Process Design Methodology for Thermochemical Production of Fuels from Biomass. Application to the Production of Synthetic Natural Gas from Lignocellulosic Resources

THÈSE N^{O} 4693 (2010)

PRÉSENTÉE LE 25 JUIN 2010

À LA FACULTÉ SCIENCES ET TECHNIQUES DE L'INGÉNIEUR
LABORATOIRE D'ÉNERGÉTIQUE INDUSTRIELLE
PROGRAMME DOCTORAL EN ENERGIE

ÉCOLE POLYTECHNIQUE FÉDÉRALE DE LAUSANNE

POUR L'OBTENTION DU GRADE DE DOCTEUR ÈS SCIENCES

PAR

Martin Gassner

acceptée sur proposition du jury:

Prof. D. Bonvin, président du jury
Dr F. Maréchal, directeur de thèse
Prof. R. Gani, rapporteur
Prof. W. Marquardt, rapporteur
Prof. A. Wokaun, rapporteur

ÉCOLE POLYTECHNIQUE
FÉDÉRALE DE LAUSANNE

Suisse
2010

Abstract

Biomass is a renewable, yet scarce resource since land is limited. This thesis addresses the question how to efficiently convert the available lignocellulosic biomass and biomass wastes to fuel and other useful energy services. In particular, it presents a systematic methodology for the conceptual design of thermochemical processes and demonstrates it at the production of Synthetic Natural Gas (SNG) through conventional biomass gasification and methanation, or hydrothermal gasification of biomass wastes. Through an appropriate mathematical decomposition of the design problem, thermo-economic process modelling, advanced process integration techniques and multi-objective optimisation are combined to provide a set of parameter- and scale-independent flowsheets for the optimal trade-off between several design targets.

The results of various design studies consistently demonstrate that process integration plays a critical role in the synthesis of energy- and cost-efficient processes. It allows both for a rational energy recovery by cogeneration and process intensification. Considerable potential is furthermore assessed for combining several complementary processes for an appropriate and complete conversion of the resource, which might decidedly improve the environmental performance of fuel production from biomass and stresses the importance of a systematic process design.

Keywords: biomass, biofuels, process design, process modelling, energy integration, process integration, polygeneration, multi-objective optimisation

Résumé

Bien que renouvelable, la biomasse est une ressource rare puisque la terre cultivable est limitée. Cette thèse examine la question comment convertir la biomasse lignocellulosique et ses déchets en carburants et autres services énergétiques utiles. En particulier, elle présente une méthodologie systématique pour le design conceptuel de procédés thermochimiques et la démontre à l'exemple de la production de Gaz Naturel de Synthèse (GNS) par gazéification conventionnelle de biomasse et méthanation, ou par gazéification hydrothermale de déchets de biomasse. Par une décomposition mathématique appropriée du problème de design, la modélisation de procédés, les techniques avancées d'intégration de procédé et l'optimisation multi-objective sont combinées afin de générer un ensemble de configurations qui réalisent un compromis optimal et indépendant de paramètres et d'échelle entre plusieurs objectifs du design.

Les résultats de diverses études démontrent de manière cohérente que l'intégration de procédé joue un rôle clé dans la conception de procédés efficaces et économiques. Elle permet non seulement une récupération rationnelle de l'énergie par cogénération, mais aussi l'intensification de procédé. Du potentiel considérable est relevé pour la combinaison de plusieurs procédés complémentaires afin de convertir la ressource de manière appropriée et complète. Ceci peut améliorer de manière décisive la performance environnementale de la production de carburants à partir de biomasse et souligne l'importance de la conception systématique de tels procédés.

Mots-clés: biomasse, biocarburants, conception de procédé, modélisation de procédé, intégration énergétique, intégration de procédé, polygénération, optimisation multi-objective

Acknowledgements

I would like to thank my thesis director François Maréchal not only for his competent guidance and inspiration, but also cordial and confident support, and friendship. His scientific passion for developing systematic methodology has been a constant driver to successfully achieving this thesis.

I have highly appreciated the collaboration with my colleagues in the motivating, interdisciplinary research project '2nd Generation Biogas' in the frame of the Competence Centre for Energy and Mobility (CCEM-CH). In particular, I would like to thank the head of this project, Samuel Stucki, for his unhesitating, cordial availability and competent advice. Furthermore, the project collaborations with Renato Baciocchi, Marco Mazzotti and the group of Fredi Vogel has been very motivating and allowed for developing detailed and accurate models.

I am very grateful to Georges Heyen for his kind support and highly qualified advice on anything in relation to thermodynamic property models and their implementation. Also, the software support and customisation by Eric Radermecker at Belsim SA has been very valuable.

It has been a great pleasure and honour to have Alexander Wokaun, Wolfgang Marquardt and Rafiqul Gani on my thesis jury headed by Dominique Bonvin. I would like to thank them for evaluating and lively discussing the thesis – although this has been somewhat hindered by infamous Eyjafjallajökull that does actually not deserve its mention in this section.

I further gratefully acknowledge the funding for this thesis provided by Erdgas Ostschweiz AG, Gasverbund Mittelland AG and Gaznat SA and their representatives Thomas Peyer, Hans Wach and Félix Guedemann for the interesting discussions at our meetings.

The lively atmosphere at the Industrial Energy Systems Laboratory has been a great environment to write this thesis. Apart its director Daniel Favrat, I would like to thank the staff of the secretariat for their friendly

and efficient administrative assistance. Working together with my office colleagues and the lenisystems group has been a pleasure and also very helpful for my research. In particular, Raffaele's developments for the modelling framework and parallel computing have been of essential value for an efficient execution of the work. Furthermore, Laurence and Léda's master and PhD projects have contributed for studying several aspects related to this thesis.

I would like to thank Kunio Yoshikawa for accepting me for an research visit at his laboratory at the Tokyo Institute of Technology. He and his students have welcomed and offered me an exciting stay in Japan.

Ganz besonders möchte ich meinen Eltern Simonette und Helmut und meiner Schwester Denise danken. Eure konstante und engagierte Unterstützung während Studium und Doktorat ist unschätzbar.

Quand je suis arrivé à Lausanne il y a presque 10 ans, je n'aurais jamais imaginé que je serais ici aussi longtemps. La meilleure raison pour rester et entamer cette thèse étaient mes amis basés ici, avec lesquels j'ai passé un temps passionnant, drôle et heureux. Je ne peux malheureusement pas tous vous mentionner – Thomas pendant les premières années, Christian plus tard, Richard tout le long, et particulièrement Yvonne et Georg, vous avez fait de cet endroit un nouveau chez moi.

Après coup, Anne, tu étais la meilleure et plus que suffisante raison pour rester.

Contents

Introduction

Biomass is a renewable, yet scarce resource since land is limited. Claimed by many as future feedstock to produce goods and provide energy (Ragauskas et al., 2006), there is growing concern about intensified forest and farmland exploitation and its inherent competition with food production. Indeed, many recent studies show that the increasingly popular production of fuels from biomass and energy crops based on industrial agriculture and forestry suffer severe sustainability issues and may even cause both greater damage to ecosystem quality, human health and greenhouse gas emissions than fossil fuels (Zah et al., 2007, Scharlemann and Laurance, 2008, Fargione et al., 2008). All these authors, including also Tilman et al. (2009), yet assert that the performance highly depends on the feedstock and conversion technologies, and that fuel production from biomass can be efficient and truly sustainable if substrates with high cellulose or lignin content that are decoupled from food production, such as sustainably harvested wood, forest and crop residues, or municipal and industrial wastes, are used.

Today, the share of biomass and biomass wastes in Switzerland's total energy consumption is of roughly 3% and currently almost exclusively used for heating purposes (BFE, 2005). At best, this input can be roughly tripled if the ecologic potential assessed by Oettli et al. (2004) can be fully exploited. If the energy consumption remains unchanged, the potential illustrated in Figure 1 allows for satisfying not much more than 10% of the primary energy consumption. However, considerable efficiency improvements in both the energy conversion system and final use might allow for meeting the 2000W society challenge (Maréchal et al., 2005a), in which biomass could contribute a significant share of up to 27% of the total demand (Table 1).

While multiple technological alternatives for an efficient low-carbon supply of heat and power exist, relatively few solutions for mitigating the important and still increasing greenhouse gas emissions in the transport sector are

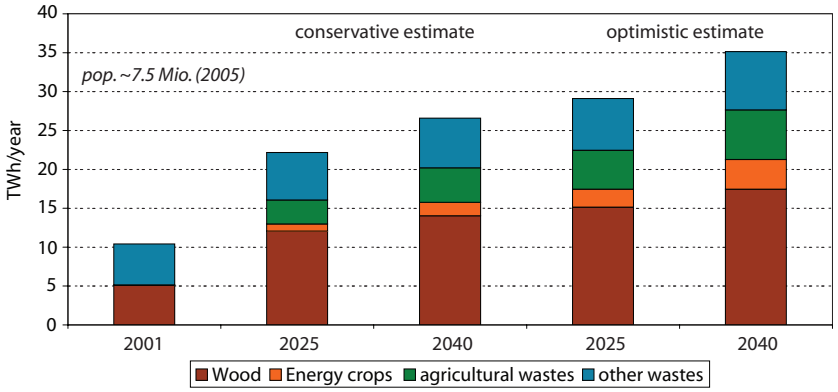

Figure 1—Biomass use today and ecological potential in Switzerland (Oettli et al., 2004).

Estimate		conservative		optimistic	
Energy consumption\Year	2001	2025	2040	2025	2040
4910 Watt/cap. (2005)	3.3%	7.0%	8.5%	9.3%	11.1%
2000 Watt/cap.		17.2%	20.9%	22.8%	27.3%

Table 1—Maximum share of biomass on total energy consumption in Switzerland (calculated from data of BFE (2005) and Oettli et al. (2004)).

emerging (BFE, 2004). The production of second-generation biofuels from lignocellulosic matter is therefore widely considered as a promising route for an effective and sustainable use of biomass.

Contrary to biological processes like biomethanation or ethanol fermentation that struggle to decompose cellulose and lignin compounds, thermochemical processing allows for a complete conversion of the lignocellulosic materials by gasification above at least 400°C. Among the candidate liquid and gaseous fuels, methane is thereby one of the most promising options since the synthesis reaction approaches chemical equilibrium, its conversion efficiency is high and also less exothermal than the one of liquid fuel. Representing the feedstock by a typical wood composition and using the carbon atom as reference, the targeted overall conversion can be expressed as:

$$\begin{aligned} \mathrm{CH_{1.35}O_{0.63}} + 0.3475\ \mathrm{H_2O} \longrightarrow 0.51125\ \mathrm{CH_4} + 0.48875\ \mathrm{CO_2}, \\ \Delta\tilde{h}_r^0 = \text{-}10.5\ \mathrm{kJ\ mol}_{wood}^{-1} \end{aligned} \tag{1}$$

Despite the overall negative heat of reaction $\Delta\tilde{h}_r^0$, the thermochemical routes typically split the conversion of Equation 1 into an endothermal decomposition at high temperature and an exothermal synthesis at lower temperature, which stresses the importance of the energy integration in the process design.

Separated from CO_2, the produced methane can be distributed as Synthetic Natural Gas (SNG) in the existing natural gas grid and used as a locally produced transport fuel in an increasingly dense network of fuel stations. If the resource is exploited in a sustainable way, the inherently carbon-neutral production could thereby even be turned into an absolute CO_2-sink for the atmosphere, since the separated biogenic CO_2 could possibly be sequestrated in the future.

Objective

The findings of the previously mentioned studies mainly rely on some reference scenarios with coarse assumptions, which is conventional practice in life cycle assessment. At another level of detail, the analysis and design of the conversion processes itself is often based on conventional simulation of some flowsheets developed by engineering knowledge and intuition[1], but lacks a systematic approach.

The objective of this work has therefore been to develop and demonstrate a methodology for the conceptual design of processes for an efficient conversion of lignocellulosic biomass and biomass wastes into fuels or other useful energy services. At the example of thermochemical SNG production, it aims at investigating the impact of the process design and its integration on the overall performance. In a field where multiple emerging conversion technologies are competing for a scarce resource, the work demonstrates how process modelling can guide research and development and serve as a design tool that allows for adapting the process configuration to variable feedstock characteristics and the specific plant location.

Themes

The issues related to the objective can be grouped into several themes.

Process modelling. In order to correctly represent to influence of design parameters on the thermo-economic performance of the process units while allowing for its evaluation at different conditions, mathematically simple, but accurate models for technologies that do not follow standard thermodynamic descriptions are required. The models should handle variable resource characteristics and allow for reconciliation with experimental data. The choice

[1]Some popular and recent examples include Tijmensen et al. (2002) and Hamelinck et al. (2004) for Fischer-Tropsch fuel, Mozaffarian and Zwart (2003) for SNG, Aden et al. (2002) and Laser et al. (2009a) for ethanol, and Zwart and Boerrigter (2005), Hamelinck et al. (2005) and Laser et al. (2009b) for the coproduction of several fuels.

or development of appropriate thermodynamic property models may also be an issue.

Energy integration and recovery. Thermochemical processing implies multiple endo- and exothermal conversions at variable temperature levels. To a large extent, the process performance thus depends on the quality of its energy integration and, in particular, the valorisation of excess heat for combined heat and power production. Conventional scenario-based flowsheeting with a predefined structure for the heat exchanger network inherently runs the risk of missing these opportunities since it lacks a systematic vision of the heat exchange. Advanced pinch technologies overcome these problems.

Process integration. In chemical process design, energy requirements are typically supplied by external utilities that only interact with the heat balance of a plant. If fuel(s) are the principal product, it is obvious that these requirements are balanced by waste and intermediate product streams available on-site. It is less obvious, however, how these requirements are balanced best.

In order to tackle this problem, the combined mass and energy balances of a plant superstructure need to be solved simultaneously with respect to an overall objective, which implies that the operating conditions depend on the process integration. Although not by orders of magnitude, such an approach allows for designing intensified processes.

Site-scale integration and biorefining. Similar to fossil resources, biomass is expected to develop as a general feedstock for the production of chemicals and/or fuels. Although originally not intended for combination, different conversion processes on the same site may thereby integrate well in terms of mass and energy. A relevant example in biofuel production is the use of the residual lignin slurry from ethanol fermentation, which is typically dried and burnt to provide heat for ethanol distillation and power cogeneration. Thermochemical conversion processes are an alternative that can be expected to substantially increase the combined fuel yield. Again, an overall appraisal of the design problem is mandatory to assess the potential synergies of such and similar biorefinery concepts.

Optimal process design? Sustainability implies good performance with respect to several incommensurable criteria. On a process design level, the performance needs to be assessed with respect to multiple thermodynamic,

economic and environmental indicators, not to mention issues related to operability and control. In the field of biomass conversion, the variability of the resource and its logistics may furthermore have an impact that might not necessarily follow conventional chemical engineering intuition.

Multi-objective optimisation is a powerful tool to preserve these multiple aspects and understand the trade-offs between individual performance indicators of complex polygeneration plants. Coupled to thermo-economic process modelling, integration and life cycle assessment, it can be used to guide research and development towards a globally sound process design instead of an isolated design of the process units, which is often reality both in industry and research.

Contributions

Methodology. The present work provides a rational process design methodology based on an appropriate mathematical decomposition of the optimisation problem, in which mass and energy integration is addressed simultaneously. Flowsheeting, equipment rating and costing is systematically coupled. In order to generate general parameter- and scale-independent sets of potentially optimal candidate configurations, it introduces a criterion for the selection of a sufficient number of objectives to be used in the multi-objective optimisation of polygeneration plants. The methodology is demonstrated at several design aspects in the thermochemical production of SNG by conventional biomass gasification and methanation, or hydrothermal gasification in supercritical water.

Process design for SNG production by conventional biomass gasification and methanation. Based on a technology review, thermodynamic and economic models are developed for the most important candidate technologies identified in a general process superstructure. In several studies, considerable insight is given in the internal energy balances and the cogeneration potential through energy integration. The effects of internal heat recovery are discussed and potential improvements are quantified. Prospects of process intensification by a tight integration of the reactive and separation systems are assessed by a detailed optimisation of the crude product separation with membranes, including also the possibility for CO_2 capture at sufficient purity for sequestration. Finally, the optimal thermo-economic performances for the combined generation of SNG, heat and power of all candidate configurations are compared. The effects of the principal design parameters on the performance is discussed and the most economic technologies are identified at several scales.

Hydrothermal SNG production in supercritical water. In order to provide a design tool for an emerging technology that is expected to convert a wide range of wet biomass and biomass waste, a simple but systematic hydrolysis scheme for substrates with variable composition is proposed. At the thermodynamic process bottleneck, a specific heat transfer model for the salt separator is developed and reconciled with experimental data. Candidate thermodynamic property models for calculating the liquid vapour equilibria of crude SNG mixtures with water are evaluated and adapted to correctly assess the interactions at the particular process conditions. A general superstructure of the alternatives for combined separation and energy recovery from the crude product is developed. The prospects of technology for unconventional high-temperature cogeneration are discussed. Separate optimisations of all candidate configurations of the process superstructure assess the general thermo-economic performance and allow for a detailed discussion of the best designs depending on catalyst deactivation, availability of key technology and scale. Finally, the influence of the substrate type on the optimal process design and performance is determined.

Outline of report

After a detailed discussion of the design methodology in Chapter 1, Chapter 2 demonstrates the thermo-economic modelling approach at the example of SNG production through conventional biomass gasification and methanation. In Chapters 3 to 5, several aspects of process integration are discussed. First, Chapter 3 demonstrates the importance of energy integration considerations at a comparison of two candidate gasification systems with respect to their thermodynamic performance as gas generators and in an overall system. The detailed design study of the product separation system in Chapter 4 then reveals the potential for process intensification. Chapter 5 illustrates the prospects of site-scale integration by thermochemically converting residues from ethanol production. In Chapter 6, the extensive discussion of the conventional route is concluded by a typefaction of the candidate process technologies and configurations with respect to thermo-economic performance at multiple scales. Finally, Chapter 7 presents a process model for hydrothermal gasification as an appropriate, emerging technology for converting wet biomass and biomass waste to SNG and power. In particular, integrated cogeneration options are introduced and the influence of the resource characteristics on the optimal process design and performance are demonstrated.

Chapter 1

Process design methodology

This chapter presents the process design methodology to be followed throughout the thesis. In its essential part, it has been published with a simple design example (Gassner and Maréchal, 2009b). The approach for combined mass- and energy integration has further been detailed in a recent submission (Gassner and Maréchal, 2009a).

1.1 Introduction

Thermochemical processes for the production of fuels from renewable resources are highly integrated energy conversion systems. In addition to the technology development, the performances of such processes relies on the quality of the design and mainly on the quality of the process integration. Most of the thermo-economic process investigations addressing the production of Fischer Tropsch (FT) liquids, Synthetic Natural Gas (SNG) and the coproduction of these fuels are based on conventional simulation of some flowsheet scenarios developed by engineers' intuition and knowledge (Tijmensen et al., 2002, Hamelinck et al., 2004, Mozaffarian and Zwart, 2003, Zwart and Boerrigter, 2005). Considering the large number of design options resulting from the choice of the available technologies and the process integration options, a systematic process design method appears to be necessary. The uncertain nature of the design parameters thereby suggests an approach using multi-objective optimisation in order to capture relationships between conflictive objectives. From engineering perspectives, understanding the links between decision variables and objective functions is also an issue.

Systematic methodologies for conceptual process design based on process integration techniques and multi-objective optimisation have already been developed and applied to power plants and solid oxide fuel cell systems design

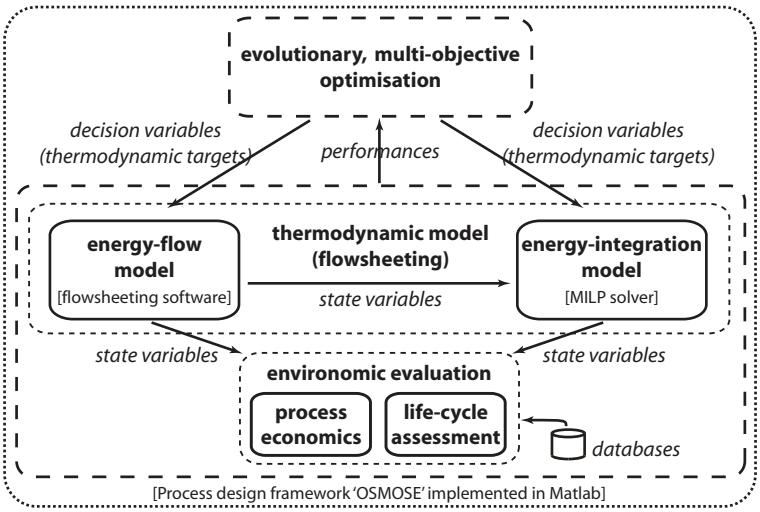

Figure 1.1—Design methodology overview.

(Bolliger et al., 2005, Palazzi et al., 2005). In the field of biofuel production, such computer aided process synthesis methodologies have not really been applied. The present chapter aims at discussing the developed process design methodology for the conceptual design of thermochemical processes for the production of fuels from biomass.

1.2 Approach

The basic concept of the developed method is the decomposition of the problem into several parts, as illustrated in Figure 1.1. Following the conceptual process design methodology (Douglas, 1985), the block flow diagram of the conversion process is first set up. After identifying suitable technology for the conversion steps, energy-flow, energy integration and economic models of the equipment and their interactions are integrated in a multi-objective optimisation framework to compute a set of optimal process configurations with respect to different design objectives. An analysis of the optimisation results with regard to environomic (i.e. thermodynamic, economic and environmental) criteria then results in the synthesis of sound conceptual plant flowsheets. The communication between the software used for the different modelling and optimisation steps has been realised by developing a computational platform programmed in Matlab-language (Bolliger, 2010).

1.3 Block flow superstructure

In the first step of the design, the product specifications and the available raw materials and energy resources are investigated and the general requirements on the process are defined. This determines feasible production pathways, required process steps and intermediate products. For the block flow diagram, suitable technologies and mandatory auxiliary operations such as feed preparation, product purification and recycling are identified and assembled in a process superstructure. The components of the heat recovery system and optional additional equipment for optimal energy conversion complete the superstructure. The definition of possible material pathways and the identification of the range of operating conditions for which the transformations are thermodynamically and technically feasible concludes the technology identification step and results in the definition of the design problem.

1.4 Flowsheet generation by thermo-economic modelling

After the definition of the block flow superstructure, there exist several ways of formulating and solving the problem of generating feasible process configurations (flowsheets). Such formulations are influenced by the chosen optimisation algorithm for the subsequent optimisation step. Considering the number of options in the process superstructure, the explicit description of the heat exchanger network (HEN) appears a priori too complex due to the combinatorial nature of the problem and the large number of possible options. One alternative is the use of a generalised heat exchanger network superstructure as proposed by Floudas et al. (1986). This however defines a very complex mixed integer non-linear programming (MINLP) problem since the heat exchanger network superstructure has to be combined with the process superstructure, in which the choice of the process options and its operating conditions have to be optimised together with the utility system and the heat exchanger network design. Alternatively, the use of the heat cascade constraints allow for modelling the performances of the HEN. Unlike conventional flowsheeting methods, this approach does not define the topology of the heat exchanger network and the fuel supply a priori, but computes it in the integration step. No restrictions are thus set on the system design and a maximum number of potential solutions are considered, which makes the method very suitable for conceptual process design. When using pinch analysis for modelling the HEN, a classical sequential approach as proposed by Douglas (1988) can be used to solve the design problem: first the energy

flows are modelled using a flowsheeting approach, then the pinch analysis is used to compute the maximum heat recovery by heat exchange and finally the heat exchanger network is designed. If in our approach, the principle of this approach is applied, the method proposed had however to be adapted in order to overcome some of the weaknesses of the classical sequential approach.

In conventional pinch analysis, only the minimum energy requirements are considered and the utility streams used to close the energy balance are considered at a given temperature (supposed to be sufficient). Furthermore, the pinch analysis does not include the combined heat and power production and the cost of the heat exchanger network is difficult to estimate since the utility streams are not considered. In order to solve the problem, a formulation as proposed by Kravanja and Glavic (1997) has been investigated to overcome such weaknesses. This approach first divides the optimisation problem into several successive mathematical programming steps. A decomposition strategy is used to partition the decision variables that affect the performances of the process flowsheet, and the problem is solved in a discretised space. The process integration and HEN targeting problem is solved as a MINLP problem. Using the results of this mathematical programming approach, a detailed model for solving and optimising the HEN design using a NLP problem is then applied. One of the major contributions of this method is the heat integration and HEN cost targeting method that is solved simultaneously with the flowsheeting aspects.

Regarding the typical problem to be solved in thermochemical biomass to fuel conversion, there are however still some unsolved problems. The first one is related to the utility system. In the case of Kravanja and Glavic (1997), the utilities are considered as external streams. In our case, there are no utility streams since the raw material (biomass), the product, the intermediate streams and even some of the waste streams are all able to produce the required heat for the conversion process. The heat requirement will therefore be satisfied by selecting the appropriate flows in the conversion process itself and the quality of the integration will define the efficiency of the process. The second difficulty relates to the process flowsheet superstructure. As different technologies may be used to realise the identified process operations, the process flowsheet is in reality a complex superstructure including a lot of different options that will be selected for their role in the production and/or in the energy integration. As the operating conditions have to be optimised together with the existence of only some of the technologies in the final design, this would require the application of disjunctive programming techniques (Türkay and Grossmann, 1996). The third difficulty is the combined heat and power (CHP) production that is used in order to valorise the exergy of the streams. The quality of the process integration therefore de-

pends on the simultaneous optimisation of the mechanical power balance and the heat integration. As steam will be used for CHP, the pressure levels have to be optimised. This would create problems in a mathematical programming formulation due to the non-continuous nature of the heat cascade when the temperature of the streams is changing. Finally, in addition to the HEN costing, the cost estimation technique for the process implies the sizing of the different technologies based on their expected operating conditions. As such sizing procedures may be discontinuous due to the application of if-then-else rules or limits of elements, this would require the use of integer variables and special constraints if one would formulate the problem as a mathematical programming problem. In addition, our goal was to use a multi-objective optimisation strategy in order to understand the trade-off between conflicting objectives and to define sets of configurations. From the mathematical programming perspective, this would require the use of integer cuts and the application of parametric programming and therefore the resolution of a large number of MINLP problems.

We have therefore reformulated the problem in order to resolve these drawbacks. The proposed method is based on the following principles:

a) The decision variables set is decomposed into two subsets: (a) the complicating variables that are handled by an evolutionary algorithm that solves a multi-objective optimisation problem and (b) the superstructure variables that are selected such that they allow for formulating the process integration model as a MILP problem. The complicating variables define the operating conditions of the different technologies. Using the flowsheeting model, these variable determine the hot and cold streams to be considered in the heat cascade as well as the mass balances from the superstructure.

b) The flowsheeting model uses an equation solver procedure and the complicating decision variables are set as specifications for the flowsheeting problem. They are selected to guarantee the convergence of the flowsheeting problem.

c) The superstructure model is formulated as a MILP problem that includes the heat cascade, the combined heat and power production and the mass balance of the technology superstructure. The objective function of this problem is a weighted sum of the produced and consumed services based on their economic or exergetic value.

d) The reference approach temperature ΔT_{ref} is considered as a complicating decision variable and is used to represent the energy recov-

ery/capital trade-off in the HEN design. It will be used as the sizing decision variable for targeting the HEN cost.

e) The cost of the HEN is estimated considering the composite curves as computed by the process integration model and the minimum number of units as obtained from the graph theory.

f) The different equipment is sized independently as a function of the operating conditions imposed by the set of complicating variables and the flows as computed in the process integration model. Their cost is then deduced from the size and not from capacity-based correlations.

g) The model is solved in three successive steps: the flowsheeting step, the process integration step and the sizing and costing step. The objective functions are calculated at the end of these three steps.

h) An evolutionary multi-objective optimiser is used to optimise the values of the complicating decision variables.

i) The set of complicating decision variables is defined such that the inequality constraints will appear either as bounds on the decision variables or as linear inequality constraints in the process integration model and therefore will be handled by the MILP algorithm.

j) The mathematical formulation of the process unit models are not available as a set of explicit equations and may be computed using different flowsheeting software.

k) The final design of the heat exchanger network will be defined after the process optimisation procedure and only for a limited number of optimal process configurations from the Pareto curves. It is assumed that the HEN design can be solved using conventional HEN design routines and that the optimal design will feature investment and operating cost that will be close to the one estimated by the composite curve model.

According to these principles, the thermodynamic conditions of the process unit operations are first calculated in the energy-flow model. The energy conversion and heat transfer system is then calculated in the energy integration model using heat cascade constraints and a combined heat and power maximisation method. As explained in mathematical detail below, this decomposition allows for inherently combining the mass and energy integration in a non-linear master and MILP subproblem optimisation.

1.4.1 Energy-flow model

The goal of the energy-flow model is to compute the material conversion in the process units, to determine their heat transfer and power requirements and to thermodynamically characterise the streams that will be used for the equipment rating. Such thermochemical transformation models are developed for all process subsystems s of the block flow superstructure and can be represented by a set of j non-linear functions $\mathcal{F}_s$:

$$c_j\,\dot{m}_j^- = \mathcal{F}_s\left(c_i, \dot{m}_i^+, \text{operating conditions}\right) \quad \forall j \tag{1.1}$$

where c and $\dot{m}$ are the mass concentrations and flows of the inlet and outlet streams i and j, respectively. While c_i and c_j are vectors of varying size, $\dot{m}$ are scalars that obviously satisfy the mass conservation, i.e.:

$$\sum_j \dot{m}_j^- = \sum_i \dot{m}_i^+ \tag{1.2}$$

Linked to this conversion, the energy balance associated with $\mathcal{F}_s$ writes:

$$\sum_{j_h}(\dot{m}\,h)_{j_h}^- + \dot{E}_j^- + \sum_{j_{th}} \dot{Q}_{j_{th}}^- = \sum_{i_h}(\dot{m}\,h)_{i_h}^+ + \dot{E}_i^+ + \sum_{i_{th}} \dot{Q}_{i_{th}}^+ \tag{1.3}$$

where h refers to the total mass enthalpy, and $\dot{E}$ and $\dot{Q}$ represent the electricity and heat consumption or generation in the subsystem, respectively.

As the subsystem models are interdependent with respect to intensive variables such as stream composition, pressure and temperature, the formulation of $\mathcal{F}_s$ in Eq. (1.1) needs to balance model complexity and robustness of its numeric resolution. In general, the use of commercial flowsheeting software that supports the implementation of user-defined, phenomenological models is adequate for this purpose. In our case, the software developed by Belsim SA based on a simultaneous resolution of all model equations has proven convenient. Based on an equation solver formulation that does not require the definition of a resolution sequence, it eases the handling of problems with stream loops and further allows for model reconciliation with experiment and pilot plant data.

1.4.2 Energy integration model

Once the chemical conversion in the process sections and its associated heat requirements determined, the combined fuel, heat and power production can be maximised by MILP in which both the mass balances between the subsystems and the heat cascade are used as constraints. In order to supply the

Exponent	0.8	0.5	0.44
$\Delta T_{min}/2$	Eq. 1.6	Linnhoff and Townsend (1982)	Bolliger et al. (2008)
2K	1'823	3'625	4'558
4K	767	906	958
8K	322	227	201
25K	78	23	16

Table 1.1—Values of α_j with different heuristics for $\alpha_{ref} = 580$ $\mathrm{Wm^{-2}K^{-1}}$, $\Delta T_{ref} = 10\mathrm{K}$ and $b_{HE} = 0.8$.

energy requirement above the pinch, combustion of fuels available on-site is considered. If the heat available from the combustion of the usable waste and retentate streams is not sufficient, process streams may be used as fuel to close the balance leading to a reduction of the flows in the main conversion route. The choice of using optional energy conversion and recovery equipment like heat pumps, gas turbines and Rankine cycles is formulated by means of integer variables. The structure and operating conditions of these units are considered as decision variables of the master problem and only the corresponding flowrates are calculated by the energy integration model.

In order to assure a feasible heat exchange and account for different values of the heat transfer coefficient, the temperatures T of all heat effects in the cascade formulation are corrected by a minimum approach temperature ΔT_{min}, i.e.:

$$T^*{}_h = (T - \Delta T_{min}/2)_h \qquad \forall h \in \{hot\,streams\} \tag{1.4}$$

$$T^*{}_c = (T + \Delta T_{min}/2)_c \qquad \forall c \in \{cold\,streams\} \tag{1.5}$$

A heuristic rule is used to estimate the value of the convective heat transfer coefficient α_j of a stream j from its minimum approach temperature contribution $\Delta T_{min}/2$:

$$(\Delta T_{min}/2)_j = \frac{\Delta T_{ref}}{2}\left(\frac{\alpha_{ref}}{\alpha_j}\right)^{b_{HE}} \tag{1.6}$$

where ΔT_{ref} is the minimum approach temperature for an an arbitrary reference heat transfer coefficient α_{ref} and b_{HE} the exponent used in Equation (1.29) for estimating the cost of the heat exchangers. Table 1.1 illustrates this approach and compares several strategies for the exponent choice in Equation 1.6[1].If the value of α_j is fixed and $\Delta T_{min}/2$ considered variable instead, the value of ΔT_{ref} can be used in the master optimisation procedure

[1]While Linnhoff and Townsend (1982) originally proposed a square-root relation, Bolliger et al. (2008) recently argued an exponent of $b_{HE}/(b_{HE}+1)$ to be more consistent.

to represent the trade-off between the investment cost and the heat recovery and energy conversion efficiency.

The selection of the objective in the MILP is arbitrary as long as the aggregation of the terms is consistent with the multiple objectives of the master optimisation problem. While we proposed to minimise the total exergy depletion in Gassner and Maréchal (2009b), a more straightforward alternative is yet to simply weight the product yields with respect to their energetic or economic value. For all subsections s that provide j output and consume i input streams through the system boundary, the target can be expressed as a function of their utilisation level f_s to be optimised, i.e.:

$$\underset{\dot{R}_r, y_s, f_s}{max} \sum_s f_s \left(\sum_j (\dot{m}\, h)_j^- C_j - \sum_i (\dot{m}\, h)_i^+ C_i \right) + \left(\dot{E}^- - \dot{E}^+ \right) C_{el} \qquad (1.7)$$

subject to:

a) Existence of subsystem s:

$$f_{min,s} y_s \leq f_s \leq f_{max,s} y_s \qquad y_s \in \{0,1\},\ \forall s = 1, ..., N_s \quad (1.8)$$

b) Superstructure model:

$$Af = b \qquad A : (N_s \times N_s),\ f, b : (N_s \times 1) \quad (1.9)$$

c) Heat balance of the temperature intervals r:

$$\sum_{s=1}^{N_s} f_s \dot{Q}_{s,r}^- + \dot{R}_{r+1} - \dot{R}_r = 0 \qquad \dot{R}_r \geq 0 \ \ \forall r = 1, ..., N_r \quad (1.10)$$

d) Overall heat balance:

$$\dot{R}_1 = 0,\ \dot{R}_{N_{r+1}} = 0 \quad (1.11)$$

e) Electricity consumption:

$$\sum_{s=1}^{N_s} f_s \dot{E}_s^- - \dot{E}_c^+ + \epsilon_d \dot{E}^+ \geq 0 \qquad \dot{E}^+ \geq 0 \quad (1.12)$$

f) Electricity exportation:

$$\sum_{s=1}^{N_s} f_s \dot{E}_s{}^- - \dot{E}_c^+ + \epsilon_d \dot{E}^+ - \frac{\dot{E}^-}{\epsilon_g} = 0 \qquad \dot{E}^+ \geq 0,\ \dot{E}^- \geq 0 \quad (1.13)$$

with:

A, b	coefficients of the linear equation system defined by the superstructure
C_j	weighting factor of product j
f_s	level of utilisation of subsystem s
$f_{max,s}$	upper bound of f_s
$f_{min,s}$	lower bound of f_s
N_r	number of temperature intervals r
N_s	number of subsystems s
$\dot{Q}^-_{s,r}$	the net production of heat of subsystem s in the temperature interval r for the reference flowrate
$\dot{R}_r$	cascaded energy from the temperature interval $r+1$ to r
$\dot{E}^+$	the consumption of electricity from the grid
$\dot{E}^+_c$	the auxiliary consumption of electricity on-site
$\dot{E}^-$	the production of electricity to the grid
$\dot{E}^-_s$	the net production of electricity of subsystem s for the reference flowrate
y_s	integer variable for the presence of subsystem s
ϵ_d	the conversion efficiency from the grid
ϵ_g	the conversion efficiency to the grid

Allowing for arbitrary reference flowrates of the different subsystems in the unit models (Eq. 1.1), the superstructure model of Eq. (1.9) consists of the mass balances between all subsections. This is illustrated by a typical block flow diagram encountered in thermochemical fuel production depicted in Figure 1.2. For instance, the connection between drying, gasification and combustion is written as:

$$\dot{m}^+{}_{wood,g} f_g + y_{wood,c} \dot{m}^+{}_{wood,c} f_{wood,c} - \dot{m}^-{}_{wood,d} f_d = 0 \tag{1.14}$$

in which $\dot{m}^+{}_{wood,g}$, $\dot{m}^+{}_{wood,c}$ and $\dot{m}^-{}_{wood,d}$ are obtained from the unit models $\mathcal{F}_s$ (Eq. 1.1) and $y_{wood,c}$ represents the choice of the technology subset that can be used as a decision variable on the master optimisation level. The non-linearities of the thermochemical conversion are thus enclosed in the coefficient matrix A of Eq. (1.9) and only the utilisation levels f_s of the subsystems are computed in the MILP problem. The only non-zero entry of b thereby fixes the reference scale of, for instance, the biomass input:

$$\dot{m}^+{}_{wood,d} \Delta h^0_{wood} f_d = cst \tag{1.15}$$

in which Δh^0_{wood} refers to the lower heating value of the feedstock.

1.4.3 Combined mass and energy integration

In general, the constraint on $\dot{R}_{N_{r+1}}$ in Eq. (1.11) is not feasible without hot utility or, in our case, burning the depleted and part of some intermediate

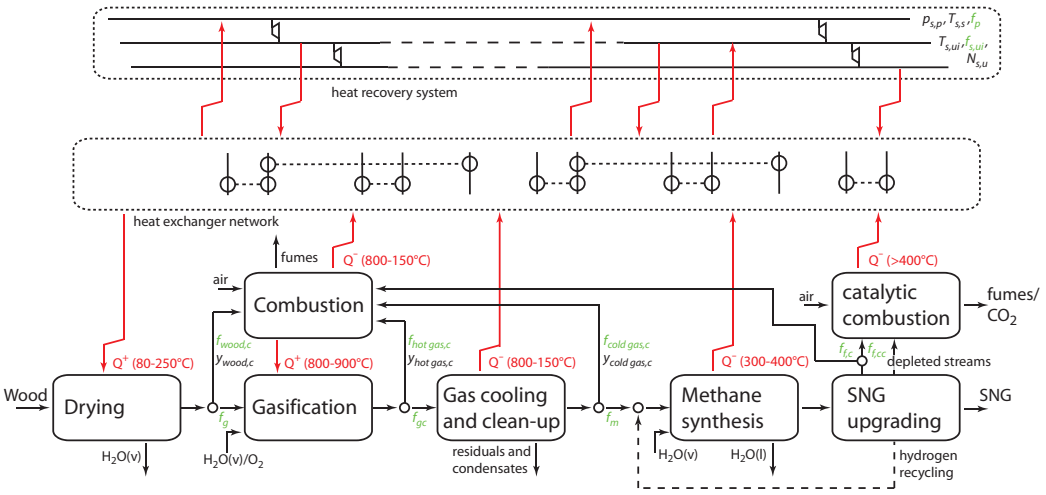

Figure 1.2—Conceptual structure of the process model illustrated at thermochemical production of SNG including the heat exchanger network and energy recovery system (simplified). Non-linear process unit models are represented by boxes. Decision variables exclusively used in the MILP are highlighted in green.

product streams. The unit model for combustion is thus of particular significance since it connects the energy and mass balances in order to satisfy the heat requirement in the highest temperature interval of Eq. (1.10) while respecting the superstructure model of Eq. (1.9). Following the formulation of Maréchal and Kalitventzeff (1998), it is possible to directly determine its optimal integration in the MILP problem by dissociating the effects of fuel and air in the combustion. Defining the heat of combustion $h_{f,r}$ as the amount of heat available from the combustion gases at an arbitrary radiation temperature T_r if the combustion is carried out with air available at this temperature, the contribution of each fuel f in the heat balance above T_r (Eq. 1.10) is written as:

$$\dot{Q}^{-}_{f,r} = \dot{m}_f h_{f,r} - \dot{m}_{air,stoich.} c_{p,air} \left(T_r - T_{air,in}\right) \tag{1.16}$$

The first term of this equation thus exclusively quantifies the contribution of the fuel at T_r, and the second one the energy required to heat up the stoichiometric amount of air from the reactor inlet temperature $T_{air,in}$ to T_r. For all candidate fuels identified in the process superstructure, $h_{f,r}$ can be determined from their lower heating value Δh^0_f, the adiabatic flame temperature ${T^0}_{ad,f}$, the oxygen required for the complete combustion of the fuel $c_{O2,req.}$

(in $\mathrm{kg}_{O2}\ \mathrm{kg}_{fuel}^{-1}$) and the mass fraction of oxygen in air $c_{O2,air}$:

$$h_{f,r} = \frac{T^0{}_{ad,f} - T_r}{T^0{}_{ad,f} - T^0} \Delta h_f^0 + \frac{c_{O2,req.}}{c_{O2,air}} c_{p,air} \left(T_r - T^0\right) \tag{1.17}$$

Similar to the effect of the fuel above T_r, its contribution in the heat balance between T_r and the stack temperature T_{stack} to be recovered by convective transfer is written as:

$$\dot{Q}_{f,c}^{-} = \dot{m}_f h_{f,c} + \dot{m}_{air,stoich.} c_{p,air} \left(T_r - T_{stack}\right) \tag{1.18}$$

for which $h_{f,c}$ can be calculated from:

$$h_{f,c} = \frac{T_r - T_{stack}}{T^0{}_{ad,f} - T^0} \Delta h_f^0 - \frac{c_{O2,req.}}{c_{O2,air}} c_{p,air} \left(T_r - T_{stack}\right) \tag{1.19}$$

The heat requirement for air preheating is separately added to the problem as cold stream with:

$$\dot{Q}_{air,c}^{+} = \dot{m}_{air,stoich.} c_{p,air} \left(T_{air,in} - T^0\right) \tag{1.20}$$

and its utilisation level f_{air} is linked to the ones of the fuels f_f by a constraint that allows for oxygen excess e_f:

$$\sum_{f=1}^{N_f} (1 + e_f) c_{O2,req.} f_f - c_{O2,air} f_{air,0} \leq 0 \tag{1.21}$$

While Eq. (1.21) assures a sufficient air flow rate for complete combustion, the air temperature at the reactor inlet $T_{air,in}$ in Eqns. (1.16) and (1.20) is a priori unknown and needs to be computed. The equations thereby show that air preheating introduces a heat pumping effect since increasing $T_{air,in}$ allows for increasing the heat available at T_r with heat below $T_{air,in}$. The determination of the optimal value of $T_{air,in}$ can be integrated in the MILP formulation by discretising the cold steam of Eq. (1.20) in N_i intervals from T_i to T_{i+1}:

$$\dot{Q}_{air,c}^{+} = \sum_{i=0}^{N_i} \dot{Q}_{air,i,c}^{+} = \dot{m}_{air,stoich.} c_{p,air} \sum_{i=0}^{N_i} \left(T_{air,i+1} - T_{air,i}\right) \tag{1.22}$$

and constraining their flow multiplication factors with:

$$f_{air,i} \geq f_{air,i+1} \qquad \forall i = 0, ..., N_i \tag{1.23}$$

where $f_{air,0}$ is the multiplication factor for ambient air. Accordingly, the temperature difference in the second term of the left-hand side of Eq. (1.16) is written by difference as:

$$\begin{aligned} T_r - T_{air,in} &= T_r - T^0 - \sum_{i=0}^{N_i} (T_{i+1} - T_i) \\ &= T_r - \sum_{i=1}^{N_i} (T_{i+1} - T_i) \end{aligned} \tag{1.24}$$

1.5 Equipment rating and cost estimation

The thermodynamic state of the process streams resulting from the energy-flow and -integration steps are used as equipment design targets. For this purpose, a preliminary rating and cost estimation procedure is implemented for each unit to take the direct influence of the design variables on the investment cost into account. Equipment design heuristics mainly from Ulrich (1984) combined with data from existing experimental and pilot plant facilities are thereby used to estimate the size of the major process equipment for a given production scale. According to the costing method of Turton et al. (1998), the bare module costs C_{BM}, defined as the installed cost of a unit considering construction material, operating pressure and indirect costs like freights and engineering expenses, are then determined with correlations from the literature. The total grass roots cost C_{GR} of the plant, i.e. the total investment cost for a new production site excluding land, is estimated by summing up and factoring the bare module costs to account for subsidiary expenses:

$$C_{GR} = (1 + c_1) \sum_i C_{BM,i} + c_2 \sum_i {C_{BM,i}}^0 \tag{1.25}$$

In this equation, c_1 accounts for contingencies and fees during construction and c_2 represents the costs for site development and auxiliary facilities. The latter are supposed to be unaffected by the construction materials and operating pressure and therefore related to the bare module costs ${C_{BM}}^0$ at base case conditions (i.e. carbon steel construction and ambiant pressure). Typically, c_1 and c_2 amount to 18% and 35%, respectively.

The capital cost of the heat exchanger network is estimated using the method of Ahmad et al. (1990) by considering the balanced hot and cold composite curves that result from the resolution of the MILP problem. The heat exchange is thereby specified as a succession of vertical exchanges between the two composite curves, whereas each vertical section is characterised

by two inlet and outlet temperatures and one heat load. Considering all the streams j and their respective heat transfer film coefficient $\alpha_{i,j}$ in the vertical heat exchange section i, and considering that the heat load $\dot{Q}_i$ of the vertical section equals $\sum_{h=1}^{n_{hot\_streams}} \dot{Q}_{h,i}$ and also $\sum_{c=1}^{n_{cold\_streams}} \dot{Q}_{c,i}$, the total area $A_{HEN,i}$ of the vertical section i is obtained by summing the contributions of the streams to the vertical exchange i. The total area of the heat exchanger network $A_{HEN,MER}$ necessary to fulfil the minimum energy requirement (MER) is then obtained by summing up the vertical sections i, as shown in Equation (1.26):

$$\begin{aligned} A_{HEN,MER} &= \sum_{i=1}^{N_{vert\,sections}} A_{HEN,i}(\Delta T_{ref}) \\ &= \sum_{i=1}^{N_{vert\,sections}(\Delta T_{ref})} \left(\frac{\dot{Q}_i(\Delta T_{ref})}{\Delta T_{lm,i}(\Delta T_{ref})} \sum_{j=1}^{N_{streams,i}} \frac{1}{\alpha_{i,j}} \right) \end{aligned} \tag{1.26}$$

The minimum number of exchangers $N_{HE,min,MER}$ to fulfil the target is obtained from the graph theory:

$$N_{HE,min,MER} = (N_s + N_{s,u}(\Delta T_{ref}) - 1) + (N_p(\Delta T_{ref}) - 1) \tag{1.27}$$

where N_s represents the number of process streams involved in the heat recovery system, $N_{s,u}$ the number of utility streams used to close the energy balance of the system and N_p the number of streams that cross the pinch points and that have to be accounted twice to estimate the number of connections.

It is then possible to estimate the heat exchanger network investment by equally distributing the overall area between the heat exchangers. Therefore, the mean area of one heat exchanger is computed by Equation (1.28):

$$A_{HE,mean} = A_{HE,mean}(\Delta T_{ref}) = \frac{A_{HEN,MER}(\Delta T_{ref})}{N_{HE,min,MER}(\Delta T_{ref})} \tag{1.28}$$

Using the investment cost estimation for the heat exchangers of Chauvel et al. (2001), the bare module cost of the heat exchanger network $C_{BM,HEN}$ may be estimated by Equation (1.29). ΔT_{ref} is the decision variable to be optimised and represents the efficiency-investment trade-off in the heat exchanger network model. Considering the property of the exponential function used to calculate $C_{BM,HE}$, this approximation overestimates the real investment of a heat exchanger network with the same total area and the same

number of exchangers (Ahmad et al., 1990).

$$C_{BM,HEN}(\Delta T_{ref}) = \sum_{HE=1}^{N_{HE}} C_{BM,HE}(A_{HE}(\Delta T_{ref})) \approx N_{HE,min,MER} \cdot C_{BM,HE}(A_{mean}(\Delta T_{ref})) \quad (1.29)$$

1.6 Multi-objective process optimisation

1.6.1 Performance indicators

The performance of energy conversion processes can be assessed by some thermodynamic, economic and environmental key indicators. In principle, these indicators are differently weighted combinations of all material, energy and monetary process inputs and outputs which can be determined from a thermo-economic process model.

1.6.1.1 Thermodynamic

Highly integrated energy conversion processes often supply multiple services and require different energy inputs. Besides the energy efficiency ϵ representing the conversion of primary into useful energy based on the first principle of thermodynamics, the exergy efficiency η takes entropy creation due to irreversible operations into account and compares the work potential of the energy flows:

$$\epsilon = \frac{\sum \Delta h_i^0 \dot{m}_i^- + \dot{Q}^- + \dot{E}^-}{\sum \Delta h_j^0 \dot{m}_j^+ + \dot{Q}^+ + \dot{E}^+} \quad (1.30)$$

$$\eta = \frac{\sum \Delta k_i^0 \dot{m}_i^- + \dot{E}_q{}^- + \dot{E}^-}{\sum \Delta k_j^0 \dot{m}_j^+ + \dot{E}_q{}^+ + \dot{E}^+} \quad (1.31)$$

In these definitions, Δh^0 and Δk^0 designate the lower heating and exergy values of products i and raw materials j, $\dot{Q}$ and $\dot{E}$ the useful heat and power and $\dot{E}_q$ the work potential of the heat. The superscripts $^-$ and $^+$ refer to produced (output) and consumed (input) services, respectively. $\dot{E}$ only occurs either in the numerator or denominator since only the overall balance is of interest. Although not directly compatible with this convention of consumed or produced quantities, net partial efficiencies for the produced fuel(s), heat

and power can be defined as, respectively:

$$\epsilon_{fuel,i} = \frac{\Delta h^0_{fuel,i} \dot{m}^-_{fuel,i}}{\sum \Delta h^0_j \dot{m}^+_j} \tag{1.32}$$

$$\epsilon_{th} = \frac{\dot{Q}^-}{\sum \Delta h^0_j \dot{m}^+_j} \tag{1.33}$$

$$\epsilon_{el} = \frac{\dot{E}^-}{\sum \Delta h^0_j \dot{m}^+_j} \tag{1.34}$$

which is a convenient normalisation to characterise the relative outputs obtained with a specific process configuration.

The overall energy and exergy indicators ϵ and η provide a strictly physical measure of the energy conversion and its quality degradation. Yet, they do not satisfactorily assess the value of the products with respect to the technical feasibility of their further conversion into final energy services and competing technology. The exergy potential of high temperature heat cannot really be recovered. This problem is especially apparent in case of fuels, whose exergy value typically exceeds the lower heating value and is technically by far not recoverable as mechanical work. An additional efficiency indicator that represents the technical value of the products is therefore worthwhile. With fuel as main product, it is convenient to define an efficiency based on the substitution of fuel-equivalents for the consumed or by-produced power and heat. Aiming a consistent weighting with efficient state-of-the-art technology, the value of electrical power is appropriately represented by the equivalent amount of (synthetic) natural gas required for its generation in a combined cycle plant. For heat cogeneration, conventional natural gas boilers do not qualify as reference although its widespread use since exergetically more efficient technologies are available. From a general energy system perspective, it is legitimate to represent the fuel equivalent of heat by the one of the electricity required to drive a heat pump. Using conversion efficiencies based on exergy, it is further possible to account for the temperature level at which the heat is delivered. A chemical conversion efficiency that correctly assesses the technical value of the by-products can thus be defined as:

$$\epsilon_{chem} = \frac{\sum \Delta h^0_i \dot{m}^-_i + \frac{1}{\eta_{NGCC}} \frac{\Delta h^0_{SNG}}{\Delta k^0_{SNG}} (\frac{1}{\eta_{HP}} \dot{Q}^- + \dot{E}^-)}{\sum \Delta h^0_j \dot{m}^+_j} \tag{1.35}$$

where η_{NGCC} and η_{HP} are the exergy efficiencies of natural gas combined cycles (NGCC) and heat pumps (HP). Contrary to the definitions (1.30) and (1.31), consumed amounts of heat and power are omitted in the denominator

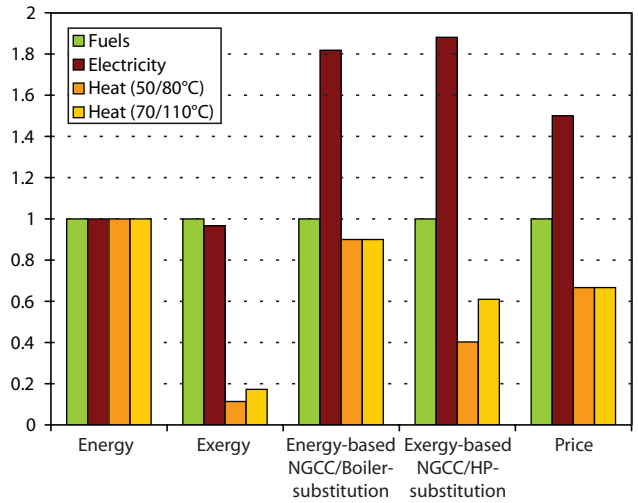

Figure 1.3—Normalised relative values of the energy vectors as assessed by the thermo-economic performance indicators. Conversion efficiencies for the substitution scenarios are $\epsilon_{NGCC} = 55\%$ and $\epsilon_{boiler} = 90\%$ for NGCC/Boiler and $\eta_{NGCC} = \eta_{HP} = 55\%$ for NGCC/HP.

and represented by negative net overall output quantities $\dot{Q}^-$ and $\dot{E}^-$ due to the applied substitution of electricity and heat by a natural gas equivalent.

A comparison of the relative values assigned to the energy vectors in terms of energy, exergy and the technological conversion scenarios is shown in Figure 1.3. As discussed above, a neutral appraisal of all services by their energy value does not do justice to the superior quality of electricity. A purely physical exergy indicator excessively corrects the value of low temperature heat, but still considerably overestimates fuel compared to electricity. While the substitution based on the energy efficiency of conventional boiler technology overestimates again the technological value of low temperature heat, an equilibrated rating is obtained with an exergy-based substitution with NGCC technology and heat pumps. Indeed, the assumption of a general exergy conversion efficiency of 55%[2] in NGCC and electricity driven heat pumps leads to a consistent and technologically reasonable appraisal of the different energy vectors (Favrat et al., 2008), which is illustrated by the resulting performance coefficients of 3.1 and 4.7 for electricity and of 1.6 and 2.5 for gas driven heat pumping to 70/110°C and 50/80°C heat networks, respectively.

[2]for methane, this corresponds to 57% in terms of energy.

1.6.1.2 Economic

In addition to the grass roots cost C_{GR} that are calculated in the economic model, the assessment of plant economics requires an indicator for the working expenses. For this purpose, the plant's operating costs C_{OP} [€ MWh_{SNG}^{-1}] normalised for the production of one unit of fuel are calculated considering the expenses for raw materials C_{RM}, utilities C_{UT}, operating labour C_{OL}, maintenance C_M and substituting the profit from the by-produced electricity and heat C_{BP}:

$$C_{OP} = C_{RM} + C_{UT} + C_{OL} + C_M - C_{BP} \tag{1.36}$$

with:

$$C_{RM} = \frac{\Delta h^0_{biomass} \dot{m}^+_{biomass}}{\Delta h^0_{SNG} \dot{m}^-_{SNG}} \cdot C_{biomass} \tag{1.37}$$

$$C_{UT} = \frac{\Delta h^0_{RME} \dot{m}^+_{RME} C_{RME} + \dot{m}^+_{O2} C_{O2} + \dot{E}^+ C_{el}}{\Delta h^0_{SNG} \dot{m}^-_{SNG}} \tag{1.38}$$

$$C_{OL} = \frac{C_{salaries}}{P_a} \tag{1.39}$$

$$C_M = 0.05 \cdot \frac{C_{GR}}{P_a} \tag{1.40}$$

$$C_{BP} = \frac{\dot{E}^- C_{el} + \dot{Q}^- C_q}{\Delta h^0_{SNG} \dot{m}^-_{SNG}} \tag{1.41}$$

In these equations, $C_{biomass}$, C_{RME}, C_{O2}, C_{el} and C_q correspond to the prices of biomass, biodiesel, oxygen, electricity and heat, $C_{salaries}$ terms the employees' total yearly salaries and P_a the yearly production of SNG. Maintenance costs are supposed to amount to 5% of the investment per year. Similar to the overall efficiency definitions of Eqs. (1.30)-(1.31), the net electricity term $\dot{E}$ occurs only in Eq. (1.38) or (1.41). By adding the discounted, annualised value of the initial investment divided by the yearly production P_a, the fixed and variable costs are combined to form the total production cost C_P [€ MWh_{SNG}^{-1}]:

$$C_P = C_{OP} + \frac{(1+i_r)^n - 1}{i_r (1+i_r)^n} \cdot \frac{C_{GR}}{P_a} \tag{1.42}$$

where i_r is the interest rate and n the economic lifetime of the plant. Considering the produced fuel as main product and accounting for the benefits of the by-products by negative contributions (as for example for electricity cogeneration in Eq. (1.38)), C_P expressed per unit of fuel assesses the competitiveness of the process compared to market prices. Although very convenient

for a single product, one drawback of this indicator in a polygeneration context is yet that the products are not equally taken into account. As the profit from selling all but the main product is included, the indicator can be misleading since it might suggest to enhance the production of by-products to the expense of the main one. This effect is avoided if the economic performance is expressed by the acceptable biomass cost for the plant to break even $C_{biomass,be}$ [€ $\mathrm{MWh}_{biomass}^{-1}$] that assesses the value of all products in a similar way:

$$C_{biomass,be} = (C_{SNG} - C_{P,SNG}) \cdot \frac{\Delta h^0_{SNG} \dot{m}^-_{SNG}}{\Delta h^0_{biomass} \dot{m}^+_{biomass}} + C_{biomass} \qquad (1.43)$$

in which the first term represents the net profit obtained from the conversion of 1 MWh of biomass.

1.6.1.3 Environmental

Since one of the fundamental aims of fuel production from renewables is the reduction of environmental impacts and in particular the mitigation of CO_2-emissions from fossil fuels, an assessment of the overall environmental balance seems essential. Life cycle assessment (LCA) provides a holistic approach for this purpose and has proven suitable for evaluating the environmental impact of well-established products and process chains, but often suffers from inconsistent and lacking information on emerging technologies. As for instance by Felder and Dones (2007) in case of SNG production, the environmental assessment is often based on the extrapolation of average data from lab- and pilot-scale facilities. The actual process design at industrial scale, and more specifically its integration and scale-up, is not considered and typically leads to an underestimation of the process performances in the life cycle assessment of emerging technologies. On the other hand, LCA is often used to only evaluate processes, but not taken into consideration in the process design, and effective measures to limit the environmental impacts are easily missed. In a conceptual process design, it is yet perfectly possible to integrate LCA in the modelling, thus provide accurate information for the environmental assessment and actively consider it as an objective in the process design. As shown by Gerber et al. (2009), the life cycle inventory (LCI) can be written as a function of the thermo-economic model, i.e. the process design variables, overall material and energy balances and equipment size. Similar to the costing, scale-up laws for the major process equipment can be developed and allow for evaluating the influence of the process scale. In this way, all impacts related to the conversion are available for the evaluation of the environmental performance of the plant and its optimisation.

A detailed discussion of the applied methodology and a comparison of the obtained results are beyond the scope of this work and left to Gerber et al. (2009).

1.6.2 Generation of optimal flowsheets

In order to identify best feasible solutions while preserving the multiple aspects of the design problem, one of the key features of the approach is the use of a multi-objective optimisation strategy. This step can be seen as the generation of a set of optimal flowsheets for a specific production setting, i.e. the available feedstock type and size and the infrastructure of energy services. It allows engineers to compare "optimal" decisions, understand the compromise between conflicting objectives and analyse their impact on the decision variables.

The optimisation procedure aims at identifying a set of Pareto optimal process configurations in the search space, i.e. configurations for which it is not feasible to further improve some objective without simultaneously deteriorating at least one other objective. Mathematically, these Pareto optimal process configurations x^* are defined by:

$$\begin{aligned} x^* \in P_k \quad \text{if} \quad & \nexists \ \{x \in S_k : (f_{\overline{o}}(x) < f_{\overline{o}}(x^*)) \ \wedge \ (f_o(x) \leq f_o(x^*))\} \\ & \forall \ \{\overline{o}, o \in O : \overline{o} \neq o\} \end{aligned} \tag{1.44}$$

where O, P_k and S_k represent the objective, Pareto and search space of a cluster k, respectively. Applying clustering techniques thereby preserves the diversity of the solutions by allowing suboptimal clusters to survive, which can be useful if it is desired to explore the entire search space and to identify break-even points of different technologies. Furthermore, the adopted algorithm developed by Leyland (2002) and Molyneaux (2002) iterates in an evolutionary procedure since the complicating decision variables (i.e. conversion pathways, equipment choices and process conditions) of the optimisation problem are of both integer and continuous type.

In principle, all the previously defined performance indicators are potential design targets, and the adopted algorithm is able to consider all of them as mathematical objectives. However, as the performance indicators f_i are different combinations of the underlying thermo-economic terms x_j (i.e. the utility and product streams and the total investment cost) and because this relation is similarly monotonic, i.e.:

$$f_i = f_i\left(x_j\right), \qquad \frac{\partial f_i}{\partial x_j} \text{ is of same sign } \forall f_i, x_j \tag{1.45}$$

these independent terms of the performance indicators are themselves used as objective functions. The condition of similar monotonicity thereby ensures that the Pareto set includes the optima not only for x_j, but all f_i. This approach reduces the number of objectives to a strict minimum and thus eases the interpretation of the numeric solutions. Moreover, it allows for generating a general set of optimal solutions that is independent on arbitrarily chosen parameters for substitution scenarios, interest rates, prices, specific emissions, etc. (cf. Eqs. 1.30 – 1.42) and guarantees to include the optima for any value of these parameters. Nevertheless, the assessment of the process performance with respect to the defined indicators is not omitted, but postponed to the results analysis that follows the generation of optimal solutions.

1.7 Results analysis

A detailed examination of the numerically generated set of optimal process configurations with regard to the multiple criteria will prepare the synthesis of a viable process. In addition to choosing an appropriate compromise, additional knowledge about the process is acquired and key issues of the process design and ongoing technology development are determined. The analysis of the dependencies and trade-offs among the objectives and performance indicators is thereby facilitated by a statistical investigation of the decision variables' influence. One possibility is to characterise the relation between decision variables and objectives by Pearson's linear correlation coefficient ρ, defined as:

$$\rho_{i,j} = \frac{\mu(x_i - \mu(x_i))\mu(x_j - \mu(x_j))}{\sigma(x_i)\sigma(x_j)} \tag{1.46}$$

where μ and σ designate the mean and the standard deviation of the observations x in the sets i and j. These coefficients provide a measure of how the observations of the sets are related: positive and negative values indicate directly and indirectly proportional relationships, values close to zero indicate that no correlation exists. In addition to ρ, partial correlation coefficients obtained from a multivariate regression are used to describe the same relation between two sets if all other decision variables are held fixed.

Although the correlation coefficients allow for statistically analysing the interdependencies between decision variables and objectives in the Pareto set, they do not give any indication about the absolute position and distribution of the optimal values of the variables in the search space. For this purpose, a histogram of their observations in the Pareto set is developed, for which some examples of typical variable distributions are displayed in Figure 1.4. On these histograms, the number of observations in the subintervals of each

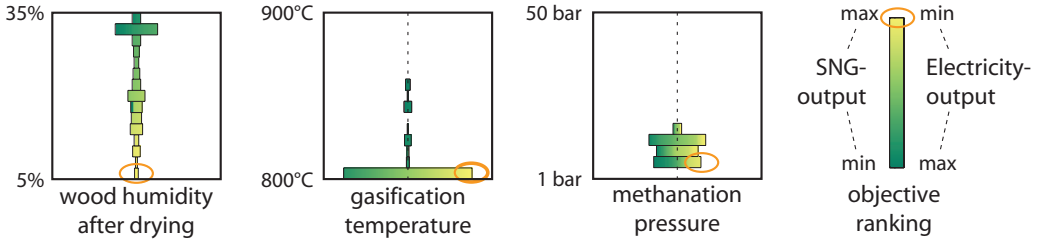

Figure 1.4—Examples for typical variable distributions in search space ranked with respect to optimisation objectives.

variable's search space is given by the bar width. The shading of the bars relate to the ranking of the points with respect to one of the objectives, which makes it possible to identify a specific design over several subplots. If the points in the set rank inversely with respect to the objectives – which occurs for example in a well developed, two-dimensional optimisation – one plot is sufficient to represent the ranking with regard to both objectives. With these plots, it is possible to identify genuine design choices that are uniformly distributed and clearly conflictive (e.g. wood humidity after drying), technological limits that inhibit better performance with respect to all objectives (gasification temperature) and less conflicting parameters that concentrate in a restricted domain inside the interval (methanation pressure).

1.8 Conclusions

Due to the separate modelling of the thermochemical conversions and the overall plant integration by an appropriate mathematical problem decomposition, the methodology presented here avoids to restrict the investigated process layouts to a very limited number of scenarios that are typically adopted by conventional simulation approaches. Instead, its coupling with cost estimation procedures that consider the specific process conditions and the use of multi-objective optimisation techniques allow for systematically generating a general set of optimal candidate flowsheets. The methodology is thus very suitable for the conceptual design of integrated plants for the production of fuels from biomass. It should be understood as a tool that efficiently eliminates solutions that are not worth investigating in detail, identifies the most promising process configurations and operating conditions, targets ideal performance and guides the efforts in R&D towards potentially optimal plants.

Chapter 2

Process model development for SNG production by conventional biomass gasification and methanation

This chapter demonstrates the approach for thermo-economic process modelling at the example of SNG production with conventional gasification and methane synthesis. Based on a review of candidate technology, a general process superstructure is introduced. Energy-flow and equipment rating models are then developed and reconciled. Like in its published version (Gassner and Maréchal, 2009c), the modelling approach is illustrated at some typical process configurations.

2.1 Introduction

Recent studies indicate that thermochemical SNG production by means of biomass gasification is technically feasible and energetic efficiencies ranging from 58% to 70% have been assessed (Mozaffarian and Zwart, 2003, Friedli and Biollaz, 2003, Duret et al., 2005, Heyne et al., 2008). Most of these works are investigations of the existing technology for the subsequent process steps provide some process scenarios. If modelled at all, the chemical transformations of the process streams have mostly been calculated assuming thermodynamic equilibrium (for instance by Schuster et al. (2001)), whereas it is known that this is not accurate in case of gasification. Furthermore, only limited energy integrations have been performed, cogeneration possibilities have not been studied in detail and the process economics have been analysed

Proximate analysis		Ultimate analysis	
Δh^{0a}	18.6 MJ kg_{dry}^{-1}	C	51.09 %wt
Δk^{0b}	20.9 MJ kg_{dry}^{-1}	H	5.75 %wt
Humidity (Φ)	50.0 %wt	O	42.97 %wt
Ash content	0.6 %wt	N	0.19 %wt

[a] Δh^0 is defined on dry basis and thus independent on humidity.

[b] Chemical exergy is calculated according to Szargut and Styrylska (1964).

Table 2.1—Proximate and ultimate analysis of woody biomass.

with capacity-based correlations disregarding the specific process conditions. Following the methodology outlined in the previous chapter, the purpose of this part is to develop detailed thermodynamic and economic models of the technological alternatives for thermochemical SNG production that are a suitable for a systematic thermo-economic process optimisation.

2.2 Process description

2.2.1 Process block flow

The conventional thermochemical conversion of lignocellulosic biomass to SNG according to Equation 1 consist in three major steps, namely gasification (endothermic), methane synthesis (exothermic) and gas separation. Considering a typical raw material such as moist wood chips with the properties of Table 2.1, a drying stage prior to gasification is necessary. Furthermore, the gas produced through gasification needs to be cleaned from impurities to prevent catalyst damage during methane synthesis. As biomass contains too much oxygen to be completely reformed into methane, CO_2 is by-produced and must be removed before or after methanation in order to meet the quality requirements of natural gas. In Switzerland, a Wobbe Index $W_{s,n}$ of 13.3-15.7 kWh Nm^{-3} and a methane content of at least 96%vol are required for unlimited injection into the national high grid that operates at around 50 bar (SVGW, 2008).

2.2.2 Technology for the process

2.2.2.1 Wood drying

The high moisture content of wood at the gasifier inlet severely decreases its performance (Schuster et al., 2001). This is mainly because high-temper-

ature heat from above the process pinch is consumed for water desorption and evaporation in the gasifier, which appears as an important exergy loss identified in Chapter 3. The presence of steam further tends to shift the equilibrium of the gas phase towards higher H_2 and CO_2 fractions and decreases the CH_4 content in the gas, which has also been observed experimentally by for example Gil et al. (1997). A drying stage before gasification is thus essential. Its level is subject to optimisation since steam is also used as gasifying agent.

Steam and air drying are reported to be the most common technologies applied in sawdust or wood chips treatment (Faaij et al., 1997, Berghel and Renström, 2002, Stahl et al., 2004). The main difference between these processes is that the use of steam allows for efficiently recovering the consumed heat by condensing the produced additional steam at its boiling temperature, while this energy is normally lost in air drying. However, operating temperatures are usually higher in steam dryers, and air drying might be advantageous if heat is available at lower temperatures (Berghel and Renström, 2002, Stahl et al., 2004). The performance of both processes depends on the integration with the rest of the process and its heat recovery possibilities. The optimal choice is thus determined by energy integration aspects, and models for both steam and air drying have been developed.

2.2.2.2 Gasification

Gasification of wood is an endothermal process where solid macromolecules are broken into mainly hydrogen, carbon monoxide, carbon dioxide, hydrocarbons, tars and ash. According to the requirement for a final gas product with high calorific value, adequate gasification technology should produce a nitrogen-free gas with high methane content. Air as gasifying agent is therefore not suitable and only steam and oxygen can be used for this purpose. Considering the equilibrium equations for the gas phase (Duret et al., 2005), high methane fractions are expected for gasification at low temperature and high pressure, having the further advantage that endothermicity of gasification decreases. Entrained flow gasification technology operating at high temperature is thus not adequate for the targeted application. The specified plant capacity further restricts the gasifier choice. Due to geometric considerations, fixed bed reactors are limited to about 10 MW_{th} (Mozaffarian and Zwart, 2003, Reimert, 1985) and thus hardly compatible with plants at industrial scale.

In this study, two types of gasifiers have been investigated, i.e. indirectly heated, steam blown FICFB-gasification (Hofbauer et al., 2002) operating at around 850°C and atmospheric pressure and directly heated, steam-oxygen

blown, pressurised CFB-gasification (Reimert and Schaub, 2009) operating at around 800℃.

2.2.2.3 Oxygen production for gasification

Oxygen required for gasification is conventionally produced by cryogenic air separation or pressure swing adsorption (PSA). According to Kirschner (2009), on-site production with these technologies gets competitive at capacities of about 1000 $Nm^3\ h^{-1}$ (0.35 kg s^{-1}) and 50 $Nm^3\ h^{-1}$ (0.02 kg s^{-1}), respectively. If smaller flow rates are required, oxygen can be purchased and delivered to the plant from an external supplier. Apart from these established technologies, high temperature air separation by ceramic ion transfer membranes may be promising in the future since they can benefit from a tight integration into the plant (van Stein et al., 2002). If temporarily cheap electricity is available, electrolysis is further an interesting option since the co-produced hydrogen can be injected into the methane synthesis, where it is bound to the abundant carbon from biomass and increases the SNG yield. Even if not operated as base load, this would allow for peak shaving electricity generated from intermittent sources (like wind power) and store it as green fuel in the gas grid (Gassner and Maréchal, 2008).

2.2.2.4 Thermal pretreatment before gasification

In addition to drying, the biomass feed can optionally be processed in a second, thermochemical torrefaction or pyrolysis pretreatment step. In the literature, these technologies are often discussed in the context of improving the solid fuel's thermal and mechanical properties like heating value or grindability (Prins et al., 2006, Svoboda et al., 2009), or the direct production of bio-oil that is further refined to liquid fuel (Zhang et al., 2005). However, thermochemical processes based on gasification can benefit in general from such a pretreatment (cf. Chapter 3 and Prins et al. (2006)). In addition to completely dry the feedstock for gasification, these technologies are characterised by an onsetting endothermal decomposition at low temperature, which decreases the energy demand at high temperature in the subsequent gasification. This directly results in a higher cold gas efficiency if the required energy for torrefaction or pyrolysis is provided from excess heat below the pinch. The product gas of a directly heated gasifier is thus less oxidised, and the fuel consumption of an indirectly heated gasifier is reduced.

As demonstrated on pilot scale by Henriksen et al. (2006), one alternative is to directly close-couple a pyrolysis screw with the gasification stage and thus feed both the gaseous and solid products into the gasifier. Another one

is to only feed the solid product to the gasifier and burn the by-produced low calorific gas. Although Prins et al. (2006) concluded that this option decreases the performance of directly heated fluidised bed gasification, it is promising in indirectly heated gasification since the volatiles can be used as fuel.

2.2.2.5 Gas cleaning

During gasification, tars are formed and traces of nitrogen, sulphur, chlorines and metals contained in the wood are reformed and transferred into the product gas. In order to prevent catalyst poisoning, the gas must be rid of these substances prior to methanation. Conventional cold gas cleaning includes a baghouse or sand filter to remove solid particles and partially tars, a scrubber for removal of ammonia, metals and residual tars as well as guard beds for scavenging hydrogen sulfide. Typical temperatures for these stages are 150-180℃ at the filter inlet, 40℃ at the scrubber outlet and around 350℃ in the guard beds (Rauch et al., 2004, Stucki, 2005). Alternatively, hot gas cleaning by particle removal with candle filters or electrostatic precipitators, thermal or catalytic cracking of the tars and high temperature adsorption of other contaminants could be applied. This would allow for a compact process design based on pressurised gasification and methanation without intermediate gas cooling and compression. A general overview on these advanced cleaning technologies for biomass gasification is given by for example Brown et al. (2009), extensive details on catalytic processes are reviewed by Torres et al. (2007) and recent technology developments are reported by Ondrey (2008), Leibold et al. (2008), Pfeifer and Hofbauer (2008).

2.2.2.6 Methane synthesis

Methane synthesis is a refining process to increase the calorific value of a gas containing high carbon monoxide and hydrogen fractions. The principal conversion is described by the methanation reaction (2.4) in Table 2.2. At typical operating temperatures of 300-400℃ and preferably under pressure, higher hydrocarbons are broken down to CO and H_2 and form additional CH_4, as shown for ethene (2.5). Depending on the initial gas composition, carbon dioxide is further reformed or produced through the water-gas shift equilibrium (2.6).

The stoichiometric coefficients of Equations (2.4)-(2.6) allow for determining the amount of hydrogen that is needed to completely reform CO, CO_2 and C_2H_4 into methane. It is thus convenient to define the stoichiometric number SN of the incoming gas stream in order to characterise the achievable

Interaction	Reaction	$\Delta\tilde{h}_r^0$	
Solid-gas			
Hydrogenating gasification	$C(s) + 2H_2 \rightleftharpoons CH_4$	-75 kJ mol^{-1}	(2.2)
Boudouard equilibrium	$C(s) + CO_2 \rightleftharpoons 2CO$	173 kJ mol^{-1}	(2.3)
Gas-gas			
Methane synthesis	$CO + 3H_2 \rightleftharpoons CH_4 + H_2O$	-206 kJ mol^{-1}	(2.4)
Ethene reforming	$C_2H_4 + 2H_2O \rightleftharpoons 2CO + 4H_2$	210 kJ mol^{-1}	(2.5)
Water-gas shift equilibrium	$CO + H_2O \rightleftharpoons CO_2 + H_2$	-41 kJ mol^{-1}	(2.6)

Table 2.2—Gasification and methanation reactions.

methane yield (Boll et al., 2009), which becomes for the considered reactions:

$$SN_{CH4} = \frac{\tilde{c}_{H2}}{3\tilde{c}_{CO} + 4\tilde{c}_{CO2} + 2\tilde{c}_{C2H4}} \tag{2.1}$$

To obtain a highly pure methane stream, this ratio must be close to unity. If it is below, the feed gas lacks hydrogen and the product gas will contain a non-negligible amount of carbon dioxide, which is the case for gases originating from wood gasification.

Methane synthesis of a $H_2/CO/CO_2$ mixture is highly exothermic and its reactor design is critical with regard to temperature control. Common installations use product gas recycle loops or multiple intercooled reactors with prior steam addition (Boll et al., 2009, Höhlein et al., 1984). Alternatively, an internally cooled fluidised bed reactor for isothermal once-through methanation has been developed and successfully operated at pilot scale for gas produced by coal gasification (Friedrichs, 1985). Ongoing research has further proven the suitability of the latter to gases produced by wood gasification (Stucki, 2005, Biollaz et al., 2009).

2.2.2.7 Carbon dioxide removal

Removal of CO_2 from natural gas is a standard operation in gas refining applications. The choice of the optimal technology depends on specific process conditions like the amount of gas treated, the partial pressure of carbon dioxide in the feed and the required purity of the produced gas (UOP LLC, last visited 04/2009). For gases containing high CO_2 fractions of more than 40% as it is the case in this application, physical absorption (Sweny and

Valentine, 1970), pressure swing adsorption (PSA) (Pilarczyk and Henning, 1987) and membrane processes (Bhide and Stern, 1993) can be identified as the most suitable options[1]. Optimal operating pressures of these processes depend considerably on the pressure of the raw gas. In general, physical absorption and membrane processes typically adapt to the gas grid pressure of 50 bar, while the maximum pressure in a PSA cycle is of 5-6 bar. Contrary to chemical absorption considered by Heyne et al. (2008), all this processes are almost neutral in thermal energy.

2.2.3 Process superstructure

From the preceding considerations, a general process superstructure is identified and depicted in Figure 2.1. The internal subsystem configuration like recycling and the integration of the utility system including hot and cold utilities as well as cogeneration possibilities by a steam Rankine cycle is not detailed. In addition to the mandatory operations outlined in Section 2.2.1, the superstructure includes the optional thermal pretreatment and also the possibility to adjust the stoichiometry of the producer gas prior to methanation. Disregarded by Mozaffarian and Zwart (2003), Friedli and Biollaz (2003), Duret et al. (2005) and Stucki (2005), this is a popular option for coal-derived producer gas that is recently also considered for biomass (Heyne et al., 2008, Haldor Topsøe A/S, 2009). The modelled, conceptual flowsheets for the process units are provided in Appendix A.

[1] Although chemical absorption with amines is a widely used technology for acid gas removal, it is not considered here since it is better suited for feeds at lower partial pressure of CO_2.

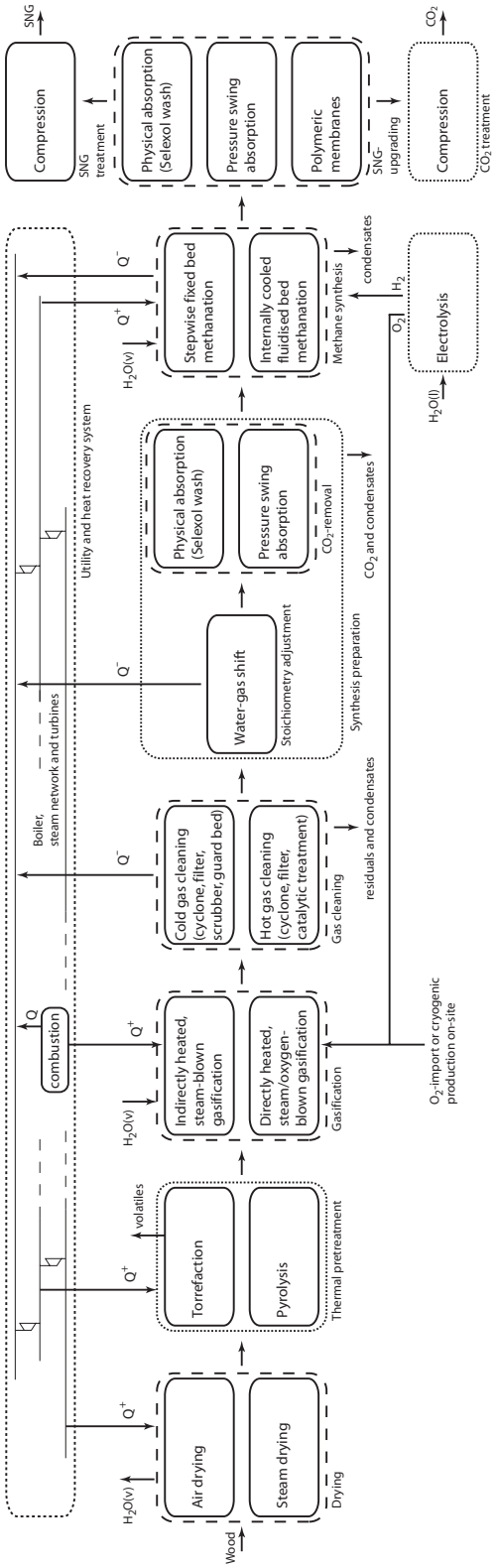

Figure 2.1—Process superstructure including main process streams without recycling loops. Dashed lines assemble investigated alternatives for different process sections and dotted lines indicate optional units.

2.3 Process modelling

2.3.1 Energy-flow models

As detailed in the applied methodology, the energy-flow models aim at defining the chemical and physical transformations occurring in the units of the superstructure. They determine the heat transfer requirements in terms of heat load and temperatures to be satisfied by the heat recovery and utility system, and further provide the necessary data for the equipment rating. In this regard, the process design method implies a trade-off between the details of the unit models and the degrees of freedom left to the process design. It requires models that are simple and robust enough to allow for evaluating different process configurations, and precise enough to accurately represent the performance of the process units. The proposed models realise this compromise without requiring detailed simulations of the heat and mass transfer dynamics and the chemical reaction kinetics. This approach is demonstrated in the following sections, and general assumptions and parameters are shown in Table 2.3.

2.3.1.1 Drying

Air drying processes are governed by the transfer of water in the solid and differences in vapour pressure at its surface and the surrounding air. The equilibrium vapour pressure at the solid's surface depends on temperature and is given by sorption isotherms. To quantify this equilibrium, an empiric equation has been fitted to data from Krischer (1978):

$$\begin{aligned}\Phi_{wood} = {} & 2.865 \cdot 10^{-2} \varphi_{air}^{1/2} \\ & + (2.307 \cdot 10^{-1} - 1.273 \cdot 10^{-3}(T - 273))\varphi_{air} \\ & - 2.519 \cdot 10^{-1} \varphi_{air}^{2} \\ & + (2.199 \cdot 10^{-1} + 8.630 \cdot 10^{-4}(T - 273))\varphi_{air}^{3}\end{aligned} \tag{2.7}$$

In this equation, Φ_{wood} terms the wood humidity in $\mathrm{kg}_{H2O}\ \mathrm{kg}_{tot}^{-1}$, φ_{air} the relative humidity of air in % and T the air temperature in K. Limited residence times in dryers prevent however that thermodynamic equilibrium is reached, and mass transfer needs to be modelled in order to estimate the outlet moisture content. In analogy to the energy transfer equation in heat exchanger calculations, the amount of transferred moisture can be written as:

$$\frac{\dot{m}_{H2O,vap}}{\dot{m}_{air}} = U_p \Delta p_{lm} \tag{2.8}$$

Section	Specification	Value
Air drying	Wood outlet temperature	$T_{air,out}$
	Dryer pressure drop	100 mbar
Steam drying	Wood outlet temperature	$T_{H2O,sat}$
	Dryer pressure drop	50 mbar
	Heat loss (w.r. to steam production)	18%
Gasification	Pressure drop in reactors	150 mbar
	Excess pressure of injected steam	12 bar
- indirectly heated	Heat loss (w.r. to heat transfer)	10%
	N_2-content in cold gas	0.5%vol
- directly heated	Heat loss (based on Δh^0_{wood})	1%
Gas cleaning	Filter inlet temperature	150°C
	Pressure drop	100 mbar
	Biodiesel consumption in scrubber	4.7 ml m^{-3}_{gas}
Methane synthesis	Reactor pressure drop	150 mbar
	Energy efficiency of electrolysis	85%
Physical absorption	CO_2-solubility in Selexol	0.18 mol $l^{-1}bar^{-1}$
	Relative solubility CO_2/CH_4	17.1
	Regeneration pressure	1 bar
	Pressure drop through column	neglected
PSA	Adsorption pressure	5.5 bar
	Purging pressure	0.2 bar
	CO_2 and CH_4 slip fraction	0.2%vol
Membranes	Material: cellulose acetate for CO_2, polysulfone for H_2 separation	
	CO_2 -permeability	9.0 (5.6) barrer
	Selectivities	
	- CO_2/CH_4, CO_2/CO, CO_2/N_2	21.1 (22.4)
	- H_2/CH_4	6.2 (56.0)
	Effective membrane thickness	1000 Å
All sections	Heat exchanger pressure drop	neglected
	Isentropic efficiency of turbomachinery	80%
Thermodynamic models	Ideal gas law, liquid phase in unsymmetric convention with solubilities from Sander (1999)	

Table 2.3—General assumptions and key parameters for the energy-flow models.

where U_p terms an overall mass transfer coefficient and Δp_{lm} the countercurrent log-mean difference of partial pressures, i.e.:

$$\Delta p_{lm} = \frac{\Delta p_1 - \Delta p_2}{\ln(\Delta p_1 / \Delta p_2)} \tag{2.9}$$

In this equation, Δp_1 terms the difference of partial pressures at the air outlet and Δp_2 at the air inlet. U_p has been fitted to data of a direct rotary drum dryer for wood (Faaij et al., 1997) and a value of $11.16 \cdot 10^{-3}$ bar^{-1} has been determined.

Contrary to air dryers, the gas phase in steam dryers is homogeneous and always above the moisture's boiling temperature. The drying process is thus controlled by heat transfer. As for air drying, an overall transfer coefficient U_T based on the amount of energy needed to evaporate the moisture has been introduced:

$$\frac{\Delta h_{vap} \dot{m}_{H2O,vap}}{\dot{m}_{steam}} = U_T \Delta T_{lm} \tag{2.10}$$

U_T has been fitted to data for a pilot-scale steam dryer (Berghel and Renström, 2002) and a value of 1117 J kg^{-1}K^{-1} has been determined.

The performance of both dryers is evaluated in terms of a thermal drying efficiency $\epsilon_{th,d}$ and the specific mechanical energy consumption ${e^+}_d$. The former is defined as the ratio between the energy used for moisture evaporation and the total thermal energy supplied to the dryer (Eq. 2.11) and the latter as the mechanical work consumed per unit mass of evaporated moisture (Eq. 2.12):

$$\epsilon_{th,d} = \frac{\Delta h_{vap} \dot{m}_{H2O,vap}}{{\dot{Q}^+}_d} \tag{2.11}$$

$${e^+}_d = \frac{{\dot{E}^+}_d}{\dot{m}_{H2O,vap}} \tag{2.12}$$

Figure 2.2 compares the computed performance of the drying processes as a function of the temperature of the heating fluid at the dryer inlet. In case of steam drying, $\epsilon_{th,d}$ is slightly decreasing with temperature and situated at around 60%. The performance of air drying is expected to increase with temperature and reaches efficiencies above 70% at high temperatures. For both systems, the specific mechanical energy consumption is decreasing with temperature and is in the order of 200 kJ $\text{kg}^{-1}_{H2O,vap}$.

2.3.1.2 Gasification

The thermochemical decomposition of solid feedstock is a complex process that is governed by chemical kinetics and heat- and mass-transfer dynamics.

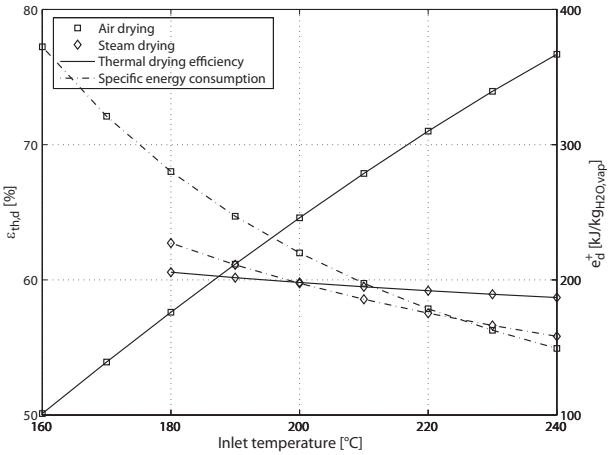

Figure 2.2—Thermal drying efficiency and specific mechanical energy consumption for steam and air drying.

As discussed by for example Pierucci and Ranzi (2008), accurate models to predict the performance of gasifiers require to handle the description of a large number of species and reactions, and thus to numerically solve a large system of differential equations. Such models, however, are not appropriate for process design purposes. In flowsheeting applications, the product composition and yield is therefore often simply fixed or computed through an equilibrium approach. Although sometimes assumed (e.g. Schuster et al. (2001)), thermodynamic equilibrium is yet not a valid assumption for fixed and fluid bed gasification that are typically operating below 1000°C, and various corrections have been proposed. Many authors, among recent studies Li et al. (2004), Pellegrini and de Oliveira Jr. (2007) and Pröll and Hofbauer (2008), therefore fix the carbon conversion and/or the fraction of methane and higher hydrocarbons, or correct the equilibrium constant with a multiplication factor (Jarungthammachote and Dutta, 2007, Huang and Ramaswamy, 2009). Introduced by Gumz (1950) and discussed for its application to biomass gasification by for instance Prins et al. (2007) and in more detail Bacon et al. (1982), Kersten (2002) and Brown (2007), a thermodynamically more significant approach is to correct the equilibrium temperature by introducing a temperature difference ΔT_{eq} to equilibrium, i.e.:

$$\hat{K}_p = K_p(T_g + \Delta T_{eq}) \tag{2.13}$$

where K_p is the theoretical equilibrium constant and $\hat{K}_p$ the apparent one corresponding tom the experimentally observed composition at the gasification

temperature T_g. They are computed with:

$$K_p(T) = \exp\left(\frac{\sum_j n_j \tilde{g}_j^0(T) - \sum_i n_i \tilde{g}_i^0(T)}{\tilde{R}T}\right) \tag{2.14}$$

$$\hat{K}_p = \frac{\prod_j p_j^{n_j}}{\prod_i p_i^{n_i}} \tag{2.15}$$

where n are the stoichiometric coefficients of the reactants i and products j, p their partial pressure, $\tilde{g}$ the Gibbs free energy and $\tilde{R}$ the ideal gas constant. Assuming that wood is converted into the gaseous components H_2, CO, CO_2, CH_4, C_2H_4, H_2O, N_2 and residual solid carbon C(s), four model equations are needed in addition to the atomic balances in order to determine the product yield and composition. Among the different possibilities, the hydrogenating gasification (2.2), Boudouard (2.3), steam ethene reforming (2.5) and water-gas shift (2.6) equilibria of Table 2.2 could be chosen as an independent set.

According to the heat of reaction of these equilibria, higher gasification temperatures would favour the formation of H_2 and CO, while CO_2, CH_4, C_2H_4 and – with the typical wood composition of Table 2.1 – C(s) are favoured at lower temperatures. This behaviour is generally confirmed for H_2, CH_4, C_2H_4 and C(s) by some extensive studies on fluidised bed gasification (Gil et al., 1997, Li et al., 2004, Rapagnà et al., 2000). In indirectly heated gasification, this trend has also been roughly confirmed for CO and CO_2 (Rapagnà et al., 2000), whereas directly heated gasification with oxygen generated more CO_2 and less CO with increasing temperature (Gil et al., 1997). These differences can partly be explained by the increasing oxygen content with temperature due to the direct heating, but must also be attributed to higher reaction rates that favour the conversion towards CO_2.

A large amount of different operating conditions has been investigated in the literature, yet surprisingly few information is available on the influence of pressure. To our knowledge, no systematic dataset has been published, and the few measurements at moderate and only slightly varying pressure do not allow for confirming the expectation from Eq. (2.15) that namely the CH_4-fraction increases with increasing pressure. Indeed, it can be argued that the pressure tends to accelerate the reaction rates, thus improves the conversion towards equilibrium and counterbalances the positive equilibrium effect of pressure on methane yield[2]. We therefore adopt a more conservative

[2]In a very recent experimental investigation, Valin et al. (2010) have observed that the CH_4 yield in a fluidised bed increases by 38% from 2 to 10 bar, which yet confirms the trend predicted by equilibrium considerations.

hypothesis concerning methane formation in the model, which is to consider not the partial pressure, but the molar fractions as activity of the species in the gas phase. A $\hat{K}_{\tilde{c}}$ is therefore defined, i.e.:

$$\hat{K}_{\tilde{c}} = \frac{\prod_j \tilde{c}_j^{n_j}}{\prod_i \tilde{c}_i^{n_i}} = \hat{K}_p \cdot p^{-(\sum_j n_j - \sum_i n_i)} \tag{2.16}$$

and used instead of $\hat{K}_p$. Equation (2.13) is therefore rewritten as:

$$\hat{K}_{\tilde{c}} = K_p(T_g + \Delta T_{eq}) \tag{2.17}$$

in which K_p is still evaluated with Equation (2.14).

By applying this approach to four independent equilibrium reactions of Table 2.2, it is feasible to determine the reaction extent and the product composition of gasification. However, it has been observed that the observed C_2H_4-fraction is excessively far from its equilibrium composition in terms of temperature, and that the amount of residual carbon is numerically sensitive and difficult to handle since it is only implicitly represented in the equations. In order to avoid a considerable deterioration of the robustness of the model, the corrected equilibrium reactions are therefore only used with the hydrogenating gasification (2.2) and the water-gas shift reaction (2.6). The amount of higher hydrocarbons represented by ethene is assumed to be proportional to the methane yield (2.18), and the carbon conversion efficiency is considered constant (2.19):

$$\tilde{c}_{C2H4} = k_{C2/C1}\tilde{c}_{CH4} \tag{2.18}$$

$$\dot{m}_{carbon,residual} = (1 - \varepsilon_{cc})\dot{m}_{carbon,biogenic} \tag{2.19}$$

By fitting the model parameters ($\Delta T_{eq,(2.2)}$, $\Delta T_{eq,(2.6)}$, $k_{C2/C1}$ and ε_{cc}) to data of existing plants, both correct product yields and energy balances around the nominal operating points are obtained. Table 2.4 shows the good agreement of the reconciliation reached for the considered gasifiers with the values of the model parameters of Table 2.5. It is thereby interesting to see that the distance to equilibrium of the reactions are identical in the two models although the principles of gasification are different. This means that the bed plays the same catalytical role in the gasifier and that the stability of methane in the gas phase preventing its decomposition is the same in the two gasifiers which are operating at similar temperatures.

Figure 2.3 depicts the dependence of the gasifier outlet composition in the interval of ±50°C of the nominal gasification temperature. For both gasifiers, lower operating temperatures are increasing the hydrocarbon and CO_2 content and decreasing the H_2 and CO fractions, resulting in an increased

Gasifier	indirectly heated[a]	directly heated[b]	directly heated (O_2)
T_g	850℃	800℃	800℃
C_2H_4	1.8 / 1.9	2.0 / 1.9	- / 4.5
CH_4	8.8 / 9.6	4.2 / 4.0	- / 9.5
H_2	37.3 / 38.5	14.8 / 14.7	- / 25.8
CO	29.4 / 27.4	15.4 / 16.0	- / 32.3
CO_2	16.2 / 15.8	15.0 / 14.7	- / 24.0
N_2	-[c] / 2.9	39.6 / 40.3	- / 0.1
H_2O	3.6 / 3.9	- / 8.4	- / 3.8
Δh^0 [MJ Nm^{-3}]	12.0 / 12.2	6.2 / 6.2	- / 12.9
SN [-]	0.24 / 0.26	0.13 / 0.13	- / 0.13

[a] Data from Rauch (written around 2004).
[b] Data from Reimert and Schaub (2009).
[c] Although no nitrogen is introduced by the gasification agent, some N_2 is used for inertisation of the raw material, which prohibits to attain the criterion on the Wobbe Index at the process outlet. In the remainder of this work, a cut-down to 0.5%vol of the dry gas by inertisation with CO_2 is assumed feasible.

Table 2.4—Reconciliation of the producer gas compositions at nominal T_g and p_g = 1 bar (Data / Calculation [%vol]).

Gasifier	indirectly heated	directly heated
$\Delta T_{eq,(2.2)}$	-280℃	-280℃
$\Delta T_{eq,(2.6)}$	-112℃	-112℃
$k_{C2/C1}$	0.205	0.476
ε_{cc}	90.3%	93.0%

Table 2.5—Reconciled gasification model parameters.

volumetric calorific value of the gas. Comparing both gasifiers, it can be seen that the CO and CO_2 fractions and thus the degree of oxidation is considerably higher in directly heated gasification. Accordingly, its product gas has a lower stoichiometric number than in indirectly heated gasification, which will lead to a lower CH_4 concentration after methanation. Figure 2.4 shows the cold gas efficiency ϵ_{cg}, defined as the ratio of the chemical energy contained in the cold product gas and the raw material (2.20), for variations of temperature and inlet wood humidity around the normal operating point.

$$\epsilon_{cg} = \frac{\Delta h^0_{gas} \dot{m}^-_{gas}}{\Delta h^0_{wood} \dot{m}^+_{wood}} \tag{2.20}$$

According to the figure, the conversion of chemical energy is more efficient in directly heated gasification and situated around 80%, while its value for

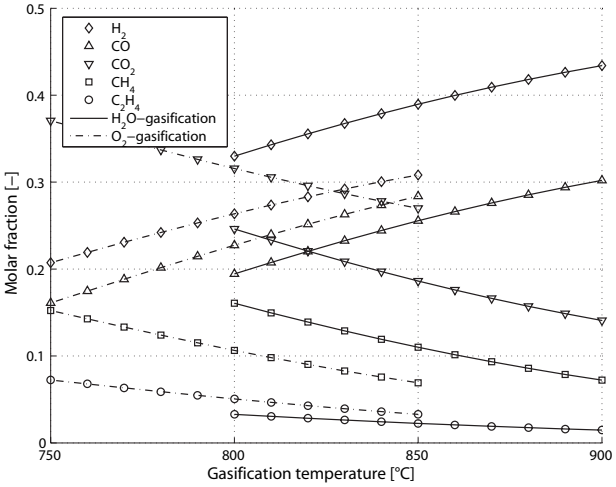

Figure 2.3—Molar compositions of the dry gas from gasification.

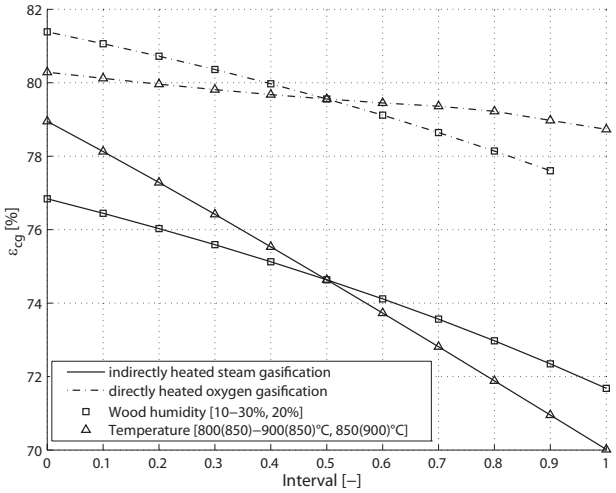

Figure 2.4—Cold gas efficiencies in parameter domain.

indirectly heated gasification is in the range of 70-80%. As discussed in Section 2.2.2.1, increasing wood humidity is markedly deteriorating the performance of both gasifiers.

2.3.1.3 Oxygen production for gasification

Since no major advantages from the integration of the SNG production with a cryogenic or adsorptive air separation plant is expected, oxygen has been

considered as a utility and the cost figures from Kirschner (2009) are used directly. In order to equitably compare configurations with and without oxygen consumption also in terms of efficiency, an electricity consumption of 1080 kJ kg_{O2}^{-1} for off-site oxygen is further included in all balances (Hamelinck et al., 2003, Annex A). If by-produced oxygen from electrolysis is used, an energy efficiency of 85% based on the lower heating value of hydrogen and the power input is assumed, and the excess heat is considered available at 120°C. A detailed analysis of this particular process configuration is reported in earlier work (Gassner and Maréchal, 2008).

2.3.1.4 Thermal pretreatment before gasification

Compared to gasification, torrefaction and pyrolysis are processes where the solid decomposition is less advanced and multiple condensable and non-condensable products are formed. An equilibrium approach to predict accurate product yields and composition is not adequate, and the processes are represented by simple conversion ratios for fixed operating conditions. From experimental torrefaction data at 260°C (Bourgois and Guyonnet, 1988), a dry solid yield of 87% has been derived, whereas the carbon mass fraction in the product is increased by 5.7% compared to its initial hydrocarbon composition, and the hydrogen and oxygen fractions are decreased by 8.4% and 5.8%, respectively. The moisture in the vapour phase is accompanied by acetic acid, methane, carbon mono- and dioxide, whereas 50.1% and 17.5% of the biogenic hydrogen and oxygen is bound in methane and carbon monoxide, respectively. For screw pyrolysis (Henriksen et al., 2006), it is assumed that the volatile fraction of the solid is completely transferred into the vapour phase, and a simplified model for calculating the heat requirement for the decomposition is used (cf. Chapter 3).

2.3.1.5 Gas cleaning

Since the conversion of impurities and tars are negligible for energy concerns, they have not been included in the models. However, the thermodynamic transformations that the cleaning operations imply obviously need to be considered. If cold cleaning is applied, the producer gas from gasification is cooled to 150°C before entering the filter. Downstream of this unit, no thermal energy can be recovered and the gas is cooled to atmospheric temperature in the scrubber, where it also reaches water saturation. In the model, it has been assumed that this heat is lost, although part of it would be available as moderately heated water leaving the scrubber. If hot cleaning is applied, the sensible heat of the gas is supposed to be entirely recoverable.

2.3.1.6 Methane synthesis

Using a similar modelling approach like in gasification, the outlet composition of the methane synthesis reactor has been computed with equilibrium equations. However, methanation is a catalytic process and the equilibrium condition is a reasonable assumption if the amount of catalytic material is sufficient. Experimental data from a laboratory reactor confirm this assumption (Duret et al., 2005). No model constants have therefore been introduced and the methanation (2.4), the steam ethene reforming (2.5) and the water--gas shift reaction (2.6) have been supposed to be in chemical equilibrium. In order to avoid carbon deposition, steam must be added to the producer gas prior to the reactor which disfavours the formation of methane. The minimum required amount is estimated based on the equilibrium data presented by Mozaffarian and Zwart (2003).

2.3.1.7 Carbon dioxide removal

All considered carbon dioxide removal processes are based on local diffusion processes and are heavily dependent on diffusion and absorption kinetics. A detailed model requires dynamic simulation, which is too complicated and not appropriate for flowsheet calculations in process design studies. For this reason, the CO_2-removal models are developed on the basis of overall performance and characteristic operation parameters.

For physical absorption, the solubilities of carbon dioxide and methane in the classic solvent Selexol reported by Sweny and Valentine (1970) are used to calculate the multicomponent separation in an absorption tower. Applying the Kremser method (Diab and Maddox, 1982), its performance is determined with respect to the number of theoretical trays and the relative solvent flow rate. While the residual humidity in the saturated gas is completely removed by the solvent, the solubility of the other non-condensable species (H_2, CO, N_2) is very low and therefore neglected in the modelling. In order to achieve a high product recovery, a typical process layout with a flash drum at moderate pressure for recycling the dissolved CH_4 is considered (Newman, 1985).

Pressure swing adsorption is a discontinuous process that removes the carbon dioxide by its adsorption under pressure following regeneration of the adsorbent at subatmospheric pressure. The purity and the amount of methane recovered in the outlet stream is essentially determined by the durations of the adsorption, recycling and purging periods. As shown on Figure 2.5, two parameters, i.e. t_{r1} and t_{r2}, are introduced and fix the relative durations of these periods. The time-averaged flow of species i that leaves the adsorber system ($\dot{m}_{i,out}$) or is recycled to its inlet ($\dot{m}_{i,rec}$) is then determined by a

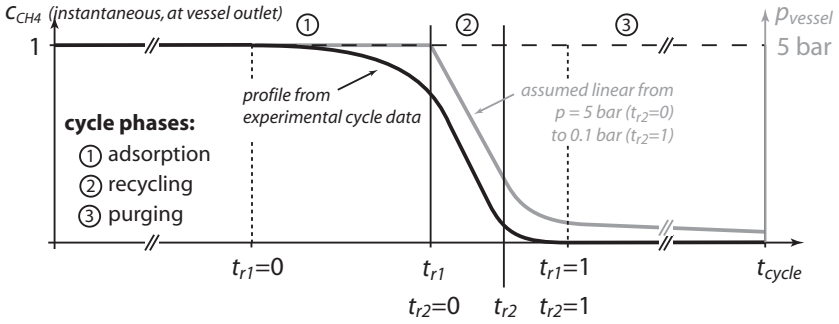

i	a_0	a_1	a_2	a_3	a_4
CO_2	0.0058	0.0305	-0.2957	1.2415	-0.6652
CH_4 and others	0.8148	0.3758	0.2021	-0.8486	0.4547

Figure 2.5—Illustration of the phenomenological model for PSA and coefficients for the regression of $f(i,t_r) = a_0 + a_1 t_r + a_2 t_r^2 + a_3 t_r^3 + a_4 t_r^4$ used in Equations (2.21) and (2.22).

relation of the form:

$$\dot{m}_{i,out} = f(i,t_{r1})\dot{m}_{i,in} \tag{2.21}$$

$$\dot{m}_{i,rec} = f(i,t'_{r2})\dot{m}_{i,in} - \dot{m}_{i,out} \tag{2.22}$$

$$\text{with } t'_{r2} = (1-t_{r1})t_{r2} + t_{r1}$$

where $f(i,t_r)$ represents the relative amount of species i that has left an adsorption vessel at t_r during one cycle. A numeric integration of pilot plant data reported by Pilarczyk and Henning (1987) for biogas separation with a carbon molecular sieve adsorbent has allowed for regressing $f(i,t_r)$ to a polynomial of 4^{th} degree whose coefficients are shown on Figure 2.5.

For SNG upgrade with membranes, a general design model for hollow-fibre modules proposed by Pettersen and Lien (1994) has been implemented in a superstructure of possible membrane arrangements. At the example of this separation technology, the integration of the crude SNG separation with the reactive process steps is discussed and optimised later in Chapter 4. As also for the PSA process, it is assumed that the saturated feed is first dried by temperature swing adsorption (TSA) over aluminium-oxide, for which 11 MJ kg^{-1}_{H2O} at 160-190°C are required (Bart and von Gemmingen, 2009).

Exploring these models, it has been determined that the Wobbe Index of 13.3 kWh Nm^{-3} can be met with all considered technologies. For upgrading the crude gas from atmospheric pressure to grid quality and pressure by PSA or physical absorption, a specific mechanical power consumption in the order of 600-800 kJ $kg^{-1}_{crudeSNG}$ is required and leads to an approximate composition of 84%vol CH_4, 12% H_2, 0.2% CO and 3.5% of inerts. With these two technologies, the residual hydrogen from the equilibrium synthesis is however not

separated from methane, which limits its purity to around 86%vol CH_4. For gas upgrading to a methane content of 96%vol, a final membrane stage for hydrogen removal can be used, from which the H_2-rich permeate is recycled to the methane synthesis. According to the information provided by Abetz et al. (2006), matrimid or polysulfone membranes are a reasonable choice for this purpose. Alternatively, an upgrading system entirely based on cellulose acetate membranes can be used, for which a specific mechanical energy consumption of 750-1100 kJ $kg^{-1}_{crudeSNG}$ depending on the targeted SNG-recovery in the separation stage is assessed in Chapter 4. In case of indirectly heated gasification, the depleted stream from the gas upgrading is thereby efficiently used as fuel, which allows for limiting the size of the separation system due to a better process integration.

2.3.2 Energy integration model

As discussed in Chapter 1, the heat requirements of all process streams determined in the energy-flow models are corrected by minimum approach temperature contributions of 25, 8, 4 and 2K for reactive, gaseous, liquid and phase changing streams, respectively, and implemented in the energy integration model to compute the optimal thermal integration by MILP. In order to supply the energy requirement of FICFB gasification, the combustion of the process wastes, i.e. ungasified char, torrefaction gas, spent biodiesel in scrubbing, recovered gas residues from flashing the wet methanation product and depleted streams from carbon dioxide removal is typically not sufficient. Intermediate products are thus required to balance the demand, for which biomass or gas upstream methanation are most suitable since the exothermal synthesis reactions convert part of the chemical energy to heat below the process pinch. While cold, clean producer gas is used for this purpose by Hofbauer et al. (2002), hot raw producer gas and dried biomass can be identified as advantageous alternatives that are discussed in detail in Chapter 3.

Available at useful temperature, the excess heat below the pinch is recovered in a steam Rankine cycle for power generation, whose superstructure (i.e. the production and usage levels) is determined on the master optimisation level. In this work, a cycle layout with one production and several utilisation levels with back pressure and condensing turbine stage efficiencies of 80% and 70%, respectively, is considered. In the latter, partial condensation to a minimum vapour fraction of 85% is allowed. Depending on the possibility of selling heat in a district heating network, the cycle may be designed for power- or heat-operation. Other utility techniques, like the use of heat pumps or combustion boosting through oxygen injection might be

used if large quantities of heat are exchanged around the pinch point or if the pinch is situated at a very high temperature level.

2.3.3 Economic evaluation

2.3.3.1 Approach

In the applied design methodology, we consider the thermodynamic conditions to be reached in the process units as decision variables. Once these conditions are determined in the flowsheet model, we compute the process performances and estimate its investment cost by rating the major process equipment to reach the thermodynamic design target. This method differs from the conventional thermo-economic approaches where either the equipment size is considered as a decision variable or the total investment cost is estimated on the components' nominal capacity, as it is done by for example Tijmensen et al. (2002).

Considering that the equipment's cost is essentially dependent on its size and construction materials, it is influenced by specific process conditions like temperature, pressure and volume flows. Hence, the information available from flowsheet calculations allow for relating the process investment cost with its thermodynamic operating conditions and performances. This is of great interest with regard to a future thermo-economic optimisation of the installation. Following the method outlined by Turton et al. (1998), the total grass roots costs C_{GR} that designate the total investment cost for a new production site without land are related to the equipment's purchase cost by Eq. (1.25), in which numeric values of 0.18 for c_1 and 0.35 for c_2 are used to provide an investment cost estimation for mature technology and established process engineering.

Unless stated otherwise, the bare module costs of the equipment is determined from correlations given by Ulrich and Vasudevan (2004) and Turton et al. (1998). For process vessels, maximum diameters of 4m (vertical) and 3m (horizontal) are assumed, and multiple units operated in parallel are considered if necessary. A complete list of parameters for the investment analysis and the considered prices for raw materials and products are provided in Table 2.6.

2.3.3.2 Equipment rating

Wood Drying The sizing of the direct rotary air dryer is based on an average velocity of wood of $u_{wood} = 0.03$ m s^{-1} occupying 12% of the dryer's cross sectional area (Ulrich and Vasudevan, 2004). Accordingly, the diameter

Parameter		Value
Marshall and Swift index (2006)		1302
Currency exchange rates		1 US$ €$^{-1}$, 1.5 CHF €$^{-1}$
Interest rate	i_r	6%
Discount period	n	15 years
Plant availability		90%
Operators[a]		4[b] per shift
Operator salary		60'000€ per year
Maintenance costs		5% of C_{GR} per year
Wood price (Φ_{wood}=50%)	C_{wood}	33 € MWh^{-1}
Biodiesel price	C_{RME}	105 € MWh^{-1}
Electricity price (green)	C_{el}	180 € MWh^{-1}
Oxygen price	C_{O2}	(Kirschner, 2009)
Industrial heat price (110/70°C)	C_q	80 € MWh^{-1}
SNG price	C_{SNG}	120 € MWh^{-1}

[a] Full time operation requires three shifts per day. With a working time of five days per week and 48 weeks per year, one operator per shift corresponds to 4.56 employees.

[b] For a plant size of 20 $MW_{th,wood}$. For other production scales, an exponent of 0.7 with respect to plant capacity is used.

Table 2.6—Assumptions for process economics.

of the drum is given by:

$$d = 2\left(\frac{\dot{m}_{wood}}{0.12\Pi\rho_{wood}u_{wood}}\right)^{1/2} \tag{2.23}$$

where $\dot{m}_{wood}$ and ρ_{wood} are the mass flow and density of wood respectively. The dryer's length is determined considering an overall heat transfer coefficient in W m^{-3}K^{-1} based on the dryers volume as given by Ulrich and Vasudevan (2004):

$$U = 240G^{0.67}/d \tag{2.24}$$

where G is the average gas mass flux that is typically in the range of 0.5 to 5 kg s^{-1}m^{-2}. The dryer's length follows from:

$$l = \frac{\Delta h_{vap}\dot{m}_{H2O,vap}}{UA\Delta T_{lm}} \tag{2.25}$$

For steam drying fixed bed design is a convenient choice and detailed information about its performance and size is provided by Berghel and Renström

(2002). Assuming the mean velocity of superheated steam being constant during scale-up, the dryer's diameter is calculated with:

$$d = 2\left(\frac{\dot{V}_{steam}}{\Pi u_{mean}}\right)^{1/2} \tag{2.26}$$

where $\dot{V}_{steam}$ is the volume flow of steam and u_{mean} its mean velocity. Using the developed energy-flow model for steam drying and data from Berghel and Renström (2002), a value of 1.4 m s^{-1} has been assessed for the latter. The height of the steam dryer is determined in the same way as for air drying and Equations (2.24) and (2.25) are used to calculate the overall heat transfer coefficient and the height of the bed. Thereby, the correlation (Eq. 2.24) has been reconciled with the data and very good accordance is observed. At an average gas mass flux of 0.645 kg $s^{-1}m^{-2}$, the observed value for U amounts to 200 W $m^{-3}K^{-1}$, while its calculated value is of 199 W $m^{-3}K^{-1}$. Finally, taking the additional height of the dryer's freeboard above the bed into account and preserving the geometry of the considered steam dryer, the overall height of the vessel has been obtained by multiplying the bed height with a factor of 1.27 (Berghel and Renström, 2002). For both the direct rotary air dryer and the fixed bed steam dryer, costing data from Ulrich and Vasudevan (2004) have been used.

Gasification and methanation The gasification and methanation reactors are of fluidised bed type and, as it is the case for the steam dryer, their mean gas velocities will typically remain constant during scale-up. The diameter of the reactors are thus calculated according to Equation (2.26), replacing $\dot{V}_{steam}$ by the total gas volume flow $\dot{V}_{gas}$. To calculate the reactor heights, an exponential law of the form:

$$h = h_0 \dot{V}_{gas}^{b} \tag{2.27}$$

has been fitted to data from existing plants (Friedrichs, 1985, Rauch, last visited 04/2009). The correlated data for Equations (2.26) and (2.27) are given in Table 2.7.

In order to take the costs associated with the gasification reactor internals and their special construction into account, the costs of the vessels have been multiplied by a factor of 4.4. This value has been derived from the total grass roots costs of the existing FICFB pilot plant, which is of 8 M€ for an installation with a nominal capacity of 8 MW_{th} (Rauch and Hofbauer, 2003). In case of a pressurised gasification, the investment for the biomass feeding system may become substantial and is thus added explicitly. The use of lock

Reactor type	u_{mean} [m s^{-1}]	h_0 [m (m^{3}s^{-1})$^{-b}$]
Gasification	0.645	4.07
FICFB-combustion	5.250	8.47
Methanation	0.093	18.0

Table 2.7—Sizing parameters for process reactors. $b = 0.188$ is reconciled for the gasification vessel and used for all reactors. Data calculated from (Friedrichs, 1985, Rauch, last visited 04/2009).

hoppers is the most common practice (Wilén and Rautalin, 1993), and a manufacturer's cost estimate reported by Swanson et al. (2002, Appendix G) is used to determine a standard scaling law for a double-train system:

$$C_{BM,lock\ hoppers} = 4.3 \cdot 10^5 \cdot \dot{m}_{dry\ wood}^{0.7} \tag{2.28}$$

with $C_{BM,lock\ hoppers}$ in US$ (2002).

For oxygen supply to directly heated gasification, cost data from Kirschner (2009) are used, who reports a range of 0.03-0.70 US$ kg^{-1} (1999) depending on the quantity required. In case production with electrolysis is considered, the bare module cost of the unit is assumed according to the US/DOE target (2010) of 300 $ kW$_{el}^{-1}$ (Newborough, 2004).

Thermal pretreatment before gasification According to a commercial design (Wyssmont Inc., last visited 04/2009), the torrefaction reactor is dimensioned as a vertical tower with a height to diameter ratio of 2, assuming that 20% of the volume are occupied by the solid with a residence time of 15 min. The purchase cost of the unit has been regressed on the reported $5.65 \cdot 10^5$ and $6.70 \cdot 10^5$ US$ for units with a volume of 115 and 145 m^3, respectively.

For pyrolysis, the design of Henriksen et al. (2006) has been investigated and procedures for a screw conveyor or rotary calcinator are used (Ulrich and Vasudevan, 2004), where the unit size is determined by the required heat transfer through the wall to the solid. With a heat transfer coefficient of 30-100 kW m^{-2}K^{-1}, scale-up of the pilot plant is however expected to be costly, since either a large temperature difference or heat transfer area is needed.

Gas cleaning While the cost of a cold gas cleaning system including a cyclone, bag filter, scrubber and guard beds can be estimated from literature data (Ulrich and Vasudevan, 2004), hot gas cleaning technology is still under development and no cost data is currently available. It is therefore assumed

that mature hot gas cleaning will roughly follow the same correlation than cold technology, and its cost is evaluated with the same relations using the gas volume flow as parameter. At an assumed temperature of 500°C, the gas volume flow to be treated is nearly doubled compared to cold processing, which leads to a multiplication of the investment in the order of 1.5.

Carbon dioxide removal The dimensions of the packed tower in the physical absorption process have been calculated according to the method of Ulrich and Vasudevan (2004). From the given data, a stage efficiency of 15% has been determined, and the tower diameter has been dimensioned considering the entrainment limit. The corresponding stripper has not been modelled in detail. As a rule of thumb, its diameter and height have been assumed to be equal to the ones of the absorption tower (Sweny and Valentine, 1970).

The size of the four pressure swing adsorption vessels necessary for continuous operation has been estimated assuming that the required adsorber volume is proportional to the amount of carbon dioxide that needs to be removed from the gas. A typical plant treating 1000 Nm^3 raw gas per hour with a CO_2 content of 40%vol is described by Riquarts and Leitgeb (1985). The diameter and height of the vessels are reported to be 1.4 and 6 meters, resulting in an specific adsorber volume of 83.13 m^3 per $Nm^3_{CO2}s^{-1}$. The shape of the vessels has been assumed constant and a height to diameter ratio of 4.3 is used.

The purchase cost of the polymeric hollow fibre membranes is estimated by updating the data reported by Bhide and Stern (1993), who considered an initial cost for the permeator modules of 108 US$ m^{-2} and a membrane element cost of 54 US$ m^{-2} that need to be replaced every three years. As detailed in Chapter 4, the required membrane area for the separation is directly computed by the design model.

In case of separation by PSA or membranes, the cost for the required TSA unit used for gas drying is determined by assuming a two-column layout with a cycle time of 12 hours and a maximum adsorbent loading of 0.12 $kg_{H2O}kg^{-1}_{adsorbent}$ (Ducreux et al., 2006). The cost of the adsorbent and its density have been assumed to 9 US$ kg^{-1} and 800 kg m^{-3}, respectively (Ulrich and Vasudevan, 2004).

If CO_2-removal is done prior to methanation, the cost estimation of the necessary shift reactor to adjust the stoichiometry is based on the preliminary design and data from Maréchal et al. (2005b).

Heat exchangers and turbomachinery The total cost of the heat recovery system including the heat exchangers of the process and the utility

system has been computed from the hot and cold composite curves assuming a reference heat transfer coefficient α_{ref} of 580 W $m^{-2}K^{-1}$ at an approach temperature ΔT_{ref} of 10K, from which the individual coefficients are determined by Equation 1.6 with 0.8 for b_{HE}. The total heat exchange area is distributed over the minimum number of heat exchangers and costing data for fixed tube sheet units from Ulrich and Vasudevan (2004) have been used. For turbomachinery, data for mainly centrifugal units are used.

2.4 Performance of exemplary technological options

The outlined thermo-economic model is developed for a systematic process optimisation that will be presented in Chapters 4 and 6. Here, the modelling approach is thus only illustrated at the example of a few technology scenarios shown in Table 2.8, which should not be considered as a portfolio of optimal process options. Indirectly heated gasification with air drying and PSA for removing CO_2 after methanation is defined as a base scenario (FICFB, base), to which different alternatives are compared. In the scenario (torr), a torrefaction unit is added to the base case, (pM) investigates the influence of a moderately pressurised methanation, and (pM, SA) compares the latter case to one where the stoichiometric number is adjusted to 1 by water-gas shift conversion and CO_2-removal prior to methanation. Indirectly heated gasification is then compared to pressurised steam/oxygen-blown gasification and methanation at the same pressure (CFB, pGM), for which the potential improvement by introducing hot gas cleaning is assessed (pGM, hot). In all cases, excess heat is recovered in a steam Rankine cycle, whose production and utilisation levels have been adjusted to reasonably fit the steam demand for gasification and methanation, and providing heat for mainly drying and torrefaction. Heat extraction for district heating is not considered, and a condensation level suitable for the cold utility is used.

	Description	FICFB				CFB	
	(case)	(base)	(torr)	(pM)	(pM, SA)	(pGM)	(pGM, hot)
Drying	Technology	Air drying					
	Conditions	drying to Φ_{wood} = 20% with $T_{air,in}$ = 200°C					
Torrefaction	Temperature	-	260°C	-	-	-	
Gasification	Technology	indirectly heated FICFB				directly heated CFB	
	Operating conditions	1 bar, 850°C				15 bar,800°C	
	Gasification agent	H_2O				H_2O/O_2	
	Steam preparation	steam to dry biomass ratio = 0.5, preheated to 300°C					
Gas processing	Gas cleaning	cold				cold	hot
	Shift temperature (min.)	-	-	-	200°C	-	
	CO_2-removal	-	-	-	PSA	-	
	Amount CO_2 removed	-	-	-	95%	-	
Methane synthesis	Pressure	1 bar	1 bar	5.5 bar	5 bar	15 bar	
	Temperature	320°C				320°C	
SNG-upgrade	Drying	flash drum & TSA				flash drum	
	CO_2-removal	PSA			-	phys. absorption	
	Pressure	5.5 bar			-	30 bar	
	CH_4-recovery	98%				98%	
	H_2-separation	polysulfone membrane at p_{grid}, permeate recycled to methanation					
	Grid specifications	50 bar, 25°C, 96% CH_4					
Steam network	Production level	60 bar (T_{sat} = 276°C), superheating to 550°C					
	Utilisation levels	14.9 bar (198°C), 4.76 bar (150°C), 1.98 bar (120°C)					
	Condensation level	0.02 bar (20°C)					

Table 2.8—Process technology and conditions of investigated cases.

2.4.1 Energetic performance

Table 2.9 shows the overall energy balance and conversion efficiencies of the scenarios defined in Table 2.8 for a capacity of 20MW$_{thwood}$. One integrated composite curves for each gasification technology is given in Figure 2.6, and Table 2.10 shows the stream compositions and flows through the systems. Although the energy balances of the different cases seem rather close, some general trends depending on the technology choice can be observed. Due to the higher cold gas efficiency for directly heated gasification assessed in Figure 2.4, the resulting SNG yield is roughly 10% higher than in case of indirectly heated gasification. As shown on the composite curve, the indirect heat supply creates a process pinch point at the gasification temperature, and satisfying this heat demand at high temperature requires to withdraw about 19% of the raw gas production of the gasifier. For this reason, more excess heat is also available below the pinch and leads to a higher co-production of electricity than in directly heated gasification. An alternative to using the excess heat in a Rankine cycle is thereby to recover it in the process through thermal pretreatment. Acting in principle as a chemical heat pump, the endothermal decomposition starts with excess heat from below the pinch, and less heat must be supplied above the process pinch point. In case of torrefaction, it is necessary to withdraw only 5% of the raw gas production for satisfying the process energy requirement, which increases the overall SNG-yield from the indirectly heated gasifier by 7%.

While the methanation pressure and prior stoichiometry adjustment influences the energetic performance to a lesser extent, hot gas cleaning is expected to considerable increase the process performance by cogenerating more electricity. Heat losses due to cooling, washing and reheating the gas are avoided, and less steam needs to be prepared for the methanation. More heat can thus be recovered in the Rankine cycle, whose gross production increase by 0.5 MW$_{el}$ and results in an positive electricity balance of the overall system also in case of directly heated gasification with oxygen.

2.4.2 Economic performance

With a common share of 68% of the total investment of 32.6 M€ illustrated in Figure 2.7, the gasification and methanation sections are dominating the capital costs of the (base)-scenario for FICFB-gasification. As shown in Table 2.11, atmospheric pressure leads to big reactors due to relatively important volumetric flows, and a much more economic plant design can be obtained by pressurising the reactors. Already at a moderate methanation pressure of 5.5 bar, the investment cost are predicted to decrease by 30% to

		FICFB				CFB	
		(base)	(torr)	(pM)	(pM, SA)	(pGM)	(pGM, hot)
Consumption							
Wood	kW	20'000	20'000	20'000	20'000	20'000	20'000
Biodiesel	kW	365	316	365	365	22	-
Electricity	kW	-	63	-	-	46[a]	-
Production							
SNG	kW	13'443	14'318	13'446	13'495	14'765	14'769
Electricity	kW	609	-	521	526	-	315[a]
Efficiencies							
ϵ	%	69.0	70.3	68.6	68.8	73.6	75.4
ϵ_{chem}	%	71.3	70.1	70.5	70.8	73.5	76.6
η	%	63.5	64.7	63.1	63.3	67.8	69.4

[a] A consumption of 311 kW (1080 kJ kg_{O2}^{-1}) for off-site oxygen production is included.

Table 2.9—Useful energy balance and efficiencies of the overall system for the scenarios defined in Table 2.8.

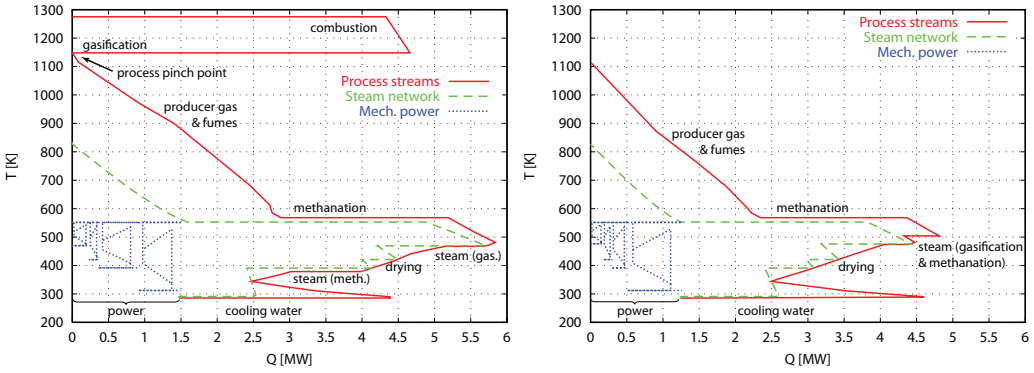

Figure 2.6—Integrated composite curves for FICFB (base, on the left) and CFB (pGM,hot) gasification as defined in Table 2.8 for an input of 20 $MW_{th,wood}$.

23.4 M€. If directly heated gasification with oxygen is used and the whole system is initially pressurised to 15 bar, a further reduction to 17.9 M€ is possible, whereas the pressurised feed train accounts for approximately 10% of the gasifier cost. If a scale-up to larger plant capacities is considered, operation at atmospheric pressure requires several units in parallel, and a pressurised system seems unavoidable.

Based on the assumptions of Table 2.6, the share of the depreciated investment and its related maintenance cost is relatively high. At base case conditions, these expenses amount to 47% of the total production cost. If methanation is moderately pressurised, the expected reduction of the invest-

		Gasification		Methanation			SNG-upgrade		
		FICFB	CFB	FICFB[a]		CFB	FICFB[a]		CFB
C_2H_4	%vol	2.3	5.5	-	-	-	-	(-)	-
CH_4	%vol	11.3	11.6	48.3	(86.1)	40.8	96.0	(96.0)	96.0
H_2	%vol	40.2	28.9	6.4	(11.4)	1.4	1.6	(1.9)	1.3
CO	%vol	26.5	17.4	0.1	(0.0)	0.0	0.3	(0.0)	0.1
CO_2	%vol	19.2	36.5	44.4	(1.1)	57.6	0.5	(0.5)	2.2
N_2	%vol	0.5	0.1	0.8	(1.4)	0.2	1.6	(1.6)	0.4
Δh^0	MW kg^{-1}	15.2	11.4	14.5	(47.4)	10.3	48.2	(47.6)	46.8
$W_{s,n}$	kWh Nm^{-3}	4.3	4.3	5.6	(13.6)	4.3	14.1	(14.1)	13.9
Load	MW_{th}	19.6	17.0	15.1	(14.7)	15.6	13.4	(13.5)	14.8

[a] Values in parenthesis are for CO_2-removal before methanation in case (pM, SA).

Table 2.10—Dry gas composition, calorific value and power balance at process section outlets.

ment allows for decreasing the share of these expenses to 38% of the total, and leads to a cost reduction by 13% in absolute terms. In the best performing case of directly heated gasification with hot gas cleaning, the share of investment and maintenance is of only 32% at 20 $MW_{th,wood}$, and can further be reduced to 23% in a plant scale-up to 150 $MW_{th,wood}$. For this directly heated option, the cost for oxygen is thereby not excessively penalising the plant economics. With the cost data from Kirschner (2009), the required 0.29 kg s^{-1} (820 Nm^3h^{-1}) at 20 $MW_{th,wood}$ are best supplied by on-site PSA. At this scale, a price of 9.4 cts kg_{O2}^{-1} is obtained, and the expenses for oxygen amount to 4.4 € MWh_{SNG}^{-1}, which correspond to 5-6% of the total production costs.

Overall, directly heated gasification tends to be the better option, for which total production costs of 80.4 (75.7) € MWh_{SNG}^{-1} with cold (hot) gas cleaning are assessed. For a plant at 150 $MW_{th,wood}$, the total costs would reduce to 63.6 (58.9) € MWh_{SNG}^{-1}. These numbers are by 10-20% better than in indirectly heated gasification with moderately pressurised methanation, for which the production costs amount to 90.9 and 80.1 € MWh_{SNG}^{-1} at 20 and 150 $MW_{th,wood}$, respectively. Compared with an expected market price of 120 € MWh_{SNG}^{-1} for the produced green gas, all these options are yet expected to be profitable.

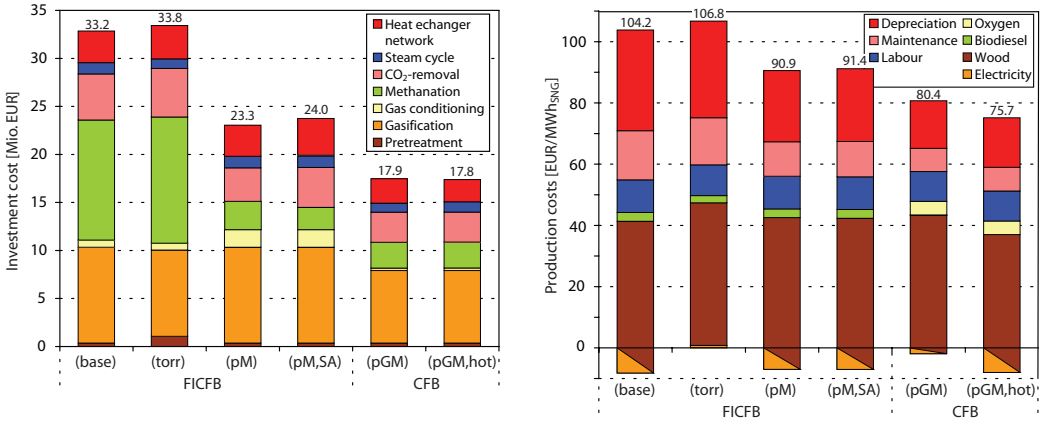

Figure 2.7—Investment (left) and total production costs for the scenarios defined in Table 2.8 at a plant capacity of 20 $MW_{th,wood}$. Negative contributions are due to profits from selling electricity.

	FICFB			CFB
	(base)	(pM)	(pM,SA)	(pGM)
N_g	1 (8)	1 (8)	1 (8)	1 (1)
d_g / $d_{g,comb.}$		3.9 m / 1.1 m		1.0 m
h_g / $h_{g,comb.}$		6.0 m / 11.6 m		3.5 m
N_m	3 (21)	1 (4)	1 (3)	1 (2)
d_m	3.8 m	2.8 m	2.5 m	1.9 m
h_m	18.2 m	16.2 m	15.4 m	14.0 m

Table 2.11—Reactor size and number of required units for a plant capacity of 20 $MW_{th,wood}$ (150 $MW_{th,wood}$, dimensions change).

2.5 Conclusions

This chapter has presented the development of a superstructure based process model for candidate technologies to produce SNG from lignocellulosic biomass by conventional gasification and methanation. Based on data from existing plants and pilot installations, simple phenomenologic unit models have been established and reconciled to accurately predict the performances of a flowsheet in a restricted domain of operating conditions. Compared to conventional simulation, the proposed model allows for assessing the thermo-economic performances of the integrated system. It thereby computes not only the energy flow using conventional flowsheeting software, but also the process integration including the combined heat and power production. The energy integration is performed without imposing any restrictions on the process topology, and therefore expected to determine the optimal choice of

utilities.

The results of this stepwise flowsheeting are used to rate the equipment and estimate the investment cost of the system. Thermodynamic variables like temperature, pressure and volume flows are thereby considered as design specifications to be met, which allows for taking the impact of the operating conditions into account. Due to this structure, the process model is adequate for thermo-economic optimisations.

In a preliminary screening of the process performance for some typical technology scenarios, it is shown that the conversion of woody biomass to SNG is a viable option with respect to both energetic and economic aspects. Recovering the excess heat by means of a Rankine cycle allows for a considerable co-production of electricity, and overall energy and exergy efficiencies of in the range of 69-76% and 63-70%, respectively, are obtained. The most efficient conversion is thereby reached with directly heated, steam/oxygen-blown gasification and hot gas cleaning. Due to reduced volume flows, moderately pressurised gasification and methanation is further advantageous with regard to investment cost. Including the equipment's depreciation, total production costs in the range of 76-107 € MWh_{SNG}^{-1} are expected for a plant capacity of 20 $\mathrm{MW}_{th,wood}$, whereas 59-97 € MWh_{SNG}^{-1} are assessed for large-scale plants at 150 $\mathrm{MW}_{th,wood}$ and above.

Chapter 3

Thermodynamic analysis of gasification concepts

As introduced in the previous chapters, the efficiency of thermochemical conversion processes largely relies on energy integration. This chapter develops this aspect for two exemplary gasification technologies at a thermodynamic analysis in terms of equilibrium, energy and exergy, and has recently been published as a paper (Gassner and Maréchal, 2009d).

3.1 Introduction

Thermochemical biomass and waste gasification is commonly considered as a rationale and carbon-neutral technology for power generation in centralised combined cycle plants (Craig and Mann, 1996, Brown et al., 2009), local combined heat and power cogeneration with gas engines (Hofbauer et al., 2002, Henriksen et al., 2006, Yoshikawa, 2006) and more recently fuel cells (Omosun et al., 2004, Karellas et al., 2008), and the synthesis of liquid and gaseous fuels (Spath and Dayton, 2003, Mozaffarian and Zwart, 2003, Hamelinck et al., 2004, Gassner and Maréchal, 2009c, Heyne et al., 2008, Ptasinski, 2008).

In process design, suitable biomass gasification technology is usually identified considering design constraints like capacity and criteria like gas composition, calorific value and contaminants that are related to the specific application (Mozaffarian and Zwart, 2003, Hamelinck et al., 2004, Stucki, 2005). Process integration aspects are regarded to a lesser extent, although heat requirements of gasifiers are generally important and influence the systems' overall performance markedly. Especially for fuel production, a high chemical gas conversion is essential since the primary product is the energy stored in the material outlet streams. Furthermore, the energy requirements

and recovery possibilities of the reforming steps after gasification are different to those in power generation, and proven technology established for this specific application does not necessarily fit the modified demand.

For this reason, the present chapter investigates the thermodynamic performance of two potential gasification systems for fuel production as producer gas generators. Several authors have recently investigated the thermodynamic and exergetic performance of gasification (Ptasinski et al., 2007, Jarungthammachote and Dutta, 2007, Prins et al., 2007) and gasification systems for the production of power (Brown et al., 2009, Prins et al., 2007, Fryda et al., 2008) and fuels (Ptasinski, 2008). Apart from Brown et al., however, all these studies disregard or discuss the effects of process integration only very briefly, and lack a systematic approach as provided by pinch analysis techniques. The present chapter therefore focusses on the integrated energetic and exergetic performance and addresses two exemplary gasification systems for whom this type of analysis has yet to be carried out. In particular, an indirectly heated fluidised bed gasifier with steam as gasifying agent (Hofbauer et al.'s FICFB process) that is currently regarded as promising option for SNG production by Stucki (2005), Heyne et al. (2008) and Biollaz et al. (2009), and a directly heated, fixed bed gasifier based on a relatively novel two-stage concept (Henriksen et al.'s Viking process) are compared.

3.2 Description of the gasification concepts

Developed by Hofbauer et al. (2002) at the Technical University of Vienna, FICFB gasification has been designed as an internally circulating fluidised bed system where heat is transferred by circulating the bed material between two physically separated gasification and combustion chambers. As shown on the left of Figure 3.1, gasifying steam is injected into a stationary fluidised bed where drying, pyrolysis and gasification of the raw material take place. The reactor is heated indirectly by transferring hot bed material via a cyclone from a combustion chamber, where the ungasified char and additional fuel are oxidised. The obtained synthesis gas is cooled to 150°C, filtered and washed with water or biodiesel in order to remove dust particles, tar and other contaminants before being used in an energy conversion unit or a fuel conversion process.

The fundamental design idea behind the Viking gasification process developed by Henriksen et al. (2006) at the Technical University of Denmark is to perform a thermally staged gasification with intermediate partial oxidation for tar cracking. As shown on the conceptual flowsheet (Fig. 3.1, right), wood is first conveyed through a screw pyrolysis unit, where it is heated

to 500-600°C and partially decomposed. After thermal cracking of the tars through partial oxidation of the gas phase, the remaining solid species are gasified in a fixed bed. The synthesis gas leaving the gasifier at 700-800°C is cooled to 90°C and filtered. Finally, the condensates are removed at ambient conditions in a gas-liquid separator.

3.3 Equilibrium analysis

Approach

Although often assumed in flowsheeting models, the producer gas of fluidised and fixed bed gasifiers do generally not reach thermodynamic equilibrium due to kinetic limitations. As detailed in Section 2.3.1.2, its composition is more appropriately represented by introducing temperature differences to equilibrium ΔT_{eq} according to Equation (2.17). Reconciling these model parameters with experimental data not only allows for evaluating the gasifier performance in terms of chemical conversion, but may also be used for analysing its suitability for a particular application with respect to process integration.

While an equilibrium-based approach is reasonably accurate for modelling the products and heat demand of gasification, it is inappropriate for taking the bulk formation of condensable hydrocarbons during pyrolysis into account. A recently published experimental study by Fassinou et al. (2009) on the screw pyrolysis unit of the Viking systems show that these condensable substances (incl. H_2O) contribute to 28-78%wt of the gaseous phase from pyrolysis. Although some yield data and the detailed non-condensable gas composition are reported, no complete mass and energy balances can be deduced from the given information. Model validation is thus impossible, and no rigorous model for the conversion of species in the pyrolysis has been developed. Instead, a simplified formulation based on a partial gasification of the biomass feed is adopted. It is considered that the atomic species in the biomass are uniformly gasified, which fixes the solid composition. Assuming further that the complete volatile fraction identified in the proximate analysis is released, two model equations are necessary to fix the gas phase composition and the heat demand. For this purpose, the hydrogenating gasification (Eq. 2.2) and water-gas shift (Eq. 2.6) reactions are used and reconciled with the consistent dataset for the overall plant.

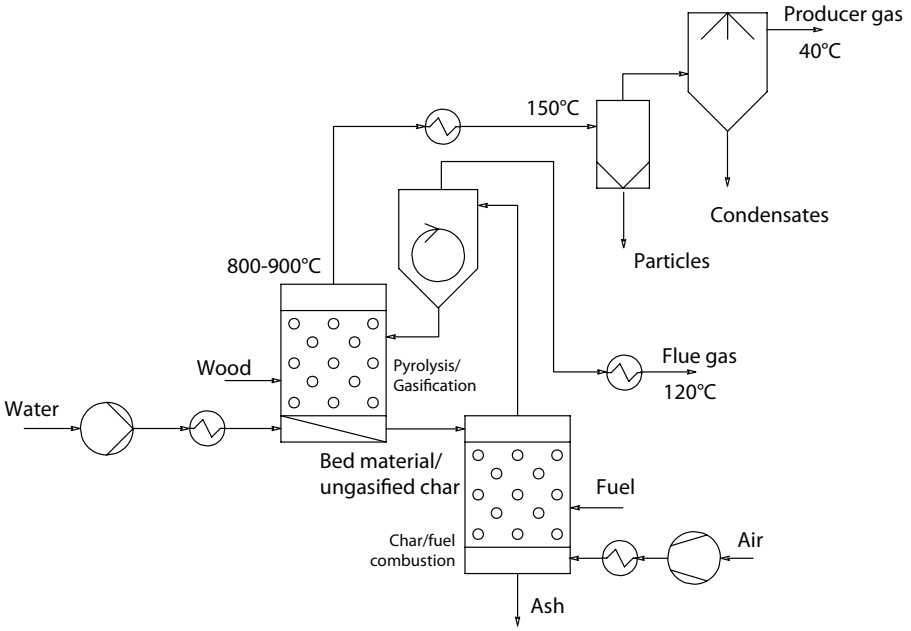

(a) FICFB gasification

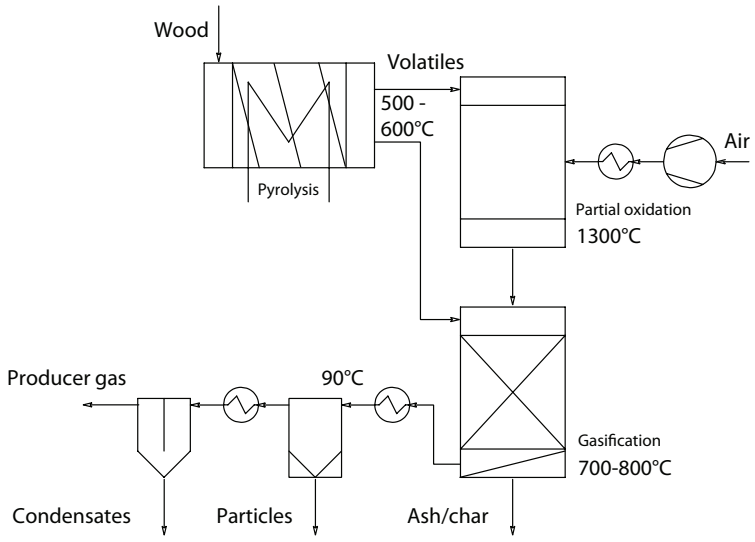

(b) Viking gasification

Figure 3.1—Conceptual flowsheets. Note: These schematics illustrate the model structure and do not correspond to the physical process layout, i.e. the pyrolysis, oxidation/combustion and gasification reactors correspond to one physical unit.

		Unit	FICFB	Viking
Model assumptions	$\epsilon_{isentropic,turbomachinery}$	%	80	80
	$\Delta p_{exchangers}$	bar	-	-
	Δp_{filter}	bar	0.10	0.10
	$\Delta p_{gasifier}$	bar	0.15	0.05
	Gasifier heat loss	%	10[a]	2[b]
	Volatile release in pyrolysis[c]	%	-	84
	Wood humidity (Φ_{wood})[c]	%wt	10	30
Operating conditions	Steam preheat temperature	°C	500	-
	Air preheat temperature	°C	600	600
	Steam/biomass ratio	-	0.6	-

[a] based on transferred heat.
[b] based on lower heating value of feed.
[c] according to data used for reconciliation (Henriksen et al., 2005, Rauch, written around 2004).

Table 3.1—Model assumptions and operating conditions for reconciliation.

Process	FICFB	Viking	
Reactor	Gasification	Pyrolysis	Gasification
$\Delta T_{eq,(2.2)}$	-280°C	-289°C	-11°C
$\Delta T_{eq,(2.3)}$	-201°C	-	-123°C
$\Delta T_{eq,(2.6)}$	-112°C	+12°C	-126°C
$k_{C2/C1}$	0.205	0	0
ε_{cc}	90.3%	-	99.0%

Table 3.2—Reconciled model parameters.

Data reconciliation

With the general assumptions and operating conditions detailed in Table 3.1, the model parameters of the gasification reactor model are determined using data of wood characteristics, process conditions and gas compositions from Gøbel et al. (2004), Henriksen et al. (2005) and Rauch (written around 2004). For FICFB gasification, the reference temperature for gasification is 850°C, while the artificial temperature differences in Viking gasification refer to pyrolysis and gasification temperatures of 600°C and 750°C respectively. The values of the identified parameters and their accuracy with respect to the measured data are given in Tables 3.2 and 3.3.

Process	FICFB		Viking		
Reactor	gasification		pyrolysis	gasification	
State	wet	dry	wet	wet	dry
C_2H_4	1.8 / 1.9	- / 2.0	- / -	- / -	- / -
CH_4	8.8 / 9.6	- / 10.0	- / 35.7	- / 1.2	1.2 / 1.2
H_2	37.3 / 38.5	- / 40.1	- / 4.9	- / 30.4	30.5 / 31.4
CO	29.4 / 27.4	- / 28.5	- / 3.0	- / 18.3	19.6 / 19.0
CO_2	16.2 / 15.8	- / 16.4	- / 33.2	- / 14.2	15.4 / 14.7
N_2	- / 2.9	- / 3.0	- / 0.2	- / 32.7	33.3 / 33.7
H_2O	3.6 / 3.9	- / -	- / 23.0	- / 3.2	- / -

Table 3.3—Gasifier outlet compositions in %vol (Data (Gøbel et al., 2004, Rauch, written around 2004) / Calculation).

Error analysis

According to Table 3.3, the model is able to reasonably reproduce the measured composition of the producer gas. As already discussed in Section 3.3, the model parameters and gas composition after pyrolysis must however be considered as artificial since the higher hydrocarbons are not explicitly included as model species, but partially accounted for by the non-condensable species and the ungasified raw material. According to experimental data, about 14%vol CH_4, 40%vol CO, 18%vol CO_2, 19%vol H_2 and 3%vol C_4H_{4-6} are typically obtained in the dry, non-condensable product at nominal conditions (Fassinou et al., 2009). However, for the validity of the following energy integration and exergy analysis, the accuracy of the intermediate composition has no influence since only a correct reproduction of the heat demand for pyrolysis is crucial. Indeed, this is assured by the computed nitrogen fraction in the producer gas, which is in very good agreement with the data from the plant. As it enters the reactor in a known ratio to oxygen, this fraction directly represents the degree of partial oxidation in the gasification. The enthalpy balance of the gasification reactor is thus accurate, which also implies that the total enthalpy of the close-coupled pyrolysis products is correct.

Discussion

Examining the reconciled model parameters, it is obvious that the synthesis gas from both gasifiers is not in thermodynamic equilibrium. All the apparent equilibrium temperatures observed in the gasification sections are below the actual reactor temperatures. Compared to equilibrium, the gasifiers produce gases that contain too much hydrocarbons and carbon dioxide and too little hydrogen and carbon monoxide. The difference from equilibrium is

thereby not as substantial in case of Viking gasification, which may be due to the different reactor types. Unlike in fluidised bed reactors were similar temperature deviations can be reasoned by similar catalytic activity of the bed, the temperature in fixed beds is not equally distributed and part of the gas might be formed at higher temperatures. In case of Viking gasification, the pyrolysis gas is furthermore heated to 1100℃ by partial oxidation in order to thermally crack the tars. Since this shifts the gas equilibrium towards H_2 and CO and reaction kinetics tend to accelerate with temperature, this might also lead to approach thermodynamic equilibrium at the gasifier outlet to a greater extent.

3.4 Energy integration

Approach

The method of separate energy-flow and integration modelling outlined in Chapter 1 inherently distinguishes the thermochemical conversion and heat transfer. Apart its suitability for conceptual process design, this also proves useful for analysing the exergy losses in the heat transfer operations while systematically considering all the possible heat recovery.

In a first analysis, the heat demand for FICFB gasification is satisfied as in the demonstration plant through combustion of ungasified char and cold producer gas. The exergy potential of excess heat below the pinch is recovered and converted to electricity by a steam Rankine cycle, for which typical small scale operating conditions of 60 bar for steam production and 500℃ for superheating are assumed. Two intermediate utilisation levels at 15.5 bar (200℃) and 1.0 bar (100℃) and one condensation level at 0.23 bar (20℃) fed with cooling water prove appropriate. For the respective stage efficiencies and minimum approach temperatures apply the assumptions outlined in Section 2.3.2.

The performance of the two gasification systems is assessed by calculating the energy balances, the cold gas efficiency ϵ_{cg} (Eq. 2.20) and the overall energy efficiency ϵ (Eq. 1.30) defined earlier. For a proper comparison, the same feedstock properties shown in Table 3.4 and an arbitrary reference input of 1 $MW_{th,wood}$ are used.

Results and discussion

The resulting energy balances and composite curves without and with a steam cycle for energy recovery are depicted in Table 3.5 and Figure 3.2. The data

Proximate analysis		Ultimate analysis	
Δh^0_{wood}	19.2 MJ kg^{-1}_{dry}	C	50.93 %wt
Δk^0_{wood} [a]	21.6 MJ kg^{-1}_{dry}	H	6.11 %wt
Φ_{wood}	30 %wt	O	42.16 %wt
		N	0.80 %wt

[a] Chemical exergy is calculated according to Szargut and Styrylska (1964).

Table 3.4—Feedstock properties.

reveals a considerable difference of the performance of the investigated gasification systems. In case of FICFB gasification, only 78% of the chemical energy input is converted into product gas, while 91% are recovered in Viking gasification. The energy loss inventory thereby illustrates that the lower carbon conversion in FICFB gasification is not the reason for the difference since it is used as fuel in the combustion. However, a significant amount of energy is lost in the gas cooling and cold utility, and a considerable by-production of electricity is observed. The composite curves show that the FICFB gasification system is pinched at 875℃, at which the endothermal heat of reaction must be supplied. From the whole demand of 266 kW_{th} MW^{-1}_{wood}, only 30% are satisfied with the ungasified char and 19% of the total cold producer gas is required to supply the remaining 70%. Consecutively, an important amount of 148 kW_{th} MW^{-1}_{wood} of sensible heat of the fumes and wet producer gas is available below the pinch, from which 36% can be recovered as electricity with a Rankine cycle (Fig. 3.2(b)). In Viking gasification, the heat demand is satisfied by partial oxidation inside the reactor and the composite curves are not pinched by heat transfer between the process streams. The key advantage of this technology in terms of gas efficiency is yet caused by the staged gasification concept. In contrast to FICFB gasification where the entire heat demand for the decomposition must be withdrawn from the chemical energy of the material streams, part of this demand is satisfied by recovering the sensible heat from the producer gas in the pyrolysis. Less excess heat is thus available from the material stream, and only a marginal 20 kW_{el} MW^{-1}_{wood} can be generated from the 52 kW_{th} MW^{-1}_{wood} that must be evacuated from the system.

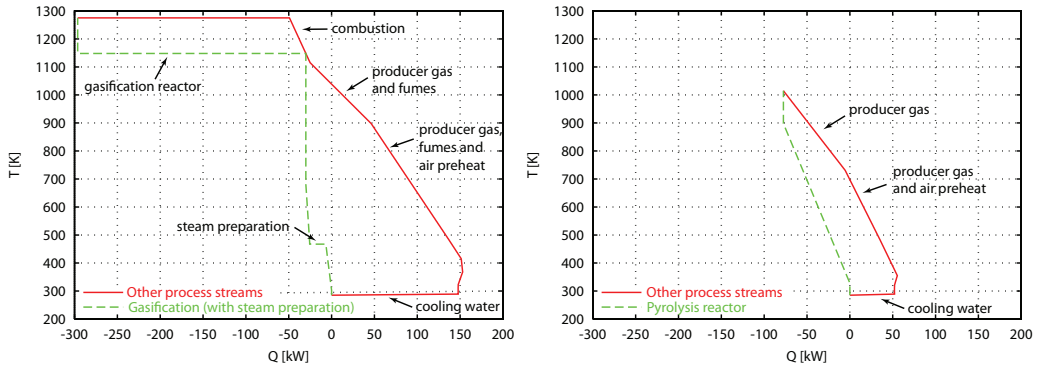

(a) Heat supply for gasification and pyrolysis from utility and process streams without steam cycle.

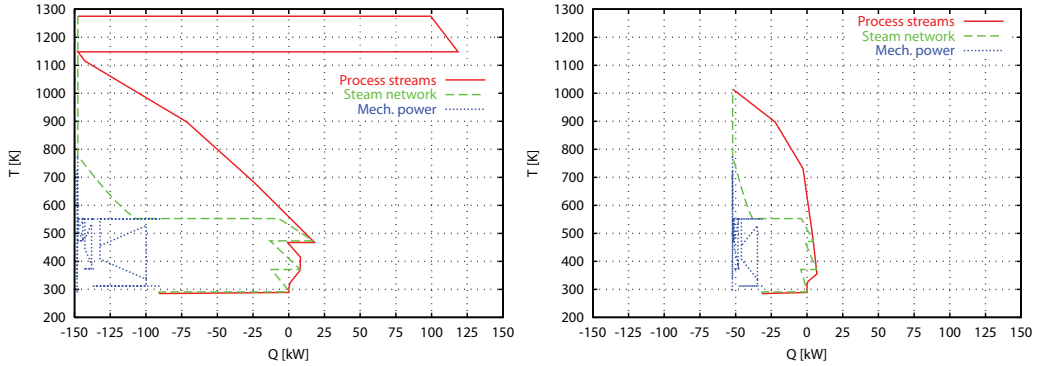

(b) Heat recovery from the process streams with a steam cycle.

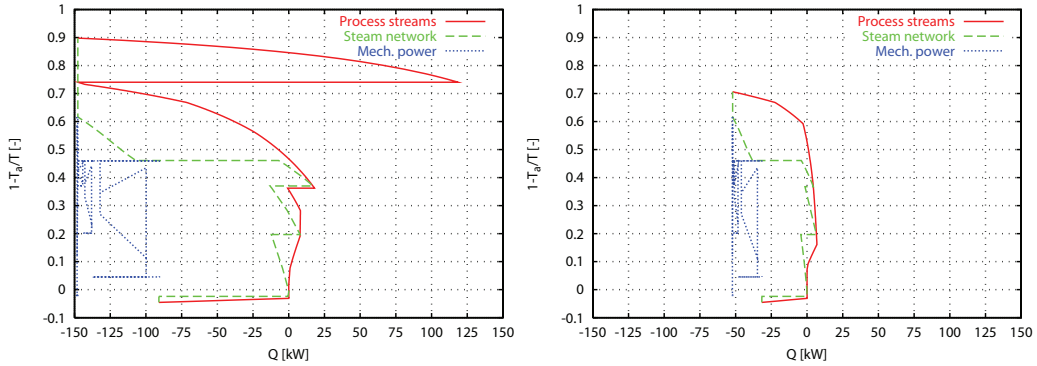

(c) Exergy representation of the heat recovery from the process streams with a steam cycle.

Figure 3.2—Composite curves for FICFB (left) and Viking gasification (right).

Type		FICFB	Viking
Consumption	Wood	1000 kW	1000 kW
	Electricity	2 kW	2 kW
Production	Gas	784 kW	907 kW
	Electricity	54 kW	20 kW
Losses	Gasification	13 kW	27 kW
	Combustion	14 kW	-
	Gas cooling	59 kW	22 kW
	Cooling water	91 kW	32 kW
	Total	177 kW	81 kW
Efficiencies	ϵ_{cg}	78.4%	90.7%
	ϵ	83.8%	92.5%

Table 3.5—Energy balances. Note that the total consumption must not necessarily equal the total production and losses since the consumption and production terms are based on lower heating value, but the gas cooling loss includes condensation.

3.5 Exergy analysis

Approach

In order to further investigate the origin of the losses in the gasification systems, exergy balances considering the exergy value of material, thermal and mechanical streams (designated $\dot{E}_y$, $\dot{E}_q$ and $\dot{E}$ respectively) are defined for all process sections. The exergy losses $\dot{L}$ (Eq. 3.1) and efficiency η (Eq. 3.2) are then calculated by balance, which is consistent with the definition of Equation (1.31):

$$\begin{aligned}\dot{L} =& \sum \dot{E_y}^+ + \sum \dot{E_q}^+ + \sum \dot{E}^+ \\ & - \left(\sum \dot{E_y}^- + \sum \dot{E_q}^- + \sum \dot{E}^- \right) \end{aligned} \tag{3.1}$$

$$\eta = 1 - \frac{\dot{L}}{\sum \dot{E_y}^+ + \sum \dot{E_q}^+ + \sum \dot{E}^+} \tag{3.2}$$

where superscripts $^+$ and $^-$ refer to streams entering and leaving the section, respectively. The exergy value of material streams is determined by adding its exergy value at atmospheric temperature T_a and the exergy necessary for

heating the stream:

$$\begin{aligned}\dot{E}_y &= \dot{m}\left[\Delta k^0 + \int_{T_a}^{T} c_p\left(1-\frac{T_a}{T}\right)dT\right] \\ &= \dot{m}\left[\Delta k^0 + c_p\left(T - T_a(1+\ln(T/T_a))\right)\right] \end{aligned} \tag{3.3}$$

where Δk^0 is the exergy value per unit mass and c_p the specific sensible heat at constant pressure. In this formulation, the contribution of the pressure is not included in $\dot{E}_y$, since the whole system operates at atmospheric pressure. The assumption of a constant c_p is also used to determine the exergy value of the thermal streams:

$$\begin{aligned}\dot{E}_q &= \int_{T_1}^{T_2}\left(1-\frac{T_a}{T}\right)d\dot{Q} \\ &= \dot{m}\int_{T_1}^{T_2} c_p\left(1-\frac{T_a}{T}\right)dT \\ &= \dot{m}c_p\left[(T_2-T_1) - T_a\cdot\ln(T_2/T_1)\right] \\ &= \dot{Q}\left(1 - T_a\cdot\frac{\ln(T_2/T_1)}{(T_2-T_1)}\right) \end{aligned} \tag{3.4}$$

Finally, the exergy value of mechanical streams equals its energy value $\dot{E}$.

Results and discussion

Complementary to the energy conversion analysis of the previous section, the exergy inventory of Table 3.6 highlights that the principal irreversible losses occur in the reactive part of the processes. A comparison of the gasifiers thereby shows that the exergy depletion in directly heated gasification is higher than in the indirectly heated reactor since partial oxidation occurs. However, this loss exactly equals out with the combined depletion in gasification and combustion of the FICFB technology. As already perceived in the energy integration analysis, it is the consequence of the combustion that induces the difference in performance. Exergy analysis thereby allows for directly quantifying the potential loss due to the degradation of valuable thermal energy in heat transfer. Since the loss in mechanical energy potential corresponds to the surface area between the uncorrected hot and cold streams in the exergy composite curves, it is clearly impossible to entirely recover the potential of the elevated amount of sensible heat of hot fumes and wet producer gas. As illustrated in Figure 3.2(c), the indirect heat transfer from combustion to gasification above the pinch increases the exergy loss of this section by 13%. Together with the depletion due to the heat transfer

	FICFB		Viking	
Section	$\dot{L}$ [kW]	η [%]	$\dot{L}$ [kW]	η [%]
Gasification[a]	176	87.4	245	80.2
Combustion	71	80.5	-	-
Heat transfer				
- above pinch	32	85.8	-	-
- below pinch	27	83.1	16	83.3
Gas cooling[b]	24	75.4	13	87.1
Steam turbine	12	86.7	4	86.0
Total	342	70.8	278	76.6

[a] including pyrolysis.

[b] The exergy efficiency of the cooling section is assessed on the basis of the theoretical work potential of the rejected heat - the separation of condensates is not considered as a transformation and the chemical exergy of the inlet material stream is not included in the denominator of Equation (3.2).

Table 3.6—Exergy losses and efficiencies.

below the pinch and the gas cooling section, this results in an overall exergy efficiency of 70.8% for FICFB gasification, while 76.6% is reached by Viking technology.

3.6 Potential process improvements

The energy integration and exergy analysis reveals that the main drawback of the FICFB gasification process is its elevated heat requirement at high temperature. This results in a relatively low cold gas efficiency, and the irreversible losses in all process sections do not allow for entirely recovering the considerable amount of sensible heat from the fumes and the wet producer gas as electricity. By mainly targeting to decrease the minimum energy requirement (MER) above the pinch and the exergy losses in the reactive steps, this section presents measures to increase the cold gas and overall process efficiency.

3.6.1 Fuel choice

In the FICFB demonstration plant, the combustion zone is fed with additional cold, clean producer gas to balance the heat demand of the gasification (Hofbauer et al., 2002). This has the main advantage that the gas handling is conveniently simple, but it consumes energy from above the pinch to heat

the cold gas up to the combustion temperature. In order to satisfy the heat demand of the gasification reactor in a more efficient way, hot producer gas could be withdrawn from the gasifier outlet. Although the actual MER of 266 kW_{th} MW_{wood}^{-1} does not change, no more heat from combustion is transferred through the pinch to preheat the fuel. As shown in Table 3.7, the exergy losses in the combustion and the energy losses in the cooling water are reduced, and less energy must be withdrawn from the product stream. An advantageous side-effect is further observed in the gas cooling section since less gas is processed. Overall, using the hot and dirty producer gas instead of clean and dry one would allow for increasing the cold gas and total efficiencies by 3% and 2%, respectively.

3.6.2 Pretreatment

In addition to changing the fuel to satisfy the energy requirement in a more efficient way, the goal of pretreating the feed is to inherently reduce the exergy losses and the heat demand of gasification. However, this requires to use additional equipment or to change the design of the gasifier. In addition to constructional modifications, a preprocessed feed is expected to decrease the ΔT_{eq} value and thus reach closer to equilibrium conditions, or it would allow for reducing the vessel size. These effects are not accounted for in this analysis.

3.6.2.1 Drying

A simple way to limit the losses in the gasifier is to remove the humidity of the feed by drying. This reduces the heat consumption above the pinch for evaporating water, which is done with sensible excess heat at low temperature instead. With the technology model for convective drying with flue gas or air developed in Section 2.3.1.1, the impact of drying on the cold gas and total efficiency of the process is assessed in Figure 3.3 for three different air preheat temperature levels. Although the drying efficiency is sharply increasing with temperature (cf. Fig. 2.2), the process efficiencies are only marginally affected due to the large amount of heat that is available in the temperature range of drying. Only for very intense drying at low temperature and efficiency, the use of heat gets conflictive with the electricity generation in the Rankine cycle. More importantly, the graph shows that the process performance is considerably increased by drying the feed. At a humidity level of 15% detailed in the comparative table (Tab. 3.7), the cold gas efficiency is increased by more than 6% compared to wood at 30% humidity. Since heat below the pinch is used, the MER is decreased by 18% from 266 to 217 kW_{th} MW_{wood}^{-1}

				FICFB				Viking
Pretreatment[a]		n	n	d	d	d	p	p
Fuel[b]		cg	hg	cg	hg	dw	cg	n
Humidity		30%	30%	15%	15%	15%	30%	30%
Consumption								
Wood	kW	1000	1000	1000	1000	1000	1000	1000
Electricity	kW	2	2	4	4	4	2	2
Production								
Gas	kW	784	814	847	869	874	888	907
Electricity	kW	56	47	30	23	23	22	20
Energy losses								
Drying	kW	-	-	19	19	19	-	-
Gasification	kW	13	13	10	10	9	9	27
Combustion	kW	14	14	12	11	10	10	-
Gas cooling	kW	59	47	59	50	50	59	22
Cooling water	kW	91	75	48	36	39	28	32
Total	kW	177	149	148	126	127	106	81
Exergy losses								
Drying	kW	-	-	12	12	12	-	-
Gasification	kW	176	176	154	154	132	150	245
Combustion	kW	71	61	57	50	71	49	-
HEN, above pinch	kW	32	33	26	27	22	23	-
HEN, below pinch	kW	27	24	34	32	30	25	16
Gas cooling	kW	24	19	24	20	20	24	13
Steam turbine	kW	12	9	2	0	1	3	4
Total	kW	342	322	309	295	288	274	278
Efficiencies								
ϵ_{cg}	%	78.4	81.4	84.7	86.9	87.4	88.8	90.7
ϵ	%	83.8	85.9	87.2	88.7	89.4	91.0	92.5
$\eta_{gasification}$	%	87.4	87.4	88.8	88.8	88.7	89.0	80.2
$\eta_{combustion}$	%	80.5	82.8	80.6	82.6	74.2	80.7	-
$\eta_{HEN,\ above\ pinch}$	%	85.8	85.7	85.8	85.6	85.9	85.7	-
$\eta_{HEN,\ below\ pinch}$	%	83.1	83.0	80.4	79.9	80.0	82.6	83.3
$\eta_{gas\ cooling}$	%	75.4	75.4	75.4	75.4	75.4	75.4	87.1
$\eta_{steam\ turbine}$	%	86.7	87.3	97.1	99.3	98.3	93.7	86.0
η_{cg}	%	66.2	68.7	71.5	73.4	73.9	75.0	75.0
η	%	70.8	72.6	73.7	75.0	75.5	76.9	76.6

[a] (d)rying, (p)yrolysis, (n)one.

[b] (c)old (g)as, (h)ot (g)as, (d)ry (w)ood, (n)one.

Table 3.7—Energy and exergy balances for system modification of the FICFB gasification. For comparison, the original performance is reprinted in the first and last rows.

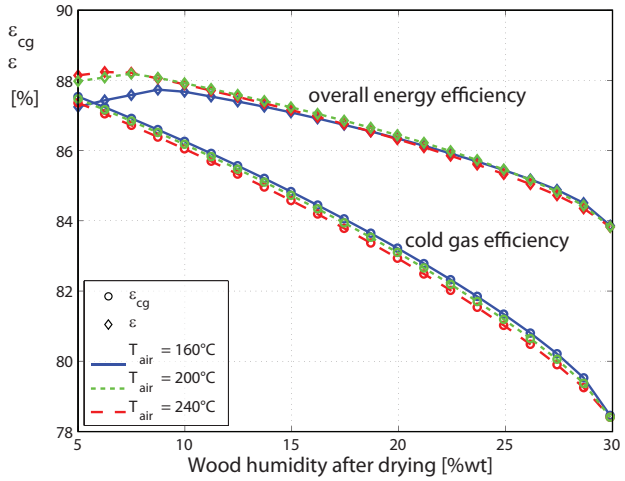

Figure 3.3—Air drying efficiency and impact of drying on the process performance.

and the exergy losses due to water evaporation at high temperature in the gasifier drop by more than 12%. Drying therefore appears as a chemical heat pump.

In analogy with using hot instead of cold producer gas, some more benefit from drying can be obtained if the heat demand is satisfied with dried wood. Since less feed material is processed, the MER is further reduced to 185 kW_{th} MW_{wood}^{-1}, and the cold gas efficiency increases by 9% overall compared to the reference technology. However, this modification would require a technical redesign of the combustion chamber and the addition of a biomass hopper.

3.6.2.2 Pyrolysis

Alternatively to installing a wood dryer, it is conceivable to feed the FICFB gasification reactor via the same type of screw pyrolysis device used in Viking gasification. This would amplify the beneficial effect on the conversion efficiency since the humidity is completely evaporated and the endothermal decomposition is set on with heat below the pinch. By reducing the MER to 185 kW_{th} MW_{wood}^{-1}, the comparative table (Tab. 3.7) shows that more than 10% improvement in cold gas and 7% in total efficiency compared to the reference solution is possible. If hot producer gas is furthermore used to supply the remaining heat, the cold gas and total efficiency increase to 90.5% and 92.2% in terms of energy and 76.4% and 77.9% in terms of exergy, respectivly. With similar pretreatment, the performance of FICFB gasification is

thus very close to Viking gasification, and might even exceed it with respect to the exergy-based indicators.

The conceptual flowsheet with a practicable structure of the heat exchanger network and the corresponding composite curve of this process option are shown in Figure 3.4. According to the calculations, the sensible heat of the producer gas balances the heat demand of the pyrolysis. It could thus be cooled in the jacket of the pyrolysis screw before entering the cold gas cleaning. The sensible heat of the fumes is left to preheat the combustion air and to produce steam in order to cogenerate electricity via the steam Rankine cycle.

3.7 Performance in SNG production

Producer gas from gasification is generally not a product on its own, but further converted to electricity, chemicals or fuels. Obviously, the overall performance of such systems does not only rely on the gasifier efficiency, but also on its integration with the rest of the system. For the two gasification systems, this effect is illustrated at the example of SNG production outlined in Chapter 2, for which staged Viking gasification is thermodynamically suitable if oxygen instead of air is used for the partial oxidation. In order to compare the performance of systems with equal boundaries, on-site oxygen production by ion transfer membranes (ITM) is considered. ITM is an emerging technology that is not yet commercially proven, but expected to consume about 147 kWh_{el} ton_{O2}^{-1} and 1.25 MWh_{th} ton_{O2}^{-1} to heat the air from 500°C up to the membrane's operating temperature of 900°C (van Stein et al., 2002).

With the process model developed in Chapter 2, the system performance for both gasifiers is determined by considering methanation at atmospheric pressure and bulk CO_2 removal by pressure swing adsorption to meet a Wobbe Index of 13.3 kWh Nm^{-3}. In order to limit the number of options to be discussed, it is assumed that the process heat demand is satisfied with cold producer gas. For Viking gasification, the steam network used for energy recovery is slightly adapted to the different process conditions. Instead of steam production at 60 bar, methanation at 320°C and a low amount of heat available above favours steam production at 50 bar and superheating to 480°C.

Table 3.8 shows the computed gas compositions for these exemplary process configurations. Compared to the reconciled data of Table 3.3, the amount of inert nitrogen is reduced, but the ratios between the species are preserved by the equilibrium-based gasification modelling approach. As the producer gas from indirectly heated, steam-blown gasification contains more

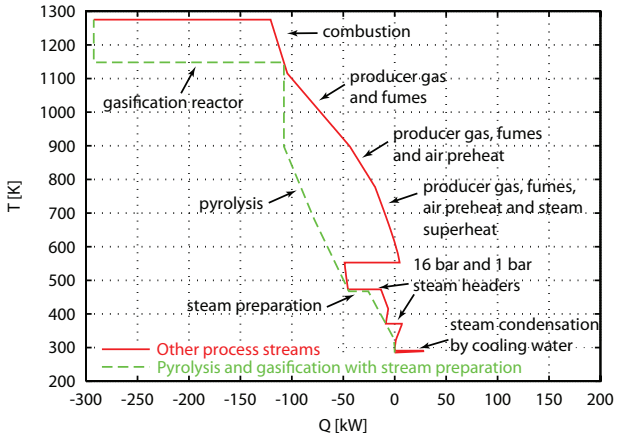

(a) Composite curve.

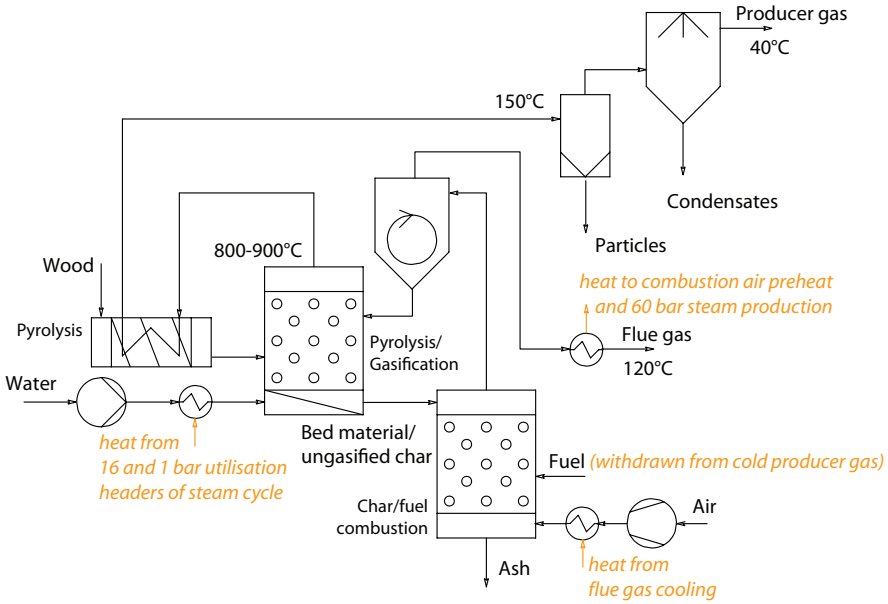

(b) Modified flowsheet with outline of heat exchanger network.

Figure 3.4—Modified FICFB gasification with feed pretreatment by Viking pyrolysis.

		gasification		methanation		CO2-removal	
	Unit	FICFB[a]	Viking	FICFB	Viking	FICFB	Viking
C_2H_4	%vol	2.4	-	-	-	-	-
CH_4	%vol	11.7	2.7	49.8	38.5	92.0	91.9
H_2	%vol	41.9	46.5	3.0	2.3	4.8	5.0
CO	%vol	22.8	28.4	0.1	0.1	0.1	0.2
CO_2	%vol	20.6	22.0	46.1	58.3	1.0	1.1
N_2	%vol	0.5	0.4	1.1	0.8	2.1	1.9

[a] it is assumed that the nitrogen fraction due to inertisation and slip can be reduced to 0.5% by constructional measures.

Table 3.8—Dry gas compositions in SNG production.

			FICFB		Viking
	Pretreatment	none	Drying	Pyrolysis	Pyrolysis
Type	O_2-production	none	none	none	ITM
Chemical energy	wood, wet, in	1000 kW	1000 kW	1000 kW	1000 kW
	wood, dry	1000 kW	1034 kW	1000 kW	1000 kW
	producer gas				
	- gross	1026 kW	1026 kW	1026 kW	931 kW
	- net	770 kW	839 kW	875 kW	896 kW
	crude SNG	672 kW	730 kW	762 kW	724 kW
	SNG, grid	645 kW	704 kW	734 kW	698 kW
Electricity	consumption	33 kW	39 kW	37 kW	57 kW
	production	109 kW	82 kW	82 kW	94 kW
	net production	76 kW	43 kW	45 kW	37 kW
Efficiencies	ϵ_{SNG}	64.5%	70.4%	73.4%	69.8%
	ϵ	72.1%	74.7%	77.9%	73.6%
	η_{SNG}	56.2%	61.2%	63.9%	60.8%
	η	62.5%	64.9%	67.6%	63.9%

Table 3.9—Chemical energy flows and overall energy balances in SNG production.

(atomic) hydrogen, the relative share of methane in the crude product is higher than the one obtained from the partially oxidised producer gas. In order to compare the performance of both in the system, the chemical energy flows and overall efficiencies are shown in Table 3.9 for the pretreatment options discussed in Section 3.6. According to the thermodynamic analysis of the gasifiers, the net producer gas yield from gasification is in all cases higher with Viking technology. After methanation, however, this advantage is considerably reduced or even lost if the FICFB feed is dried or pyrolysed. As less methane is present in the partially oxidised producer gas, the equilibrium

conversion to methane is higher, and more energy is released in the exothermal methanation reactions. The system with FICFB gasification actually benefits from the fact that the producer gas is further away from equilibrium because the gasification reactions are less endothermal – and the ones in methanation less exothermal. As for the isolated performance, drying and pyrolysis further increase the cold gas efficiency by 6% and 9%, respectively. With a potential overall efficiency of almost 78% for FICFB gasification, this technology seems thus clearly advantageous for SNG production compared to fixed bed Viking gasification due to process integration aspects.

3.8 Conclusions

Using a modelling approach based on adjusted equilibrium equations and performing the process integration with pinch analysis, indirectly heated, fluidised bed gasification with steam as gasifying agent (FICFB) and two-stage, fixed bed gasification with air as gasifying agent (Viking) have been compared with respect to thermodynamic performance. It has been shown that the modelling approach allows for accurately reproducing experimental gas compositions and quantifying the difference to thermodynamic equilibrium. Directly heated, fixed bed gasification is observed to be closer to equilibrium than FICFB gasification, which is suspected to be due to an unequal temperature distribution in the reactor and intermediate heating of the pyrolysis product for tar cracking.

In order to analyse the overall performance and identify the origin of major losses, the energy integration has been completed with an exergy analysis of the different process sections. Due to the pinch of FICFB gasification at high temperature, its heat requirements balanced by cold producer gas are elevated and the exergy potential of the sensible heat is only partially recovered. Viking gasification proves efficient since part of the sensible heat is used to dry and start the endothermal decomposition at low temperature. With the current technology at demonstration status, the advantage of a nitrogen free product gas with high calorific value obtained from FICFB gasification is thus penalised by a 12% lower cold gas and 9% lower overall energy efficiency for wood at 30% humidity. However, process integration allows for partly compensating the exergy losses and substantial improvements can be obtained by satisfying the heat requirement of the plant with other streams and using additional technology. In particular, balancing the heat requirement with hot producer gas would increase the cold gas and total energy efficiencies by 3% and 2%, drying the feed to 15% humidity allows for a 6% and 3% increase, and using the same type of screw pyrolysis than in Viking

gasification improves these efficiencies by 10% and 7%, respectively. By applying several of these modifications, the gap to Viking gasification is reduced in terms of energy efficiency, and even surmounted in terms of exergy.

A final comparison of the performance of both gasification technologies in an integrated plant for SNG production shows that the advantage in cold gas efficiency is quickly compensated by a higher heat release in methanation. The fact that the producer gas from fluidised bed gasification is further away from equilibrium turns out to be an advantage since the endothermicity of the gasification reactions is restrained and less chemical energy is released in the exothermal synthesis reactions below the pinch.

Chapter 4

Integrated design of a gas separation system for the upgrade of crude SNG with membranes

In a process that uses its waste and intermediate products as fuel to balance the heat demand, the process performances may considerably benefit from process integration. This chapter assesses the advantage of combining mass- and energy-integration in the design of a gas separation system for upgrading crude SNG to grid quality. The detailed comparison of isolated and integrated design strategies presented here has been published in Gassner et al. (2009). The optimisation of the overall system design is detailed in the recent advancements on combined mass- and energy integration and not reported here (Gassner and Maréchal, 2009a).

4.1 Introduction

While several recent studies have investigated suitable technology and processes for SNG production (Mozaffarian and Zwart, 2003, Duret et al., 2005, Heyne et al., 2008, Luterbacher et al., 2009), the issue of the gas upgrading to grid quality has not received much attention. The separation of carbon dioxide from methane is considered as a conventional operation in the removal of sour gas from natural gas in petrochemical applications, and relatively mature technology for the upgrade of biogas is available (Urban et al., 2008). For SNG production, different candidate technologies have been identified and some basic performance data reported for physical absorption (Mozaffarian and Zwart, 2003), chemical adsorption (Heyne et al., 2008), membrane permeation (Duret et al., 2005) and pressure swing adsorption. In Chapter 2

of this work, relatively simple design or phenomenological models have been developed for screening the performances of these technologies.

The detailed design of a gas separation system for the upgrading of thermochemically produced SNG needs not only to adapt to the quality and impurities of the crude product, but can also exploit the advantages of process integration. The present chapter therefore investigates different design strategies for upgrading crude SNG to grid quality. Through the example of gas separation with membranes, it aims at showing in particular the benefits of a holistic design approach that considers a tight integration of the separation system with the reactive sections of the process. A suitable thermo-economic model of the membrane system is presented and coupled to a process model for crude SNG production. Multi-objective optimisation is used to compare different design approaches and optimal system layouts, and operating conditions for processes with and without CO_2-capture are proposed.

4.2 Process design problem

4.2.1 Production of crude SNG

Discussed in detail in Chapter 2, the currently technically preferred route to produce SNG from lignocellulosic biomass consists in conventionally gasifying the feedstock and converting the obtained producer gas into methane and carbon dioxide. As depicted in Figure 4.1, the raw material is thereby dried prior to gasification in order to prevent excessive losses due to water evaporation. The presence of dust, tars and catalyst poisons like sulphur compounds requires to clean the producer gas before entering the methane synthesis, where it is converted in a catalytic fluidised bed operated at 300-400°C and requires upgrading before being fed to the grid. From the current state of research and process development carried out by Stucki (2005) and Biollaz et al. (2009), it is expected that the first installations will be based on indirectly heated fluidised bed gasification technology of FICFB-type that has been developed and commercialised by Hofbauer et al. (2002).

Using the detailed process model developed in Chapter 2, expected gas compositions of the producer gas and the crude methanation product for this technology are reported in Table 4.1. The corresponding properties of the feed and the process conditions considered for this base case are given in Tables 2.1 and 4.2, respectively. Depending on the operating conditions of the methanation reactor, cold, crude SNG contains around 50%vol of methane and 45%vol carbon dioxide. Especially at low pressure where the conversion

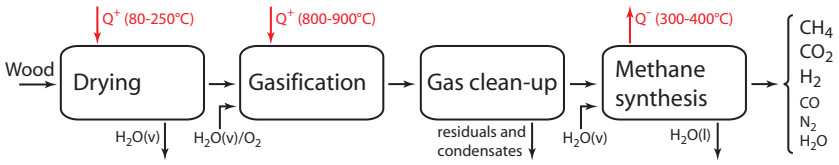

Figure 4.1—Block flow diagram of crude SNG production from wood.

		C_2H_4	CH_4	H_2	CO	CO_2	N_2	H_2O
Gasification	hot	1.9	9.2	32.8	21.5	15.7	0.4	18.5
(FICFB, 1123 K)	cold	2.2	10.9	38.8	25.5	18.6	0.5	3.5
Methanation	hot	-	26.7	3.6	0.1	27.1	0.6	41.9
(1 bar, 593 K)	cold	-	44.8	5.9	0.1	45.1	1.0	3.1
Methanation	hot	-	27.6	1.2	0.0	26.9	0.6	43.7
(10 bar, 593 K)	cold	-	52.1	1.7	0.0	44.7	1.2	0.3

Table 4.1—Composition of producer gas and crude SNG calculated with the process model for the operating conditions of Table 4.2 (%vol).

is limited by thermodynamic equilibrium, a non-negligible residue of hydrogen and traces of carbon monoxide remain in the gas. According to Rauch (written around 2004), up to 5%vol of nitrogen is furthermore present in the producer gas due to its use for the inertisation of the gasification feed and some slip from the adjacent combustion chamber. Since the methanation reaction reduces the volume of the reactants, the molar fraction of the inert species increases, which would prevent to meet the grid specifications for SNG without a special removal of nitrogen. In this work, it is assumed that this issue can be resolved by using CO_2 for feed inertisation and taking special care of nitrogen in an improved gasifier design, which allows for attaining a nitrogen content of 0.5%vol in the dry producer gas.

The stoichiometric design equation outlined earlier (Eq. 1) shows that the overall conversion of wood to methane is exothermic and releases about 450 kJ kg^{-1}_{wood} of heat. The block flow diagram (Fig. 4.1) illustrates, however, that this net release is distributed over the gasification and methanation reactions. The first one is endothermic and requires heat at high temperature, whereas the second one is exothermic and releases heat at lower temperature. The process thus requires additional energy and the quality of the process integration will define the overall process efficiency. The grand composite curve of the process streams shown in Figure 4.2 highlights that the process is pinched at the gasification temperature and that 200 - 250 kW of high temperature heat at 850 - 900°C are typically required to convert 1 MW of

Section	Operating conditions	Value
Drying	Inlet temperature	473 K
	Outlet wood humidity	20%wt
Gasification	Pressure	1 bar
	Gasification temperature	1123 K
	Steam preheat temperature	573 K
	Steam/dry biomass ratio	0.5
Methanation	Pressure	1 bar
	Inlet temperature	593 K
	Outlet temperature	593 K

Table 4.2—Typical operating conditions of the process.

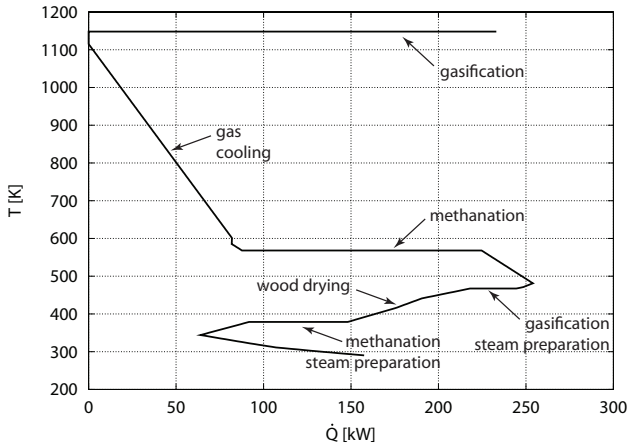

Figure 4.2—Grand composite curve of the minimum energy requirement normalised for the conversion of 1 MW of wood.

wood to crude SNG.

4.2.2 Gas grid specifications

According to the Swiss directive for the supply of biogas (also applying to synthetically produced gas) to the natural gas grid, unlimited amounts of gas can be fed in if its methane content is higher than 96%vol and the CO_2, H_2 and CO content less than 6, 4 and 0.5%vol, respectively (SVGW, 2008). Among other conditions, it is furthermore required that the dew point of the gas at grid pressure ($\leq$ 70 bar) is lower than -8°C. The limit with respect to methane content is thereby based on the fact that biogas as a binary mixture of methane and carbon dioxide does not meet a Wobbe index between 13.3

	C_2H_4	CH_4	H_2	CO	CO_2	N_2	H_2O
Methanation (1 bar, 593 K)	-	44.8	5.9	0.1	45.1	1.0	3.1
– without H_2O, CO_2	-	86.4	11.3	0.3	-	2.0	-
– without H_2O, CO_2, H_2	-	97.4	-	0.3	-	2.3	-
Methanation (10 bar, 593 K)	-	52.1	1.7	0.0	44.7	1.2	0.3
– without H_2O, CO_2	-	94.7	3.0	0.1	-	2.2	-
– without H_2O, CO_2, H_2	-	97.6	-	0.1	-	2.3	-
grid specifications		> 96	< 4	< 0.5		< 6	265 K

Table 4.3—Gas upgrading requirements (%vol).

and 15.7 kWh Nm^{-3} if its methane content is below 96%vol, which is the usual norm for H-quality natural gas.

4.2.3 Design problem definition

Table 4.3 compares the obtained gas compositions after methanation with the grid specifications. Assuming that nitrogen cannot be separated from methane, it shows the maximum obtainable purities after complete removal of water, carbon dioxide and hydrogen. Although a cut-down of the nitrogen fraction in the producer gas to 0.5%vol is considered feasible, it is not sufficient to remove only the carbon dioxide. Provided that an ideal separation process for removing CO_2 from the SNG is used, the hydrogen concentration of the SNG is expected to rise to around 3-11% depending on the methanation conditions. The CH_4 purity will be at best around 94% and at least some of the unconverted hydrogen must be removed. Apart from the separation of the bulk species, the table also shows that the residual carbon monoxide might be an issue. While for pressurised methanation, its fraction in the concentrated methane is at 0.1%vol, it approaches the directive's limit in case of a reactor at atmospheric pressure.

The identification of the minimum energy requirements of the process adds a supplementary aspect to the design problem. Gasification has a relatively important heat demand at high temperature, which is usually supplied by burning producer gas. In the combined heat and power application for which the gasification technology has originally been developed, few other fuel alternatives are available. However, in an SNG plant that necessarily suffers from a non-ideal separation, depleted gas streams from the SNG upgrading section could be used instead of the intermediate product. The condition for this is that its flame temperature is sufficiently higher than the gasification temperature. If the depleted gas is too diluted, it must in any case be treated in a catalytic combustion to eliminate the residual methane due to its high

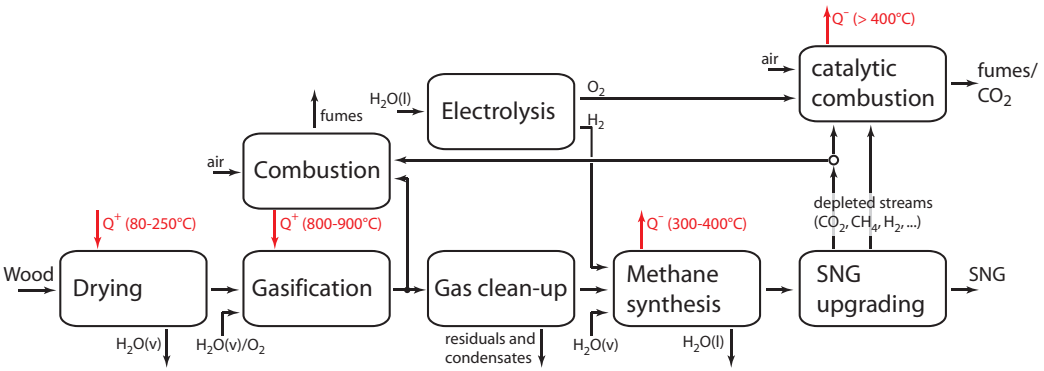

Figure 4.3—Block flow diagram of process integration options for SNG upgrading.

environmental impact as a greenhouse gas.

From these considerations, it is obvious that the design of the separation system is not a trivial problem. It requires the development of an appropriate multicomponent separation system including gas drying, while also considering possible cost and energy savings originating from the trade-off between using the producer gas or a depleted gas as hot utility. In the framework of the actions aimed at climate change mitigation, rather pure carbon dioxide (95% minimum) may also represent a valuable by-product. In a near future, carbon dioxide storage sites are expected to be developed, and carbon dioxide could be transported to the storage sites through dedicated pipelines (Meth et al., 2005). If sequestration instead of venting the separated carbon dioxide is targeted, care must be taken not to dilute this by-product with nitrogen from combustion with air. A possible option is thereby to use oxygen produced by electrolysis in the catalytic combustion. As already discussed in earlier work (Gassner and Maréchal, 2008), the additional hydrogen could be supplied to the methane synthesis and would increase the SNG output since the producer gas lacks hydrogen to be completely reformed into methane. A general block flow diagram of these different upgrading options is given in Figure 4.3.

4.3 Thermo-economic modelling

From the candidate technologies for SNG upgrading reviewed in Gassner et al. (2009), multi-stage membrane separation has been chosen for a detailed modelling in order to investigate the impact of process integration on the optimal design of the separation system and the reactive sections of the plant. Preliminary to the simultaneous bulk separation of CH_4, H_2 and CO_2, gas

drying in a TSA unit with an activated alumina adsorbent is considered, which allows for attaining a dew point of -70℃ with a heat consumption of 11 MJ kg_{H2O}^{-1} for regeneration at 160-190℃ (Bart and von Gemmingen, 2009).

4.3.1 Unit models for membrane separation

According to the theory of gas separation by membranes, a practical description of the permeation process through a membrane has to consider the difference of partial pressure in the bulk as driving force (Hwang and Kammermeyer, 1975). Using a phenomenological constant termed permeability P_i, the permeation of species i is described as:

$$\frac{d\dot{n}_{i,p}}{dA} = \frac{P_i}{\delta} \ (p_{i,r} - p_{i,p}) \tag{4.1}$$

where $\dot{n}_{i,p}$ is the partial molar flow of i that permeates the membrane, A the membrane area, δ its thickness, and $p_{i,r}$ and $p_{i,p}$ the partial pressure of species i on the retentate and permeate side, respectively. The permeability P_i is thereby often given in barrer [$cm^2s^{-1}cmHg^{-1}$], which corresponds to $7.5005 \cdot 10^{-18}$ [$m^2s^{-1}Pa^{-1}$] in SI-units. Furthermore, it is convenient to specify the relative permeabilities of two different species i and j by the selectivity $\alpha_{i,j}$ of i over j:

$$\alpha_{i,j} = P_i / P_j \tag{4.2}$$

As the permeation is described by a set of i differential equations of the same type as Equation (4.1), its resolution depends on the flow pattern of the membrane. Typical patterns discussed in the literature, for example by Hwang and Kammermeyer (1975) or Rautenbach and Dahm (1985), are the completely mixed, cross-flow (also termed plug-flow) and parallel flow (either co- or counter-current) types and apply to plate and frame, spiral wound and hollow fibre modules, respectively. Analytic solutions for these different flow schemes have been developed in pioneering work by mainly Weller and Steiner (1950) for binary mixtures and are comprehensively compared by Hwang and Kammermeyer (1975). For multicomponent systems no analytic solutions have been reported, but some simplified analytic or numeric procedures are suggested. Hogsett and Mazur (1983) present a simplified design approach for spiral wound membranes, in which fast and slow permeating gases are lumped together and a log-mean average of the feed and retentate streams is claimed to be empirically accurate enough to determine the partial pressure on the rich side. Rautenbach and Dahm (1985) doubt on the accuracy of this approach and present advanced iterative procedures for all flow patterns. However, such an approach is impractical for

flowsheet calculations since it lacks numerical robustness. For this reason, Pettersen and Lien (1994) developed and validated a simplified design model for hollow-fibre modules in counter-current operation, where the analogy to heat exchangers is exploited. Using the Paterson approximation to the logarithmic mean, they have formulated an algebraic multicomponent model in a quadratic form, from which the permeate molar fraction $\tilde{c}_{ip}$ of a substance i is explicitly calculated by:

$$\tilde{c}_{ip} = \frac{-b_i + \sqrt{b_i^2 - 4a_i c_i}}{2a_i} \tag{4.3}$$

were the parameters a_i, b_i and c_i are combinations of the feed fraction $\tilde{c}_{if}$ and design parameters like the absolute pressure ratio Π_r, the molar stage cut θ and a dimensionless permeation factor R_i, which is also interpreted as a dimensionless area of the membrane:

$$\begin{aligned} a_i = {} & \frac{\Pi_r}{3}\left(\frac{2\theta}{R_i} - \Pi_r\right) + \left(\frac{\theta}{R_i}\right)^2 \\ & + \frac{\theta}{3(1-\theta)}\left(\frac{\theta}{R_i} + \frac{\theta}{12(1-\theta)} - \Pi_r\right) \end{aligned} \tag{4.4}$$

$$\begin{aligned} b_i = {} & \frac{\tilde{c}_{if}}{3}\left(1 + \frac{1}{1-\theta}\right)\left(\Pi_r - \frac{\theta}{R_i}\right) \\ & + \frac{\theta\tilde{c}_{if}}{18(1-\theta)}\left(7 - \frac{1}{1-\theta}\right) \end{aligned} \tag{4.5}$$

$$c_i = \left(\frac{\tilde{c}_{if}}{6(1-\theta)}\right)^2 (\theta^2 + 12\theta - 12) \tag{4.6}$$

with Π_r, θ and R_i defined as:

$$\Pi_r = \frac{p_p}{p_f} \tag{4.7}$$

$$\theta = \frac{\dot{n}_p}{\dot{n}_f} \tag{4.8}$$

$$R_i = \frac{AP_i p_f}{\delta \dot{n}_f} \tag{4.9}$$

In order to compare the quality of the separation for the different flow schemes, the characteristics of a single membrane stage are computed for a typical binary biogas mixture of 60/40% CH_4/CO_2. The selected material is cellulose acetate, which is a commercial membrane used for the removal of CO_2 from natural gas and in enhanced oil recovery (Bhide and Stern, 1993).

P_{CO2}	9.00 barrer	δ	1000 Å
P_{H2}	2.63 barrer		
P_{CH4}, P_{CO}, P_{N2}	0.426 barrer		

Table 4.4—Properties of cellulose acetate membranes (Bhide and Stern, 1993, Phair and Badwal, 2006).

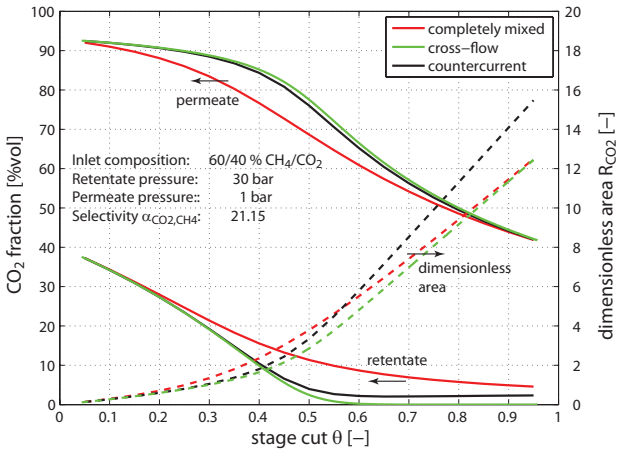

Figure 4.4—Single-stage performance of different membrane unit models.

Typical properties of such membranes, which are available as spiral wound or hollow fibre modules, are given in Table 4.4. As shown in Figure 4.4, considerable differences occur between a completely mixed and the more advanced cross- and countercurrent flow patterns. Especially for stage cuts between 0.2 and 0.6 which provide a reasonable trade-off between purity and recovery, completely mixed modules suffer from the continuous dilution of the retentate with fresh feed. The obtained CH_4-purity is up to 10% lower than in the other cases, and more membrane area is required for a worse separation. The performances of the cross- and countercurrent modules are very similar. Small differences occur only at very high cut rates which are not interesting in practice since not only the fast species but also a large amount of the slow one permeates the membrane. In this domain, the countercurrent retentate contains some residual CO_2 since a log-mean average for its partial pressure across the membrane is used. In a cross-flow scheme, the fast permeator completely diffuses through the module due to the assumption that it is immediately swept away from the membrane surface on the permeate side.

4.3.2 Flowsheet options

In principle, the most general operational scheme of a membrane system is a network of membranes where the permeate and retentate streams of each module can connect to the inlet of all other membranes or mix to the CH_4- or CO_2-rich outlet. All these modules can operate at different feed and permeate pressures, and the most general network definition includes a stream conditioning unit for each connection. If the subsequent stage of an outlet stream is at higher pressure, it requires compression and cooling, while lower pressure allows for power recovery by a reheat and expansion stage. However, as it is generally not advantageous to remix priorly separated species, the membrane stages are typically arranged in cascades where the depleted streams are recycled to a preceding stage of lower purity. Although a systematic problem formulation with a superstructure model solved by mixed integer optimisation (like for example in Girardin et al. (2006)) could have been used, preliminary calculations with a typical biogas mixture of 60/40% CH_4/CO_2 for countercurrent cascades of 1 to 4 stages and simplified schemes with less recycle options have been conducted to better understand the system interactions. The three most promising configurations of the general superstructure depicted in Figure 4.5(a) for the considered membrane properties have been selected for the design study. They include a two-stage countercurrent cascade with the feed location on the CO_2-rich side of stage 1 (Fig. 4.5(b)), a three-stage countercurrent cascade with a splitted feed to the CO_2-rich stage 1 and the intermediate stage 2 (Fig. 4.5(c)), and a simplified three-stage scheme with a common recycle of the depleted permeate streams from the intermediate stage 2 and CH_4-side stage 3 to the CO_2-rich stage 1 (Fig. 4.5(d)). In the preliminary calculations, not only the membrane system configuration, but also its integration in the production plant depicted in Figure 4.3 has been investigated. Especially when the separated streams are valuable products or recovered as combustibles to provide high temperature heat, the quality of the depleted stream(s) is important and depends on the location where it is withdrawn from the membrane system. If CO_2-capture is not considered, the first stage retentate has been identified as the most advantageous location for extracting the diluted mixture. If CO_2 is a valuable by-product, it is promising to withdraw it from the additional enriching stage E1 and use its retentate as fuel. It is further observed that gradually increasing the operating pressure from low to high CH_4-purity stages is advantageous since the gas grid pressure is at higher pressure than the crude gas. Power recovery by expansion of the gas is thus disregarded, and only compression stages of 80% isentropic efficiency are retained for the feed and recycling streams.

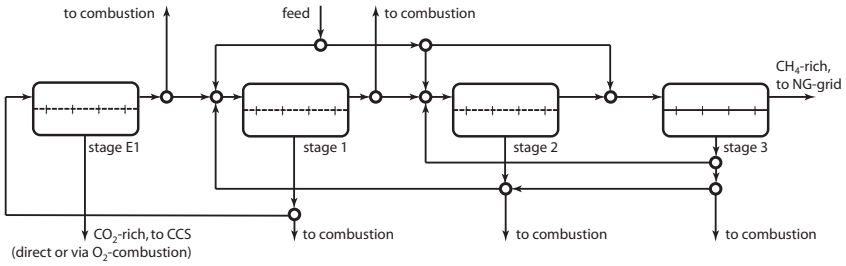

(a) All investigated options of the membrane superstructure.

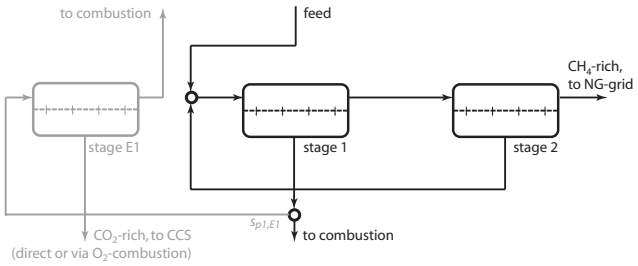

(b) Two-stage, countercurrent recycling.

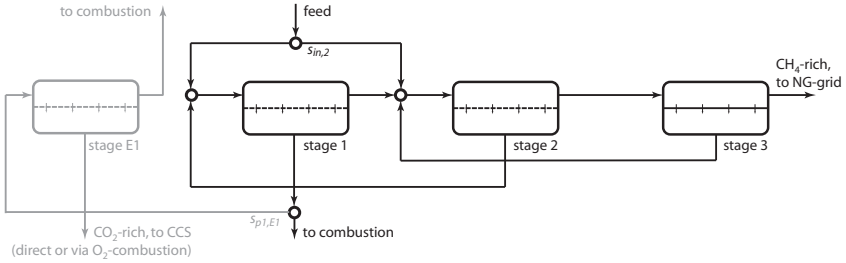

(c) Three-stage, countercurrent recycling.

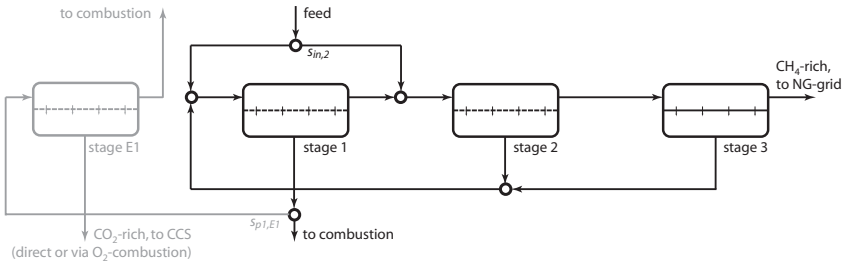

(d) Three-stage, one common recycle loop.

Figure 4.5—All investigated and most promising layouts of the membrane system. The additional stage for CO_2-enrichment (E1, in grey) instead of combusting the permeate of stage 1 is only considered in Section 4.4.4.

4.3.3 Economic model

According to the approach outlined in Chapter 1, the investment cost for the separation system is computed by factoring the cost contributions from the membranes and the compressors to account for other expenses associated with the construction of the plant. The purchase cost of the membranes is assessed by updating the cost data reported by Bhide and Stern (1993), who considered an initial permeator module cost of 108 US\$ m^{-2} and a membrane element cost of 54 US\$ m^{-2} that needs replacement every 3 years. For the compressors, cost data from Turton et al. (1998) for centrifugal compressors and appropriate electric drives are used. The preceding two-column TSA unit for gas drying is sized by assuming a cycle time of 12 h and a maximum adsorbent loading of 0.12 kg_{H2O} $kg^{-1}_{adsorbent}$ (Ducreux et al., 2006). According to Ulrich and Vasudevan (2004), the cost of the adsorbent and its density have been assumed to 9 US\$ kg^{-1} and 800 kg m^{-3}, respectively. Detailed sizing and costing information for all other process units is reported in Chapter 2.

4.4 Design study

4.4.1 Approach

Following the design methodology, the process model is coupled to a multi-objective optimisation algorithm to assess the most promising membrane separation layouts, its operating conditions and the possible energy integration options. In order to highlight the influence of the design strategy, several process optimisations for fixed operating conditions of the crude SNG production are carried out. The flowsheets generated by the optimisation algorithm are then analysed with respect to different sets of performance indicators. A first set of indicators is chosen in order to represent the performance of the isolated separation system, while a second one assesses the performance of the integrated plant. Definitions of these sets are given in Section 4.4.2. Solutions that appear optimal with respect to the different sets of indicators are identified and compared to each other.

In addition to the comparison of the design approach and the assessment of the optimal setup for basic SNG upgrading (Section 4.4.3), the model is explored for the design of a separation system that also produces CO_2 in adequate quality for sequestration (Section 4.4.4).

4.4.2 Performance indicators

Isolated separation system. In order to compare an isolated with a holistic design approach, different sets of thermo-economic indicators representing the performance of the separation system and the overall plant are required. The energetic performance of the membrane separation is assessed by its energy efficiency, defined as (Eq. 4.10):

$$\epsilon^{sep} = \frac{\Delta h^0_{SNG} \dot{m}^-_{SNG}}{\Delta h^0_{crudeSNG} \dot{m}^+_{crudeSNG} + \dot{E}^{sep,+}} \tag{4.10}$$

where superscripts ^{sep} refers to the separation system. As economic indicator, all the costs C_P^{sep} related to the separation are considered. Similar to the definition for the overall system in Equation (1.42), these costs include the investment and operating costs, i.e. the discounted investment $C^{sep}_{GR,d}$, maintenance costs C^{sep}_M, expenses for utilities C^{sep}_{UT} and a cost reflecting the loss of the raw materials' energy content in the depleted stream C^{sep}_{RM} (Eq. 4.11):

$$C_P^{sep} = C^{sep}_{GR,d} + C^{sep}_M + C^{sep}_{UT} + C^{sep}_{RM} \tag{4.11}$$

$$\text{with} \quad C^{sep}_{GR,d} = \frac{(1+i_r)^n - 1}{i_r(1+i_r)^n} \, \frac{C^{sep}_{GR}}{P_a} \tag{4.12}$$

$$C^{sep}_M = 0.05 \, \frac{C^{sep}_{GR}}{P_a} \tag{4.13}$$

$$C^{sep}_{UT} = \frac{\dot{E}^{sep,+}}{\Delta h^0_{SNG} \dot{m}^-_{SNG}} \, C_{el} \tag{4.14}$$

$$C^{sep}_{RM} = \left(\Delta h^0_{crudeSNG} \dot{m}^+_{crudeSNG} - \Delta h^0_{SNG} \dot{m}^-_{SNG}\right) \, C_{SNG} \tag{4.15}$$

where C^{sep}_{GR} stands for the initial investment, P_a for the yearly SNG production, i_r for the interest rate and n for the discount period of the plant.

Integrated plant. For evaluating the performance of the entire plant, the energy efficiency ϵ of Equation (1.30) and the total production cost C_P as defined in Equations (1.36) - (1.42) is used. Compared to C_P^{sep}, the economic evaluation of the overall process with C_P is completed by a term for operating labour and the actual expenses for wood are used as cost for the raw material instead of accounting for the gas loss in the separation. As already before, Equations (4.11) - (4.15) and (1.36) - (1.42) are evaluated with the parameters given in Table 2.6.

Operating conditions		Unit	2-stage	3-stage
Stage cut of stage 1	θ_1	-	[0.2 0.5]	[0.2 0.6]
Stage cut of stage 2	θ_2	-	-	[0.2 0.6]
Stage cut of stage E1[a]	θ_{E1}	-	[0.2 0.8]	[0.2 0.8]
Permeate pressure of stage 1	p_{p1}	bar	[1 5]	[1 5]
Permeate pressure of stage 2	p_{p2}	bar	[1 5]	[1 5]
Permeate pressure of stage 3	p_{p3}	bar	-	[1 5]
Permeate pressure of stage E1[a]	p_{pE1}	bar	[0.2 0.8]	[0.2 0.8]
Feed pressure of stage 1	p_{f1}	bar	[5 50]	[5 50]
Feed pressure of stage 2	p_{f2}	bar	[5 50]	[5 50]
Feed pressure of stage 3	p_{f3}	bar	-	[5 50]
Fraction of feed to stage 2	$s_{in,2}$	-	-	[0 1]
Fraction of permeate 1 to E1[a,b]	$s_{p1,E1}$	-	-	[0 1]

[a] CCS only (Section 4.4.4).

[b] direct capture only.

Table 4.5—Decision variables of the membrane system.

4.4.3 Optimal design of the SNG upgrading system

The optimal design of the SNG upgrading system to 96%vol pure CH_4 is performed for the fixed base case conditions of the crude gas production Table 4.2. The decision variables are therefore chosen among the operating conditions of the membranes system. In all cases, they include the stage cuts of each stage but the last (CH_4-rich) one as well as the total pressure on the permeate and the feed sides. For the three-stage layouts, the fraction of the inlet stream that is fed to stage 2 is furthermore considered as a decision variable. The search space for all decision variables is given in Table 4.5.

The objective functions used in the mathematical problem formulation must allow for generating a complete set of optimal solutions with respect to the selected performance indicators. In the present case, maximising the SNG recovery r_{SNG} (Eq. 4.16) and minimising both the specific power consumption e^{sep}_{spec} (Eq. 4.17) and the investment cost of the separation system C^{sep}_{GR} have proven to be adequate and efficient for this purpose:

$$r_{SNG} = \frac{\Delta h^0_{SNG} \dot{m}^-_{SNG}}{\Delta h^0_{crudeSNG} \dot{m}^+_{crudeSNG}} \tag{4.16}$$

$$e^{sep}_{spec} = \frac{\dot{E}^{sep,+}}{\Delta h^0_{crudeSNG} \dot{m}^+_{crudeSNG}} \tag{4.17}$$

The numeric optimisation results are shown in Figure 4.6 as two-dimensional projections of the three-dimensional objective space. The plots show

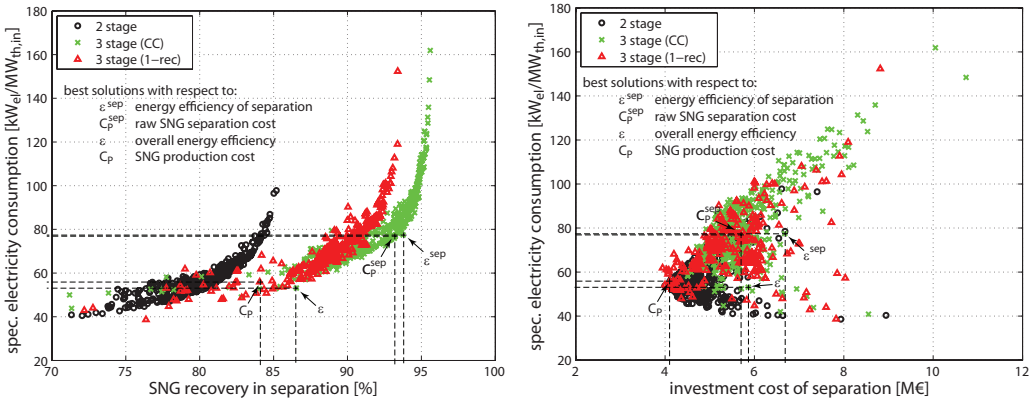

Figure 4.6—Projections of the Pareto-optimal solutions of the separation system: trade-off between SNG recovery and power consumption (left) and investment cost and power consumption (right).

that the SNG recovery and specific power consumption are clearly conflictive, whereas no general trend is observed for the investment cost. For high recovery ratios, the latter is positively correlated with the specific power consumption since it is dominated by the need for powerful compressors. For low recoveries, this trend is reversed by the increasing cost for larger membrane areas that are necessary to achieve higher stage cuts. Comparing the different layouts, it is observed that a two-stage system limits the SNG recovery to about 85%, while more than 95% are achievable with a countercurrent three-stage system. The limit of the alternative three-stage layout with one recycle is at about 93% recovery. However, for values above 90%, its specific power consumption is clearly higher than the one of the countercurrent scheme.

Figure 4.7 shows the thermo-economic performance indicators for the separation system and the total process. Details of the optimal solutions with respect to energy efficiency and production cost are given in Tables 4.6 and 4.7, respectively. Considering the isolated performance of the separation system (plots and columns on the left), it is observed that all membrane layouts pass through an optimal value for the SNG recovery with respect to efficiency and cost. At low recovery levels, the performance suffers from elevated gas losses, whereas at high recoveries, the power consumption and cost of the compression get excessive. The two-stage scheme is clearly suboptimal due to its lowest recovery level. Although the three-stage systems are close for a large recovery range, the countercurrent scheme performs best since highest recoveries are attained. At values of 93.2% and 93.8%, it reaches a minimum separation cost and maximum efficiency of 32.4 € MWh^{-1} and 87.0%,

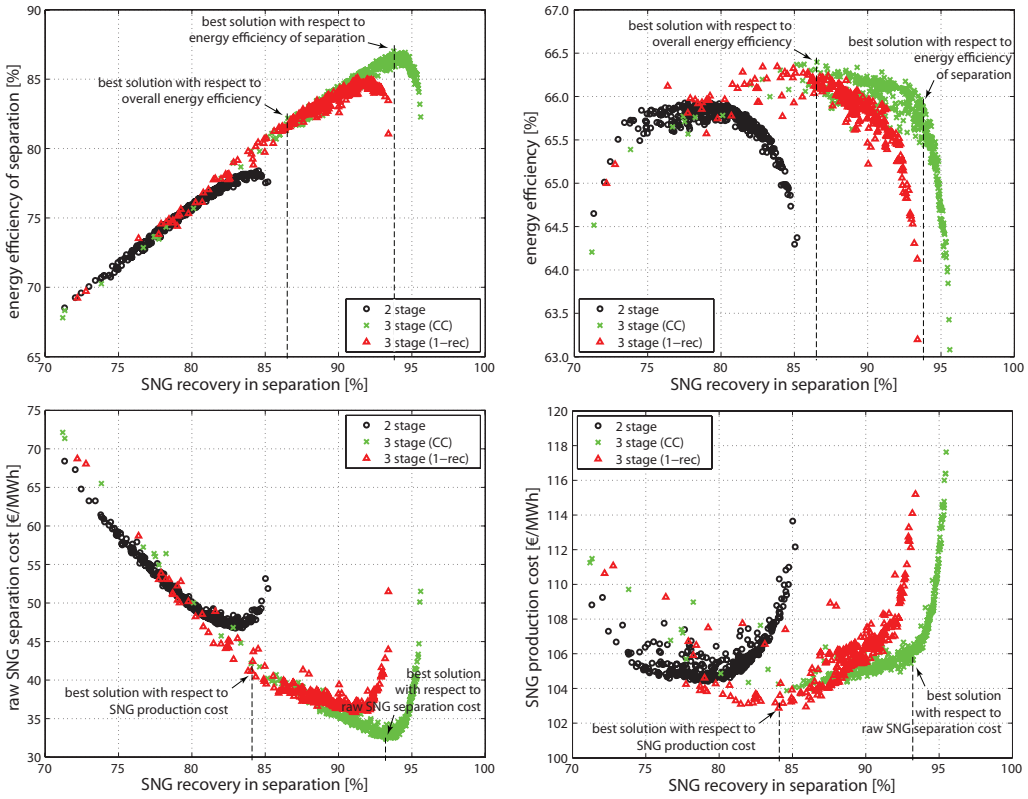

Figure 4.7—Energy efficiency (top) and production costs (bottom) of the separation system (left) and the total process (right).

respectively. Comparing the generated solutions with respect to the overall performances (plots and columns on the right), it is observed that the slope of the curves are flatter and that increasing the recovery above 85% does not have any beneficial effect. When considering the integrated system, both the operating conditions and system layout are changed. As indicated in Tables 4.6 and 4.7, the value of $s_{in,2}$ shows that the best feed location switches from stage 2 to 1. Rather than using a countercurrent scheme, the most efficient and economic solutions are obtained with the three-stage one-recycle layout at 83.8% and 84.1% SNG recovery, respectively. Implementing the optimal solution suggested by the analysis of the isolated performance of the separation system (i.e. a three-stage countercurrent scheme with 93.2-93.8% recovery) would thus lead to a suboptimal system solution. The data in the tables shows that the membrane area would be oversized by 58-60%, leading to investment costs that are 39-46% higher than for the global optimum.

These results clearly indicate that the depleted permeate stream is not lost and its quality is sufficient to be valuable as hot utility. As shown

		Optimal process with respect to:					
		separation system			overall plant		
		2s	3s, 1-rec	3s, CC	2s	3s, 1-rec	3s, CC
θ_1	-	0.28	0.32	0.57	0.46	0.39	0.38
θ_2	-	0.72	0.58	0.47	0.46	0.33	0.44
θ_3	-	-	0.48	0.55	-	0.34	0.38
p_{p1}	bar	1.0	1.1	1.0	1.0	1.0	1.3
p_{p2}	bar	1.0	3.8	2.1	1.0	2.2	2.9
p_{p3}	bar	-	1.1	1.2	-	1.0	1.3
p_{f1}	bar	15.5	11.7	12.2	16.6	14.8	11.0
p_{f2}	bar	49.5	26.0	21.4	49.8	35.9	27.3
p_{f3}	bar	-	49.4	47.0	-	44.5	42.0
$s_{in,2}$	-	-	0.94	1.00	-	0.02	0.07
r_{SNG}	%	84.5	91.3	93.8	78.0	83.8	86.5
e^{sep}_{spec}	$kW_{el}MW^{-1}_{th}$	78.5	72.9	77.4	49.1	50.7	53.1
C^{sep}_{GR}	M€	6.7	7.0	6.7	4.4	4.6	5.9
$\tilde{c}_{CO2,p}$	%	79.9	85.0	86.9	75.8	79.7	81.5
$\tilde{c}_{H2,p}$	%	9.9	10.2	10.4	9.2	9.5	9.8
$\tilde{c}_{CH4,p}$	%	9.9	4.6	2.5	14.6	10.5	8.5
A	m^2	6024	7317	6537	3911	4129	6490
C^{sep}_P	€ MWh^{-1}	49.1	36.7	33.2	52.2	41.2	38.9
$\Delta h^0 \dot{m}$							
- dry wood	MW	20.0	20.0	20.0	20.0	20.0	20.0
- crude SNG	MW	15.0	14.0	13.7	16.1	15.1	14.7
- grid SNG	MW	12.7	12.8	12.9	12.6	12.7	12.7
$\dot{E}^{sep,+}$	MW	1.18	1.02	1.06	0.79	0.77	0.78
$\dot{E}^{-}$	MW	0.28	0.35	0.31	0.63	0.59	0.55
ϵ^{sep}	%	78.4	85.1	87.0	74.4	79.8	82.2
ϵ	%	64.9	65.9	65.9	65.9	66.3	66.4
C_{GR}	M€	32.5	32.2	31.7	30.9	30.3	31.4
C_P	€ MWh^{-1}	110.8	108.2	107.6	104.5	103.2	105.0

Table 4.6—Decision variables, objectives, performance indicators and key properties of best designs with respect to energy efficiency.

		Optimal process with respect to:					
		separation system			overall plant		
		2s	3s, 1-rec	3s, CC	2s	3s, 1-rec	3s, CC
θ_1	-	0.35	0.40	0.56	0.44	0.39	0.45
θ_2	-	0.62	0.58	0.52	0.48	0.40	0.44
θ_3	-	-	0.39	0.46	-	0.24	0.32
p_{p1}	bar	1.0	1.1	1.0	1.0	1.0	1.1
p_{p2}	bar	1.0	3.8	3.0	1.1	2.2	4.3
p_{p3}	bar	-	1.1	1.1	-	1.4	1.8
p_{f1}	bar	17.4	20.1	12.1	22.8	24.4	23.5
p_{f2}	bar	49.9	49.7	35.9	47.7	49.0	49.5
p_{f3}	bar	-	49.9	50.0	-	49.0	50.0
$s_{in,2}$	-	-	0.94	0.98	-	0.00	0.21
r_{SNG}	%	83.0	91.2	93.2	79.3	84.1	85.6
e^{sep}_{spec}	$kW_{el}MW^{-1}_{th}$	63.9	80.2	76.9	54.2	55.9	60.0
C^{sep}_{GR}	M€	5.3	5.4	5.7	4.3	4.1	4.6
$\tilde{c}_{CO2,p}$	%	78.9	85.0	86.6	76.6	79.9	80.8
$\tilde{c}_{H2,p}$	%	9.7	10.1	10.3	9.3	9.4	9.7
$\tilde{c}_{CH4,p}$	%	11.1	4.8	3.0	13.7	10.4	9.2
A	m^2	4423	3712	4675	3304	2928	3466
C^{sep}_P	€ MWh^{-1}	46.7	35.8	32.4	50.6	41.2	40.0
$\Delta h^0 \dot{m}$							
- dry wood	MW	20.0	20.0	20.0	20.0	20.0	20.0
- crude SNG	MW	15.3	14.1	13.8	15.9	15.1	14.9
- grid SNG	MW	12.7	12.8	12.9	12.6	12.7	12.7
$\dot{E}^{sep,+}$	MW	0.98	1.13	1.06	0.86	0.84	0.89
$\dot{E}^{-}$	MW	0.45	0.32	0.35	0.59	0.56	0.52
ϵ^{sep}	%	78.0	84.4	86.6	75.2	79.6	80.7
ϵ	%	65.6	65.7	66.0	65.9	66.2	66.2
C_{GR}	M€	31.2	30.6	30.7	30.6	29.9	30.2
C_P	€ MWh^{-1}	106.5	106.1	105.6	104.4	102.9	103.7

Table 4.7—Decision variables, objectives, performance indicators and key properties of best designs with respect to production cost.

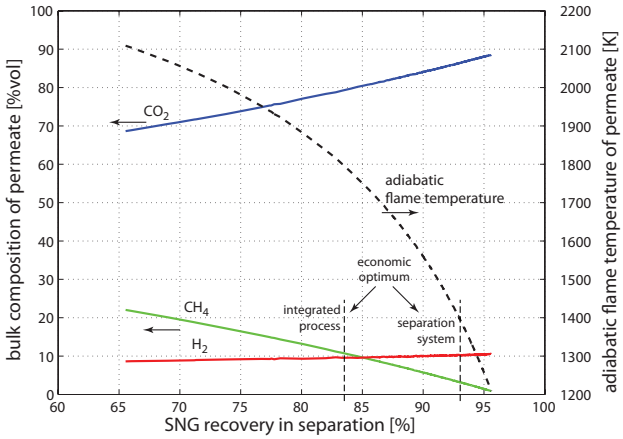

Figure 4.8—Molar composition and adiabatic flame temperature of the permeate stream.

in Figure 4.8, it still contains a considerable amount of methane beneath the hydrogen that permeates very fast in the cellulose acetate membrane. The adiabatic flame temperature of the stream is therefore high enough to transfer heat to the gasification reactor, which is illustrated by the energy flow diagram depicted in Figure 4.9. At 95% recovery, 19.9% of the chemical energy content of the producer gas is directly used as utility, 11.0% is lost as methanation reaction heat, 3.5% is used as utility in the form of depleted membrane permeate and 65.6% is present as final product. At 85% recovery, only 11.7% of the producer gas is withdrawn from the process stream, and the share of the depleted membrane permeate used as utility is close to 50%. Although this results in a decreasing utility demand from 23.4% to 23.1% due to the more advantageous combustion properties of the permeate, a slight decrease to 64.7% of final product is caused by an increase of the methanation reaction heat loss to 12.2%. At about 75%, the complete heat demand of the gasifier is satisfied by the membrane permeate, and no more savings of producer gas can be obtained below.

4.4.4 Process optimisation for CO_2 capture

In the previous sections, the design of the separation system is only focussed on the upgrading of the main product to grid quality and the CO_2-rich stream is considered as waste. In order to prevent the emission of the remaining highly active greenhouse gas CH_4 to the atmosphere, the final membrane permeate is completely oxidised. In the most economic designs, the purity

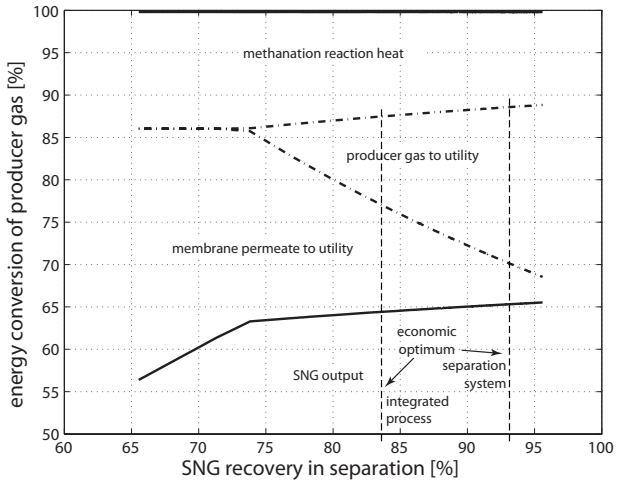

Figure 4.9—Conversion of the chemical energy in the producer gas through the system.

of the CO_2 in this stream does thereby not exceed 80%, which allows for recovering its heating value at a sufficiently high temperature to be useful for the process.

A priori, the elevated amount of CO_2 in the bulk composition of the crude SNG encourages for producing not only SNG, but also recovering the CO_2 as a by-product. In case of SNG production from biomass, applying carbon capture and storage (CCS) would thereby turn the process into an atmospheric CO_2-sink if the resource is exploited in a sustainable way (i.e. no deforestation and limited impact from biomass processing). In fact, the complete oxidation of biogenic carbon does not produce net emissions of CO_2, since it has previously been extracted through photosynthesis during plant growth and the carbon cycle is closed. When the reemission of CO_2 is partly prevented by its capture at the conversion plant and sequestration, the net balance of emitted greenhouse gases becomes indeed negative considering the entire life cycle of the product.

In order to facilitate approaching a typical purity requirement of 95% for CCS, preliminary calculations suggest to complete the membrane process layout with an enriching stage of the same material. As shown in Figures 4.5(b)-(d), the retentate of the additional stage E1 is thereby not recycled to the stripping section (stage 1), but withdrawn from the membrane system. The separation of the main product is thus not additionally loaded by diluting the feed, and the heating value of the low-value retentate of stage E1 can be used as utility with more advantageous fuel properties

than the originally used permeate from stage 1. To attain the purity requirement for sequestering the permeate from E1, two strategies are envisaged. On the one hand, it could be directly brought to sufficient purity and captured, including the residual H_2, CH_4 and minor amounts of CO and N_2. Alternatively, the residual H_2, CH_4 and CO may be completely oxidised to CO_2, in which case the captured CO_2 is only accompanied by 5%vol of inert N_2. As shown in Figure 4.3, this can be done by catalytically combusting the E1-permeate with enriched air, for which the required oxygen is obtained through electrolysis. The by-produced H_2 can thereby be fed to the methanation and results in an increase of the SNG yield (Gassner and Maréchal, 2008).

In order to find optimal process configurations for CCS, the multi-objective optimisation strategy is applied to the most promising layouts. As objectives, the amount of captured carbon per total carbon in the biomass feed (hereafter termed as carbon capture ratio) is maximised while the production cost defined in Equation (1.42) for SNG including CCS is minimised. Like in Section 4.4.3, base case conditions for the crude gas production are assumed and the same decision variables for the stripping section are considered (Table 4.5). Figure 4.10 shows the computed impact of the carbon capture on the production cost of SNG and the process efficiency, as well as the specific power consumption and cost for the recovery of 95% pure CO_2 at atmospheric pressure and temperature. In Table 4.8, the operating conditions and performance of some selected process designs that are highlighted in Figure 4.10 are given.

For small amounts of captured carbon, direct capture without catalytic combustion proves to be better. Since no additional equipment for electrolysis and catalytic combustion is needed and only additional membrane surface and compression power is required, the production cost increases and the energy efficiency decreases almost continuously from the best solution without capture. When the capture ratio reaches about 15%, it becomes more and more difficult to attain the purity requirement, the penalties on cost and efficiency increase considerably and direct capture gets suboptimal. At higher capture ratios, catalytic combustion with enriched air becomes profitable due to the less strict purity requirement of the permeate and the advantage of recovering its heating value. For this setup, the cost and efficiency penalty increases considerably from about 30% onwards. At this ratio, the flame temperature of enriched air combustion also begins to exceed the pinch point of the process and the stream must be used as a heat service for the gasification. The gasifier design would thus become more complex since heat needs to be supplied from two physically separated combustion chambers (one with normal, one with enriched air). At this technological barrier, 30% of carbon

Mode of capture, selection criteria[a]		A	B	C	D
θ_1	-	0.39	0.35	0.41	0.37
θ_2	-	0.40	0.43	0.34	0.35
θ_3	-	0.24	0.28	0.27	0.36
θ_{E1}	-	-	0.35	0.48	0.63
p_{p1}	bar	1.0	2.2	3.4	3.6
p_{p2}	bar	2.2	2.4	2.1	3.0
p_{p3}	bar	1.4	1.1	1.1	1.3
p_{pE1}	bar	-	1.1	1.1	1.2
p_{f1}	bar	24.4	27.0	33.9	32.8
p_{f2}	bar	49.0	49.3	47.1	45.2
p_{f3}	bar	49.0	49.9	49.1	48.6
p_{fE1}	bar	-	12.1	6.7	13.8
$s_{in,2}$ and $s_{p1,E1}$	-	0	0	0	0
r_{SNG}	%	84.1	85.5	82.2	83.8
e^{sep}_{spec}	$\mathrm{kW}_{el}\mathrm{MW}^{-1}_{th}$	55.9	71.2	63.7	69.4
C^{sep}_{GR}	M€	4.1	5.0	4.9	5.1
$\tilde{c}_{CO2,p}$	%	79.9	95.0	93.6	93.0
$\tilde{c}_{H2,p}$	%	9.4	4.3	5.1	5.6
$\tilde{c}_{CH4,p}$	%	10.4	0.7	1.3	1.3
A	m^2	2928	3253	3516	3532
C^{sep}_P	€ MWh^{-1}	41.2	43.0	47.4	46.0
$\Delta h^0_{wood}\dot{m}^+_{wood}$	MW	20.0	20.0	20.0	20.0
$\Delta h^0_{crudeSNG}\dot{m}^+_{crudeSNG}$	MW	15.1	15.0	15.6	15.4
$\Delta h^0_{SNG}\dot{m}^-_{SNG}$	MW	12.7	12.8	12.8	12.9
$\dot{E}^{sep,-}$	MW	0.84	1.07	0.99	1.07
$\dot{E}^-$	MW	0.56	0.29	0.27	0.11
ϵ^{sep}	%	79.6	79.8	77.3	78.3
ϵ	%	66.2	65.5	65.3	65.0
C_{GR}	M€	29.9	30.6	31.2	31.4
C_P	€ MWh^{-1}	102.9	106.8	108.0	109.9
carbon capture ratio	%	-	16.2	23.4	29.8
carbon in SNG	%	34.7	35.0	35.0	35.3
carbon emitted on site	%	65.3	48.8	41.6	34.9
$C^{electrolysis\ \&\ cat.\ comb.}_{GR}$	k€	-	-	189	302
rel. increase of C_{GR}	%	-	2.4	4.3	5.0
spec. power for CCS	$\mathrm{kWh}_{el}\mathrm{ton}^{-1}_{CO2}$	-	234	172	208
C_{CO2} (180 € MWh^{-1}_{el})	€ ton^{-1}_{CO2}	-	42.5	38.8	41.6
C_{CO2} (40 € MWh^{-1}_{el})	€ ton^{-1}_{CO2}	-	9.8	14.7	12.5

[a] A: no capture, min. C_P; B: direct capture, min. C_P; C: capture via cat. comb. with enriched air, min. C_P; D: capture via cat. comb. with enriched air, techn. barrier.

Table 4.8—Decision variables, objectives, performance indicators and key parameters of selected designs for CCS in comparison with the reference solution without capture.

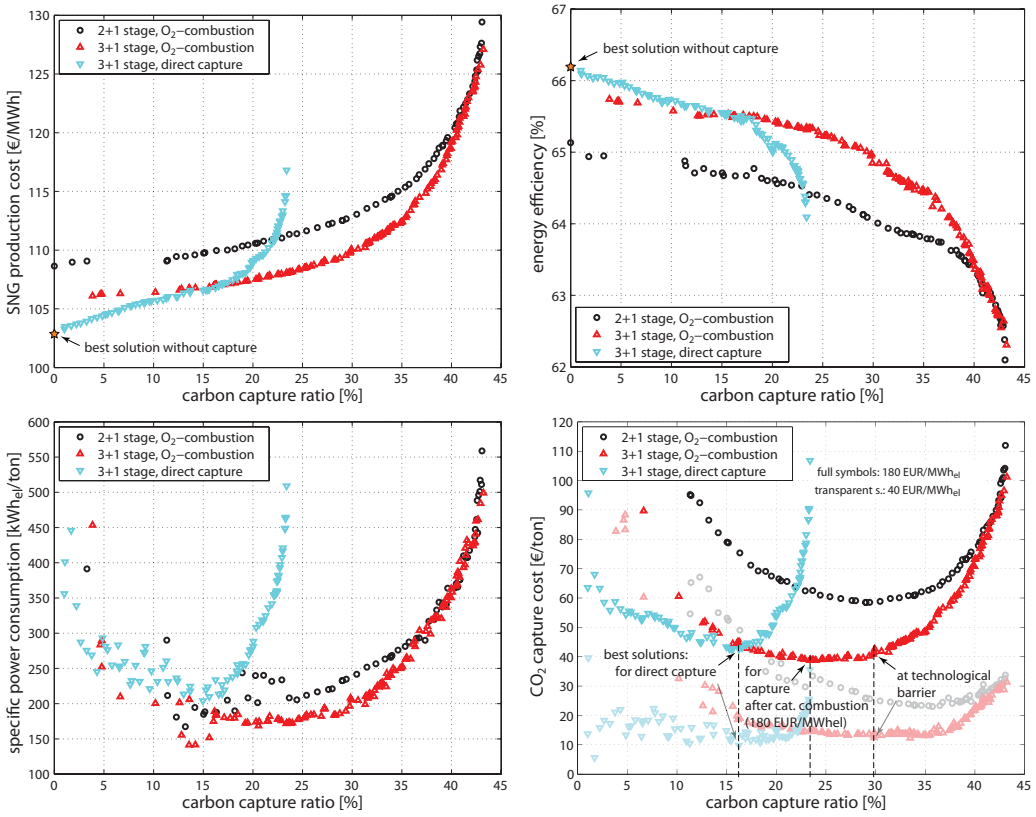

Figure 4.10—Pareto-optimal solutions for CO_2-capture (top, right) and its impact on the process efficiency (top, left). Specific electricity consumption (bottom, left) and relative cost (bottom, right) of capture for two different electricity prices.

contained in the biomass is captured, 35% of the carbon leaves the process as SNG and 35% is released to the environment in the on-site flue gas.

If the specific cost and power consumption per ton of CO_2 is considered, the optimal carbon capture ratio lies around 15% for direct capture and at 25-30% for capture after catalytic combustion. At these ratios, the net specific power consumption for CO_2 purification is in the order of 200 kWh ton^{-1}, and the process efficiency is decreased by 0.5-1%. The cost of capture is therefore strongly dependent on the cost of electricity. If a price of 180 € MWh^{-1} for green electricity is considered, the share of expenses for electricity contributes to more than 80% at the optimal capture ratios, the rest being related to the additional investment. If typical electricity generation costs of 40 € MWh^{-1} for new coal and natural gas power plants without CCS are assumed (Meth et al., 2005), the cost of captured – and avoided – CO_2 drops from 40 € ton^{-1} to below 15 € ton^{-1}. This value is considerably lower than

the ones compiled by Meth et al. (2005) for CCS from fossil fuel power plants. It is therefore potentially more economic to do CCS via an SNG plant that doing the capture at the power plants itself, and trading CO_2 certificates could be used as a way to increase the profitability of the SNG production.

4.5 Conclusions

By implementing a thermo-economic model for multicomponent membrane gas separation in the process model for SNG production, different design approaches for SNG upgrading to grid quality have been compared. Using multi-objective optimisation, it has been shown that the resulting system design and performance depends markedly on the level of process integration that is implemented. If the interactions between the separation system and the reactive parts of the process are disregarded and only the isolated performance of the separation system is considered, the size, cost and electricity consumption of the separation are significantly exaggerated. By including the process integration in the design problem, advantage is taken from using depleted gas from the separation as utility and less product recovery is required. For the considered membrane properties and design constraints, a globally optimal system recovers only about 84% instead of 93% of the crude SNG and satisfies about 50% of the heat demand with depleted membrane permeate.

Finally, different strategies for simultaneously purifying the by-produced CO_2 to fulfil the requirements for long-term storage have been investigated. It has been shown that completely oxidising the residual CH_4, H_2 and CO in a catalytic combustion with enriched air from electrolysis is promising. This is because less effort must be put into the gas separation, the heating value of the residues is recovered and the by-produced hydrogen increases the SNG yield. The cost of captured and avoided CO_2 is strongly dependent on the cost of electricity and lies in the range of 15 to 40 € ton^{-1}, which is lower than the cost for avoiding CO_2 at a fossil power plant. Capturing CO_2 at the SNG plant using electricity from a centralised power plant is thus potentially more economic than investing in an end-of-pipe capture at the power plant.

Chapter 5

Prospects of site-scale integration

This chapter concludes the discussion of the energy and process integration aspects by an outlook to site-scale integration of combined ethanol and SNG production from lignocellulosic biomass.

5.1 Ethanol production from lignocellulosic biomass

In the public and scientific debate on biofuels, ethanol from lignocellulosic biomass is one of the most popular alternatives that may allow for a sustainable production. Compared to thermochemical processing of biomass which assures a complete conversion of the feedstock, it yet suffers from an inherently lower fuel yield since lignin resists to biological degradation.

Following the method outlined in this thesis, Zhang et al. (2009) recently developed a process model for fuel ethanol production from lignocellulosic biomass based on double acid hydrolysis. According to the block flow diagram of the principal process steps depicted in Figure 5.1 (left), Zhang et al. modelled the biomass hydrolysis in two stages at 155-165°C with conversion yields of 80%, 70% and 10% for the degration of cellulose to glucose, hemicellulose to xylose and further to furfural, respectively. After removing the suspended solids, glucose and xylose are then fermented to ethanol and CO_2 at conversion yields of 95% and 60%, respectively. The distillation is carried out in three columns, where ethanol is subsequently concentrated from 2.7%wt to 40% and further to the azeotrope at 95%wt, from which it is rectified with cyclohexane as entrainer to 99.5%wt. After recovery of the residual ethanol and cyclohexane by stripping, 90% of the organic matter in the wastewater is recovered as biogas by anaerobic digestion. For these conversions, the composite curve in Figure 5.1 (right) assesses a minimum en-

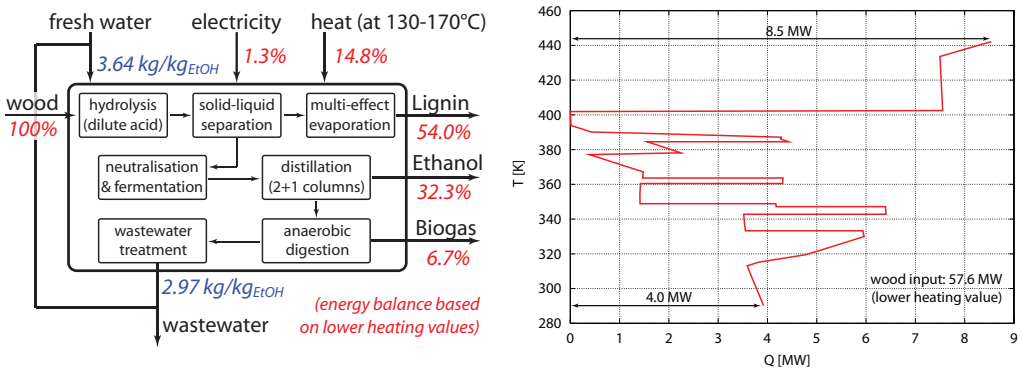

Figure 5.1—Principal mass and energy balances of ethanol production according to the model of Zhang et al. (2009).

ergy requirement (MER) at 130-170°C of roughly 15% of the biomass input, which also includes the multi-effect evaporation from 75 to 35%wt humidity of the lignin-rich slurry recovered from hydrolysis. With a dry biochemical composition of 12.3%wt hemicellulose, 25.9%wt cellulose and 61.8%wt lignin, this residue represents more than 50% of the feedstock's chemical energy due to the modest yields assumed in hydrolysis and fermentation.

5.2 Energy integration and recovery

5.2.1 Conventional combustion and power cogeneration

The most straightforward use of the residual lignin slurry and biogas is to supply the process MER by combustion and cogenerate power from the excess heat in a steam Rankine cycle, which is the solution proposed in NREL's reference design (Aden et al., 2002). Despite the considerable heat demand of distillation, Figure 5.2(a) highlights that combustion of the residues generates a lot of excess heat which is recovered at a very modest efficiency. Assuming a single steam production level at 80 bar (295°C), superheating to 550°C, steam utilisation at 14.9 bar (198°C) and 3.6 bar (140°C) and condensation at 0.02 bar (20°C), the energy balance of Table 5.1 assesses a net partial electric efficiency of 17.1% based on the overall plant input, which corresponds to an electricity yield of roughly 34% from the residuals. In this configuration, the Rankine cycle operates largely independent of the ethanol plant and an important amount of energy is lost in the cooling water due the exergy losses in the heat recovery. Benefits from process integration are small.

Lignin use	combustion	gasification	SNG (gasification & methanation)		
	steam cycle	comb. cycle	-	steam cycle	& heat pumps
Fig.	5.2(a)	5.2(b)	5.2(c)	5.3(b)	5.3(c)
ϵ_{EtOH}	32.3%	32.3%	32.3%	32.3%	32.3%
ϵ_{SNG}	-	-	40.3%	35.2%	41.9%
ϵ_{el}	17.1%	21.5%	-3.0%	1.9%	-0.5%
ϵ	49.4%	53.8%	70.5%	69.4%	73.6%
ϵ_{chem}	62.3%	70.0%	67.3%	70.8%	73.2%
η	52.5%	56.9%	74.9%	73.8%	78.5%

Table 5.1—Screening of partial and total efficiencies defined by Equations (1.30) to (1.35) for different lignin valorisation and process integration options (without any optimisation).

5.2.2 Gasification alternatives

Compared to the chemical energy potential of the residuals, the process heat demand is relative small and cogeneration technologies with a low heat share are thus preferable. For this purpose, the use of an integrated gasification combined cycle (IGCC) has been investigated by Hamelinck et al. (2005) and later also Laser et al. (2009a). By generating power from the producer gas in a gas turbine, the exergy losses at high temperature are reduced and the total power output thus increased (cf. Fig. 5.2(b)). With a topping cycle design similar to the one proposed by Brown et al. (2009), IGCC based on pressurised, oxygen blown gasification allows for increasing the power cogeneration from 17.1% to 21.5% of the total biomass input compared to a simple steam Rankine cycle.

In order to increase the overall fuel yield, a second alternative would be to thermochemically convert the residual lignin slurry to other liquid or gaseous products. Compared to the power generation options discussed in the previous sections, the share of excess heat of this processes is generally lower, and less exergy losses are thus expected in the conversion. While Laser et al. (2009b) discuss scenarios for the coproduction of Fischer-Tropsch fuels, dimethyl ether or hydrogen, we briefly explored the suitability of SNG production at a case based on conventional indirectly heated gasification (Zhang et al., 2009). As illustrated by the composite curve of Figure 5.2(c), the excess heat available from the conversion of the residual lignin slurry into SNG matches well with the requirement for ethanol distillation. Together with the sensible heat of the producer gas and fumes, the excess heat from the exothermal methane synthesis just balances with the demand for ethanol production, and the total cooling requirement equals the strict MER assessed

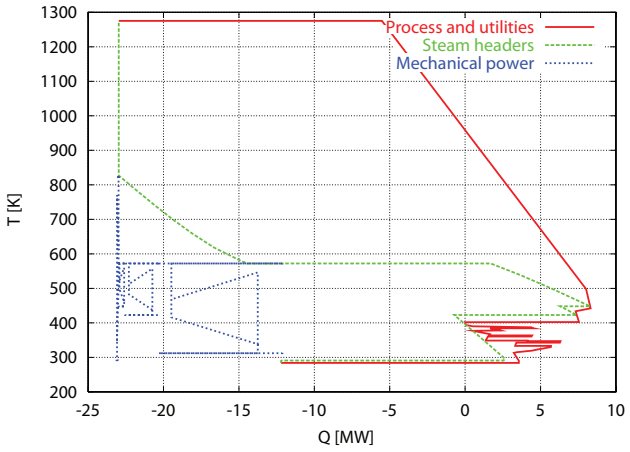

(a) Combustion and steam cycle.

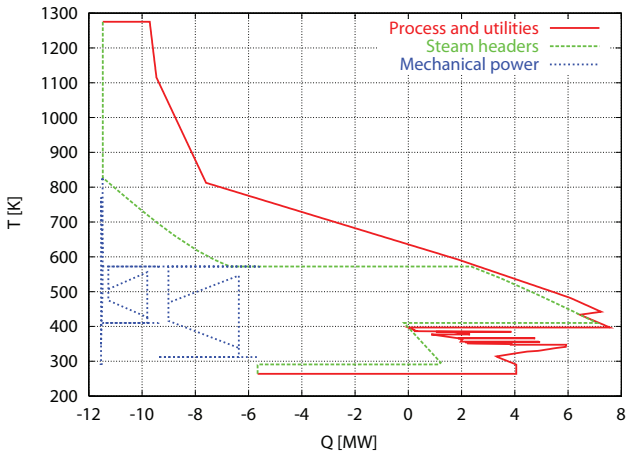

(b) IGCC (gasification, gas turbine and steam cycle).

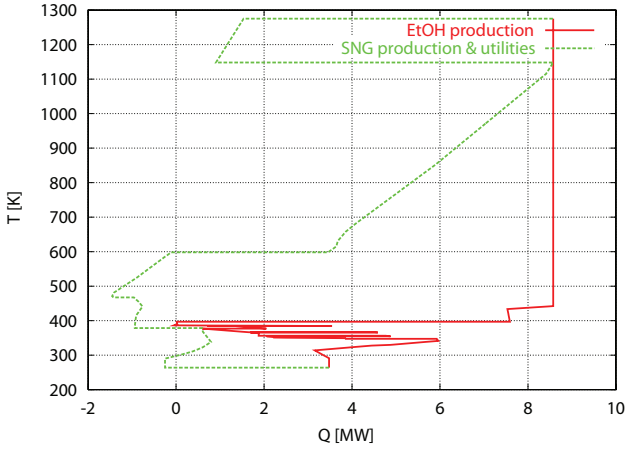

(c) SNG production (gasification and methanation).

Figure 5.2—Composite curves for different alternatives of lignin valorisation in the production of ethanol from wood (biogas is combusted in all cases).

in Figure 5.1. In this setup, SNG production allows for increasing the combined fuel yield to over 70%. However, no excess excess heat is available for power cogeneration and an equivalent net amount of 3% of the biomass input is consumed by the process (Tab. 5.1).

5.2.3 A paradox of energy and exergy

Transforming the section composite curves of Figure 5.2(c) into a single grand composite curve of Figure 5.3(a) reveals a paradoxal situation in waste heat recovery: Although high-temperature exergy is potentially available, there is no heat excess in the system for its extraction as mechanical power. Cogeneration is thus limited by the first law of thermodynamics and not, as usual, by the second. In order to overcome this limitation and valorise the exergy potential at high temperature, energy must be supplied to the system above the process pinch at 104℃.

One alternative is the combustion of additional producer gas to not only satisfy the pinch at gasification temperature, but also provide supplementary energy for power cogeneration. Such a situation is illustrated in Figure 5.3(b). As just as much energy to extract the exergy potential of the high-temperature streams is supplied, a marginal electric efficiency $\Delta\epsilon_{el}/\Delta\epsilon_{SNG}$ of 96% is obtained since no thermodynamic, but only thermal and mechanical losses in the boiler and turbomachinery occur. The according energy balances of Table 5.1 highlight that this allows for a gross power generation of roughly 5% of the total biomass input and results in an overall positive balance of the integrated plant.

Another, thermodynamically more promising alternative is to supply the required energy not by combustion of producer gas, but by heat pumping across the low temperature pinch. While combustion only transforms the chemical energy of an intermediate product without second-law losses into power, heat pumping adds more energy from below the process pinch – or the environment – above the process pinch. This allows for generating a net supplement of useful energy in the form of power, and not just the conversion of chemical into mechanical energy. The prevailing temperature profiles enable water as working fluid of two heat pump cycles from 68 to 107℃ (0.28 to 1.29 bar) and 91 to 128℃ (0.72 to 2.53 bar). With a combined shaft power of only 560 kW_{el}, these cycles provide 3.9 MW_{th} above the pinch, which allows the power cycle to extract 2.0 MW_{el} of the available high-temperature exergy. Overall, the net recovery of 1.4 MW_{el} almost balances the electricity demand of the plant. At the same time, the SNG yield is not only constant but even increased, since the heat pumps also substitute heat that

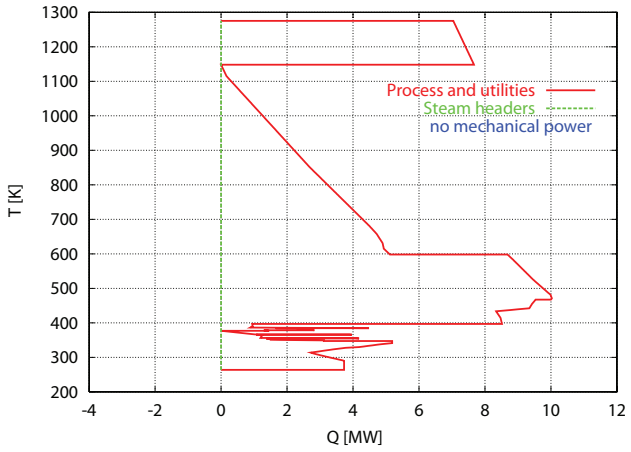

(a) Without exergy recovery (identical to Fig. 5.2(c)).

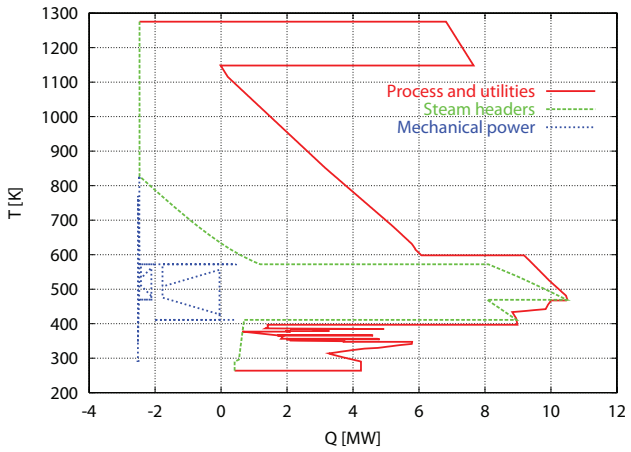

(b) Steam cycle with partial producer gas combustion.

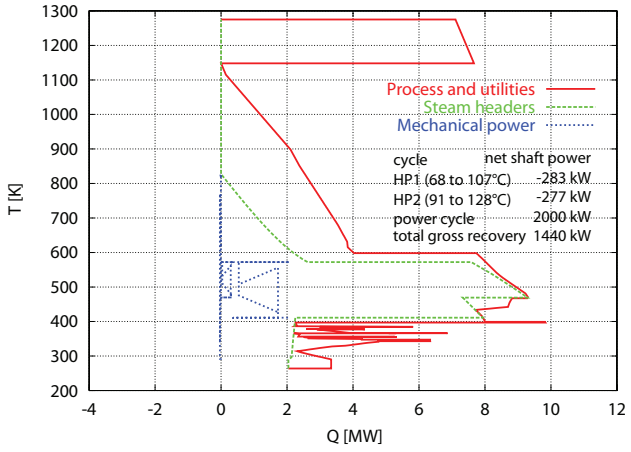

(c) Steam cycle with heat pumping.

Figure 5.3—Exergy recovery in combined ethanol and SNG production.

has previously been transferred across the high temperature pinch by only partially preheating the combustion air.

5.3 Conclusions

Table 5.1 summarises the benefit of designing site-scale integrated processes. Starting from an overall energy efficiency of 49.4% for the conventional process design, the combined production of SNG and ethanol from lignocellulosic resources allows for increasing the efficiency to up to 73.6%.

This brief outlook thus detects substantial potential in the polygeneration of fuels by exploiting the synergies between complementary conversion processes. The proper, overall-site integration of mass and energy is thereby a necessary condition to fully exploit the resource, which can only be realised by a systematic approach. In this regard, the findings with respect to thermal exergy recovery are not restricted to applications in the biofuel sector. Instead of addressing a waste heat recovery problem from the process streams' energy excess, it should be formulated as a problem of exergy minimisation, in which energy and exergy conversion technologies symmetrically allow for exchanges between the process streams and the environment.

Chapter 6

Process typefaction

Based on the process model developed in Chapter 2, this chapter presents a systematic typefaction of all candidate technology and process configurations for the polygeneration of SNG, heat and power. It thereby discusses the influence of the process technology, operating conditions and process integration on the thermo-economic performance of optimised plant configurations. Furthermore, the economic scaling is quantified and the most profitable flowsheets for different energy prices and scale are identified.

6.1 Introduction

As illustrated by the general process superstructure developed in Figure 2.1 of Chapter 2, thermochemical fuel production from biomass proceeds through several conversion steps for which several major technological options are available. This results in a multitude of possible configurations, in which the candidate technologies of the process sections adapt and integrate differently with each other. The distinct thermo-economic characteristics and cogeneration potentials of these alternatives are furthermore expected to scale differently. The choice of the optimal plant configuration is yet not only scale-dependent, but also very specific to the prevailing or projected economic conditions in which the relative value of both capital and the multiple energy services may change.

In this context, the objective of a process typefaction is to systematically assess the thermo-economic performance of the process configurations and identify the most promising technologies and their optimal matches in terms of operating conditions, process scale and the economic environment.

Previous studies in the field of fuel production from biomass have carried out this kind of task by defining some typical flowsheet scenarios by hand.

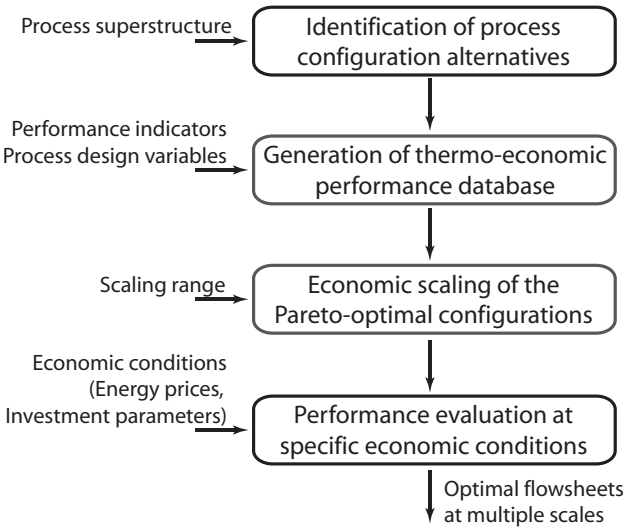

Figure 6.1—Typefaction sequence.

For SNG production with conventional gasification and methanation, this has been done by Mozaffarian and Zwart (2003), and for model illustration purposes in Chapter 2 of this work. Luterbacher et al. (2009) studied some technology scenarios for hydrothermal SNG production, and popular examples of this approach applied to the production of Fischer-Tropsch fuels are Tijmensen et al. (2002) and Hamelinck et al. (2004).

In order to systematically address the typefaction of candidate technology and process configurations for thermochemical SNG production, the present chapter follows the approach illustrated in Figure 6.1. In a first step, all potentially adequate technology routes are identified from the process superstructure of Figure 2.1. For these candidate configurations, a set of thermo-economically optimal flowsheets is then generated by multi-objective optimisation of their design with respect to adequate performance indicators. This database of Pareto-optimal flowsheets is scaled, which finally allows for evaluating the performance of all technology routes with respect to different economic conditions at multiple scales.

6.2 Typefaction by multi-objective optimisation

Multi-objective optimisation techniques have been introduced in the conceptual design of energy conversion systems in order to provide an enlarged set of candidate solutions to a design problem that is characterised by several

conflictive objectives such as efficiency, cost and environmental impact. Due to their ability of handling non-linear and non-continuous objective functions, evolutionary algorithms have thereby proven as a robust method for solving these complex programming problems.

In the context of energy conversion system design, Toffolo and Lazzaretto (2002) discuss the basic concept of Pareto optimality and evolutionary algorithms for multi-objective optimisation. They demonstrate its usefulness at a benchmark cogeneration problem, in which they consider the exergy efficiency and total cost including expenses for plant operation (i.e. fuel) and investment as objectives. By introducing a pollution cost in their economic objective function, Sayyaadi (2009) and Lazzaretto and Toffolo (2004) generalise the thermo-economic benchmark problem to an environomic one. While Lazzaretto and Toffolo introduce a third objective targeting the minimim emissions and thus follow the approach's underlying intention of dissociating objectives of different kinds, Sayyaadi aggregates the economic and environmental criteria in a conventional way.

Based on an evolutionary algorithm developed by Leyland (2002) and Molyneaux (2002), Maréchal et al. (2005b) and Autissier et al. (2007) apply multi-objective optimisation to energy conversion systems based on fuel cells. Contrary to the studies of Sayyaadi, Lazzaretto and Toffolo, they completely dissociate the effects of conversion efficiency and system cost by considering only the investment as economic target in their objective definition. The same has been done by Brown et al. (2009) for biomass-based integrated gasification combined cycles, whereas Li et al. (2006) applied the algorithm targeting minimum total cost and CO_2-emissions for natural gas combined cycles.

In an attempt to uncouple the generated set of optimal solutions from weighting parameters, a systematic choice of the objectives in the problem formulation for polygeneration systems has been proposed in Chapter 1 of this work. Although useful for a detailed system design demonstrated in Chapter 4, this approach is yet less suitable for typefaction purposes since the increasing problem complexity requires a far more detailed analysis of the numeric results that is beyond the scope of a typefaction. For this reason, an optimisation problem with a more conventional two-dimensional objective space is formulated and solved in Sections 6.3 and 6.4. In the last part of the chapter (Section 6.5), the systematic typefaction of candidate SNG-technology is concluded by investigating the influence of process scale on the thermo-economic characteristics and the optimal configurations, which is an issue that has not been addressed in any of the previously mentioned studies.

6.3 Optimisation problem formulation

6.3.1 Production setting

The previous chapters have shown that thermochemical conversion processes are highly integrated installations that can generate several energy services from biomass. The relative amounts of these products are adjusted in the process design, which might result in the use of different technologies and operating conditions for different demands of energy services. The best configuration for a specific production setting is therefore dependent on the biomass availability, local heat cogeneration possibilities and economic boundary conditions such as energy prices. In order to highlight the influence of this specific conditions, the process typefaction is carried out for all candidate configurations without and with industrial heat cogeneration at 110°C (70°C return temperature). For the entire analysis, wood with the properties of Table 2.1 is considered as raw material. SNG at 96%vol CH_4 is delivered dry to the grid at 50 bar and 25°C.

6.3.2 Process configuration alternatives

Based on the developed process model for the superstructure depicted on Figure 2.1, all principal technology combinations for SNG production by gasification and methanation are considered for the optimisation. According to the operating conditions detailed in Table 6.1, both drying technologies are optimised with respect to the residual humidity level and the temperature of the drying medium. In case of steam drying, operating pressure is also used as a decision variable since it determines the temperature at which the latent heat is recovered. For gasification, indirectly heated FICFB technology at nominal operating conditions and directly heated, pressurised steam-oxygen gasification are considered. Although currently not demonstrated in practice, the benefits of an advanced indirectly heated gasifier operated under pressure are explored in additional runs. By expanding the fumes from combustion, such a facility would represent a gasifier that shares its combustion chamber with a gas turbine. Yet technically very challenging, this would allow for generating additional power and thus increase the cogeneration efficiency.

Among the thermal pretreatment options for gasification, only torrefaction in connection with indirectly heated gasification is considered, in which the volatiles released during torrefaction are used for heat supply. Pyrolysis is not included in the candidate configurations since the scale-up of the investigated pilot pyrolysis unit is expected to be very costly (cf. Chapter 2).

For all candidate configurations, cold gas cleaning including biodiesel scrubbing is used as reference technology. In case of pressurised gasification and methanation, the benefits obtained through advanced hot gas cleaning is further assessed. For gasification at atmospheric pressure or CO_2-removal upstream of methanation, no benefit is expected from this technology since the producer gas needs to be cooled anyway for compression or separation. In all configurations, methane synthesis is considered to be carried out in an internally cooled fluidised bed that is recently successfully demonstrated at pilot scale (Biollaz et al., 2009).

In order to find the best technology matches, all possible combinations of the crude SNG production and its upgrade are considered in the optimisation. Whereas pressure swing adsorption and physical absorption with Selexol are suitable for CO_2-removal both up- or downstream of methanation, membrane technology can only be applied downstream due to the fast permeation of hydrogen. For this case, three cellulose acetate membrane stages arranged as shown on Figure 4.5(d) have been identified as the best subsystem configuration. Similar to the other CO_2-removal options, a final polysulfone membrane for hydrogen removal and recycling to the methane synthesis reactor has further proven useful. All other depleted streams from the liquid-vapour and gas separation units are preheated to 400°C and either used for energy supply or disposed by catalytic combustion. If necessary, cold producer gas is withdrawn as supplementary fuel to balance the energy requirement of the indirectly heated gasifier. Compared to the other candidate fuels discussed in Chapter 3, this is the less performing, yet currently implemented solution due to its technical convenience. In all runs, excess heat is recovered in a Rankine cycle whose header layout and operating conditions are optimised according to Table 6.1.

Overall, the typefaction covers 60 (20 FICFB, 16 CFB-O2 and 2·12 pressurised FICFB) technology combinations that are individually optimised for operation with and without industrial heat cogeneration. Since the applied evolutionary algorithm does not feature a convergence criterion, the optimisations are stopped after 10'000 iterations. The large computational effort has been managed by parallel computing on the EPFL pleiades cluster in roughly 480 net days on an equivalent single 2.67 GHz processor (EPFL Pleiades cluster, last visited 11/2009).

Section	Technology	Operating conditions		Unit	Value/Range
Drying	Air drying	Air inlet temperature	$T_{d,in}$	°C	[180 240]
	Steam drying	Steam inlet temperature	$T_{d,in}$	°C	[180 240]
		Pressure	p_d	bar	[1 5]
	- both	Humidity after drying	$\Phi_{d,wood}$	%wt	[10 30]
Thermal pretreatment	Torrefaction	Inlet temperature	$T_{t,in}$	°C	[300 400]
		Outlet temperature	$T_{t,out}$	°C	260
Gasification	Ind. heated FICFB	Temperature	T_g	°C	850
		Pressure	p_g	bar	1 / p_m[a]
	Dir. heated CFB	Temperature	T_g	°C	800
		Pressure	p_g	bar	p_m
	- both	Steam to dry biomass ratio	$r_{S/B}$	-	0.5
		Steam/O_2 preheat temperature	$T_{g,ph}$	°C	300
Methane synthesis	Internally cooled FB	Inlet temperature	$T_{m,in}$	°C	[300 400]
		Outlet temperature	$T_{m,out}$	°C	[300 400]
		Pressure	p_m	bar	[1 30]
Gas separation	PSA &	Wobbe Index[b]	$W_{s,n}$	kWh Nm^{-3}	[13.0 13.5]
	Phys. absorption	Amount CO_2 removed[c]	$r_{CO2,rem}$	%	[95 99]
		Methane recovery	r_{CH4}	%	[95 99]
	PSA	Adsorption pressure	p_{PSA}	bar	5.5
	Phys. absorption	Column pressure	p_{sel}	bar	[30 50]
		Absorption factor	A_{sel}	-	[1 1.8]

[a] pressurised operation only in advanced configurations.
[b] CO_2-removal after methanation.
[c] CO_2-removal before methanation.

Table 6.1—Principal fixed operating conditions and decision variables for optimisation.

Section	Technology	Operating conditions		Unit	Value/Range
Gas separation *(cont.)*	Membranes	Wobbe Index	$W_{s,n}$	kWh Nm^{-3}	[13.0 13.8]
		Stage cut of stage 1	θ_1	-	[0.2 0.6]
		Stage cut of stage 2	θ_2	-	[0.2 0.6]
		Feed pressure of stage 1	p_{f1}	bar	[5 50]
		Feed pressure of stage 2	p_{f2}	bar	[5 50]
		Feed pressure of stage 3	p_{f3}	bar	[5 50]
		Fraction of feed to stage 2	$s_{in,2}$	-	[0 1]
Steam network	Production header	Production pressure	$p_{s,p}$	bar	[40 120]
		Superheat temperature	$T_{s,s}$	℃	[350 550]
	Utilisation headers	Number of utilisation levels	$N_{s,u}$	-	[1 4]
		Temperature of utilisation level 3[d]	$T_{s,u3}$	℃	[50 250]
		Condensation level temperature[e]	$T_{s,c}$	℃	[20 110]

[d] levels 1 and 2 are adjusted to steam requirements for gasification and methanation.

[e] corresponds also to lowest utilisation level.

TABLE 6.1 *(cont.)*—Principal fixed operating conditions and decision variables for optimisation.

6.3.3 Performance indicators and objectives

As discussed in Chapter 1, the multiple thermodynamic, economic and environmental indicators defined to measure the process performance are weighted combinations of all material, energy and monetary input and output streams. On this basis, it is argued that the use of all independent flows as objectives is the most consequent choice, since it allows for generating a general set of optimal configurations that is independent on the weighting factors. Although feasible in principle, this approach is yet cumbersome to comprehensively compare all potential process configurations included in a large superstructure as the one for SNG-production developed in Figure 2.1. Instead, a more conventional two-dimensional approach with one thermodynamic and one economic objective seems more appropriate for this purpose.

In most of the previous multi-objective thermo-economic optimisations, exergy efficiency has been chosen as thermodynamic objective since it provides a physically strict appreciation of heat and power in cogeneration applications (Toffolo and Lazzaretto, 2002, Lazzaretto and Toffolo, 2004, Sayyaadi, 2009, Brown et al., 2009). Although no physical argument objects its use in the trigeneration of fuel, heat and power, the analysis in Section 1.6.1 has yet shown that it disproportionately favours the fuel output from a technical point of view. For a balanced weighting of technical relevance, the chemical efficiency ϵ_{chem} based on a SNG-equivalent for heat and power defined in Equation (1.35) is therefore chosen as thermodynamic objective for the typefaction. As economic objective, the specific investment cost c_{GR} obtained by normalising the grass roots cost of Equation (1.25) with the process scale is used:

$$c_{GR} = \frac{C_{GR}}{\Delta h^0_{biomass} \dot{m}^+_{biomass}} \tag{6.1}$$

which is similar to the economic objective used by Maréchal et al. (2005b). In our case, an arbitrary reference scale of 20 $MW_{th,biomass}$ has been chosen for the optimisation step.

Compared to the minimisation of the total production cost by Sayyaadi, Lazzaretto and Toffolo, minimising c_{GR} considers the plant scale directly and eliminates the thermodynamic performance from the economic objective. It thus provides the complete range of optimal plant configurations by extending the Pareto front at the low-cost extreme, which is limited in Lazzaretto and Toffolo's (2004) approach to the economic optimum at fixed economic conditions and process scale.

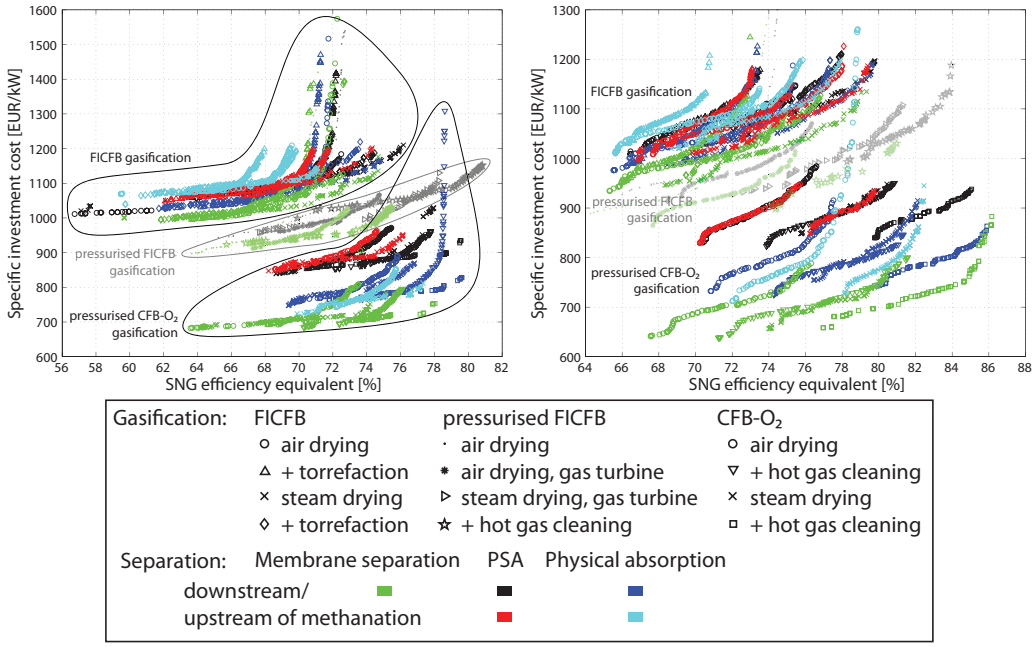

Figure 6.2—Pareto-optimal solutions of all examinated process configurations without (left) and with heat cogeneration.

6.4 Thermo-economic performance of the candidate technology

Figure 6.2 provides a general overview of the optimal thermo-economic performances for all candidate processes at the reference scale of 20 $MW_{th,biomass}$, which are discussed in detail in the following sections. Without industrial heat cogeneration, most of the configurations based on indirectly heated gasification at atmospheric pressure reach chemical (i.e. SNG-equivalent) efficiencies between 60 and 76% at specific investment costs of 1000 to 1300 € kW^{-1}. For directly heated, oxygen-blown gasification under pressure, the Pareto fronts range from 68 to 80% efficiency at 700 to 1000 € kW^{-1} and clearly dominate the ones of its competitor. Industrial heat cogeneration allows for slightly decreasing the investment costs and increasing the chemical efficiency up to 80% and 86% for indirectly and directly heated technology, respectively. If indirectly heated gasification could be operated under pressure, the gap between the two technologies narrows. A combined gasification/gas turbine configuration could reach over 80% chemical efficiency without heat cogeneration and thus even become globally optimal at the high-efficiency end.

Figure 6.3 illustrates the product outputs at a regression of the partial efficiencies ϵ_i defined in Equations (1.32) on the the chemical efficiency ϵ_{chem}. For each process configuration, (a) shows the mean values of ϵ_{SNG}, ϵ_{el} and ϵ_{th} on a Pareto front and (b) the slope of their on ϵ_{chem}. In most of the cases, $\Delta\epsilon_{SNG}/\Delta\epsilon_{chem}$ is close to zero, which highlights that the amount of SNG produced by a specific technology combination is constant on a Pareto front. The operating conditions of the thermochemical conversion are thus not conflictive with respect to investment cost and SNG yield, and the trade-off between efficiency and cost within a specific process configuration is mainly related to the cogeneration of heat and power.

6.4.1 Drying and thermal pretreatment

Figure 6.4 compares some typical performance curves for the pretreatment options at the example of FICFB gasification with PSA and membrane separation technology. If industrial heat cogeneration is not considered, air drying is assessed as the better drying technology at the low-efficiency end. Above approximately 67 to 69% for PSA and membrane separation, respectively, the Pareto fronts intersect and steam drying gets clearly dominating at higher efficiencies. The same qualitative behaviour is observed for all other configurations and is due to the possibility for latent heat recovery from steam at useful temperature. If this heat can be valorised directly in a distribution grid, steam drying is the better technology in the entire Pareto domain, which is characterised by a constant translation from air to steam towards considerably higher efficiencies at slightly higher costs.

The optimal drying temperatures and their distribution are dependent on the technology and can be explained with the individual equipment performance. As shown earlier in Figure 2.2, the thermal efficiency of air drying is markedly increasing with its inlet temperature $T_{d,in}$, which is beneficial for the overall process since more excess energy is available for heat and power cogeneration. In the optimisation, $T_{d,in}$ of air is not conflictive and always at its higher bound defined in Table 6.1. If steam drying is used, the heat requirement and the specific power consumption for drying are slightly decreasing with temperature (Fig. 2.2). Contrary to air drying, $T_{d,in}$ of steam is thus conflictive with respect to the thermo-economic performance of the entire process and tends to its lower bound for more efficient solutions and to its higher bound for the less costly ones. In all configurations with steam drying, the operating pressure is preferably chosen at the upper limit, and a compact process setup might consist in operating the dryer as a steam generator for methane synthesis.

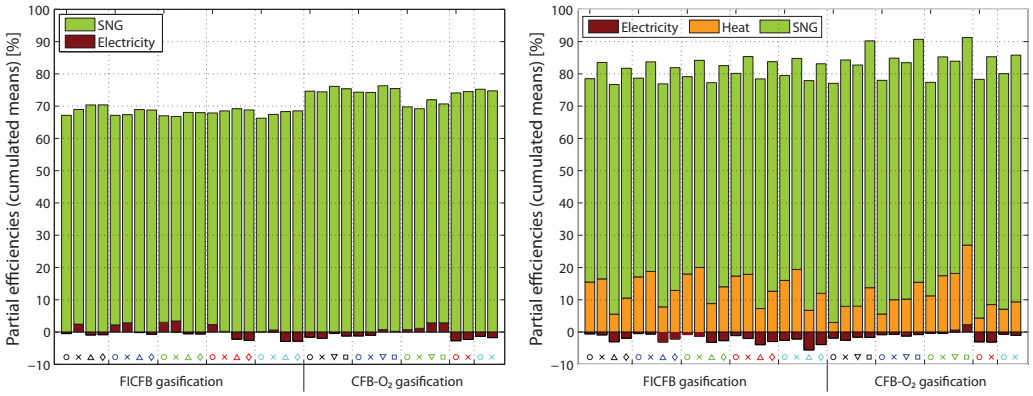

(a) - Mean values of ϵ_{SNG}, ϵ_{el} and ϵ_{th}.

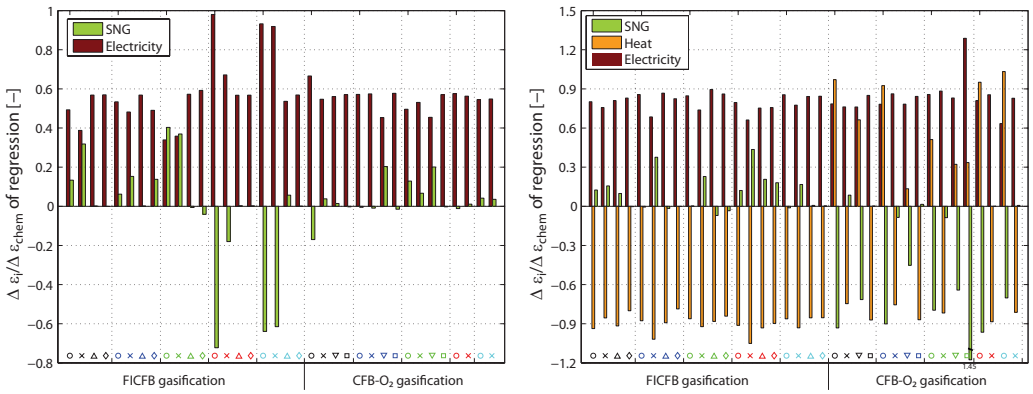

(b) - Slopes of the regression.

Gasification:	FICFB	pressurised FICFB	CFB-O_2
	○ air drying	· air drying	○ air drying
	△ + torrefaction	* air drying, gas turbine	▽ + hot gas cleaning
	× steam drying	▷ steam drying, gas turbine	× steam drying
	◇ + torrefaction	☆ + hot gas cleaning	□ + hot gas cleaning

Separation: Membrane separation PSA Physical absorption

downstream/ upstream of methanation

Figure 6.3—Regressed product distribution on a Pareto front.

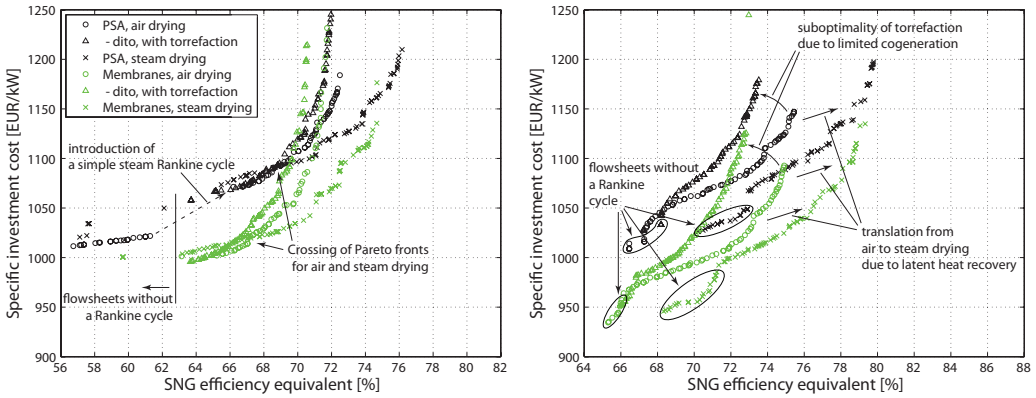

Figure 6.4—Pareto-optimal solutions without (left) and with heat cogeneration: Comparison of some selected pretreatment options for FICFB-gasification.

Independently on specific technology, the residual humidity of the dried biomass is a key variable in any process design. As discussed in Chapter 3, limiting the humidity content in the gasifier feed allows for decreasing its energy requirement at high temperature and the exergy loss during gasification. This may affect the cold gas efficiency ϵ_{cg} (Eq. 2.20) in a 10% order of magnitude as observed for FICFB technology in Figure 3.3, which is yet partially compensated with respect to overall performance by heat and power cogeneration from the increased excess heat below the pinch. The decision variable is thus conflictive with respect to the partial yields and thus within the thermodynamic objective itself. For most of the configurations, a value of $\Phi_{d,wood}$ at the considered lower bound of 10% is beneficial for high chemical efficiency but also requires a higher investment. However, for air drying with heat cogeneration or air drying coupled to torrefaction, decreasing $\Phi_{d,wood}$ at the expense of a high dryer heat load is not worthwile, the variable is not conflictive and always at its upper bound of 30%.

Similar energy integration effects are observed when the gasifier feed is completely dried and partly decomposed by torrefaction. Compared to configurations without a second thermal pretreatment step, this allows for further enhancing the SNG yield to the expense of heat and power cogeneration. The weighting applied by ϵ_{chem} does however not balance the reduced contribution of the by-products with increased fuel output, and the Pareto fronts of the configurations with torrefaction on Figure 6.4 drop away from the optimal performance at elevated chemical efficiency. In all cases, $T_{t,in}$ tends to its upper bound of 400°C.

6.4.2 Gasification and fuel synthesis

6.4.2.1 Gasification

As already discussed in the introductory section, the general performance overview of Figure 6.2 highlights the distinctive character of the gasification technology with respect to the process performance. Independently of co-generation, indirectly heated gasification at atmospheric pressure is clearly suboptimal compared to directly heated steam-oxygen gasification under pressure. On the one hand, the indirect heat supply at atmospheric pressure requires a complex twin-reactor, bulky gas cleaning and intermediate compression, which is more expensive than a compact process design with a directly heated pressurised vessel (cf. Fig. 2.7). Efficiency, on the other hand, is limited by the relatively low cold gas efficiency (cf. Fig. 2.4) due to the pinch at elevated temperature and the power required for intermediate gas compression. Compared to the Viking gasifier analysed in Chapter 3, directly heated fluidised bed gasification does not suffer from a producer gas that approaches equilibrium at high temperature, but operates slightly colder and equidistant to thermodynamic equilibrium than FICFB gasification (cf. Tab. 2.4). The heat release during methanation is thus moderate, and pressurised operation eliminates the need for intermediate gas compression.

Although technically challenging, a pressurisation of the FICFB gasification reactor could at least partially compensate its disadvantages with respect to performance. As illustrated in Figure 6.5, increasing the vessel pressure to the one of methanation is expected to decrease the system cost by roughly 10%. If the power requirement for air compression is not recovered, efficiency is yet decreased as well. A beneficial effect on cost and efficiency is only obtained if it is possible to expand the fumes in a turbine, which converts part of their abundant specific excess heat at high exergy value into additional power.

6.4.2.2 Gas cleaning

In addition to the immediate benefit of pressurised gasification on the process performance, it constitutes the basis for the use of hot gas cleaning technology since intermediate gas cooling, vapour condensation and compression is made redundant. Figure 6.5 illustrates that closely coupling the gasification and methanation reactors through hot cleaning increases ϵ_{chem} by up to 3% to 5% for the setups without and with heat cogeneration, respectively. In case of directly heated gasification with CO_2-removal by physical absorption, the previously favoured solution of gas separation upstream of synthesis becomes

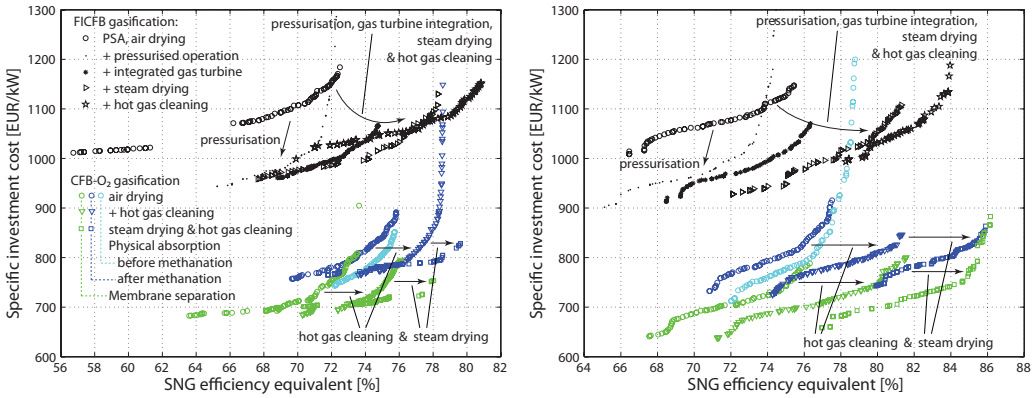

Figure 6.5—Pareto-optimal solutions without (left) and with heat cogeneration: Advanced technologies (hot gas cleaning and pressurised FICFB).

suboptimal compared to its downstream arrangement since hot cleaning is only beneficial in the latter case.

Combined with steam drying, this advanced technology thus constitutes the globally optimal process configurations with directly heated gasification and membrane separation at the low-cost end, and downstream physical absorption in the mid-range of the Pareto domain. With an increased SNG yield due to the use of hot gas for balancing the heat requirement, pressurised FICFB gasification combined with gas separation by PSA might further complement the globally optimal configurations at the top efficiency end.

6.4.2.3 Methane synthesis

In all candidate configurations, methanation in an internally cooled fluidised bed is considered as the reference technology with a linear enthalpy profile between the reactor inlet and outlet temperatures. Except for upstream CO_2-removal, these variables are not conflictive and tend to their upper and lower bounds, respectively, which allows for an efficient design of the steam network while limiting the residual H_2 and CO concentration. If CO_2 is removed before methanation, cheaper configurations are obtained for lower gas temperatures at the reactor inlet.

As indicated by the mean values for the different process configurations shown in Figure 6.6, the optimal synthesis pressure is dependent on the gasification and gas separation technology. Within a specific configuration, the pressure is thereby slightly conflictive. While efficiency typically decreases monotonously with pressure due to increased power requirements, considerable cost savings are obtained with a compact, mildly pressurised reactor. If

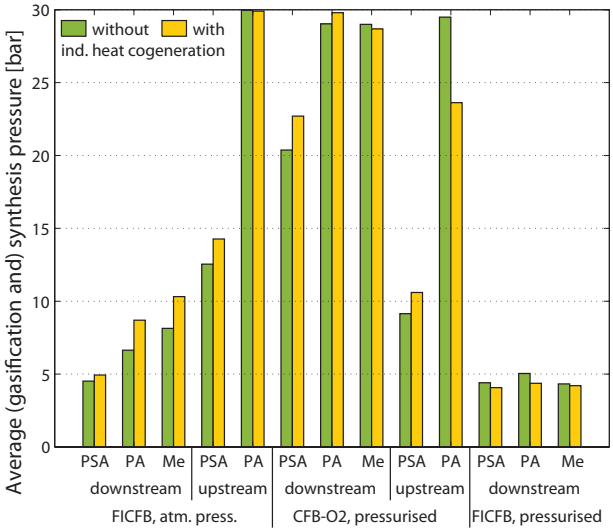

Figure 6.6—Averages of optimal synthesis pressures for different gasification technologies with gas separation down- or upstream of methanation (PSA: Pressure swing adsorption, PA: Physical absorption, Me: Membranes).

pressure is further increased, this benefit is yet outweighed by an increasing cost factor related to the construction material.

In case of FICFB gasification at atmospheric pressure, optimal configurations perform the synthesis at a mild pressurisation of 3 to 10 bar. Slightly higher values are thereby obtained for the pressure-driven physical absorption and membrane separation processes. If CO_2 is removed prior to synthesis, the operating pressure of these sections are preferably matched in order to avoid supplementary turbomachinery. In case of directly heated gasification at the synthesis pressure, gas compression requirements are minimised at elevated system pressure and its optimal values are all in the upper half of the search space. In pressurised indirectly heated gasification, the twin reactor dominates the system performance and its optimal pressure is independent on the gas separation technology.

6.4.3 Gas separation

Figure 6.7 compares the representative thermo-economic process characteristics of the candidate CO_2-removal with air drying and cold gas cleaning, and thereby highlights that the best technology matches depend on the gasification technology. For an indirectly heated reactor, gas separation by membranes dominates a large part of the Pareto domain and gets only suboptimal

at the top-efficiency end where PSA is the preferable choice. The performance of absorptive separation with Selexol is always worse than membrane technology whose permeate is appropriate for heating the gasification reactor (cf. Chapter 4). Furthermore, the pressure levels imposed by upstream CO_2-removal are not favourable for process configurations based on FICFB technology and result in suboptimal performance.

Due to its suitability to elevated operating pressures, directly heated gasification matches much better with physical absorption, and PSA with its relatively low operating pressure gets secondary. For cold gas cleaning, an upstream separation column performs thereby even better than its downstream alternative, but cannot benefit from hot cleaning. Although dominating the low-cost configurations, membrane technology suffers from a relatively inefficient permeate disposal that is not usable in directly heated gasification. The obtained SNG yield is thus lower compared to the other CFB-O2 configurations, and the higher heat and power share does not compensate for the decrease in gas efficiency.

For pressure swing adsorption, the decision variables of Table 6.1 are not conflictive and the best performance is always obtained at the upper purity- and recovery-limit of the technology. In Selexol absorption, somewhat lower purity and intermediate recovery levels should be targeted, although no general trends emerge. In any case, the optimal separation pressure sticks to its lower bound of 30 bar to limit the compression requirements. The column design is thereby conflictive in terms of absorption factor, which is positively correlated with both efficiency and investment cost. In accordance with the results of Chapter 4, the cellulose acetate membranes are generally best arranged in a three-stage cascade with a common recycling loop and crude feed to the first stage of Figure 4.5(d). In order to limit the compression requirement from p_m to p_{grid}, a high separation in the first stages and increasing pressure on the retentate side of the subsequent stages seems worthwhile. Accordingly, decreasing stage cuts and optimal operating pressure of 35 to 45 bar, 40 to 45 bar and 50 bar for the 1^{st}, 2^{nd} and 3^{rd} stage, respectively, are assessed.

6.4.4 Energy recovery

As discussed at Figure 6.3, energy recovery by a steam Rankine cycle has an essential impact on the thermo-economic plant performance and causes a large part of the variation within the Pareto front of a specific configuration. Although a priori considered in all runs, the optimisation algorithm may prevent the implementation of a Rankine cycle by imposing infeasible conditions, and thus provide some Pareto-optimal solutions at low invest-

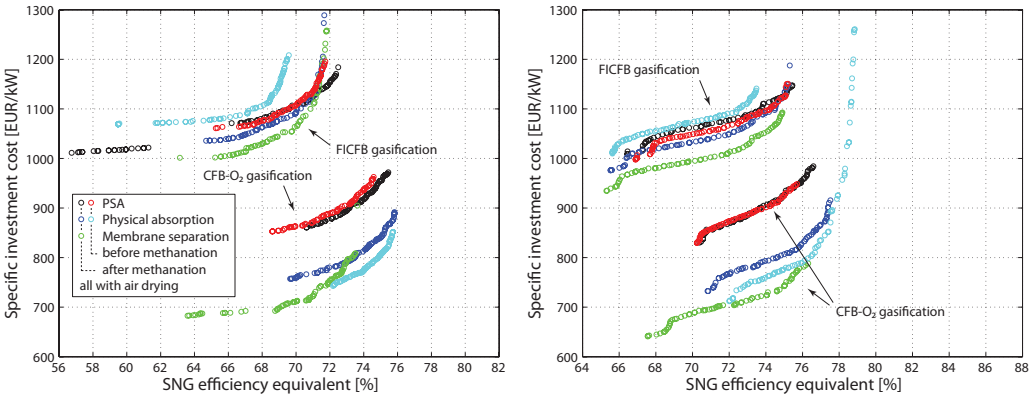

Figure 6.7—Pareto-optimal solutions without (left) and with heat cogeneration: Comparison of the CO_2-removal options for both gasification technologies in case of air drying.

ment cost. These configurations indicate that the chemical process efficiency is limited to 62% and 71% for conventional FICFB and pressurised CFB-O_2 gasification, respectively, if no energy at all is recovered from excess heat. If at least heat can be valorised, the lack of a steam cycle allows for 73% and 80% equivalent efficiency for the same cases. Figure 6.4 thereby highlights that the introduction of a steam cycle generates a jump discontinuity in the Pareto front if only power is cogenerated, or an inflection point if the power output rivalises with the one of heat. With a gross power generation of up to 10% of the biomass input, the SNG-equivalent process efficiency is improved by 4% to 14% if power is the only by-product. If both power and heat can be valorised, around 35% of the heat output can be fully substituted by power. This corresponds to a gross power production of 5% to 8% of the raw material's heating value and improves the chemical process efficiency by up to 7%. Except the steam turbine inlet temperature that is positively correlated with process efficiency and cost, the operating conditions of the steam cycle do not follow general trends and need to be adjusted with a specific process configuration.

6.5 Economic process scaling

6.5.1 Approach

As stated in the problem formulation, all thermo-economic process optimisations have been carried out for a reference plant capacity of 20 $MW_{th,biomass}$. However, the relative economic performance of the technology is expected to

change with scale, which needs to be accounted for if a general comparison of the candidate technology is targeted. Individual process optimisations at multiple scales would thus be necessary in principle, but are cumbersome since they require a large computational effort. Assuming that the operating conditions within a set of Pareto-optimal flowsheets do not substantially change with process scale, it would be possible to select the optimal plants at different scales by extrapolating the optimised flowsheets from the reference scale. It should be noted that this does not mean that the best process flowsheet with respect to a particular performance indicator is scale-independent, but that it may be chosen from a scale-independent set of Pareto-optimal solutions. Since the thermodynamic objective is inherently independent on scale, suboptimality may thereby only arise with respect to investment cost. This simplifying hypothesis has been tested for the major process configurations (i.e. FICFB and CFB-O_2 gasification with air and steam drying and PSA, Selexol and membrane separation after methanation) at 5 and 100 $MW_{th,biomass}$ with and without heat cogeneration. The plots in Appendix B compare the Pareto fronts obtained by optimisation at the specific scale with the extrapolated ones from the reference scale and confirm that the differences are indeed relatively small. In more than half of the 24 test cases, the difference in investment cost is within 1-2%, in one third of the cases it is smaller than 5%, and in none of the cases bigger than 7%. For some configurations, the performance of the extrapolated flowsheets is even better than the one of the optimised configurations. This highlights that the error commited through the extrapolation is in the same order of magnitude than the incertainty of not finding the global optimum with an evolutionary algorithm that inherently lacks of a convergence criterion.

6.5.2 Scaling correlations

In order to provide a measure of the economies of scale to be expected for the process technology, the investment cost of the Pareto-optimal configurations can be regressed on the plant scale with a conventional scaling law of the form:

$$C_{GR} = C_{GR,ref} \left(\frac{\Delta h^0_{biomass} \dot{m}^+_{biomass}}{(\Delta h^0_{biomass} \dot{m}^+_{biomass})_{ref}} \right)^b \tag{6.2}$$

or, for a specific cost formulation:

$$c_{GR} = c_{GR,ref} \left(\frac{\Delta h^0_{biomass} \dot{m}^+_{biomass}}{(\Delta h^0_{biomass} \dot{m}^+_{biomass})_{ref}} \right)^{(b-1)} \tag{6.3}$$

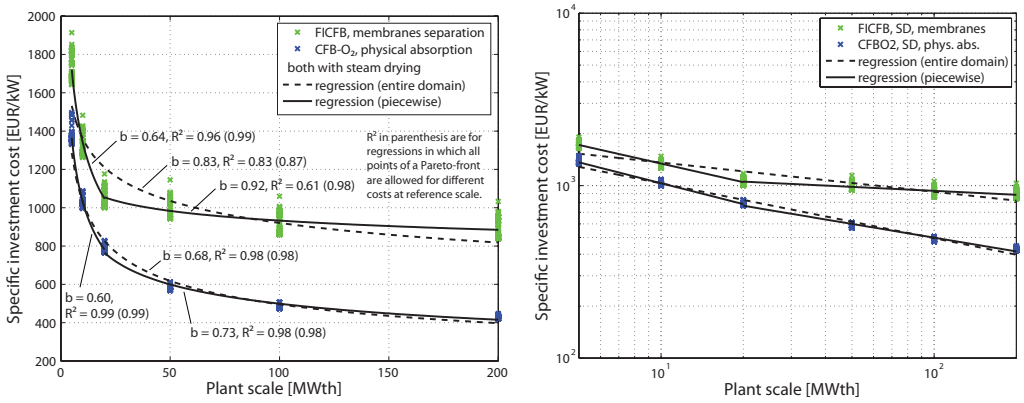

Figure 6.8—Regression of the exponent in the cost correlation of Eq. (6.3) for two exemplary process configurations on linear (left) and logarithmic scale.

Separation\Gasification	FICFB		CFB-O2		FICFB (press.)	
Range [$MW_{th,biomass}$]	[5 20]	[20 200]	[5 20]	[20 200]	[5 20]	[20 200]
PSA	0.63	0.90	0.64	0.78	0.64	0.80
Physical absorption	0.60	0.89	0.58	0.73	0.58	0.76
Membranes	0.64	0.92	0.64	0.78	0.64	0.81

Table 6.2—Regressed cost exponents for principal process configurations. The coefficient of determination R^2 is between 0.97 and 0.99 if individual costs values at reference scale are allowed. The reference value of $c_{GR,ref}$ in Eq. (6.3) for a specific configuration is given directly in one of the Figures 6.2-6.7.

Cost advantages are principally due to decreasing specific costs of the process units with scale, for which the cost exponent b is smaller than unity. For chemical process equipment, typical values of b range from 0.4 to 0.9 and means between 0.6 and 0.7 are often assumed (Ulrich and Vasudevan, 2004). However, the size of the process units, and in particular vessels, is limited to manageable dimensions. As introduced in Chapter 2 and illustrated in Table 2.11, parallel arrangement might therefore be required at larger scales and leads to a linearisation of Equation 6.2.

Figure 6.8 compares the scaling characteristics of two exemplary process setups regressed piecewise and over its entire domain at 5, 10, 20, 50, 100 and 200 MW with a unique cost exponent for all configurations of a Pareto-front. At small plant scales, the lines for FICFB and CFB-O2 gasification are nearly parallel in logarithmic coordinates and economies of scale are significant. Not much above 20 $MW_{th,biomass}$, however, the bulky vessels operated near atmospheric pressure reach their limits and parallel processing in several units is necessary in case of FICFB gasification. As a consequence, the

		Price scenario			CH-market[a]	
Energy vector	Unit	green	mid	low	1999	2008/09
Electricity	€ MWh^{-1}	180	90	60	90-135	80-160
Automotive fuel & SNG	€ MWh^{-1}	120	60	40	80-95	130-140
Industrial heat	€ MWh^{-1}	80	40	26.6	20-35	40-65

[a] including tax. Figures for 1999 are from Previdoli and Beck (2001), 2008/09 is approximate.

Table 6.3—Energy price scenarios.

slope of the large-scale regression flattens considerably and justifies the use of a piecewise correlation for up- and downscaling the investment cost from the reference scale. This effect is much less pronounced in the configurations based on pressurised gasification since their process units can be operated at higher capacity. Furthermore, it has been shown that pressurised gasification matches better with liquid absorption technology, for which more important economies of scale than with the inherently linearly scaling of PSA or membrane separation can be obtained.

The overall cost exponents for the principal technology groups reported in Table 6.2 confirm these trends. Similar to Figure 6.8, they have been obtained by regressing a unique cost exponent for all Pareto-optimal configurations. Each process flowsheet is thereby allowed for an individual specific reference cost $c_{GR,ref}$ at 20 $MW_{th,biomass}$ that can be identified directly from one of the Figures 6.2-6.7 or the optimal configurations discussed in the following section and detailed Tables 6.4 and 6.5.

6.6 Optimal configurations at different scales

The last step of the conceptual process design consists in selecting a specific flowsheet from the generated set of thermo-economically optimal process configurations. For this final choice, an economically rational criterion such as the overall production costs or the process profitability may be supposed. Whereas this obviously depends on the general economic assumptions for investment depreciation and plant operation defined in Table 2.6, it is particularly sensible to raw material costs and product prices. In our case, multiple competing energy services can be produced or consumed, and the economic decision criterion may not be unique. As discussed in Section 1.6.1.2, the most balanced choice is to consider the break-even cost for biomass defined in Equation (1.43) since it appreciates all potential products in an identical

way.

In order to investigate the influence of the energy price on the selection of the best plant at a specific scale, the flowsheets that allow for the maximum biomass break-even cost are chosen for three price scenarios outlined in Table 6.3. As in the previous studies, the relatively high energy prices are considered as reference and compared to a mid- and low-price scenario for which the economic value of the energy vectors are decreased to 50% and 33%, respectively. While the former might only be obtained for labelled renewable energy that possibly benefits from tax exemption, the two latter are in the range of current and previous market prices for fossil energy.

Figures 6.9 and 6.11 summarise the characteristics of an economically rational process scaling for FICFB and CFB-O_2 gasification, respectively. Part (a) shows the maximum break-even costs obtained for a specific process configuration and (b) the chemical efficiency for the overall most profitable flowsheet. Part (c) displays this evolution on the Pareto fronts at 5, 20 and 100 MW. In addition, Tables 6.4 and 6.5 show the decision variables and some performances of the best flowsheets for green energy prices at small, mid and large scale. Figures 6.10 and 6.12 illustrate these configurations at 20 $MW_{th,biomass}$.

With current market prices for wood of 30 to 35 € MWh^{-1}, the figures indicate that plants can operate profitably if high prices for the produced energy vectors can be obtained, and considerable economies of scale can be expected up to 20 to 30 MW. The distribution of the maximum break-even costs for the different technologies is rather wide, and the economically best process configuration and its operating conditions change with scale. The Pareto fronts shown in Part (c) of the figures illustrate that the best process technologies scale considerably different indeed. Membrane separation is a well suited technology for small to medium-sized plants, but suffers from poor economy of scale. In our application, the technology is especially beneficial if heat and power cogeneration is considered since the quality of the depleted streams allows for an efficient recovery. With increasing plant size, it is yet outperformed by pressure swing adsorption or dedicated large-scale physical absorption technology.

According to the general expectation, the efficiency of the economically best flowsheet increases with scale since the influence of the investment on the plant economics is decreases. The obtained prices for the products thereby affects this characteristic essentially. When energy is expensive, renewable SNG, electricity and heat are more precious than heat exchanger area and steam turbines, and very efficient solutions are already economic at relatively small production scales. The effect of scale on the efficiency of the best flowsheets is more pronounced for lower energy prices, which probably better

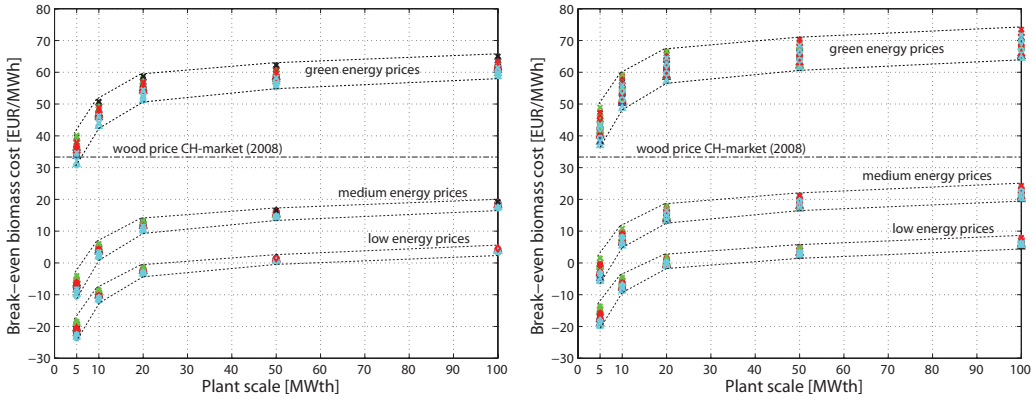

(a) - Maximum biomass break-even costs for each of the candidate configurations.

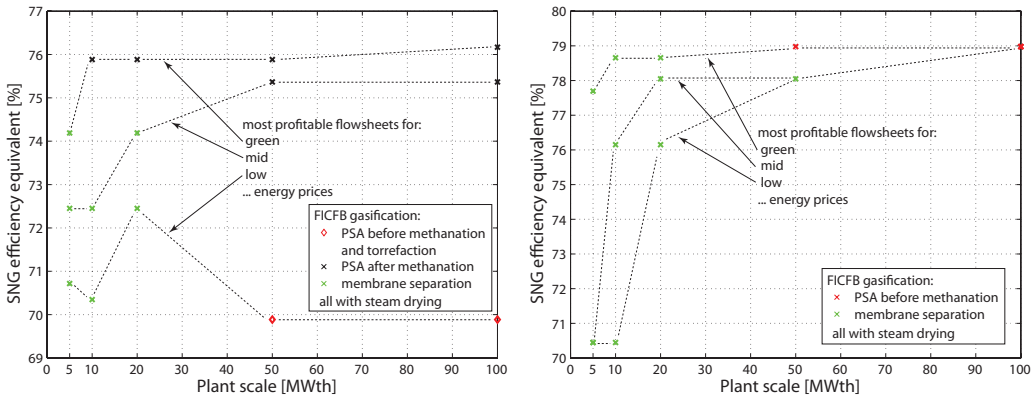

(b) - Process efficiency of the most competitive configurations.

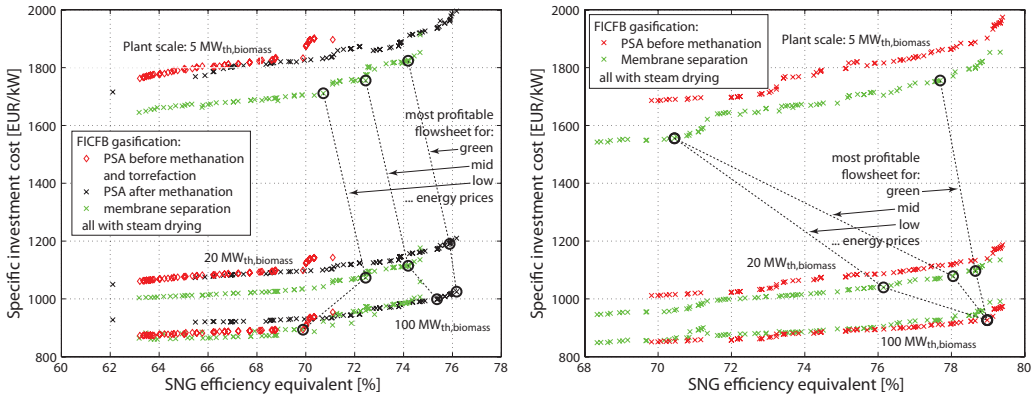

(c) - Evolution of the thermo-economic Pareto-front.

Figure 6.9—Optimal thermo-economic scaling for FICFB gasification without (left) and with heat cogeneration

	Heat cogeneration		without			with		
	Scale	MW	5	20	100	5	20	100
Drying	Technology		steam drying					
	$T_{d,in}$	℃	180	180	180	188	188	187
	p_d	bar	5.0	5.0	5.0	5.0	5.0	5.0
	$\Phi_{d,wood}$	%wt	10.1	10.0	11.1	13.8	13.8	12.3
Gas cleaning	Technology		cold					
Methanation	$T_{m,in}$	℃	399	399	399	396	396	372
	$T_{m,out}$	℃	300	329	339	306	326	301
	p_m	bar	4.5	4.4	4.4	12.3	12.2	16.7
Separation	Technology[a]		Me	PSA	PSA	Me	Me	PSAu
	$W_{s,n}$	-	13.4	13.5	13.5	13.5	13.5	-
	$r_{CO2,rem}$	%	-	-	-	-	-	97.2
	r_{CH4}	%	-	99.0	99.0	-	-	99.0
	θ_1	-	0.46	-	-	0.45	0.45	-
	θ_2	-	0.22	-	-	0.23	0.23	-
	p_{f1}	bar	26.3	-	-	30.4	30.3	-
	p_{f2}	bar	42.8	-	-	41.2	41.0	-
	p_{f3}	bar	46.2	-	-	46.3	46.5	-
	$s_{in,2}$	-	0.0	-	-	0.0	0.0	-
Steam cycle	$p_{s,p}$	bar	70.1	86.8	84.1	98.0	97.8	112.9
	$T_{s,s}$	℃	547	549	549	530	531	550
	$N_{s,u}$	-	3	3	3	3	3	3
	$T_{s,u3}$	℃	127	126	168	56.4	122	122
	$T_{s,c}$	℃	21	21	21	98	97	94
Efficiencies	ϵ_{SNG}	%	66.7	69.3	69.1	65.9	65.9	68.9
	ϵ_{el}	%	4.3	3.7	4.0	1.0	1.8	0.5
	ϵ_{th}	%	0.0	0.0	0.0	17.6	16.9	16.3
	ϵ	%	71.0	73.0	73.1	84.5	84.6	85.7
	η	%	65.3	67.2	67.2	64.4	65.0	66.4
	ϵ_{chem}	%	74.2	75.9	76.2	77.7	78.7	79.0
Costs	c_{GR}	€ kW^{-1}	1823	1190	1025	1755	1096	927
	C_P	€ MWh^{-1}	109.9	84.0	74.9	96.7	70.4	62.7
	$C_{biomass,be}$	€ MWh^{-1}	40.2	58.7	65.0	48.9	66.6	73.5

[a] Me: Membrane separation, PSA: Pressure swing adsorption, PSAu: Pressure swing adsorption upstream of methanation.

Table 6.4—Decision variables and performance of the economically optimal plant configurations for FICFB gasification at atmospheric pressure.

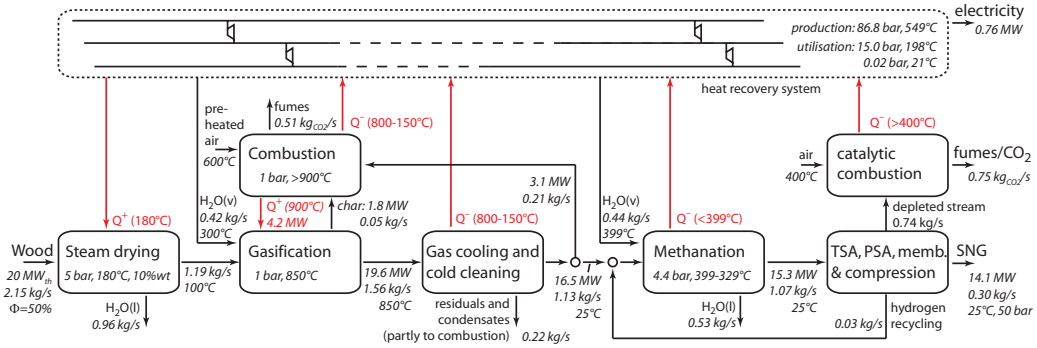

(a) Without heat cogeneration.

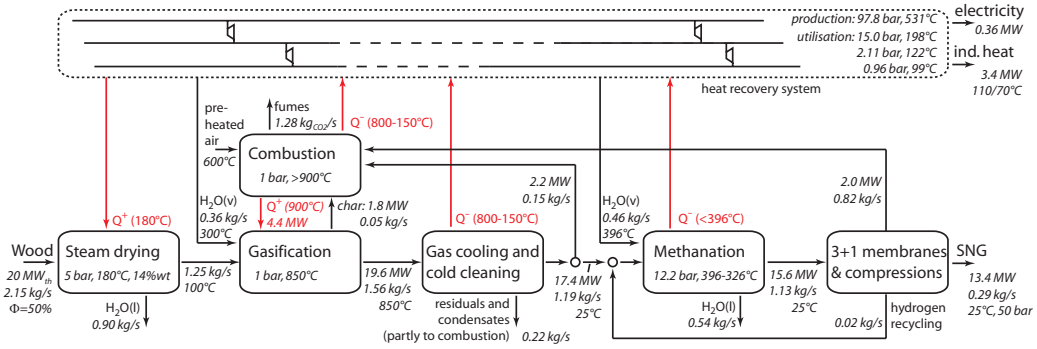

(b) With heat cogeneration.

Figure 6.10—Schematic flow diagrams for most economic plants at 20 $MW_{th,biomass}$ based on indirectly heated gasification at atmospheric pressure.

meets the engineers' intuition. One particularity is thereby observed for FICFB gasification without heat cogeneration, in which the efficiency of the optimal flowsheet for the low-price scenario tends decreases with scale. This can be explained by the influence of the relative product yields. With the assumed low prices, power cogeneration becomes secondary and the bulk SNG has a more important influence on the process profitability. A flowsheet with torrefaction becomes therefore optimal since the share of SNG on the plant output is higher. This example illustrates the sensibility and limits of the simplified typefaction approach for polygeneration plants that aggregates the products in the definition of ϵ_{chem}.

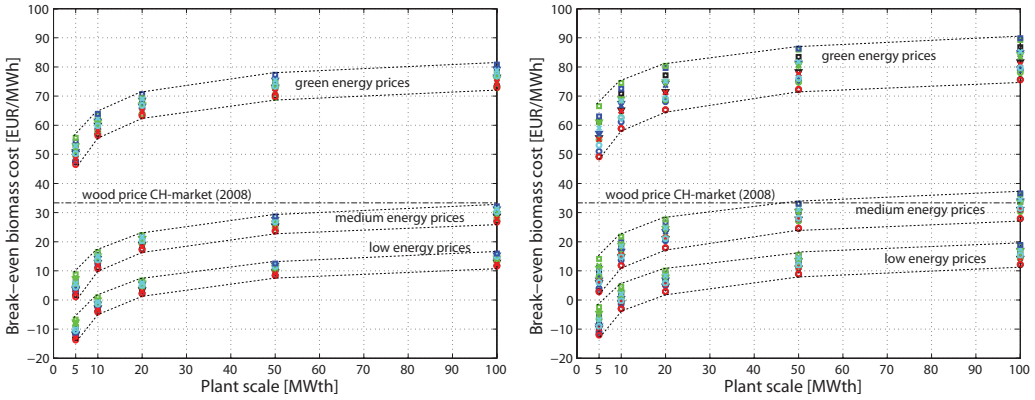

(a) - Maximum biomass break-even costs for each of the candidate configurations.

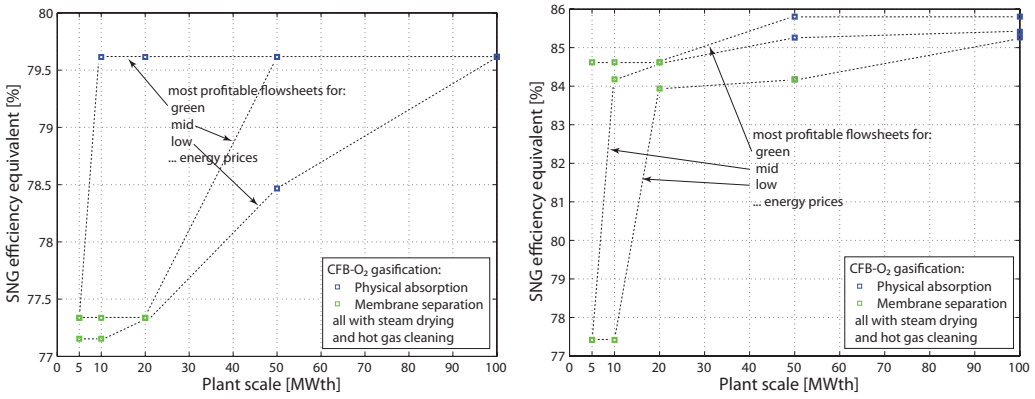

(b) - Process efficiency of the most competitive configurations.

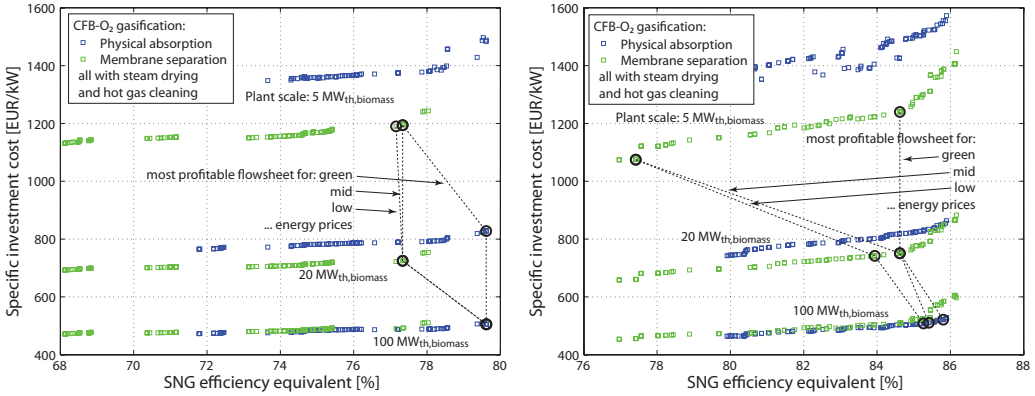

(c) - Evolution of the thermo-economic Pareto-front.

Figure 6.11—Optimal thermo-economic scaling for CFB-O2 gasification without (left) and with heat cogeneration

	Heat cogeneration		without			with		
	Scale	MW	5	20	100	5	20	100
Drying	Technology				steam drying			
	$T_{d,in}$	℃	180	185	185	181	181	184
	p_d	bar	5.0	5.0	5.0	5.0	5.0	4.5
	$\Phi_{d,wood}$	%wt	10.3	11.1	11.1	10.2	10.2	10.0
Gasification	p_g[a]	bar	29.2	29.4	29.4	29.9	29.9	30.0
Gas cleaning	Technology				hot			
Methanation	$T_{m,in}$	℃	326	375	375	344	344	395
	$T_{m,out}$	℃	311	300	300	303	303	300
Separation	Technology[b]		Me	PA	PA	Me	Me	PA
	$W_{s,n}$	-	13.2	13.4	13.4	13.4	13.4	13.4
	r_{CH4}	%	95.7	97.4	97.4	96.8	96.8	97.6
	p_{sel}	bar	-	30.0	30.0	-	-	30.0
	A_{sel}	-	-	1.35	1.35	-	-	1.32
	θ_1	-	0.54	-	-	0.54	0.54	-
	θ_2	-	0.21	-	-	0.25	0.25	-
	p_{f1}	bar	29.3	-	-	30.3	30.3	-
	p_{f2}	bar	34.1	-	-	45.2	45.2	-
	p_{f3}	bar	35.3	-	-	48.4	48.4	-
	$s_{in,2}$	-	0.0	-	-	0.0	0.0	-
Steam cycle	$p_{s,p}$	bar	99.9	115.3	115.3	115.6	115.6	92.1
	$T_{s,s}$	℃	546	546	546	509	509	550
	$N_{s,u}$	-	2	2	2	3	3	3
	$T_{s,u3}$	℃	121	178	178	175	175	177
	$T_{s,c}$	℃	20	20	20	98	98	99
Efficiencies	ϵ_{SNG}	%	67.8	75.0	75.1	68.1	68.1	75.4
	ϵ_{el}	%	5.4	2.6	2.6	3.0	3.0	1.4
	ϵ_{th}	%	0.0	0.0	0.0	19.8	19.8	13.8
	ϵ	%	73.2	77.6	77.7	90.9	90.9	90.7
	η	%	67.3	71.4	71.4	68.5	68.5	72.9
	ϵ_{chem}	%	77.3	79.6	79.6	84.6	84.6	85.8
Costs	c_{GR}	€ kW^{-1}	1194	828	505	1240	751	521
	C_P	€ MWh^{-1}	87.1	70.3	56.7	71.2	50.9	45.0
	$C_{biomass,be}$	€ MWh^{-1}	55.7	70.7	80.8	66.6	80.4	89.9

[a] corresponds also to the methanation pressure (less pressure drop).

[b] Me: Membrane separation, PA: Physical absorption downstream of methanation.

Table 6.5—Decision variables and performance of the economically optimal plant configurations for pressurised CFB-O_2 gasification.

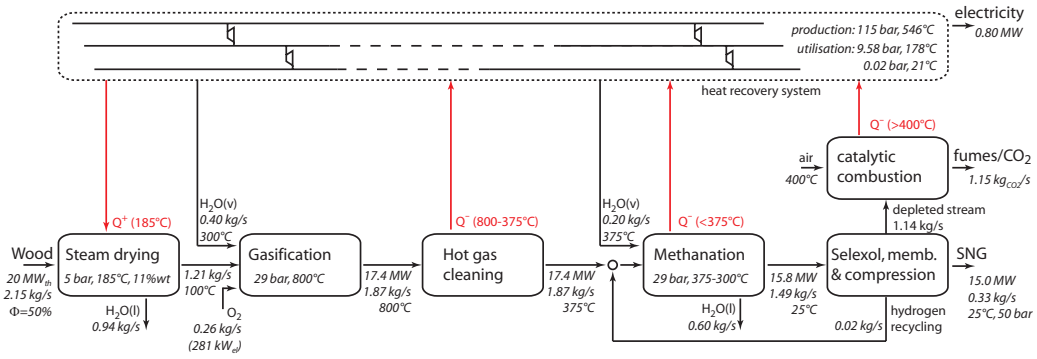

(a) Without heat cogeneration.

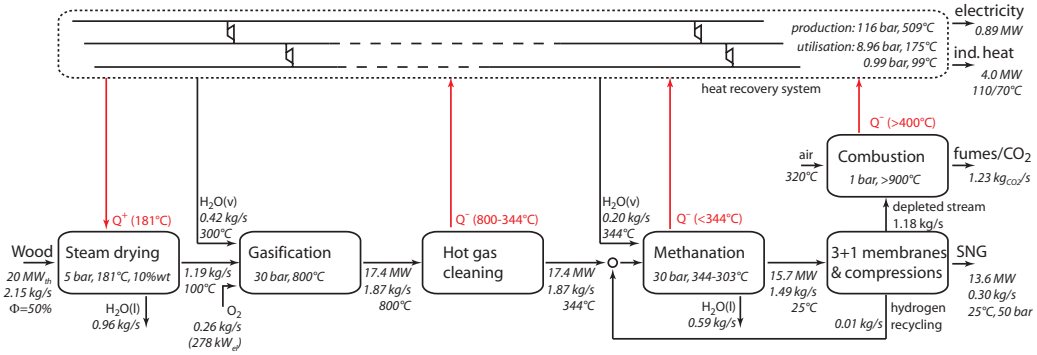

(b) With heat cogeneration.

Figure 6.12—Schematic flow diagrams for most economic plants at 20 $MW_{th,biomass}$ based on directly heated, pressurised gasification.

6.7 Conclusions

This chapter has presented a thermo-economic typefaction of the technologies for thermochemical production of SNG from lignocellulosic biomass by gasification and methanation. Coupling a process model with multi-objective optimisation techniques, a general set of Pareto-optimal flowsheets has been systematically generated for all potential combinations of the candidate technologies.

The analysis has shown that the gasification technology is the most distinctive and critical choice that dominates the entire process design. The developed process model thereby suggests that pressurised, directly heated gasification with oxygen and steam clearly outperforms indirectly heated gasification at atmospheric pressure with respect to both polygeneration efficiency and investment cost. Pressurisation of the FICFB-technology might partially compensate its disadvantage, and even close the gap in terms of

efficiency if it is technically feasible to integrate a gas turbine in the gasifier design. Among the pretreatment technologies, steam drying emerges as the best choice since it allows for efficiently recovering the latent heat. Although an additional torrefaction pretreatment step increases the SNG yield, it limits the cogeneration of heat and power and appears suboptimal in terms of combined production. Once mature, hot gas cleaning technology might increase the chemical efficiency by 3 to 5%. This benefit is yet limited to pressurised gasification close-coupled to methanation. For an optimal process design, the gas separation technology needs to be matched with the gasification and the operating conditions of the synthesis. A membrane cascade is typically less costly than the other options and performs best at small to mid-scale and especially if heat can be valorised in a distribution grid. From medium to large scale, FICFB gasification performs best with the slightly more efficient and costly pressure swing adsorption. Due to its elevated operating pressure, CFB-O2 gasification matches particularly well with physical absorption, which particularly benefits from economies of scale. In any case, energy recovery by a steam cycle is mandatory for a efficient conversion of the resource.

In the last part of the analysis, the economic process scaling is discussed and parameters for a regression of the investment cost on plant scale are provided. Depending principally on the price for energy, the most competitive process configurations at different scales are finally identified.

Chapter 7

Optimal process design for hydrothermal production of SNG from waste biomass

While the previous chapters have addressed conventional technology for SNG production from relatively dry matter, this chapter deals with hydrothermal gasification of wet biomass and biomass waste. It present a detailed model that can be used as a tool for the process design. Based on a superstructure for combined product separation and energy recovery, the potential for fuel and power cogeneration is systematically assessed. Detailed optimisations of the thermo-economic plant performance investigate the optimal process design with respect to the availability of technology, catalyst deactivation, plant scale and feedstock characteristics.

7.1 Introduction

Hydrothermal gasification of biomass in supercritical water is a promising process alternative to the production of SNG through conventional gasification and methanation. By omitting the requirement for a dry feedstock, it grants access to a large range of low quality feedstocks such as wet lignocellulosic biomass and biomass wastes that are difficult to valorise by other means and thus relatively cheap.

In general, hydrothermal gasification is considered for the production of methane, hydrogen or combinations of those. Typically focussed on pathways for hydrogen, Matsumura et al. (2005), Kruse (2008, 2009), Elliott (2008) and Peterson et al. (2008a) provide reviews on process fundamentals, chemistry, catalysis and principal technological developments and issues. Experimen-

tally, Waldner and Vogel (2005) and Vogel et al. (2007) have demonstrated the production of methane in a batch reactor from wood substrate. During the subsequent development of a continuous process setup, the required salt separation in supercritical conditions has emerged as a main technological bottleneck. To understand this complex process step, Peterson et al. (2008b, 2009) have performed visualisations of salt precipitation in a vertical tubular vessel, and Schubert et al. (2010a,b) have led an extensive experimental study of the separation of different types of salt from supercritical water. Luterbacher et al. (2009) has reported on an overall process model and provided a first investigation of the process design and life cycle assessment for the hydrothermal production of SNG from wood and manure. Recently, microalgae have received growing attention as a feedstock since its production and gasification in a closed nutrient cycle would decouple energy crop based biofuels from food production (Haiduc et al., 2009, Stucki et al., 2009).

Among these previous studies which either discuss general process principles, present lab and pilot units or focus on detailed experimental investigations, Luterbacher et al. (2009) have presented the only process design model that quantitatively takes energy integration and recovery into account. At the time of their developments, only limited insight into the salt separator design and the product separation was yet available. Energy integration has been performed on a scenario basis without optimisation, and the synergies between the reaction and separation subsystems through process integration have been disregarded.

The objective of this chapter is to systematically address the conceptual process design of hydrothermal gasification for the cogeneration of SNG and power from wet lignocellulosic biomass and biomass wastes that are not accessible to the conventional technology investigated in the previous chapters. For this purpose, candidate thermodynamic models are first discussed and further developed to appropriately represent the physical properties at the particular process conditions. Luterbacher et al.'s model is then improved with both more general and detailed technology models that are reconciled and validated with data from experimental investigations. A general superstructure for integrated product separation, power recovery and heat supply for the process is developed, and multi-objective optimisation is finally applied to explore the design alternatives and performances for selected candidate substrates.

7.2 Process description

7.2.1 Thermodynamic considerations

The conversion of biomass into methane and carbon dioxide outlined in Equation (1) requires a heterogeneous catalyst and is thus impossible to perform directly with the solid biomass feed since the big macromolecules cannot access the active sites. The most envisaged conventional route discussed in the previous chapters is thus to first decompose the solid feedstock by gasification and then catalytically synthesise the obtained H_2/CO-rich producer gas into CH_4 and CO_2. Equation (1) therefore splits up in an endothermal gasification step at high temperature (typically > 800°C) and an exothermal synthesis step at 300 to 400°C at which CH_4 is thermodynamically favoured. This limits the product yield since a considerable part of the energy content of the feed is required to form intermediate H_2/CO and is then converted into excess heat in its highly exothermal methanation.

Contrary to this two-step layout, the hydrothermal route omits the endothermal step at high temperature and targets a direct conversion at 300 to 400°C into CH_4 and CO_2. Instead of forming an intermediate gas, the biomass is hydrolysed and gasified in a supercritical aqueous environment at around 300 bar, which allows for an efficient contact with the catalyst (Waldner and Vogel, 2005). The thoroughly fluid processing thereby requires a feed in form of a pumpable slurry with typical total solid contents of 20-50%wt depending on the type of substrate (Waldner and Vogel, 2005, Vogel et al., 2007). Although this makes the process suitable for wet biomass since the heat requirement up to the gasification temperature is reduced by high pressure and drying is not required, the design must take care of the high amount of water that accompanies the reacting species throughout the process. As this represents the major share of the heat transfer requirements, the overall performance gets sensitive to the energy integration of the plant.

7.2.2 Technical process layout

Depending on the humidity and type of biomass that is processed, the first step in the block flow diagram of Figure 7.1 is to mechanically dry or grind and dilute the feed. The slurry is then compressed to 300 bar and heated close to pseudo-critical conditions, during which hydrolysis occurs (Waldner and Vogel, 2005). When passing the pseudo-critical point, inorganics present in the feedstock will precipitate as salts and risk to plug the equipment and deactivate the catalyst if they are not efficiently removed. To do so, the subcritical slurry is injected through a dip-tube in a heated vessel, in which

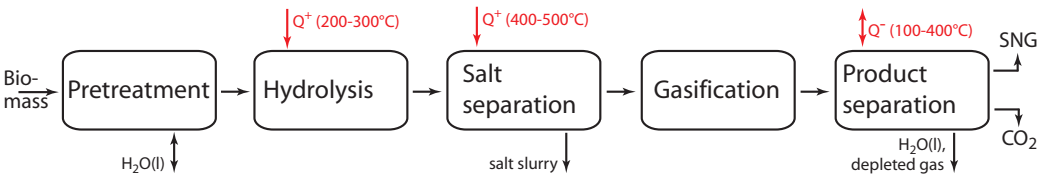

Figure 7.1—Block flow diagram for supercritical hydrothermal gasification.

supercritical conditions are reached, the salts precipitate and the main flow reverses and leaves the vessel at the top (Peterson et al., 2008b, 2009, Schubert et al., 2010a,b). The supercritical hydrolysate then passes through a fixed bed of nickel- or ruthenium-based catalyst, which converts, at ideal conditions, more than 99.9% of the organic matter into CH_4, CO_2 and some residual H_2 and only traces of CO (Vogel et al., 2007).

In order to inject the produced methane at the required purity of 96%mol into the natural gas grid (SVGW, 2008), it must be separated from water, carbon dioxide and possibly hydrogen. For a typical lignocellulosic feedstock (Eq. 1) diluted to 20%wt total solids, the crude product thereby contains approximately 84%mol of H_2O and 8%mol of each CH_4 and CO_2 in a supercritical mixture at 300-400°C and around 300 bar. As indicated in Figure 7.1, the process furthermore requires additional heat for the salt separator. The design of the product separation should therefore not only consider the grid quality specifications for SNG, but also the recovery of the exergy potential of the crude and the supply of required heat for the plant. For a similar separation problem in conventional SNG production, Chapter 4 has shown that the overall process benefits from a tight integration of the reactive and separation systems, and similar effects can be expected for a hydrothermal plant.

7.3 Process modelling

7.3.1 Thermodynamic models

Due to the targeted biomass conversion in supercritical water, the process design is confronted with rather particular thermodynamic conditions throughout the process. With the bulk substance H_2O present at reduced pressures $p_r = p/p_c$ up to 1.4 and temperatures $T_r = T/T_c$ in the range of 0.5 to 1.1, the operations are carried out in very different regions of the phase diagram. In hydrolysis, a suspended organic solid is decomposed at subcooled conditions into a large range of hydrocarbons. The mixture is then heated across the pseudocritical point, where the inorganic fraction precipitates and needs

to be removed in the salt separator. Gasification is carried out at supercritical conditions, and the crude product then separated somewhere in the gas- and two-phase regions at different compositions.

In order to ensure a reliable process design, several requirements are to be met by the thermodynamic model. The bulk of accompanying water causes the enthalpy-temperature profiles of the hot and cold streams to be non-linear and very tight. A change in a few degrees may considerably disturb the pinch point and thus the performance of the process. The prediction of these profiles must therefore be valid and consistent over the entire range of the process. A second crucial requirement is the accurate evaluation of the liquid vapour equilibrium (LVE) in the bulk separation, which needs to be able to reproduce the considerable non-idealities due to the polarity of H_2O and the fact that the conditions in the separation may approach the critical point of CO_2 at 304 K and 74 bar. Finally, the process design methodology imposes a thermodynamic model that is computationally robust in order to evaluate the process model at very different conditions.

Although simple linear models like Henry's law are very convenient at low pressure, they fail at higher pressures where the assumption of infinite dilution does not hold anymore. Approaches based on a general equation of state (EOS), as for example the classic ones by Peng and Robinson (1976) or Lee and Kesler (1975), are better suited for the high pressure domain, but lack precision for LVE equilibria in the present mixture. Peng-Robinson is a Van der Waals type EOS and thus suitable to represent moderate non-idealities, but has poor precision for polar mixtures (Heyen, 2008b). The Lee-Kesler EOS is reasonable for general purposes, but not precise enough to represent the phase equilibrium of the H_2O-CO_2-CH_4 system. For this reason, Duan et al. (1992a,b) developed and parametrised a modified form of the Lee-Kesler equation with experimental pTV and binary solvus data over a very large temperature and pressure range (273(323)-1273 K, 0-8000(1000) bar). Since promising for our application, this equation has been investigated for the prevailing process conditions, which has revealed some major weaknesses that prevent its direct application.

A hybrid approach as detailed in Appendix C is finally adopted. Above 523 K, the homogeneous EOS of Duan et al. (1992a,b) proves valid for LVE calculations and assures coherency in the critical zone. Below 523 K, however, the EOS looses both accuracy and robustness and a heterogeneous solubility model is used instead. For this purpose, the binary models for the H_2O-CO_2 and H_2O-CH_4 systems proposed by Duan and Sun (2003) and Duan and Mao (2006) are extended to the ternary by regressing activity coefficients that account for the interactions between CO_2 and CH_4 that have recently been observed in the ternary data of Qin et al. (2008). Throughout the process,

enthalpy is consistently evaluated with the original Lee-Kesler equation since the Duan EOS shows severe deviation from reliable data for pure water.

7.3.2 Energy-flow models

7.3.2.1 Hydrolysis

The breakdown of lignocellulosic biomass into its macromolecular components cellulose, hemicellulose and lignin and their hydrolysis into a wide spectrum of smaller molecules follows multiple complex reaction paths whose details are impractical to account for in process modelling. In a liquefaction experiment at 303℃ and 122 bar in water and presence of a nickel catalyst, Waldner and Vogel (2005) have identified the main intermediate species in the decomposition and developed a simplified reaction network. In the model of Luterbacher et al. (2009), these findings have been used to adjust an approximate hydrolysate composition based on a few model species for wood and manure. They have thereby followed a procedure by hand, which is not generalisable since the decomposition into model species is underdetermined and further infeasible for certain potentially interesting substrates.

In order to generalise the scope of the process model, a simple and systematic decomposition scheme that is feasible for a wide range of substances has been developed. The model species are thereby chosen among the principal experimentally observed substances that are located in the ternary diagram of Figure 7.2(a). Following the considerations of Waldner and Vogel (2005), different reaction pathways for lignin and (hemi-)cellulosic parts are expected, and the biomass is first divided into these two macromolecular groups:

$$biomass \rightarrow (hemi-)cellulose + lignin$$

i.e.:

$$\mathrm{CH}_{bmH}\mathrm{O}_{bmO} \rightarrow (1-\tilde{r}_{lignin})\ \mathrm{CH}_{celH}\mathrm{O}_{celO} + \tilde{r}_{lignin}\ \mathrm{CH}_{ligH}\mathrm{O}_{ligO} \tag{7.1}$$

with:
$$celH = \frac{bmH - ligH}{1-\tilde{r}_{lignin}} + ligH$$
$$celO = \frac{bmO - ligO}{1-\tilde{r}_{lignin}} + ligO$$
$$\tilde{r}_{lignin} = \frac{\tilde{m}_{biomass}}{\tilde{m}_{lignin}}\ r_{lignin}$$

Assuming a typical lignin composition of 62.7/6.0/31.3%wt C/H/O (ECN, last visited 06/2009) and a default lignin fraction r_{lignin} of 28%wt, Eq. (7.1)

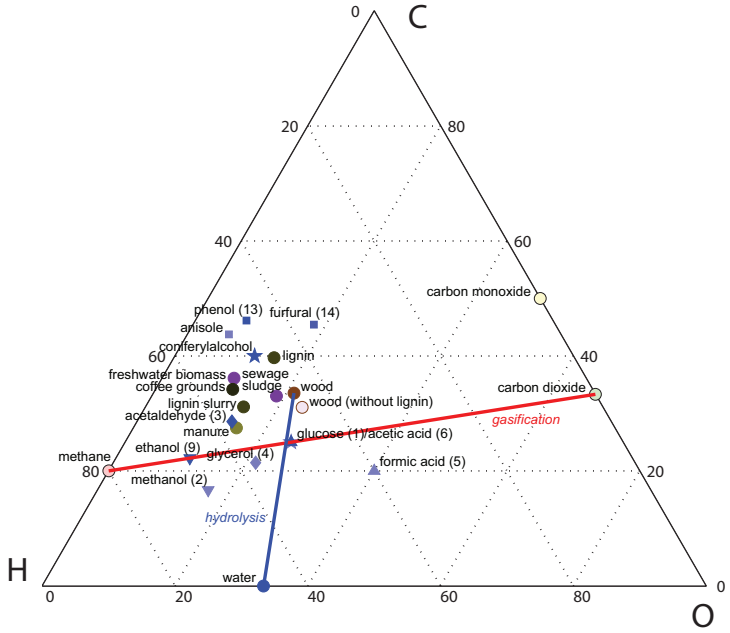

(a) Potential feedstocks, main intermediate hydrolysis products, global reactions and final products.

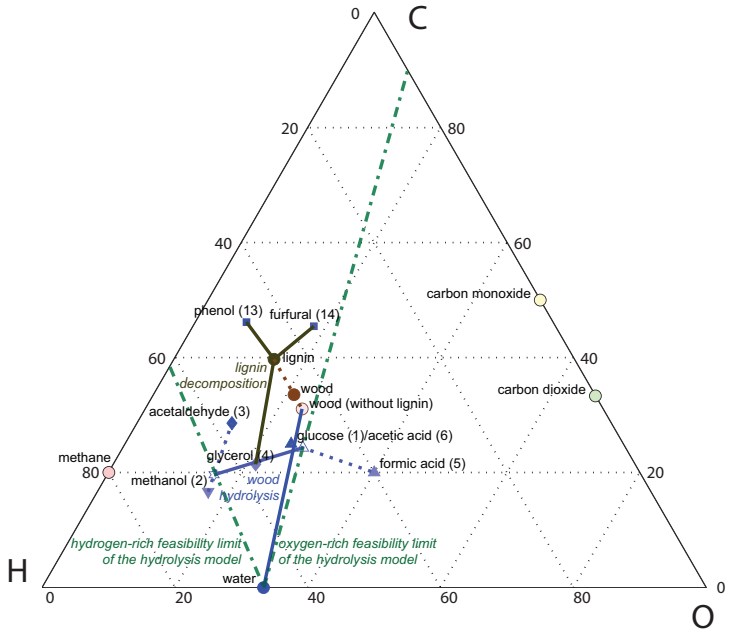

(b) Decomposition of wood and feasibility range of the model.

Figure 7.2—Molar ternary diagram of the hydrolysis model. Numbers in parenthesis indicate the quantitative rank of the substances detected in the liquefaction experiment by Waldner and Vogel (2005).

decomposes the biomass macromolecule of Eq. (1) to:

$$CH_{1.35}O_{0.63} \rightarrow 0.66\ CH_{1.46}O_{0.76} + 0.34\ CH_{1.14}O_{0.38} \tag{7.2}$$

During hydrolysis, the (hemi-)cellulosic parts are degraded to glucose and further (via 5-hydroxymethyl furfural, 5-HMF) to carboxylic acids, aldehydes and alcohols (Waldner and Vogel, 2005). Among the experimentally identified substances, the most abundant have been chosen as model species, and Eq. (7.1) is further developed as:

$$\begin{aligned}(hemi-)cellulose + water \rightarrow\ & acetic\ acid + formic\ acid \\ & + acetaldehyde + methanol\end{aligned}$$

i.e.:

$$\begin{aligned}CH_{celH}O_{celO} + \tilde{r}_{H2O}\ H_2O \rightarrow\ & \tilde{r}_{acetic\ acid}\ CH_3COOH + \tilde{r}_{formic\ acid}\ HCOOH \\ & + \tilde{r}_{acetaldehyde}\ CH_3CHO + \tilde{r}_{methanol}\ CH_3OH\end{aligned} \tag{7.3}$$

In addition to the three atomic balances of C, H and O, two more specifications are needed to determine the stoichiometric coefficients of this hydrolysis reaction. For this purpose, the data of Waldner and Vogel (2005) is used to assess typical ratios between the most abundant intermediates:

$$\tilde{r}_{acids} = \frac{\tilde{r}_{acetic\ acid}}{\tilde{r}_{formic\ acid}} = \frac{\tilde{c}_{acetic\ acid}}{\tilde{c}_{formic\ acid}} = \frac{\tilde{c}_{acetic\ acid+glucose}}{\tilde{c}_{formic\ acid}} = 3.82 \tag{7.4}$$

$$\tilde{r}_{alcohol/aldehyde} = \frac{\tilde{r}_{methanol}}{\tilde{r}_{acetaldehyde}} = \frac{\tilde{c}_{methanol}}{\tilde{c}_{acetaldehyde}} = 3.57 \tag{7.5}$$

where glucose as principal decomposition product is included in the share of acetic acid due to their identical molar composition. On the ternary diagram of Figure 7.2(b), these ratios fix the intermediate points on the blue-dotted lines and determine the amount of water that is consumed during hydrolysis.

Lignin is typically converted to phenolic and aromatic compounds and then further to the same final products as above. In order to represent the more carbon-rich lignin-derivates, phenol and furfural are included as model species, and the lignin decomposition is balanced with the abundant glycerol:

$$lignin \rightarrow phenol + furfural + glycerol$$

i.e.:

$$CH_{1.14}O_{0.38} \rightarrow 0.072\ C_6H_6O + 0.086\ C_5H_4O_2 + 0.045\ C_3H_8O_3 \tag{7.6}$$

which is shown by the brown lines on Figure 7.2(b). In this way, the decomposition model includes the main families of the observed species, and is feasible for a broad range of potential substrates. According to the conservative estimate for the hydrolysis kinetics of Luterbacher et al. (2009), these reactions are assumed to take place between approximately 250 and 350℃ with a peak at 320℃.

7.3.2.2 Salt separation

The currently envisaged design of the salt separator consists of a vertical, tubular vessel in which the hydrolysate is injected through a dip tube (Peterson et al., 2008b, Schubert et al., 2010a). By externally heating the vessel, the mixture passes its pseudo-critical point, at which the solubility of the salts decreases and causes them to precipitate in a salt brine that is withdrawn at the vessel bottom. As the fluid temperature increases, the bulk flow reverses towards the top exit of the vessel, which is schematically shown in Figure 7.3. At the time Luterbacher et al. (2009) developed their model, the detailed equipment design was not yet considered, and the thermodynamic, linear hT-profile from inlet to outlet has been assumed accessible to the heating medium with a minimum approach temperature contribution $\Delta T_{min}/2$ of only 4℃. From an engineering perspective, this is most likely a too optimistic assumption for the heat transfer at the technological bottleneck and pinch point of the process.

Based on the experimentally measured temperature profiles along the vessel axis by Schubert et al. (2010a), a technological representation of the heat requirement during salt separation is proposed here. As shown in Figure 7.3, the heat exchange is divided into several zones with distinct characteristics. In the dip tube area, heat is exchanged internally between the entering fluid and the main exit stream, and through the outer wall between the exit stream and the external heating medium. Since the heat transfer is dependent on the flow pattern, it is further expected to be different in the flow reversal and salt brine layer zone. Using Schubert's (2010a) experimental data for different operating conditions of the salt separator, global heat transfer coefficients U for these zones are reconciled with the general law of the form:

$$\dot{Q} = AU\Delta T_{lm} = \Pi l d_{lm} U \Delta T_{lm} \qquad d_{lm} = \frac{d_o - d_i}{\ln(d_o/d_i)} \tag{7.7}$$

where $\dot{Q}$ is the exchanged heat, A the area, l the section length, d_i and d_o the inner and outer diameter of the heat exchanger tube, respectively, and ΔT_{lm} the log-mean temperature difference in the heat exchange zone. As the heat transfer is dependent on the flow regime (i.e. Reynolds and Prandtl

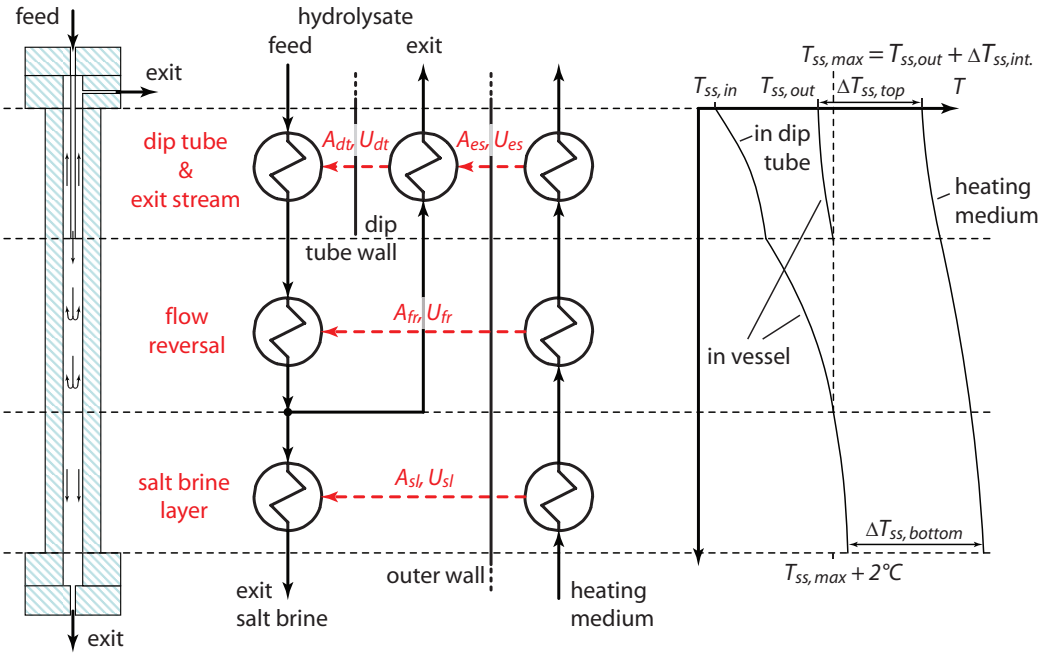

Figure 7.3—Schematic of the salt separator and its heat transfer model representation.

numbers), the reconciled values for U shown in Table 7.1 are not valid for diameters and flowrates different from the ones in the experimental setup.

Equation (7.7) used with distinct transfer coefficients for each zone represents the basis of a thermo-economic model for the salt separator, for which the hT-profiles are related to the required size of the separator tube. For scale-up, the vessel could be designed as a bundle of vertically arranged separator tubes including each a dip tube. The required area of this shell-and-tube like heat exchanger is then determined by specifying the targeted inlet and outlet temperatures of the hydrolysate and the heating medium. This approach complies with the proposed methodology that considers the thermodynamic requirements as a target for the equipment design.

In order to assess the catalyst poisoning in the gasifier by residual diluted sulphur, the salt loading at the separator outlet is estimated with the correlation of Leusbrock et al. (2008) for Na_2SO_4-solubility in pure supercritical water. Due to the lack of data for organic mixtures at these conditions, the correlation based on the fluid's molar density is applied without any modification. At the same temperature and pressure, this results in an increased salt solubility due to the increased density of the organic mixture compared to pure water. As Peterson et al. (2009) and Schubert et al. (2010b) reason that the separation does not occur at the hottest point, the arithmetic

Zone and exchanging fluids		Flow pattern[a]	d_i	d_o [mm]	d_{lm}	U[b] [$Wm^{-2}K^{-1}$]	Conf.[c] [%]
Dip tube							
dip tube	exit stream	cnt	1.5	3.0	2.16	4'190	15.0
exit stream	heating medium	co/cnt	50	12	26.6	477	13.0
Flow reversal							
mixed fluid	heating medium	co/cnt	50	12	26.6	268	10.2
Salt brine layer							
salt brine	heating medium	co/cnt	50	12	26.6	13	25.0

[a] Experiments have been conducted with an electric heating block at constant temperature and do thus not correspond to a flow pattern. For the process design, the reconciled U can be used for both co- and countercurrent modes (abbreviated co and cnt).

[b] U is dependent on d and thus not valid for other diameters than the ones reported here.

[c] 95%-confidence interval relative to U assuming a normal distribution.

Table 7.1—Salt separator heat transfer model reconciliation using data from Schubert et al. (2010a).

average of the molar density and temperature ($(\rho_{ss,max} + \rho_{ss,out})/\tilde{m}/2$ and $(T_{ss,max} + T_{ss,out})/2$) between the flow reversal and the top exit are considered in the correlation. For the organic loss in the salt brine, a conservative value of 10% of the salt separator feed based on the experience acquired by Schubert et al. (2010a,b) is furthermore assumed.

7.3.2.3 Gasification

Originally demonstrated in a batch reactor, the current development of a continuous process envisages a downdraft fixed bed design for the slightly endothermal gasification reaction (Vogel et al., 2005, 2007, Schubert et al., 2010a). The experimental results indicate that equilibrium conversion to CH_4, CO_2, residual H_2 and traces of CO can be reached with a weight hourly space velocity (WHSV) of no more than 2 $kg_{biomass,dry}kg_{cat}^{-1}h^{-1}$ and for gasification temperatures at approximately 400°C. If the temperature drop due to the endothermicity causes the reaction to fade away, preheating the feed after the salt separator or external heating of the reactor tubes might be envisaged to assure a good conversion. Catalyst deactivation is estimated assuming that 1 mol of sulphur poisons 1 mol of ruthenium, which is dispersed to 100% and represents 2%wt of the total catalyst mass (Schubert et al., 2010a).

7.3.2.4 Crude product separation and expansion

The crude product from gasification contains more than 80% H_2O, approximately equal amounts of CH_4 and CO_2, and some marginal H_2 and CO. Due to the supercritical conditions, its upgrade and expansion to grid conditions potentially allows for recovering mechanical energy, which however competes with the supply of thermal energy required for hydrolysis and salt separation. Another important aspect of the separation system design is the quality of the depleted stream, which may be used to supply the required heat and thus relax the need for a high methane recovery in the separation. The given boundary conditions thereby suggest two different separation strategies. Apart from conventional absorptive separation at grid pressure with a dedicated physical solvent followed by a membrane stage to remove residual hydrogen, the better solubility of CO_2 compared to CH_4 in water may become technically relevant at the prevailing process pressure. As shown by the absolute and relative solubilities of CO_2 towards CH_4 in their binary mixtures with water depicted in Figure 7.4(a), the relative solubility deteriorates with increasing pressure, and a trade-off between selectivity and good absolute solubility might occur. In any case, the separation is best at low temperature, and additional water is required for absorbing the bulk CO_2 to reach grid quality. The expected separation performance for a typical crude composition as calculated with the thermodynamic model of Appendix C is shown on Figure 7.4(b). Compared to a simple flash stage where only a marginal separation occurs, the use of a number of theoretical equilibrium stages and additional water allows for purifying the crude product up to the required 96%mol methane. The increase in purity is thereby rather steep at low rates of additional water, but flattens out at higher rates, which has a considerable impact on the pump power required to attain high purity. As expected from the trade-off observed in Figure 7.4(a), decreasing the absolute pressure increases the methane recovery due to the change in relative solubility and only marginally affects the attained purity.

In order to recover mechanical energy from the crude product at high pressure, the separated vapour phase – or the entire supercritical bulk, if no high pressure separation is applied – may be expanded through turbines. It might thereby be advantageous or even necessary to preheat the stream, which increases the thermal efficiency of the recovery and prevents an expansion to far into the two-phase region. Compared to an isenthalpic expansion through valves, this causes less heat to be available from the crude product stream since energy is withdrawn at high temperature, and can lead to suboptimality if done above the process pinch. For the liquid phase obtained from the separation at high pressure, the available exergy can be recovered

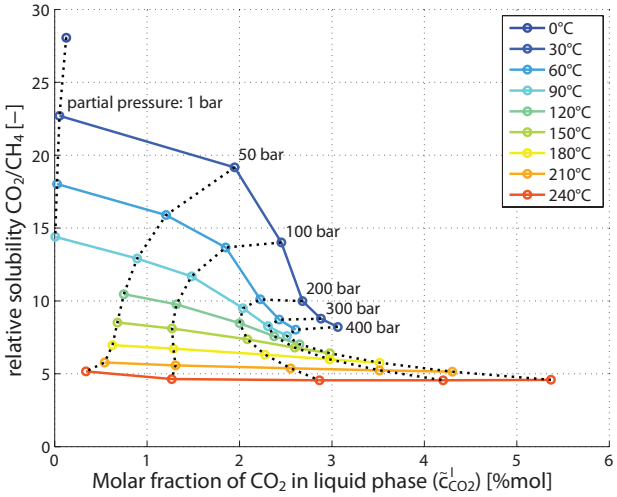

(a) Relative solubilities of CO_2 and CH_4 in their binary mixture with water (data according to Duan and Sun (2003), Duan and Mao (2006).

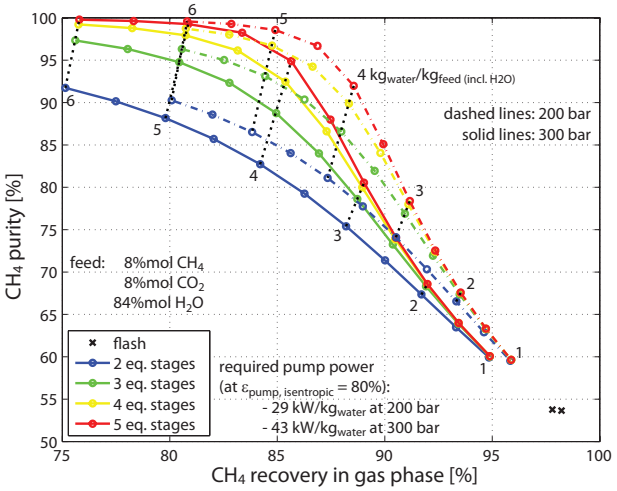

(b) Performance of CO_2/CH_4-separation in an absorption column with water.

Figure 7.4—Characteristics of the separation of CO_2 and CH_4 with water under high pressure.

by liquid expanders. This technology is currently being commercialised in natural gas liquefaction plants, where it also copes with expansions that partially result in a vapour phase (Perlmutter et al., 2004). As an alternative, the liquid phase could also be reheated and expanded into the the vapour domain, which would allow for extracting more mechanical energy from the available potential, but also requires a considerable amount of heat to be supplied.

A general superstructure with all these options for combined product separation and expansion is outlined in Figure 7.5. If the product is not upgraded to grid quality at high pressure, the liquid vapour (LV) and gas separation need to be carried out after the expansion of the crude product. In this case, the same technologies and models as for the more conventional SNG production by methanation of producer gas can be applied. For the complete gas separation at grid pressure, a Selexol column seems appropriate. The combination of both high pressure and grid pressure separation is also conceivable. In order to reduce the amount of required additional water and thus pump power, the gas could only be pre-separated at high pressure and a single polymeric membrane stage at grid pressure could be used. For a good separation performance of the latter, the partial pressure of CO_2 in the membrane feed should however not exceed 10-20 bar to avoid a decrease in selectivity due to plasticisation (Houde et al., 1996).

7.3.3 Energy integration

7.3.3.1 Minimum energy requirements

Figure 7.6 shows the minimum energy requirements of the principal flowsheeting options for wood with properties of Table 2.1 at the default operating conditions of Table 7.2. The composite curves that identify the contributions of the process sections (Fig. 7.6(a)) highlight that the layout of the product separation and expansion section determines the pinch point and influences the energy demand markedly. If no power recovery from the crude product is performed (Fig. 7.6, left), the process pinch is situated at the salt separator where 186 kW $MW_{biomass}^{-1}$ are required at 440°C. Below, the specific and latent heat of the crude product is sufficient for preheating and hydrolysis of the feed, and an excess of about 150 kW $MW_{biomass}^{-1}$ can be recovered between 250 and 400°C (Fig. 7.6(b)). Limited power recovery by liquid expansion of the high pressure condensate and/or expansion of the incondensable mixture with previous reheating to the process pinch does not change the MER and only marginally influences the amount of excess heat (not shown on figures).

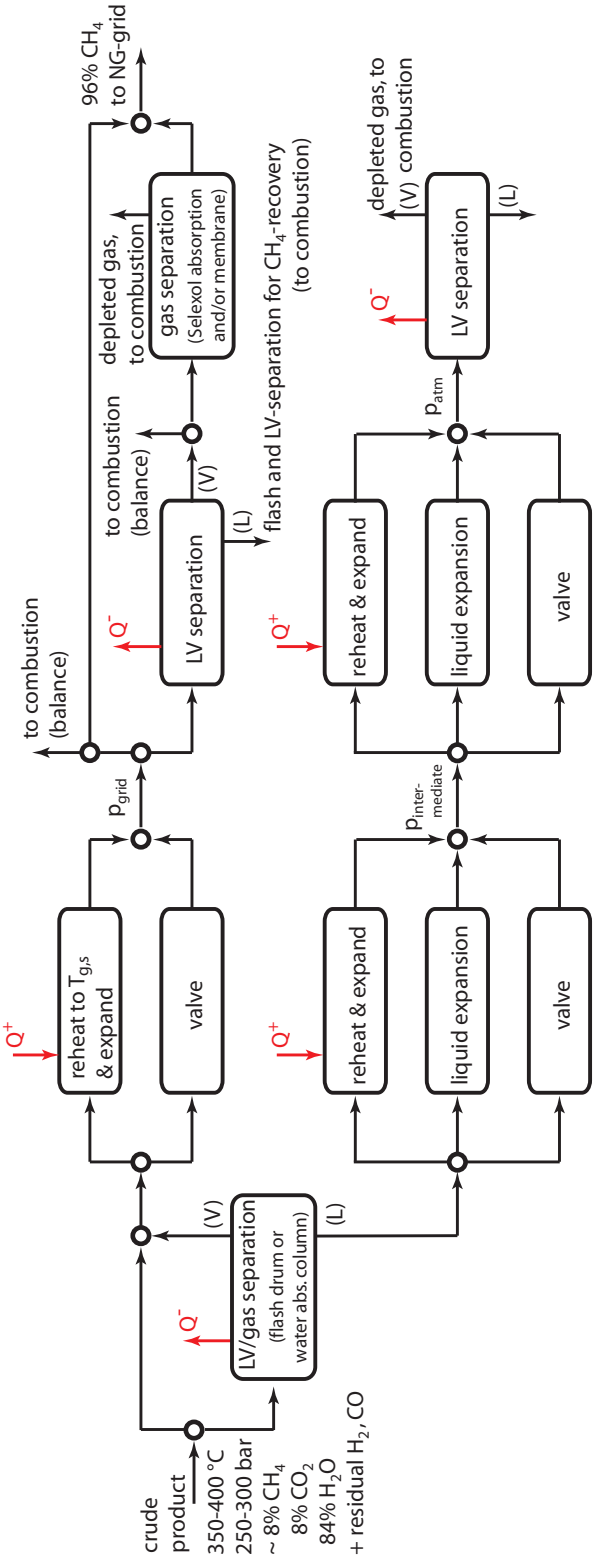

Figure 7.5—Superstructure including all possibilities for combined crude product separation and expansion.

Section	Operating conditions		Unit	Default	Range
General	Process pressure	p_{tot}	bar	300	[250 350]
	Feed total solids content		%wt	20	
Salt separation	Inlet temperature	$\Delta T_{ss,in}$	°C	350	
	Separation temperature	$T_{ss,max}$	°C	430	[430 550]
	Internal heat decrease	$\Delta T_{ss,int.}$	°C	20	[10 70]
	Outlet temperature	$\Delta T_{ss,out}$	°C	410	
	ΔT at bottom	$\Delta T_{ss,bottom}$	°C	20	[10 70]
	ΔT at top	$\Delta T_{ss,top}$	°C	30	[10 70]
	Organic loss in salt brine		%	10	
Gasification	Inlet temperature	$T_{g,in}$	°C	410[a]	
	Outlet temperature	$T_{g,out}$	°C	393[a]	[330 400]
Water column	Bottom temperature		°C	30	
	Pressure	$p_{hp,sep}$	bar	300	[100 350][b]
	Equilibrium stages	$N_{s,H2O}$	-	5	[3 5]
	CH_4 purity[c]	$\tilde{c}_{CH4,hp,out}$	%mol	n/a	[80 95]
Selexol column	CH_4 recovery	$r_{CH4,sel}$	%	98	[95 99]
	Absorption factor	A_{sel}	-	1.4	[1 1.8]
	CH_4 purity[c]	$\tilde{c}_{CH4,sel,out}$	%mol	n/a	[90 96]
SNG membrane	Material[c]	$y_{memb.}$	integer	n/a	[1 2]
Power recovery	Vapour phase	y^v_{prec}	integer	1	[0 1]
	Liquid phase	y^l_{prec}	integer	1	[0 1]
	Reheat temperature of vapour	$T_{g,s}$	°C	var	[300 600]

[a] obtained without feet preheating after salt separation.
[b] limited to process pressure.
[c] only for final SNG-upgrading with a polymeric membrane (material choice: 1: cellulose acetate, 2: polysulfone with properties given in Chapter 2).

Table 7.2—General assumptions, fixed operating conditions and decision variables for optimisation.

Section *(cont.)*	Operating conditions		Unit	Default	Range
Turbomachinery	Efficiency (isentropic)		%	80	
Rankine cycle	Steam production pressure	$p_{s,p}$	bar	var	[20 120]
	Steam superheat temperature	$T_{s,s}$	°C	var	[300 550]
	Intermediate utilisation level	$T_{s,u}$	°C	var	[50 250]
	Condensation level[d]		°C	19	
	Efficiency, backpressure stages		%	80	
	Efficiency, condensation stage		%	70	
POX-turbine	Pressure	p_{POX}	bar	14	[5 30]
	Fuel choice[e]	y_{fuel}	integer	1	[1 7]
	Additional steam per fuel i	$r_{fi,H2O}$	kg kg^{-1}	0.5	[0 1]
Energy integration	Fuel preheat temperature		°C	400	
	Minimum approach temperatures	$\Delta T_{min}/2$	°C		
	- vapour/supercritical streams		°C	8	
	- liquid streams		°C	4	
	- phase-changing streams		°C	2	
	- reactive streams		°C	25	

[d] corresponds also to the low-temperature utilisation level.

[e] candidate fuels: 1: (crude) SNG, 2: recovered depleted stream from flash, 3: membrane permeate, combinations: 4: 1&2, 5: 1&3, 6: 2&3, 7: all.

Table 7.2 *(cont.)*—General assumptions, fixed operating conditions and decision variables for optimisation.

If no separation at high pressure is applied and the crude product including the bulk water vapour is expanded in a turbine, the energy withdrawn as mechanical work is not available anymore at the gasification outlet temperature. As a consequence, the pinch point shifts to the turbine outlet temperature and results in an increased MER at lower temperature (Fig. 7.6, right). Reheating the crude might thereby be required to avoid condensation in the final turbine stages and enhances the thermodynamic conversion efficiency, which leads not only to an increased power output but also heat demand.

If the condensable phase from separation at high pressure is evaporated, reheated and expanded to atmospheric pressure, the characteristics of the process integration change drastically. For such a configuration, the pinch point would shift to the saturation temperature of the mixture at atmospheric pressure and the MER increases to 64-68% of the raw material's heating value. This would require to burn a large part of the produced gas and thus turn the generation of electrical power to the plant's main purpose.

7.3.3.2 Heat supply and cogeneration options

As mentioned earlier, the residual amount of methane and hydrogen in the depleted streams from the product separation may contribute to satisfy the process MER and reduce the amount of fuel to be withdrawn from the product stream in order to balance the heat demand. In the separation system superstructure of Figure 7.5, the waste streams considered for this purpose are the vapour phase recovered by the flash drums at atmospheric pressure, the offgas from the Selexol regeneration column and the membrane permeate in the SNG postprocessing after bulk removal of CO_2. If these are not sufficient, crude SNG at grid pressure is identified as the appropriate stream to balance the heat requirement.

In addition to the embedded power generation from the exergy potential of the high pressure product, excess heat below the pinch can be recovered in a Rankine cycle to cogenerate electricity and industrial heat. In our model, the energy recovery potential of such a cycle is calculated with water as working fluid, although the temperature levels identified on Figure 7.6(b) suggest an organic fluid as a technically more relevant option. Complementary to conventional waste heat recovery in a bottoming cycle, the pinch at a still moderate temperature level might also allow for high temperature cogeneration. Although Luterbacher et al. (2009) demonstrated that gas engines or standard gas turbines are not adequate since the temperature level of the cogenerated heat is too low to efficiently balance the MER, less conventional gas turbine technology might yet be an option. One possibility is thereby not to control the turbine inlet temperature by lean combustion, but to with-

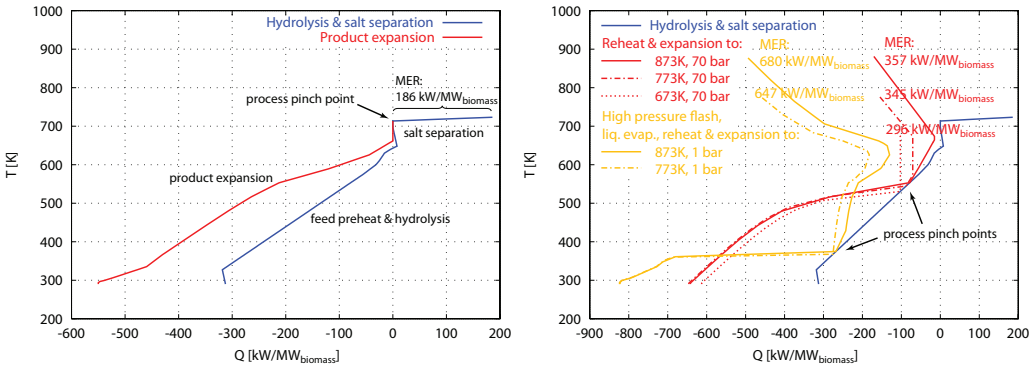

(a) Composite curves of pre- and post-gasification sections.

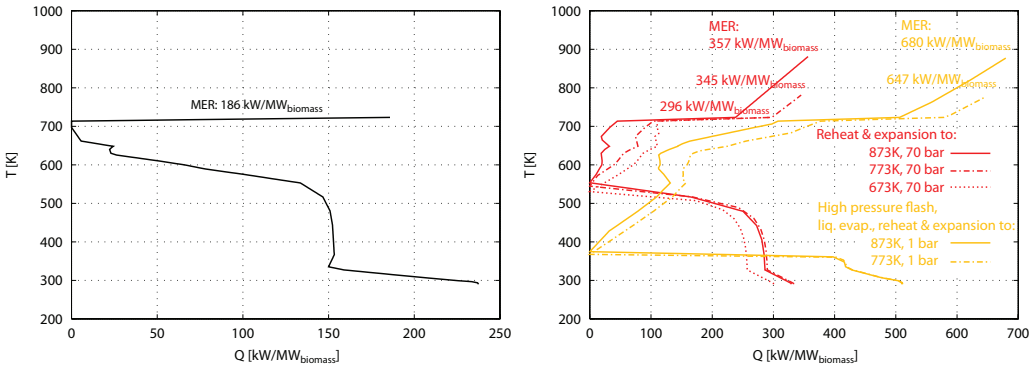

(b) Grand composite curves.

Figure 7.6—Minimum energy requirements for product expansion without power recovery (left) and for complete power recovery by reheating of entire condensable phase.

draw high temperature heat by radiative transfer from the combustion to satisfy the MER. Another option is to only partially oxidise the fuel in the gas turbine and complete the combustion after expansion. As shown in the exemplary energy balances of Table 7.3, these options provide substantially more heat at the identified process pinch point, and internal heat recovery for air preheating and steam injection might further increase the cogeneration efficiency.

In order to illustrate the thermodynamic performance of the principal flowsheeting and cogeneration options, Table 7.4 shows a screening of energy balances and efficiencies for the default operating conditions of Table 7.2. Comparing the alternatives for product separation with a high pressure stage, the detailed electricity balance highlights the elevated pump power required for complete separation in a water column at 300 bar. Power recovery through liquid expanders thus appears mandatory. From a pure efficiency

	Power	Heat		
Technology		$T > T_{pinch}$	$T < T_{pinch}$	stack loss
Expansion and combustion	2.0%	97.7%	-0.2%	0.6%
Gas turbine				
- conventional lean, simple cycle	26.5%	16.0%	44.4%	13.0%
- with radiative HE	9.6%	74.7%	11.9%	3.9%
Partial oxidation (POX) gas turbine				
- simple cycle	7.9%	85.7%	4.6%	1.8%
- air preheating to 800°C	7.8%	86.4%	4.2%	1.6%
- steam injection (0.3 kg kg_{SNG}^{-1})	8.7%	84.6%	1.9%	4.7%
- with radiative HE	8.6%	80.4%	8.2%	2.7%

Table 7.3—Typical energy balances for cogeneration options from SNG at 20 bar. Fuel and steam are preheated to 400°C, air to $T_{pinch} = 440$°C ($T_{stack} = 120$°C).

point of view, bulk gas separation at grid pressure is still more competitive due to its lower power consumption. For both these options, the power recovery potential from expanding the crude vapour phase to grid pressure is relatively modest and only feasible at large production scales. This is illustrated in Figure 7.7, which shows the power recovery potential and the minimum rotational speed of a radial turbine to reach an isentropic efficiency of 80% according to Balje (1981). If the liquid phase is separated at gasification pressure, the rotational speed required to efficiently expand the dense gas phase is indeed elevated and the turbine design might be challenging.

A Rankine cycle may generate around 4% of the biomass input as electricity and allows for a positive net power balance. Due to the high marginal electric efficiency approaching 60%, the use of a partial oxidation turbine for high-temperature cogeneration might slightly increase the chemical efficiency-equivalent although the power potential is limited. If no high pressure separation is applied and the crude bulk is reheated, expanded and separated at grid pressure, the product balance shifts towards an increased electricity generation to the expense of SNG. Both the product expansion turbine and the bottoming cycle generate substantially more power and integrate particularly well with a partial oxidation turbine. For all options, the largest part of the energy loss is related to the heat evacuation by cold utility, and a substantial chemical potential is lost in the substrate accompanying the salt brine withdrawn from the separator.

		High pressure gas separation		water absorption		flash drum		-	
		Grid pressure gas separation		-		selexol absorption		selexol absorption	
		Vapour reheat temperature $T_{g,s}$		400 °C		400 °C		600 °C	
		POX turbine fuel		-	SNG	-	crude SNG	-	crude SNG
Consumption	Biomass		kW	20'000	20'000	20'000	20'000	20'000	20'000
	Electricity	- process	kW	192	192	192	192	192	192
		- separation	kW	943	942	218	195	155	122
Production	SNG		kW	12'888	12'611	12'864	11'521	9'088	7'167
	Electricity	- vapour exp.	kW	134	124	331	296	1'909	1'782
		- liquid exp.	kW	652	652	92	92	21	21
		- POX turbine	kW	-	162	-	833	-	1'606
		- Rankine cycle	kW	848	859	792	744	1'371	1'146
		- net	kW	499	663	805	1'578	2'954	4'241
Losses		Total	kW	6'613	6'726	6'331	6'901	7'958	8'592
		- salt brine	kW	1'910	1'910	1'910	1'910	1'910	1'910
		- cooling water	kW	3'542	3'559	3'596	3'331	5'045	4'226
		- fumes	kW	404	411	410	494	706	820
		- latent heat[a]	kW	757	846	415	1'166	297	1'636
Efficiencies		ϵ_{SNG}	%	64.4	63.0	64.3	57.6	45.4	35.8
		ϵ_{el}	%	2.5	3.3	4.0	7.9	14.8	21.2
		ϵ	%	66.9	66.3	68.3	65.5	60.2	57.0
		η	%	61.6	61.0	62.8	60.0	55.0	51.8
		ϵ_{chem}	%	68.8	68.9	71.4	71.5	71.4	73.1
		$\Delta\epsilon_{el,\ POX}$[b]	%	-	59.2	-	57.6	-	67.0

[a] Difference in latent heat of the combustion products from biomass, SNG and on-site flue gas which is not accounted for in energy balances based on lower heating value. Calculated by difference.

[b] defined as $\Delta\dot{E}/(\Delta h^0_{SNG}\Delta\dot{m}_{SNG})$.

Table 7.4—Typical energy balances and efficiencies for the principal flowsheeting and power recovery options of Figure 7.5 for wood.

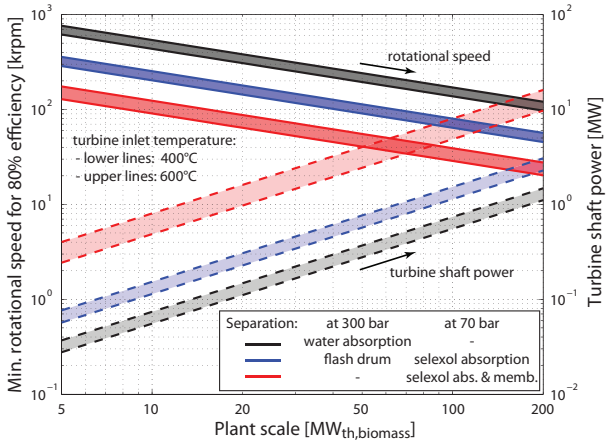

Figure 7.7—Power recovery potential from high pressure vapour and minimum rotational speed required to reach 80% turbine efficiency determined with the correlation of Autissier et al. (2007) for Balje's (1981) radial turbomachinery data. Tip speed is between 350 and 550 m s^{-1} and always subsonic.

7.3.4 Economic evaluation

As outlined in Chapter 1, the investment cost of a flowsheet is estimated through rating and costing the major process equipment required to reach the targeted conversion. Following classic process design procedures by Ulrich and Vasudevan (2004) and Turton et al. (1998), the process vessels for reaction and separation are roughly sized for the specific operating conditions. Costing data from the same sources is then used to determine the investment required for the plant.

Before diluting and pressurisation, solid biomass feedstock has to be ground, whereas wet feedstock is dewatered in a sedimentation centrifuge. If sanitarily problematic waste biomass such as manure is used, the excess water is further purified by reverse osmosis, which also allows for recovering the nutrient salts and dissolved organic matter. The required membrane area for the unit has been reconciled with cost data from Luterbacher et al. (2009) and Ulrich and Vasudevan (2004). For the salt separator, the heat transfer area is determined in the energy-flow model and directly used for its costing as a shell and tube heat exchanger with a fixed tube sheet in titanium alloy. The gasification reactor is rated for a WHSV of 2 $kg_{biomass}kg_{cat}^{-1}h^{-1}$ considering a dry catalyst bed density of 260 kg m^{-3}. The equipment for LV separation and gas absorption is sized according to the recommendations by Ulrich and Vasudevan (2004). Both for water and Selexol as solvent, a tray efficiency of 15% is assumed. Whereas Selexol regeneration requires a

stripper, the saturated water is simply expanded and flashed at atmospheric pressure to recover the residual fuel. For the final membrane stage, the same cost data as in Chapter 2 is used. The cost of combustion equipment is assessed with Ulrich and Vasudevan's correlation for alloy steel reformer furnaces. For the heat exchanger network, the total heat transfer area and the minimum number of exchangers is estimated from the balanced composite curves following Ahmad et al. (1990). The cost of the network is assessed for fixed tube sheet heat exchangers of mixed carbon-steel/nickel-alloy construction at maximum process pressure with the averaged surface areas obtained for a reference heat transfer coefficient of 580 $Wm^{-2}K^{-1}$ in Equation (1.6). For all turbomachinery, centrifugal units are considered.

The operating expenses are assessed for the prices for raw materials, electricity, maintenance and labour of Table 2.6. In addition, the cost for catalyst renewal due to deactivation is assessed with a price of 200 € kg^{-1}. The total production costs are obtained by summing up the operating expenses and capital depreciation over 15 years with an interest rate of 6%. For currency conversions, parity between € and US$ and 1.5 CHF $€^{-1}$ are used.

7.4 Thermo-economic optimisation of the process design

In order to explore and optimise the performance of the different process design alternatives illustrated in the separation superstructure of Figure 7.5 and discussed in Section 7.3.3.2, separate optimisations of the major flowsheet alternatives are carried out. As already introduced in Table 7.4, these are (1) LV and gas separation in a water column at high pressure, (2) bulk LV separation in a high pressure flash drum and gas separation at grid pressure by selexol absorption and (3m) no high pressure separation, but both LV and gas separation by a flash drum and selexol absorption at grid pressure followed by a membrane for the selective removal of residual hydrogen. While the use of membrane technology as an additional downstream separation step at grid pressure to allow for hydrogen removal is mandatory in case (3), it has also been identified as promising for flowsheets that include a separation step at high pressure (i.e. options (1m) and (2m)), since it also allows for relaxing the required methane purity in the bulk separation. All these alternatives are optimised without and with partial oxidation turbine technology fed with the different candidate fuels identified in Figure 7.5. A complete list of the decision variables for all optimisations is given in Table 7.2.

7.4.1 SNG and power cogeneration potential

As illustrated earlier in Table 7.4, the process design for hydrothermal conversion of biomass is particularly flexible with respect to the co-production of fuel and power. In order to explore this particular trade-off, the maximum cogeneration potential is determined in a first optimisation step that targets the partial efficiencies of both SNG and power defined in Equations (1.32) and (1.34), respectively. The influence of the available power recovery technology is thereby highlighted by separately optimising all process configurations with and without power generation from the crude product expansion and the use of a partial oxidation turbine.

Figure 7.8 shows the computed partial outputs in the Pareto domain and the resulting overall chemical efficiency defined in Equation (1.35). The operating conditions and performances of the solutions that maximise the latter are summarised in Table 7.5. The optimisations have revealed that a supplementary membrane has only marginal influence on the thermodynamic performance, and the data for alternatives (1m) and (2m) are thus omitted in this analysis for simplicity.

The plots indicate that up to 75% or 40% of the biomass input can be converted into SNG or power, respectively. In between, the outputs are substitutable over a very large domain. If power recovery from the high pressure vapour phase is not feasible (Fig. 7.8, left), the most efficient solutions for the combined production are situated close to the top-end SNG generation at which the power consumption for a higher gas yield drastically increases. Below a partial SNG efficiency of approximately 70%, the marginal increase in power generation to the expense of SNG is lower than the benchmark efficiency η_{NGCC} for a combined cycle and the overall combined efficiency steadily decreases. If power recovery from the high pressure bulk phase is feasible (Fig. 7.8, right), a particularly high marginal efficiency for supplementary power generation is obtained at lower SNG rates. Combined with a partial oxidation gas turbine, a second peak of the combined efficiency is reached at only 35% and 24% partial output for SNG and electricity, respectively. In general, the optimisation of the process design and its integration allows for increasing the equivalent chemical efficiency by up to 4 to 7 points compared to the default scenarios discussed in Table 7.4.

For the conceptual process design, some key variables can be identified from the decision variable distribution of the optimal configurations. In general, high pressure facilitates high SNG and chemical efficiency since it considerably reduces the heat requirement of the process. Decreasing pressure requires the combustion of more SNG to supply the MER and emphasizes power cogeneration from the excess heat. The inverse effect is observed for

High pressure vapour power rec.		no			yes		
	Unit	(1)	(2)	(3m)	(1)	(2)	(3m)
Design variables							
p_{tot}	bar	350	335	350	348	350	348
$T_{ss,max}$	°C	460	458	432	448	433	488
$\Delta T_{ss,int.}$	°C	70	67	49	59	43	10
$T_{ss,out}$	°C	390	391	383	389	390	478
$\Delta T_{ss,bottom}$	°C	27	37	53	10	26	19
$\Delta T_{ss,top}$	°C	28	46	21	30	10	44
$T_{g,in}$	°C	372	376	373	373	372	402
$T_{g,out}$	°C	330	330	330	330	330	364
$p_{hp,sep}$	bar	100	335	-	100	350	-
$N_{s,H2O}$	-	5	-	-	5	-	-
$r_{CH4,sel}$	%	-	96.8	95.2	-	95.2	96.6
A_{sel}	-	-	1.00	1.00	-	1.00	1.21
$\tilde{c}_{CH4,sel,out}$	%	-	-	94.8	-	-	95.9
$y_{memb.}$	-	-	-	2	-	-	2
y^{v}_{prec}	-	-	-	-	1	1	1
y^{l}_{prec}	-	1	1	1	1	1	1
$T_{g,s}$	°C	-	-	-	573	313	585
$p_{s,p}$	bar	66.4	74.5	23.2	71.0	44.7	22.2
$T_{s,s}$	°C	547	550	377	550	507	492
$T_{s,u}$	°C	166	124	132	150	143	103
p_{POX}	bar	-	14.7	24.8	10.6	-	24.2
y_{fuel}	-	-	4	1	4	-	1
$r_{f1,H2O}$	-	-	0.10	0.01	0.19	-	0.01
$r_{f2,H2O}$	-	-	0.15	-	0.05	-	-
Efficiencies							
ϵ_{SNG}	%	73.6	69.7	73.8	68.0	74.4	34.7
ϵ_{el}	%	1.1	3.7	-0.1	4.4	1.5	24.1
ϵ	%	74.7	73.3	73.7	72.5	75.9	58.8
η	%	68.7	67.4	67.9	66.6	69.9	53.4
ϵ_{chem}	%	75.5	76.1	73.6	75.8	77.1	77.1
Costs							
c_{GR}[a]	€ kW^{-1}	743	1095	860	863	1017	1147
C_{OP}[b]	€ MWh^{-1}	59.0	58.9	62.8	56.1	59.7	13.2
C_{P}[b]	€ MWh^{-1}	72.5	79.9	78.4	73.1	77.9	57.5
C_{cat}	€ MWh^{-1}	3768	2787	7788	4805	5820	129
$C_{biomass,be}$[b]	€ MWh^{-1}	68.3	61.2	64.0	65.2	64.6	55.0

[a] at a nominal capacity of 20 $MW_{th,biomass}$.

[b] without catalyst.

Table 7.5—Design variables and performances of the optimal process configurations with respect to ϵ_{chem}.

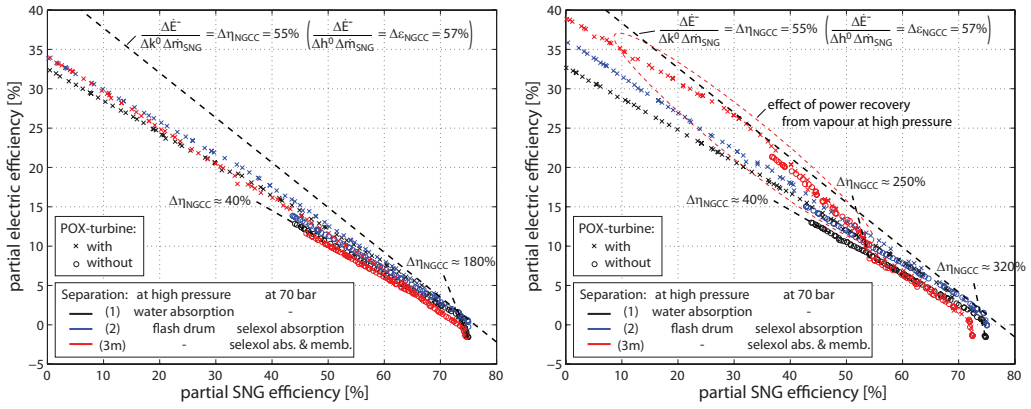

(a) Partial efficiencies (Pareto front).

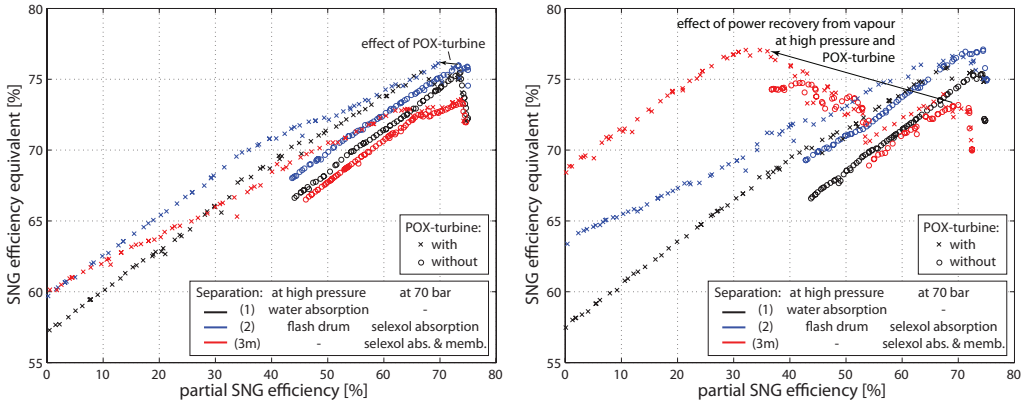

(b) Chemical efficiency.

Figure 7.8—Maximum process efficiency without (left) and with power recovery from the high pressure vapour phase.

the temperatures in the salt separator. Essentially determining the process pinch point, low temperature is favourable for high SNG output, while high temperatures increase the share of cogenerated power. For the most efficient process design without power recovery from the crude product at high pressure, the composite curve in Figure 7.9 (left) highlights that the optimisation of the process pressure and salt separation temperatures reduces the MER by 50% compared to the default solution shown earlier in Figure 7.6 (left), while keeping the pinch point at 430°C.

The gasification outlet temperature essentially determines the amount of residual hydrogen and is therefore linked to the choice and operating conditions of the separation system. Generally tending towards its lower bound, low temperatures are particularly favoured if no supplementary membrane

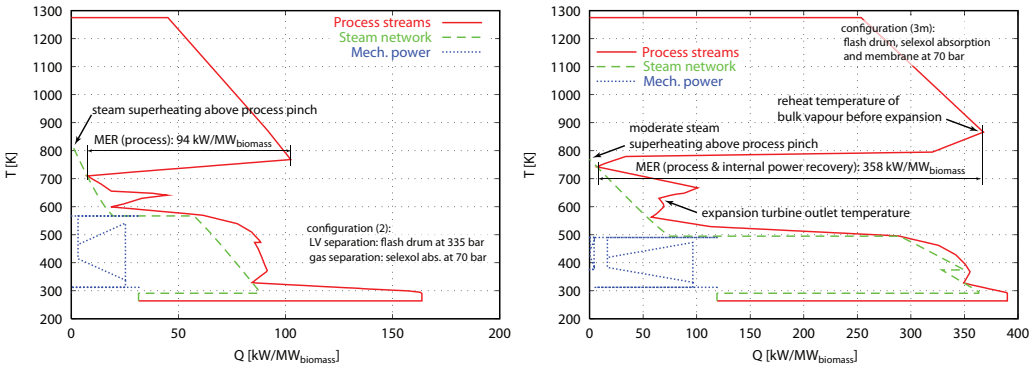

Figure 7.9—Grand composite curves for the most efficient process configurations without (left) and with power recovery from the bulk at high pressure.

separation is carried out and if high SNG output is targeted. However, such low temperatures might be hard to realise due to reaction kinetics and require a very efficient catalyst. For separating the crude product in a water column, a very pronounced trend to the lower limit for pressure confirms the conclusions from Figure 7.4 that high pressure mainly increases the pump power without being essential for the separation performance in the integrated system. If a supplementary membrane is used, relatively low methane purity in the high pressure column is further advantageous to limit the power requirement. Contrary to the LV and gas separation in a water column, high pressure is yet advantageous for pre-separating the crude product in a flash drum. The remaining decision variables for the separation system are not conflictive with respect to the relative output, but influence the thermo-economic trade-off discussed in Section 7.4.2.

In any case, power recovery from the high pressure streams increases the process efficiency. While liquid expanders should especially be considered if the gas is washed with additional water, power recovery from the vapour phase represents a major advantage if the entire bulk is expanded in the vapour phase and separated at grid pressure. Reheating across the pinch is thereby favourable in any case, although it slightly decreases the gas output by increasing the MER. Combined with a topping partial oxidation turbine and a bottoming Rankine cycle, the composite curve of Figure 7.9 (right) provides the characteristics of this efficient alternative with a high power share. In this setup, the partial oxidation turbine is preferably operated at 20 to 25 bar and fuelled by crude SNG without additional steam. For the Rankine cycle, moderate steam pressure or an organic fluid seems appropriate.

7.4.2 Optimal thermo-economic plant design

Having explored the thermodynamic cogeneration potential of the hydrothermal conversion, the following sections address the optimal thermo-economic plant design by considering process economics. As indicated in Table 7.5, catalyst deactivation is of crucial importance in this regard and prevents a priori the most efficient flowsheets to be economically feasible by orders of magnitude. In order to elaborate this particular impact on the process design and performance, separate optimisations with and without considering the catalyst cost in the process economics are carried out. As already distinguished in the previous paragraph, the individual optimisation of flowsheets with and without power recovery from the crude product at high pressure is furthermore maintained.

7.4.2.1 Catalyst deactivation without regeneration

In a first optimisation step, catalyst poisoning by residual, dissolved sulphur that has not precipitated in the salt separator is considered by assuming that deactivated catalyst is disposed and replaced by new charges at full cost. In order to cover both the thermodynamic and economic design targets and allow for a clear analysis of the results, two consistently aggregated performance indicators are used as objectives. The chemical efficiency defined in Equation (1.35) represents the thermodynamic performance and covers all costs and profits directly linked to it (i.e. raw material, labour and returns from the products). The purely economic aspects that are not directly linked to the energetic process inputs and outputs (i.e. equipment, maintenance and auxiliaries) are assessed by the specific investment cost plus the total catalyst cost over the whole plant lifetime n [years], i.e.:

$$c_{GR,cat} = \frac{C_{GR} + 27.7 \cdot 10^6 n \, C_{cat} \dot{m}^+_{cat}}{\Delta h^0_{biomass} \dot{m}^+_{biomass}} \tag{7.8}$$

The performance of the flowsheet alternatives optimised with respect to these two objectives and their impact on the overall process economics are shown in Figure 7.10. Analogous to Chapter 6, the latter is assessed by the biomass break-even cost defined in Equation (1.43) as the maximum acceptable raw material cost for the plant to break even. Tables 7.6 and 7.8 summarise the overall economically optimal process configurations that maximise this aggregated indicator for flowsheets without and with power recovery from the high pressure vapour phase.

If power recovery from the vapour phase is not considered, LV separation in a high pressure flash drum and gas separation by physical absorption with

	Catalyst deactivation considered						
		Unit	(1)	(1m)	(2)	(2m)	(3m)
Design variables	p_{tot}	bar	250	251	250	250	252
	$T_{ss,max}$	℃	500	498	500	523	521
	$\Delta T_{ss,int.}$	℃	68	67	60	69	68
	$T_{ss,out}$	℃	432	431	440	454	453
	$\Delta T_{ss,bottom}$	℃	58	61	66	54	48
	$\Delta T_{ss,top}$	℃	38	30	56	60	30
	$T_{g,in}$	℃	380	381	381	379	397
	$T_{g,out}$	℃	334	338	340	332	394
	$p_{hp,sep}$	bar	100	101	250	250	-
	$N_{s,H2O}$	-	5	5	-	-	-
	$\tilde{c}_{CH4,hp,out}$	%	-	80.3	-	-	-
	$r_{CH4,sel}$	%	-	-	95.9	95.1	95.7
	A_{sel}	-	-	-	1.27	1.17	1.28
	$\tilde{c}_{CH4,sel,out}$	%	-	-	-	90.3	90.3
	$y_{memb.}$	-	-	2	-	2	2
	y^{l}_{prec}	-	1	1	1	1	1
	$p_{s,p}$	bar	54.6	43.1	60.7	54.3	58.8
	$T_{s,s}$	℃	520	484	505	519	550
	$T_{s,u}$	℃	130	104	124	125	150
	y_{fuel}	-	-	-	-	-	-
Efficiencies	ϵ_{SNG}	%	54.9	56.0	54.2	52.5	52.5
	ϵ_{el}	%	8.4	7.8	9.0	10.4	8.3
	ϵ	%	63.3	63.7	63.2	62.9	60.8
	η	%	58.0	58.5	57.9	57.6	55.8
	ϵ_{chem}	%	69.6	69.6	70.0	70.8	67.2
Costs	c_{GR}	€ kW^{-1}	729	722	824	808	793
	C_{OP}	€ MWh^{-1}	55.1	55.9	54.8	51.5	58.4
	C_{cat}	€ MWh^{-1}	5.1	5.5	4.5	3.2	3.6
	C_P	€ MWh^{-1}	72.9	73.1	75.1	72.1	78.6
	$C_{biomass,be}$	€ MWh^{-1}	56.4	56.5	55.2	56.8	53.2

Table 7.6—Design variables and performance of the optimal process configurations at 20 $MW_{th,biomass}$ with respect to break-even biomass costs without power recovery from the high pressure vapour phase and fully considering catalyst cost.

		Catalyst deactivation	not considered				
		Unit	(1)	(1m)	(2)	(2m)	(3m)
Design variables	p_{tot}	bar	350	332	347	339	350
	$T_{ss,max}$	°C	441	433	438	439	432
	$\Delta T_{ss,int.}$	°C	51	41	46	49	44
	$T_{ss,out}$	°C	390	392	392	390	388
	$\Delta T_{ss,bottom}$	°C	60	62	65	60	69
	$\Delta T_{ss,top}$	°C	18	15	12	43	31
	$T_{g,in}$	°C	373	377	373	375	372
	$T_{g,out}$	°C	330	330	330	330	330
	$p_{hp,sep}$	bar	100	101	326	327	-
	$N_{s,H2O}$	-	5	5	-	-	-
	$\tilde{c}_{CH4,hp,out}$	%	-	91.8	-	-	-
	$r_{CH4,sel}$	%	-	-	95.1	95.6	95.0
	A_{sel}	-	-	-	1.36	1.22	1.07
	$\tilde{c}_{CH4,sel,out}$	%	-	-	-	90.5	90.1
	$y_{memb.}$	-	-	1	-	1	1
	y^{l}_{prec}	-	1	1	1	1	1
	$p_{s,p}$	bar	33.5	33.4	30.5	39.0	21.7
	$T_{s,s}$	°C	456	454	436	482	432
	$T_{s,u}$	°C	123	167	121	134	120
	y_{fuel}	-	-	-	-	-	-
Efficiencies	ϵ_{SNG}	%	74.3	73.0	73.3	73.4	74.4
	ϵ_{el}	%	0.6	1.1	1.7	1.1	-0.6
	ϵ	%	74.9	74.1	75.0	74.5	73.9
	η	%	68.9	68.2	69.0	68.6	68.1
	ϵ_{chem}	%	75.3	74.9	76.2	75.3	73.3
Costs	c_{GR}	€ kW^{-1}	678	655	797	742	679
	C_{OP}	€ MWh^{-1}	59.0	58.6	58.3	59.1	61.9
	C_{cat}	€ MWh^{-1}	-	-	-	-	-
	C_{P}	€ MWh^{-1}	71.2	70.7	72.9	72.7	74.1
	$C_{biomass,be}$	€ MWh^{-1}	69.6	69.3	67.9	68.1	67.4

Table 7.7—Design variables and performance of the optimal process configurations at 20 $MW_{th,biomass}$ with respect to break-even biomass costs without power recovery from the high pressure vapour phase and without considering catalyst cost.

	Catalyst deactivation		considered				
		Unit	(1)	(1m)	(2)	(2m)	(3m)
Design variables	p_{tot}	bar	250	250	250	251	252
	$T_{ss,max}$	℃	508	491	507	508	540
	$\Delta T_{ss,int.}$	℃	70	69	69	64	66
	$T_{ss,out}$	℃	438	422	438	444	474
	$\Delta T_{ss,bottom}$	℃	69	55	58	65	68
	$\Delta T_{ss,top}$	℃	24	40	55	49	65
	$T_{g,in}$	℃	379	379	382	380	382
	$T_{g,out}$	℃	331	331	343	334	341
	$p_{hp,sep}$	bar	100	106	250	251	-
	$N_{s,H2O}$	-	5	4	-	-	-
	$\tilde{c}_{CH4,hp,out}$	%	-	81.4	-	-	-
	$r_{CH4,sel}$	%	-	-	95.9	95.1	95.4
	A_{sel}	-	-	-	1.46	1.23	1.16
	$\tilde{c}_{CH4,sel,out}$	%	-	-	-	91.5	90.0
	$y_{memb.}$	-	-	2	-	1	2
	y^{v}_{prec}	-	0	1	1	1	1
	y^{l}_{prec}	-	1	1	1	1	1
	$T_{g,s}$	℃	356	318	410	436	364
	$p_{s,p}$	bar	35.3	45.1	66.0	69.3	21.3
	$T_{s,s}$	℃	462	489	550	549	467
	$T_{s,u}$	℃	136	99	129	128	99
	y_{fuel}	-	-	-	-	-	-
Efficiencies	ϵ_{SNG}	%	55.6	57.0	53.6	52.9	50.5
	ϵ_{el}	%	7.5	7.4	10.2	10.6	13.1
	ϵ	%	63.2	64.5	63.7	63.5	63.5
	η	%	57.9	59.1	58.4	58.1	58.1
	ϵ_{chem}	%	68.9	70.1	71.4	71.5	73.4
Costs	c_{GR}	€ kW^{-1}	722	715	855	836	815
	C_{OP}	€ MWh^{-1}	56.9	55.8	51.9	51.0	44.2
	C_{cat}	€ MWh^{-1}	4.3	6.7	4.5	4.2	2.6
	C_{P}	€ MWh^{-1}	74.3	72.6	73.2	72.1	65.9
	$C_{biomass,be}$	€ MWh^{-1}	56.3	56.5	56.0	56.5	59.4

Table 7.8—Design variables and performance of the optimal process configurations at 20 $MW_{th,biomass}$ with respect to break-even biomass costs with power recovery from the high pressure vapour phase and fully considering catalyst cost.

		Catalyst deactivation	not considered				
		Unit	(1)	(1m)	(2)	(2m)	(3m)
Design variables	p_{tot}	bar	350	323	348	339	331
	$T_{ss,max}$	°C	447	438	449	450	432
	$\Delta T_{ss,int.}$	°C	59	45	65	62	34
	$T_{ss,out}$	°C	388	393	384	388	398
	$\Delta T_{ss,bottom}$	°C	46	64	66	51	63
	$\Delta T_{ss,top}$	°C	47	27	55	37	28
	$T_{g,in}$	°C	372	380	373	375	379
	$T_{g,out}$	°C	330	332	330	330	332
	$p_{hp,sep}$	bar	100	101	332	337	-
	$N_{s,H2O}$	-	4	3	-	-	-
	$\tilde{c}_{CH4,hp,out}$	%	-	81.8	-	-	-
	$r_{CH4,sel}$	%	-	-	95.0	95.4	95.1
	A_{sel}	-	-	-	1.31	1.30	1.18
	$\tilde{c}_{CH4,sel,out}$	%	-	-	-	90.0	90.9
	$y_{memb.}$	-	-	2	-	1	2
	y^{v}_{prec}	-	0	0	1	1	1
	y^{l}_{prec}	-	1	1	1	1	1
	$T_{g,s}$	°C	316	364	314	331	300
	$p_{s,p}$	bar	20.4	38.4	20.0	23.1	20.0
	$T_{s,s}$	°C	496	495	401	418	441
	$T_{s,u}$	°C	122	160	126	124	124
	y_{fuel}	-	-	-	-	-	-
Efficiencies	ϵ_{SNG}	%	74.1	71.7	74.6	73.8	70.9
	ϵ_{el}	%	0.5	1.7	1.1	1.3	1.1
	ϵ	%	74.7	73.4	75.7	75.1	72.0
	η	%	68.8	67.6	69.7	69.1	66.3
	ϵ_{chem}	75.1	74.7	76.5	76.1	72.9	
Costs	c_{GR}	€ kW^{-1}	665	650	790	762	678
	C_{OP}	€ MWh^{-1}	59.2	58.1	58.6	58.4	60.5
	C_{cat}	€ MWh^{-1}	-	-	-	-	-
	C_{P}	€ MWh^{-1}	71.2	70.3	72.8	72.3	73.4
	$C_{biomass,be}$	€ MWh^{-1}	69.5	69.0	68.5	68.6	66.4

Table 7.9—Design variables and performance of the optimal process configurations at 20 $MW_{th,biomass}$ with respect to break-even biomass costs with power recovery from the high pressure vapour phase and without considering catalyst cost.

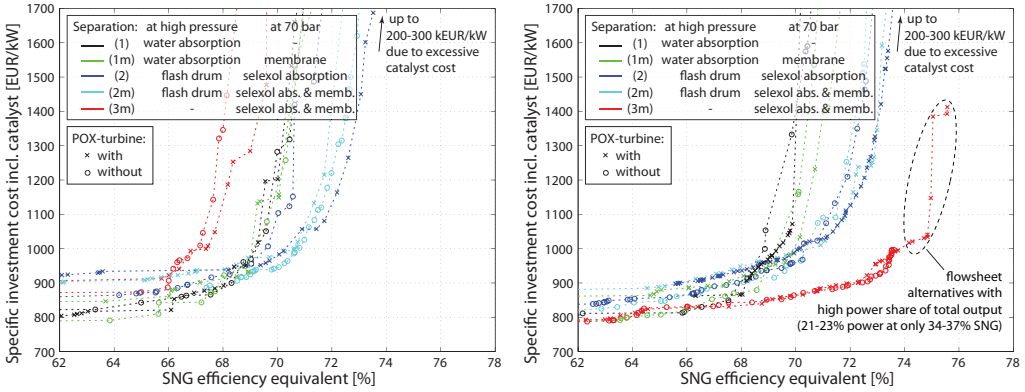

(a) Specific investment costs incl. catalyst vs. chemical efficiency (Pareto front).

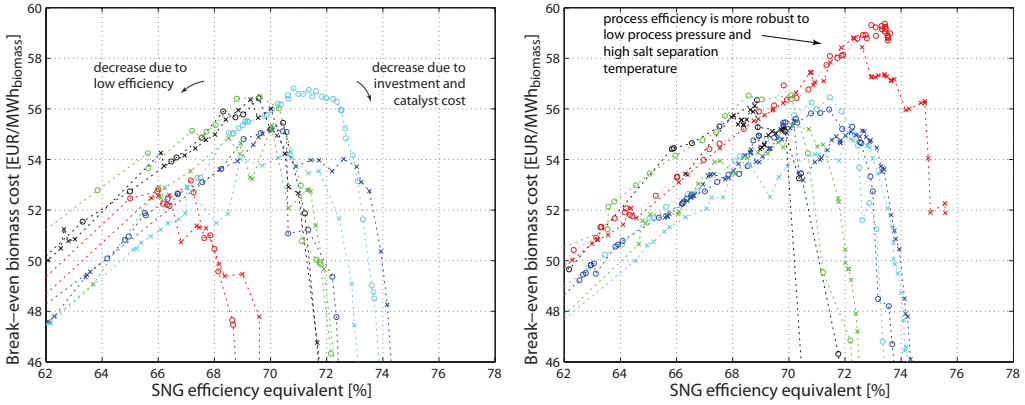

(b) Evolution of the biomass break-even cost on the Pareto front.

Figure 7.10—Optimal thermo-economic trade-off fully considering catalyst costs at 20 $MW_{th,biomass}$ without (left) and with power recovery from the high pressure vapour phase. Dotted lines are for indication only.

Selexol dominates a large part of the Pareto domain. An additional membrane stage for supplementary removal of hydrogen is thereby advantageous since the combustion of the depleted permeate supplies useful heat to the process, and the size of the bulk separation system is limited without detrimental effect on the process efficiency due to process integration. Water as washing medium is slightly suboptimal compared to the dedicated solvent, and configurations without LV separation at high pressure are clearly worst.

While power recovery from the vapour phase at high pressure has only a marginal impact on the process configurations with LV separation prior to expansion, it allows for increasing the combined efficiency by 6 to 8 points if the entire bulk phase is expanded. If catalyst costs are considered, configuration

(3m) thus clearly becomes the optimal solution overall. With modest partial SNG yields of 50 to 57%, all economically optimal flowsheets are fairly different to the most efficient configurations shown in Figure 7.8. In this range, however, layout (3m) profits overproportionally from the power cogeneration due to an efficient expansion of the bulk. Although this configuration is in principle not more efficient than the others, it has a crucial advantage since its efficiency is more robust to design constraints imposed by keeping the catalyst deactivation at an acceptable level. According to the correlation of Leusbrock et al. (2008), the solubility of Na_2SO_4 increases markedly with pressure and decreases with temperature, which is conflictive with the process efficiency that is favoured by high pressure and low salt separation temperature. As the catalyst cost is dominating the economically best solutions, all optimal configurations of Tables 7.6 and 7.8 are at the minimum bound for the process pressure and at distinctively higher separation temperatures than those of Tables 7.7 and 7.9 that disregard catalyst cost. Accordingly, superheating and expansion of the bulk is the unique flowsheet alternative that allows for a high process efficiency despite unfavourable process pressure and salt separation temperature.

Apart p_{tot}, $T_{ss,max}$ and $\Delta T_{ss,int.}$ that are governed by the influence of catalyst deactivation, the other decision variables are mainly subject to the conventional thermo-economic trade-off between investment and efficiency. The temperature differences for the heat transfer in the salt separator follow the classical compromise between cost for exchanger surface and energy efficiency. As reaction kinetics are not modelled in detail, the gasification outlet temperature is not conflictive and low values are preferable to limit the amount of residual hydrogen. If the catalyst does not allow for reasonable conversion at temperatures below 400°C, a benchmark optimisation has revealed that the decrease in chemical efficiency depends on the process configuration and might amount to up to 4 points.

For the gas separation in a water column, an increasing number of equilibrium stages has a positive effect on the separation efficiency, but is obviously more costly in terms of investment. Gas posttreatment in a membrane stage thereby reduces the importance of the separation performance and allows for a smaller tower. A similar trend is observed for the absorption factor used in the Selexol column model, with which investment cost and separation efficiency are negatively correlated. The choice of the membrane material is slightly conflictive. Polysulfone is more selective with respect to hydrogen and thus more efficient, while cellulose acetate is more permeable and cheaper. In general, high product recovery in the separation is secondary with respect to plant profitability since the depleted streams are used to supply the required heat. If absorptive and diffusive separation are combined, low purity after

the first step is identified as optimal since the resulting elevated membrane permeate flowrates are not penalising. The pressure at which the crude gas is (pre-)separated is not influenced by process economics. As in the previous section, it clearly trends to its lower or higher limit if an absorption tower or flash drum is used, respectively.

Power recovery is always beneficial for high efficiency but obviously requires some more investment. In a steam Rankine cycle, a steam generation pressure below 40 bar is sufficient. Superheating slightly above the process pinch is rationale, although the optimal temperature is moderate to match steam pressure. In any case, the investment for a partial oxidation turbine is not cost-effective at the considered scale since the applied pricing slightly disfavours power generation compared to SNG by a lower economic than thermodynamic value.

7.4.2.2 Without catalyst deactivation

In order to provide a benchmark solution for comparing the impact of catalyst deactivation on the process design, a second set of optimisations without considering the catalyst cost is carried out. This corresponds to the assumption that catalyst poisoning or its economic impact can be prevented by a chemical guard for the diluted sulphur or that its regeneration is possible at negligible cost. The optimisation setup is identical to the previous case, except that the specific investment c_{GR} without catalyst cost is considered as economic objective. Figure 7.11 and Tables 7.7 and 7.9 provide the results for these runs.

The thermo-economic characteristics of the flowsheet alternatives differ substantially from the ones that fully consider catalyst deactivation. The catalyst cost, or eventual measures to prevent its fast poisoning by diluted sulphur, is thus crucially influencing the choice of the best process configuration and its operating conditions. If an excessive deactivation or its economic impact can be prevented by other means than low process pressure and high separation temperature, the flowsheets with power generation from the superheated bulk are not competitive since the alternatives with at least LV separation at high pressure do not suffer from these design constraints. While the performance of the former stagnates, the most profitable flowsheets with a separation step at high pressure gain 5 to 6 efficiency points. While LV separation in a flash drum at high pressure and Selexol wash at grid pressure has the highest top-end efficiency, absorption in a water column is less costly and dominates the Pareto domain over a large range. Accordingly, the optimisation results suggest that this is clearly the most profitable solution at a plant scale of 20 $MW_{th,biomass}$.

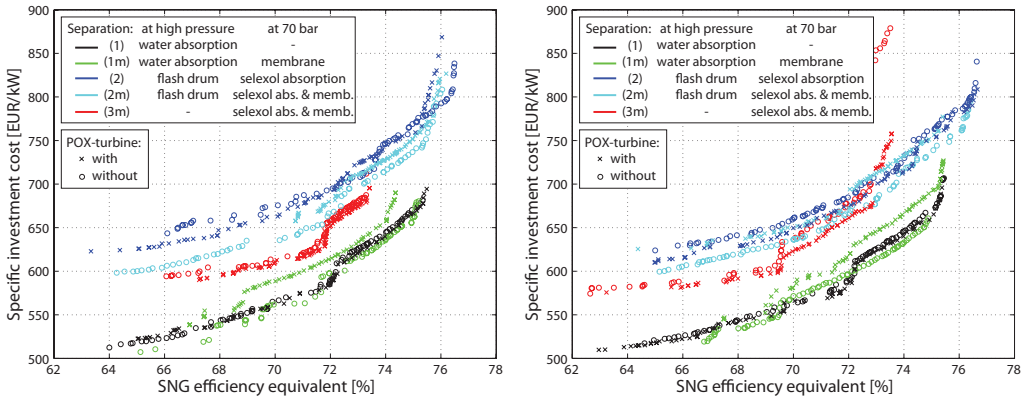

(a) Specific investment costs vs. chemical efficiency (Pareto front).

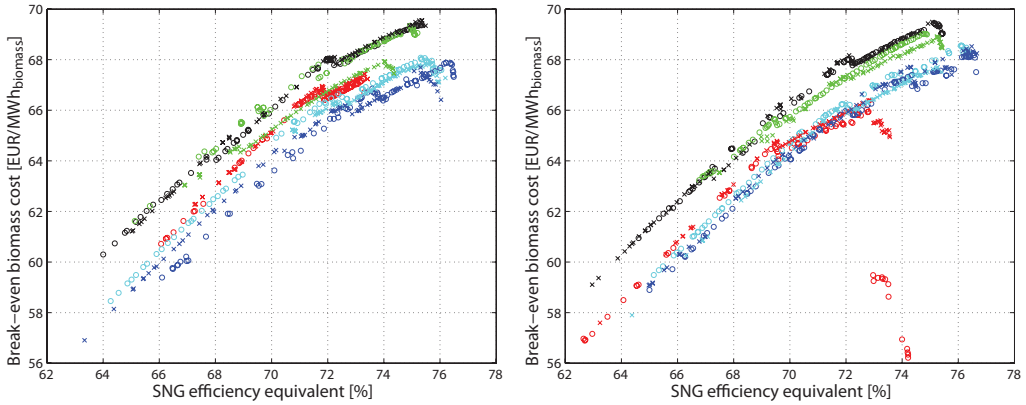

(b) Evolution of the biomass break-even cost on the Pareto front.

Figure 7.11—Optimal thermo-economic trade-off without considering catalyst costs at 20 $MW_{th,biomass}$ without (left) and with power recovery from the high pressure vapour phase.

Contrary to the process optimisations in which the catalyst cost is considered, a good thermodynamic efficiency is assured by high process pressure and low temperatures in the salt separator. The need for a very efficient separation and energy recovery system design is thus less pronounced, and flowsheets with smaller equipment and slightly lower investment costs emerge as the most profitable ones.

7.4.2.3 Economic process scaling

The most economic plant design and its performance is generally dependent on the production scale and configurations different to those reported in Tables 7.6 to 7.9 may become optimal for other biomass inputs. In order to

Range [$MW_{th,biomass}$]	[5 20]			[20 200]		
Catalyst deact.\Configuration	(1)	(2)	(3)	(1)	(2)	(3)
considered	0.68	0.59	0.62	0.84	0.80	0.81
not considered	0.71	0.67	0.68	0.87	0.84	0.86

Table 7.10—Regressed cost exponents for principal process configurations. The coefficient of determination R^2 is higher than 0.968 if individual costs values at reference scale are allowed.

determine the thermo-economic process scaling, Chapter 6 has shown that it is valid to assume that the operating conditions within a set of Pareto-optimal flowsheets do not substantially change with process scale and that it is thus possible the select the optimal plants among the Pareto-optimal configurations extrapolated from the reference scale. The influence of the process scale on its specific investment is conveniently expressed by the cost exponents defined in Equation 6.2, which are provided for the major flowsheet alternatives in Table 7.10. With values between 0.6 to 0.7 for inputs below 20 $MW_{th,biomass}$ and higher than 0.8 above, substantial economies of scale are obtained from small- to mid-scale, but become less significant above roughly 50 MW. In general, they are greatest for the configurations with LV separation at high and gas separation at grid pressure and least for those with LV and gas separation in a high pressure water column.

If catalyst deactivation is unavoidable and power recovery from the high pressure vapour phase infeasible, configuration (2m) generates maximum profit at and above 20 $MW_{th,biomass}$ while (1m) is best below due to investment savings at lower efficiency. If power recovery is feasible, the bulk expansion in the vapour phase of configuration (3m) is best at any scale. In case catalyst costs need not to be considered, complete separation in a water column with configuration (1) is best at any scale without power recovery and also up to roughly 100 $MW_{th,biomass}$ with power recovery. Above, configuration (2) becomes optimal due to its greater top-end efficiency.

7.5 Process performance for selected substrates

In the previous sections, wood with the same properties as in the previous chapters on more conventional processing by separate gasification and methanation has been used as exemplary feedstock to demonstrate the process design and provide a coherent assessment of its performance. The process concept of hydrothermal gasification yet principally addresses the conversion of wet biomass and biomass waste, and relatively dry, clean and increasingly

	Proximate analysis			Ultimate analysis					Eq. (1)	
	Φ	ash	Δh^0	C	H	O	N	S	CH_4	CO_2
	%wt	$\%wt_{dry}$	$MJkg^{-1}_{daf}$			$\%wt_{daf}$			-	-
Wood[a]	50	0.6	18.6	51.1	5.8	42.9	0.2	n/a	0.51	0.49
Manure[b]	97	24.9	21.2	48.0	8.3	36.1	7.0	0.6	0.62	0.38
Sewage sludge[c]	73	47.8	19.2	49.2	6.0	37.6	7.2	n/a	0.54	0.46
Coffee grounds[d]	50	0.3	26.0	60.1	8.5	29.6	1.6	0.2	0.62	0.38
Lignin slurry[e]	75	0.6	23.4	55.8	8.2	36.0	n/a	n/a	0.60	0.40
Microalgae[f]	87	12.5	25.3	57.7	7.6	25.3	8.1	1.3	0.61	0.39

[a] identical to Table 2.1.
[b] pig manure as analysed by Waldner (2007).
[c] internal data (Descoins, 2009) for a mixture of conventionally digested primary and secondary sludges, ash content and humidity from ECN (last visited 06/2009).
[d] ID 2190 from ECN (last visited 06/2009).
[e] residue of ethanol production from lignocellulosic biomass according to Zhang et al. (2009).
[f] Phaeodactylum tricornutum of Haiduc et al. (2009).

Table 7.11—Properties of the candidate feedstock.

expensive wood is not the originally preferred feedstock. For this reason, the influence of the substrate properties on the process design and performance is discussed here at some representative examples.

7.5.1 Candidate substrates

Table 7.11 provides the relevant properties of a selection of candidate feedstocks for hydrothermal gasification. Among the potential substrates, manure and sewage sludge are abundant biomass wastes with a large potential. Coffee grounds and lignin slurry represent typical energetically exploitable by-products. While the former is a residue from the food industry, large amounts of biomass are retrieved as slurries with high lignin content in the pulp and paper industry or in a future production of fuel ethanol from lignocellulosic biomass. In case of the latter, excess heat from the SNG production might thereby also satisfy the requirement for biomass pretreatment and ethanol distillation, and very favourable effects might emerge from process integration (Zhang et al., 2009). Finally, microalgae are considered as a photosynthetically efficient energy crop that are cultivable in photobioreactors on marginal land (Haiduc et al., 2009, Stucki et al., 2009), from which a reduced environmental impact compared to land-based energy crops can be expected.

Compared to wood, all these substrates offer a higher hydrogen fraction and thus an increased theoretical methane yield from the dry, ash-free substance according to Equation (1). Except coffee grounds and lignin slurry,

they yet suffer from a higher ash content which reduces the effective biomass content if diluted to the same dry solids content. Among the substrates, manure suffers from a particular low solids content on an as-received basis and is the only substrate for which water purification by reverse osmosis is considered necessary.

7.5.2 Process optimisation

As in the previous section, the process optimisation is addressed by first assessing the fuel and power cogeneration potential and subsequent thermo-economic optimisation with and without considering catalyst cost. In addition to the decision variables outlined in Table 7.2, the choice of the separation subconfigurations (1)-(3m) is left to the multi-objective algorithm in order to limit the computational time and data volume. Figure 7.12 provides the Pareto fronts of the overall best configurations for all substrates in the different optimisation steps.

The maximum partial efficiencies in (a) assess a nearly equal cogeneration potential for coffee grounds and lignin slurry, which are performing slightly better than wood. Microalgae, manure and sewage sludge are consecutively worse. In comparison with Table 7.11, this order mainly follows the ash content of the substrates. With an equal total solids content of 20%, the net dilution of the reactive biomass in water almost doubles in the worst case of sewage sludge and has a fatal impact on process efficiency since the amount of water to be entrained is doubled as well. As discussed in detail for wood, power recovery from the high pressure vapour phase has a similar influence on the performance for all substrates. In addition to the maximum combined efficiency situated close to the maximum SNG yield, it allows for a high marginal efficiency in substituting the SNG by electrical power generation. This leads to a second peak with respect to the combined efficiency at net SNG yields below roughly 50%, which is particularly beneficial for low quality substrates like sewage sludge.

The efficiency considerations have a big impact on the thermo-economic performance of the conversion. Compared to coffee grounds and lignin slurry which are dominating the common Pareto domain, the conversion of wood is slightly less efficient and more expensive due to the higher CO_2 share in the crude product that requires more effort for separation. Although potentially more efficient, it is thus competing with microalgae whose conversion is disfavoured by a slightly higher ash content. The waste substrates are clearly worst. While sewage sludge is seriously penalised by its low thermodynamic performance, manure suffers from high investment cost for dewatering and especially wastewater treatment by reverse osmosis.

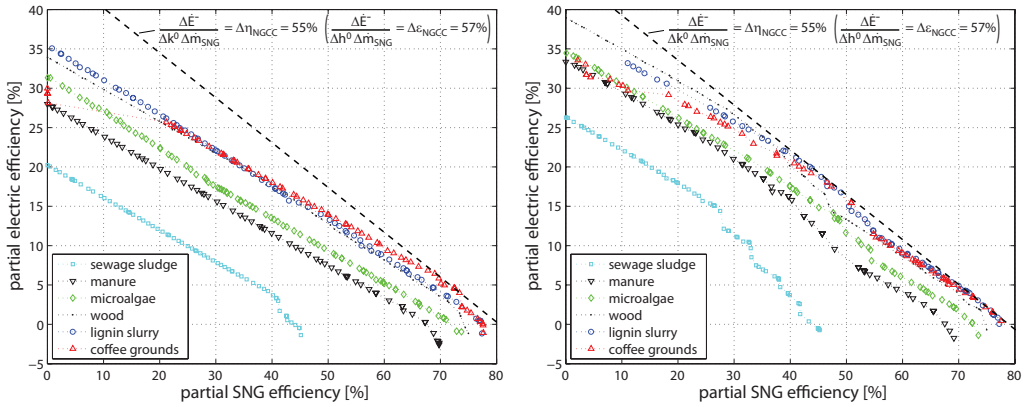

(a) Maximum partial efficiencies.

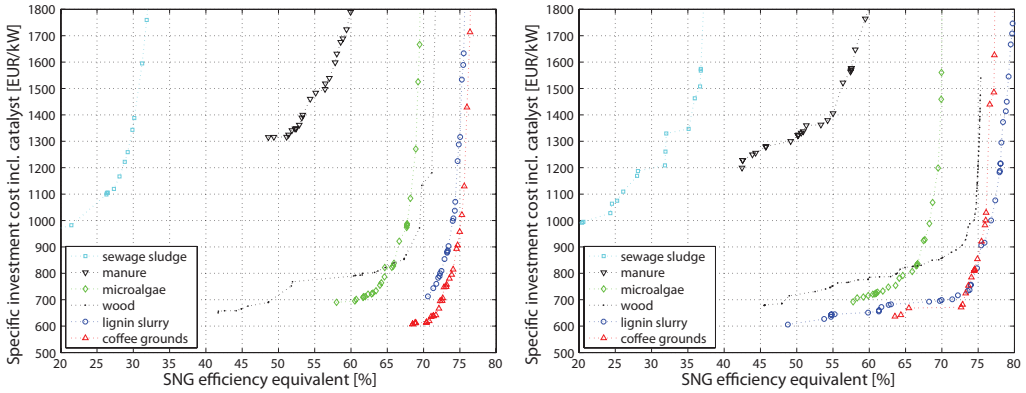

(b) Full consideration of catalyst cost.

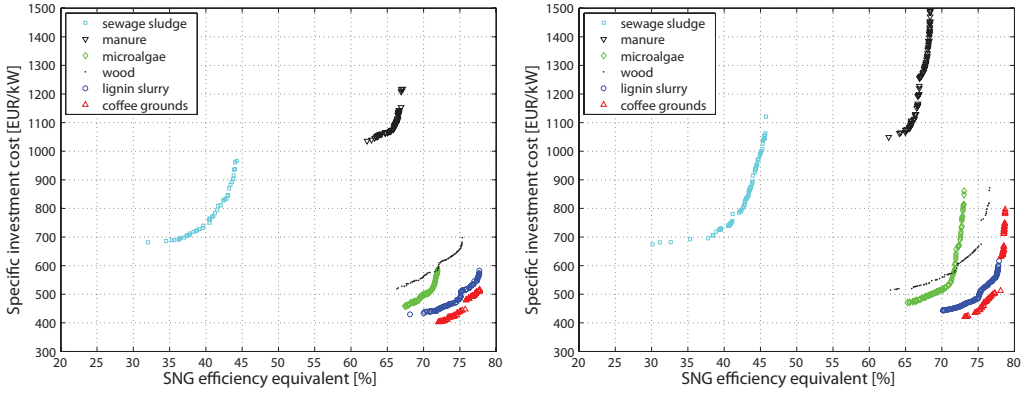

(c) Without catalyst deactivation.

Figure 7.12—Optimal thermodynamic and thermo-economic trade-off at 20 $MW_{th,biomass}$ without (left) and with power recovery from the high pressure vapour phase.

Figure 7.13 illustrates the evolution of the process configuration on the thermo-economic Pareto fronts and clearly highlights that the optimal choice depends not only on the availability of energy recovery technology, catalyst deactivation and plant scale, but also on substrate properties. According to the trends observed in the detailed design study for wood, the use of a single separation technology is more efficient, but its combination with a membrane is less costly since the purification requirement is relaxed. The flowsheets with absorption of CO_2 in water thereby require less investment than Selexol, but are disfavoured at higher efficiency. An exception is observed if power recovery from high pressure vapour is excluded and catalyst cost can be disregarded, for which water absorption is the unconditionally best technology for all substrates. If catalyst cost is considered and power recovery feasible, superheating and expansion of the bulk crude product emerges again as an interesting alternative since its efficiency is less sensible to the design constraints imposed to avoid excessive deactivation. For the economically best configurations, the yield distribution is similar to those obtained for wood. While an almost neutral power balance at high SNG yield seems best if catalyst deactivation does not need to be considered, converting up to 10% of the biomass input into power is more advantageous otherwise. The assessed break-even costs for coffee waste, lignin slurry and microalgae are thereby similar or higher to those of wood, which may result in considerably higher plant profitability if lower substrate prices apply. Although manure conversion suffers from high investment cost, such plants might yet be profitable since also low compensations for the feedstock can be expected. With the assumed inert fraction and dilution limit, the conversion of sewage sludge increases the energy efficiency of wastewater treatment, but economical benefits should principally emerge from avoiding another type of waste treatment.

7.6 Conclusions

The present chapter has presented a systematic analysis of the process design alternatives for hydrothermal production of SNG from wet biomass and biomass waste. For this purpose, technology models have been developed, reconciled and validated with data from experimental investigations and process demonstration. Based on a general superstructure for combined product separation and internal energy recovery from the supercritical conditions, the possibilities for an efficient cogeneration of SNG and power have been explored. Simultaneously considering the mass and energy balances in the process integration has thereby allowed for linking the synthesis of the sep-

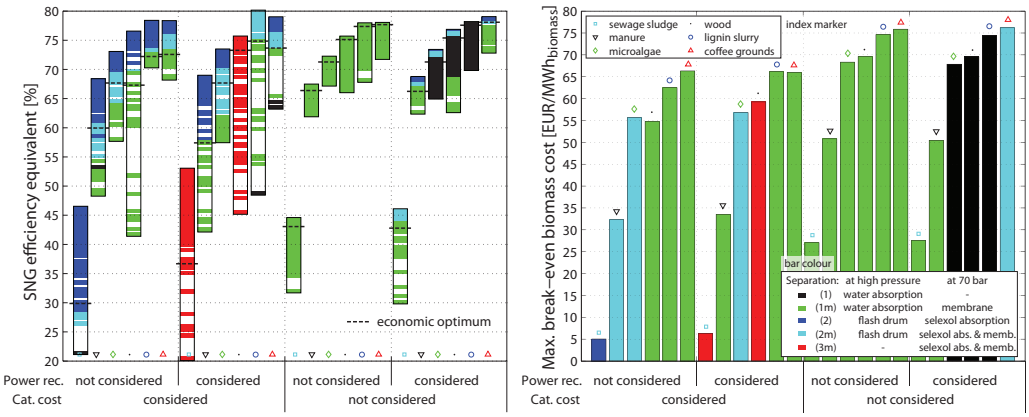

Figure 7.13—Evolution of the process configuration on the Pareto front (left) and characteristics of the most economic one at 20 $MW_{th,biomass}$ for the selected substrates.

aration and energy recovery systems while considering the depleted streams as fuels to balance the heat demand of the process.

Even with conservative hypothesis on practical design limitations such as a maximum total solids content of 20% in the feed and the loss of 10% of the hydrolysate in the salt slurry, a sound process integration and energy recovery allows for an energetically and economically viable process design. Multiple thermo-economic optimisations have revealed that the hydrothermal conversion should thereby be regarded as a polygeneration system in which SNG and electricity yields are to a large extent on a par. In a detailed design study for wood substrate, it has been observed that catalyst deactivation and the availability of energy recovery technology crucially affect the process design and lead to solutions with substantially different characteristics. If catalyst deactivation or its economic impact can be avoided by other means than low pressure and high temperatures in the salt separator, flowsheets with 72 to 75% SNG yield close to the maximum and an almost neutral power balance are economically optimal. If excessive catalyst cost can only be avoided by keeping the salt solubility in the separator on a low level, flowsheets with a substantially lower gas yield of 50 to 57% and an increased power generation of 7 to 13% become optimal. In this circumstances, superheating and expanding the bulk crude product proves as a particularly energy- and cost-efficient design alternative.

In the last part of the analysis, it is demonstrated that the process design and performance is not only influenced by available technology, catalyst deactivation and plant scale, but also the characteristics of the processed

substrate. Wet but energetically valuable industrial by-products with a high hydrogen and low ash content such as lignin slurries or coffee grounds have been identified as a particularly well suited feedstock that allow for greater efficiencies than wood. Biomass wastes with high ash content such as manure and digested sewage sludge are less advantageous since their effective biomass content is severely reduced if processing is limited to slurries containing no more than 20% total solids. From the perspective of waste treatment with disposal as principal objective, also marginal profit from a complete energy recovery from wastes might yet be valuable.

Conclusions

In this thesis, a systematic methodology for the conceptual design of efficient processes for converting biomass to fuels, heat and power has been developed and demonstrated. Based on an appropriate mathematical decomposition of the design problem into an intensive non-linear and an extensive linear model, it allows for generating parameter- and scale-independent sets of potentially optimal process configurations and operating conditions with respect to multiple objectives. The approach is thus well-suited to target best possible performance and eliminate solutions that are not worth investigating in detail. In this regard, it may serve as a tool to guide research efforts and process development towards optimal plant design, which is too easily missed by the conventional simulation of some scenarios.

Based on the analysis of feasible conversion pathways arranged in a general process superstructure, a database of thermo-economic models for promising technologies for the thermochemical conversion of biomass has been developed and validated. Due to its modular structure, it facilitates the comparison of multiple candidate process configurations and may conveniently be enriched in the future. The models thereby consider the variable characteristics of the resource and realise a trade-off between the level of detail and numerical robustness. Contrary to conventional studies that typically assess equipment cost based on capacity, a preliminary equipment rating and costing is performed. This allows for properly investigating the thermo-economic performance by multi-objective optimisation with respect to process configuration and operating conditions.

At the example of thermochemical production of SNG from wood, several studies have shown that process integration plays a crucial role in the definition of energy- and cost-efficient system designs. The individually most efficient technologies are thereby not necessarily the best ones from an overall perspective. For instance, Viking gasification is outperformed by indirectly

heated FICFB gasification with respect to integrated system performance despite its considerably higher cold gas efficiency of 91% compared to 78% for FICFB. Another example is the design of the separation system for upgrading crude SNG to grid quality. If the separation section is designed as an individual package, it is possibly oversized by up to 60% with 46% higher investment costs compared to a design that fully takes the process integration into account. Apart such benefits from process intensification, considerable potential has been assessed for site-scale integration. For a conservative process design for ethanol production from lignocellulosic biomass, it has been shown that the fuel yield can be more than doubled if the unfermented residues are thermochemically converted into SNG instead of conventionally burnt for power cogeneration in a steam Rankine cycle. This strengthens not only the economic plant competitiveness, but also highlights the influence of the process design on environmental performances, since the same fuel output is obtained with less than half as much cropland and related impacts. Again, the full potential is thereby only accessible if a systematic approach for extracting the available exergy for combined heat and power cogeneration is applied.

In a general typefaction of the candidate process configurations, the best technologies and technology matches for the polygeneration of SNG, industrial heat and power have been identified. A detailed discussion of the influence of the operating conditions reveals the interaction of the optimal values between the different sections and their relation with the process integration. It is further shown how the best process configurations depend on the possibility for local heat cogeneration, plant scale and the projected economic conditions.

Overall, the production of SNG from lignocellulosic biomass by conventional gasification and methanation suggests itself as an efficient and sustainable option for biomass-to-fuel conversion. Depending on technology, process scale and energy prices, the most economic configurations may provide a net fuel yield of 66 to 75% from wood at 50%wt humidity based on the lower heating value of the dry substance. Cogeneration allows for a total useful energy yield ranging from 71 to 91%. This corresponds to an equivalent gas yield of 74 to 86% if electricity and heat are substituted by the gas consumed for their generation in a combined cycle and heat pumps at an exergy efficiency of 55%. Assuming prices of 33 € MWh^{-1} for wood and 80 and 180 € MWh^{-1} for industrial heat and electricity generated from renewables, respectively, these efficiencies result in overall production costs of 51 to 84 € MWh_{SNG}^{-1} at a plant scale of 20 $MW_{th,biomass}$ or as low as 45 € MWh_{SNG}^{-1} for mature large-scale production above 100 $MW_{th,biomass}$. Directly heated, pressurised fluidised bed gasification thereby clearly emerges as the best technology, al-

though maybe contradictory to results obtained for conventional flowsheet scenarios based on intuition. From the stoichiometry of the main reaction, CO_2 is a by-product of the fuel production that must be separated from SNG in order to reach grid quality. This biogenic carbon dioxide might be captured and avoided at a price of 15 to 40 € ton^{-1} depending on the price of electricity. Capturing CO_2 at a SNG plant using cogenerated electricity is thus potentially more economic than end-of-pipe capture at a fossil power plant and allows for extracting net CO_2 from the atmosphere during plant growth.

Instead of using conventional gasification, hydrothermal gasification in supercritical water is an alternative process that is suitable for wet biomass and biomass wastes. For this emerging technology, a detailed process model has been developed based on experimental laboratory results for the production of crude SNG. In order to correctly predict the phase equilibria for the particular conditions in the product separation, a suitable thermodynamic property model has been identified and adapted to recently available ternary data for the H_2O-CO_2-CH_4 system. Promising alternatives for the combined separation and energy recovery from the crude product have been assembled in a superstructure. As such, the model may be used as an adaptive design tool in the development of a pilot, demonstration or later commercial plant.

In a detailed design study, the impact of available technology, catalyst deactivation and process scale has been quantified for selected candidate substrates. Hydrothermal gasification thereby appears as a flexible process with a wide spectrum of relative fuel and power yields at efficiencies that are relatively close. Based on conservative hypothesis, efficiencies of up to 75 to 80% in terms of SNG equivalents have been assessed for integrated processes. While substrates such as coffee grounds, microalgae or the unfermented lignin slurry from ethanol production are very promising for generating considerable profit, the process may at least extract valuable residual energy from low-quality substrates such as manure or sewage sludge and thus contribute to a rational and sustainable use of otherwise unemployed resources.

Perspectives

Life cycle assessment. The modular character of the model architecture allows for readily implementing life cycle assessment (LCA) for the process technology and streams. On the one hand, this provides accurate projections of industrial-scale process data to environmental analysts, which is usually lacking for emerging technologies. On the other hand, the process developers

may actively consider the environmental impact as an objective in the design phase, and thus efficiently avoid environmental harm at an early stage. As demonstrated by Gerber et al. (2009, 2010), an integrated process design for industrial-scale may indeed drastically improve the environmental performance of lab and pilot facilities. By linking the LCA model to geographic information system data, the impact of plant location and scale may further be considered. For distributed resources like biomass where transport is an issue, this might critically influence the appropriate choice of the dimensions of the plant.

Liquid fuels. The global debate on biofuels is dominated by liquid transportation fuels such as ethanol or Fischer-Tropsch products, or hydrogen as the overarching energy vector of the future. Probably due to its gaseous nature and conventionality, SNG is often disregarded. Tock et al. (2009) investigated the production of the liquid diesel substitutes such as Fischer-Tropsch fuel, dimethyl ether and also methanol with the method described in this thesis. The results indicate that Fischer-Tropsch is the best of these options. With a conversion efficiency that is roughly 15 points lower than the one for SNG, the price for the convenience of a liquid energy carrier is yet high. From a process design perspective, it is more interesting that contrary to SNG production, indirectly heated gasification proves as the more efficient and economic choice for liquid fuel production than directly heated pressurised gasification since the abundant off-gas from the liquid synthesis may readily be used to supply the gasifier's energy requirement, which avoids costly recycling. The conventional flowsheeting approach upon which the reference papers by Tijmensen et al. (2002) and Hamelinck et al. (2004) are based does not allow for systematically considering such integration aspects. The authors thus exclude this overall more efficient solution either through their results or even a priori. Such conclusions should be revisited.

Chemicals and biorefining. With a certain pertinence, the chemical industry is claiming for a material use of biomass instead of an energetic one. Indeed, as long as fossil methane is converted to syngas for the synthesis of chemicals, the conversion of biomass via producer gas to methane may be questioned since it multiplies conversion losses in the overall system. The methodology presented here is perfectly apt to investigate this field and might contribute to a rational design of biomass-based production of chemicals. Complex biorefinery systems are thereby a challenge of particular interest.

References

Abetz, V., Brinkmann, T., Dijkstra, M., Ebert, K., Fritsch, D., Ohlrogge, K., Paul, D., Peinemann, K.-V., Nunes, S. P., Scharnagl, N., Schossig, M., 2006. Developments in membrane research: From material via process design to industrial application. Advanced Engineering Materials 8, 328–358.

Aden, A., Ruth, M., Ibsen, K., Jechura, J., Neeves, K., Sheehan, J., Wallace, B., 2002. Lignocellulosic biomass to ethanol process design and economics utilizing co-current dilute acid prehydrolysis and enzymatic hydrolysis for corn stover. Tech. rep., NREL, Colorado, USA.

Ahmad, S., Linnhoff, B., Smith, R., 1990. Cost optimum heat exchanger networks – 2. Targets and design for detailed capital cost models. Computers and Chemical Engineering 14 (7), 757–767.

Autissier, N., Palazzi, F., Marechal, F., van Herle, J., Favrat, D., 2007. Thermo-economic optimization of a solid oxide fuel cell, gas turbine hybrid system. Journal of Fuel Cell Science and Technology 4 (2), 123–129.

Bacon, D., Downie, J., Hsu, J., Peters, J., 1982. Fundamentals of thermochemical biomass conversion. Elsevier, London, Ch. Modeling of fluidized bed wood gasifiers, pp. 717–732.

Balje, O., 1981. Turbomachines. A guide to design, selection and theory. Wiley, New York.

Bart, H.-J., von Gemmingen, U., 2009. Adsorption. In: Ullmann's encyclopedia of industrial chemistry, 7th Edition. Wiley-VCH.

Belsim SA, last visited 04/2009. Vali IV. www.belsim.com.

Berghel, J., Renström, R., 2002. Basic design criteria and corresponding results performance of a pilot–scale fluidized superheated atmospheric condition steam dryer. Biomass and Bioenergy 23, 103–112.

References

BFE, 2004. Aufdatierung der Standortbestimmung CO_2-Gesetz. CO_2-Perspektiven und Sensitivitäten. Bundesamt für Energie, Bern.

BFE, 2005. Schweizerische Gesamtenergiestatistik. Bundesamt für Energie, Bern.

Bhide, B., Stern, S., 1993. Membrane processes for the removal of acid gases from natural gas. I. Process configurations and optimization of operating conditions. Journal of Membrane Science 81, 209–237.

Biollaz, S., Schildhauer, T., Ulrich, D., Tremmel, H., Rauch, R., Koch, M., 2009. Status report of the demonstration of BioSNG production on a 1 MW scale in Güssing. In: 17th European Biomass Conference and Exhibition. Hamburg, Germany.

Boll, W., Supp, E., Hochgesand, G., Higman, C., Kalteier, P., Müller, W.-D., Kriebel, M., Schlichting, H., Tanz, H., 2009. Gas production, chap. 5: Gas treating. In: Ullmann's encyclopedia of industrial chemistry, 7th Edition. Wiley-VCH.

Bolliger, R., 2010. Méthode généralisée de synthèse et d'analyse de systèmes de conversion d'énergie. Ph.D. thesis, Ecole Polytechnique Fédérale de Lausanne, to be submitted.

Bolliger, R., Favrat, D., Maréchal, F., 2005. Advanced power plant design methodology using process integration and multi-objective thermo-economic optimisation. In: Proceedings of the 18th International conference on efficiency, cost, optimization, simulation and environmental impact of energy systems (ECOS).

Bolliger, R., Palazzi, F., Maréchal, F., 2008. Heat Exchanger Network (HEN) costs and performances estimation for multi-period operation. In: 18th European Symposium on Computer Aided Process Engineering (ESCAPE18). Lyon, France.

Bourgois, J., Guyonnet, R., 1988. Characterization and analysis of torrefied wood. Wood Science and Technology 22, 143–155.

Brown, D., 2007. Development and application of an equilibrium reaction modelling approach and of heat integration methodologies for the conceptual design of biomass gasification energy conversion systems. Ph.D. thesis, Tokyo Institute of Technology.

Brown, D., Gassner, M., Fuchino, T., Maréchal, F., 2009. Thermo-economic analysis for the optimal conceptual design of biomass gasification energy conversion systems. Applied Thermal Engineering 29, 2137–2152.

Chauvel, A., Fournier, G., Raimbault, C., 2001. Manuel d'évaluation économique des procédés. Technip, Paris.

References

Craig, K., Mann, M., 1996. Cost and performance analysis of biomass-based integrated gasification combined-cycle power systems. Tech. rep., NREL, Colorado, USA.

Descoins, N., 2009. Internal data for a mixture of digested primary sewage sludges. Laboratory for Industrial Energy Systems, EPFL.

Diab, S., Maddox, R. N., December 1982. Here are the techniques for choosing a solvent and calculating the column size required for a specific process in which a gas is absorbed into a liquid. Chemical Engineering 89 (27), 38–56.

Douglas, J. M., 1985. Hierarchical decision procedure for process synthesis. AIChE Journal 31, 353–362.

Douglas, J. M., 1988. Conceptual design of chemical processes. McGraw-Hill, New York.

Duan, Z., Mao, S., 2006. A thermodynamic model for calculating methane solubility, density and gas phase composition of methane-bearing aqueous fluids from 273 to 523 K and from 1 to 2000 bar. Geochimica et Cosmochimica Acta 70, 3369–3386.

Duan, Z., Møller, N., Weare, J. H., 1992a. An equation of state for the CH_4-CO_2-H_2O system: I. Pure systems from 0 to 1000°C and 0 to 8000 bar. Geochimica et Cosmochimica Acta 56, 2605–2617.

Duan, Z., Møller, N., Weare, J. H., 1992b. An equation of state for the CH_4-CO_2-H_2O system: II. Mixtures from 50 to 1000°C and 0 to 1000 bar. Geochimica et Cosmochimica Acta 56, 2619–2631.

Duan, Z., Sun, R., 2003. An improved model calculating CO_2 solubility in pure water and aqueous NaCl solutions from 273 to 533 K and from 0 to 2000 bar. Chemical Geology 193, 257–271.

Ducreux, O., Lavigne, C., Nedez, C., 2006. Air and gas drying with activated alumina. www.axens.net, Axens IFP Group Technologies.

Duret, A., Friedli, C., Maréchal, F., 2005. Process design of Synthetic Natural Gas (SNG) production using wood gasification. Journal of Cleaner Production 13, 1434–1446.

ECN, last visited 06/2009. Phyllis, database for biomass and waste. www.ecn.nl/phyllis.

Elliott, D. C., 2008. Catalytic hydrothermal gasification of biomass. Biofuels, Bioproducts and Biorefining 2 (3), 254–265.

References

EPFL Pleiades cluster, last visited 11/2009. pleiades.epfl.ch.

Esser, G., 2008. Étude thermodynamique d'un procédé de gazéification de biomass à pression élevée. Master's thesis, Université de Liège.

Faaij, A., van Ree, R., Waldheim, L., Olsson, E., Oudhuis, A., van Wijk, A., Daey-Ouwens, C., Turkenburg, W., 1997. Gasification of biomass wastes and residues for electricity production. Biomass and Bioenergy 12, 387–407.

Fargione, J., Hill, J., Tilman, D., Polasky, S., Hawthorne, P., 2008. Land clearing and the biofuel carbon debt. Science 319 (5867), 1235–1238.

Fassinou, W. F., Van de Steene, L., Toure, S., Volle, G., Girard, P., 2009. Pyrolysis of pinus-pinaster in a two-stage gasifier: Influence of processing parameters and thermal cracking of tar. Fuel Processing Technology 90, 75–90.

Favrat, D., Marechal, F., Epelly, O., 2008. The challenge of introducing an exergy indicator in a local law on energy. Energy 33 (2), 130–136.

Felder, R., Dones, R., 2007. Evaluation of ecological impacts of synthetic natural gas from wood used in current heating and car systems. Biomass and Bioenergy 31 (6), 403–415.

Floudas, C., Ciric, A., Grossmann, I., 1986. Automatic synthesis of optimum heat exchanger network configurations. AIChE Journal 32, 276–290.

Friedli, C., Biollaz, S., 2003. Ecogaz, projet bois-méthane. Tech. rep., EPFL-PSI, Switzerland.

Friedrichs, G., 1985. Methanisierung von Kohlevergasungsgasen im Wirbelbett. Pilot–Entwicklungsstufe. Tech. rep., Thyssengas Gmbh, Duisburg.

Fryda, L., Panopoulos, K. D., Karl, J., Kakaras, E., 2008. Exergetic analysis of solid oxide fuel cell and biomass gasification integration with heat pipes. Energy 33, 292–299.

Gassner, M., Baciocchi, R., Maréchal, F., Mazzotti, M., 2009. Integrated design of a gas separation system for the upgrade of crude SNG with membranes. Chemical Engineering and Processing 48, 1391–1404.

Gassner, M., Maréchal, F., 2008. Thermo-economic optimisation of the integration of electrolysis in synthetical natural gas production from wood. Energy 33, 189–198.

Gassner, M., Maréchal, F., 2009a. Combined mass and energy integration in process design at the example of membrane-based gas separation systems. submitted upon invitation for the special edition of Computers and Chemical Engineering dedicated to the PSE conference 2009.

References

Gassner, M., Maréchal, F., 2009b. Methodology for the optimal thermo-economic, multi-objective design of thermochemical fuel production from biomass. Computers and Chemical Engineering 33, 769–781.

Gassner, M., Maréchal, F., 2009c. Thermo-economic process model for thermochemical production of Synthetic Natural Gas (SNG) from lignocellulosic biomass. Biomass and Bioenergy 33, 1587–1604.

Gassner, M., Maréchal, F., 2009d. Thermodynamic comparison of the FICFB and Viking gasification concepts. Energy 34, 1744–1753.

Gerber, L., Gassner, M., Maréchal, F., 2009. Integration of LCA in a thermo-economic model for multi-objective process optimisation of SNG production from woody biomass. In: 19th European Symposium on Computer Aided Process Engineering (ESCAPE19). Cracow, Poland.

Gerber, L., Gassner, M., Maréchal, F., 2010. Integration of LCA in the optimal design of energy conversion systems: The example of SNG production from lignocellulosic biomass. To be submitted to Computers and Chemical Engineering.

Gil, J., Aznar, M. P., Caballero, M. A., Francet's, E., Corella, J., 1997. Biomass gasification in fluidized bed at pilot scale with steam-oxygen mixtures. product distribution for very different operating conditions. Energy and Fuels 11, 1109–1118.

Girardin, L., Maréchal, F., Tromeur, P., 2006. Methodology for the design of industrial hydrogen networks and the optimal placement of purification units using multi-objective optimisation techniques. In: 16th European Symposium on Computer Aided Process Engineering and 9th International Symposium on Process Systems Engineering.

Gøbel, B., Henriksen, U., Ahrenfeldt, J., Jensen, T., Hindsgaul, C., Bentzen, J., Sørensen, L., 2004. Status – 2000 hours of operation with the Viking gasifier. In: Proceedings of the 2nd World Conference and Technology Exhibition on Biomass for Energy and Industry. Rome.

Gumz, W., 1950. Gas producers and blast furnaces. Wiley, New York.

Haiduc, A. G., Brandenberger, M., Suquet, S., Vogel, F., Bernier-Latmani, R., Ludwig, C., 2009. SunCHem: An integrated process for the hydrothermal production of methane from microalgae and CO2 mitigation. Journal of Applied Phycology 21 (5), 529–541.

Haldor Topsøe A/S, 2009. From solid fuels to substitute natural gas (SNG) using TREMP. www.topsoe.com.

References

Hamelinck, C. N., Faaij, A. P. C., den Uil, H., Boerrigter, H., 2003. Production of FT transportation fuels from biomass; technical options, process analysis and optimisation, and development potential. Tech. rep., ECN, Petten, Netherlands.

Hamelinck, C. N., Faaij, A. P. C., den Uil, H., Boerrigter, H., 2004. Production of FT transportation fuels from biomass; technical options, process analysis and optimisation, and development potential. Energy 29, 1743–1771.

Hamelinck, C. N., van Hooijdonk, G., Faaij, A. P., 2005. Ethanol from lignocellulosic biomass: Techno-economic performance in short-, middle- and long-term. Biomass and Bioenergy 28 (4), 384–410.

Henriksen, U., Ahrenfeldt, J., Bentzen, J., 2005. Langtidsforsøg med totrinsforgasseren "Viking". Tech. Rep. MEK-ET-2005-7, DTU, Lyngby, Denmark.

Henriksen, U., Ahrenfeldt, J., Jensen, T., Gøbel, B., Bentzen, J., Hindsgaul, C., Sørensen, L., 2006. The design, construction and operation of a 75 kW two-stage gasifier. Energy 31, 1542–1553.

Heyen, G., 2008a. Implantation de l'équation d'état de Duan et al.. Conclusions des tests. Tech. rep., LASSC, Université de Liège, Belgium.

Heyen, G., 2008b. Numerical methods for physical properties evaluation. Lecture notes for course given in doctoral school in energy, EPFL.

Heyne, S., Thunman, H., Harvey, S., 2008. Integration aspects for synthetic natural gas production from biomass based on a novel indirect gasification concept. In: PRES 2008, 11th Conference on Process Integration, Modelling and Optimisation for Energy Saving and Pollution Reduction. Prague.

Hofbauer, H., Rauch, R., Löeffler, G., Kaiser, S., Fercher, E., Tremmel, H., 2002. Six years experience with the FICFB-gasification process. In: Proceedings of the 12th European Conference and Technology Exhibition on Biomass for Energy, Industry and Climate Protection. Amsterdam, Netherlands.

Hogsett, J., Mazur, W., 1983. Estimate membrane system area. Hydrocarbon Processing 62 (8), 52–54.

Höhlein, B., Niessen, H., Range, J., 1984. Methane from synthesis gas and operation of high-temperature methanation. Nuclear Engineering and Design 78, 241–250.

Houde, A. Y., Krishnakumar, B., Charati, S. G., Stern, S. A., 1996. Permeability of dense (homogeneous) cellulose acetate membranes to methane, carbon dioxide, and their mixtures at elevated pressures. Journal of Applied Polymer Science 62 (13), 2181–2192.

References

Huang, H., Ramaswamy, S., 2009. Modeling biomass gasification using thermodynamic equilibrium approach. Applied Biochemistry and Biotechnology 154, 14–25.

Hwang, S.-T., Kammermeyer, K., 1975. Membranes in separation. Vol. 7 of Techniques of chemistry. Wiley, New York.

Jarungthammachote, S., Dutta, A., 2007. Thermodynamic equilibrium model and second law analysis of a downdraft waste gasifier. Energy 32, 1660–1669.

Karellas, S., Karl, J., Kakaras, E., 2008. An innovative biomass gasification process and its coupling with microturbine and fuel cell systems. Energy 33, 284–291.

Kersten, S., 2002. Biomass gasification in circulating fluidized beds. Ph.D. thesis, Twente University, Enschede.

Kirschner, M. J., 2009. Oxygen. In: Ullmann's encyclopedia of industrial chemistry, 7th Edition. Wiley-VCH.

Kravanja, Z., Glavic, P., 1997. Cost targeting for HEN through simultaneous optimization approach: a unified pinch technology and mathematical programming design of large HEN. Computers and Chemical Engineering 21, 833–853.

Krischer, O., 1978. Die wissenschaftlichen Grundlagen der Trocknungstechnik. Springer–Verlag, Berlin.

Kruse, A., 2008. Supercritical water gasification. Biofuels, Bioproducts and Biorefining 2 (5), 415–437.

Kruse, A., 2009. Hydrothermal biomass gasification. Journal of Supercritical Fluids 47 (3), 391–399.

Laser, M., Jin, H., Jayawardhana, K., Lynd, L. R., 2009a. Coproduction of ethanonl and power from switchgrass. Biofuels, Bioproducts and Biorefining 3 (2), 195–218.

Laser, M., Larson, E., Dale, B., Wang, M., Greene, N., Lynd, L. R., 2009b. Comparative analysis of efficiency, environmental impact, and process economics for mature biomass refining scenarios. Biofuels, Bioproducts and Biorefining 3 (2), 247–270.

Lazzaretto, A., Toffolo, A., 2004. Energy, economy and environment as objectives in multi-criterion optimization of thermal systems design. Energy 29 (8), 1139–1157.

Lee, B. I., Kesler, M. G., 1975. Generalized thermodynamic correlation based on three-parameter corresponding states. AICHE Journal 21 (3), 510–527.

References

Leibold, H., Hornung, A., Seifert, H., 2008. Hthp syngas cleaning concept of two stage biomass gasification for ft synthesis. Powder Technology 180, 265–270.

Leusbrock, I., Metz, S. J., Rexwinkel, G., Versteeg, G. F., 2008. Quantitative approaches for the description of solubilities of inorganic compounds in near-critical and supercritical water. Journal of Supercritical Fluids 47, 117–127.

Leyland, G. B., 2002. Multi-objective optimisation applied to industrial energy problems. Ph.D. thesis, Ecole Polytechnique Fédérale de Lausanne.

Li, H., Maréchal, F., Burer, M., Favrat, D., 2006. Multi-objective optimization of an advanced combined cycle power plant including CO2 separation options. Energy 31 (15), 3117–3134.

Li, X. T., Grace, J. R., Lim, C. J., Watkinson, A. P., Chen, H. P., Kim, J. R., 2004. Biomass gasification in a circulating fluidized bed. Biomass and Bioenergy 26, 171–193.

Linnhoff, B., Townsend, D., 1982. A user guide on process integration for the efficient use of energy. The Institution of Chemical Engineers.

Linstrom, P., Mallard, W. (Eds.), 2009. NIST Chemistry WebBook, NIST standard reference database number 69.

Luterbacher, J., 2006. The improvement of thermodynamic property estimation in a hydrothermal gasification simulation. Tech. rep., EPFL-PSI, semester project.

Luterbacher, J., Fröling, M., Vogel, F., Maréchal, F., Tester, J. W., 2009. Hydrothermal gasification of waste biomass: Process design and life cycle assessment. Environmental Science and Technology 43, 1578–1583.

Maréchal, F., Favrat, D., Jochem, E., 2005a. Energy in the perspective of the sustainable development: The 2000 W society challenge. Resources, Conservation and Recycling 44 (3 spec. iss.), 245–262.

Maréchal, F., Kalitventzeff, B., 1998. Process integration: Selection of the optimal utility system. Computers and Chemical Engineering 22, S149–S156.

Maréchal, F., Palazzi, F., Godat, J., Favrat, D., 2005b. Thermo-economic modelling and optimisation of fuel cell systems. Fuel Cells 5, 5–24.

Matsumura, Y., Minowa, T., Potic, B., Kersten, S. R. A., Prins, W., Van Swaaij, W. P. M., Van De Beld, B., Elliott, D. C., Neuenschwander, G. G., Kruse, A., Antal Jr., M. J., 2005. Biomass gasification in near- and super-critical water: Status and prospects. Biomass and Bioenergy 29 (4), 269–292.

References

Meth, B., Davidson, O., de Coninck, H., Loos, M., Meyer, L. (Eds.), 2005. IPCC special report on carbon dioxide capture and storage. IPCC.

Molyneaux, A., 2002. A practical evolutionary method for the multi-objective optimisation of complex integrated energy systems including vehicle drivetrains. Ph.D. thesis, Ecole Polytechnique Fédérale de Lausanne.

Mozaffarian, M., Zwart, R. W. R., 2003. Feasibility of biomass/waste-related SNG production technologies. Tech. rep., ECN, Petten.

Newborough, M., 2004. A report on electrolysers, future markets and the prospects for ITM Power LTD's electrolyser technology. www.h2fc.com/newsletter.

Newman, S. A., 1985. Acid and sour gas treating processes. Gulf Publishing Company, Houston.

Oettli, B., Blum, M., Peter, M., Schwank, O., Bedniaguine, D., Gnansounou, E., Chételat, J., Golay, F., Hersener, J.-L., Meier, U., Schleiss, K., 2004. Potenziale zur energetischen Nutzung von Biomasse in der Schweiz. Schlussbericht. Tech. rep., Bundesamt für Energie, Bern.

Omosun, A. O., Bauen, A., Brandon, N. P., Adjiman, C. S., Hart, D., 2004. Modelling system efficiencies and costs of two biomass-fuelled sofc systems. Journal of Power Sources 131, 96–106.

Ondrey, G., 2008. Chementator: Cleaning syngas at high temperatures. Chemical Engineering 115 (12), 11.

Palazzi, F., Maréchal, F., van Herle, J., Autissier, N., 2005. A methodology for thermo-economic modeling and optimization of SOFC systems. Chemical Engineering Transactions 7, 13–18.

Pellegrini, L. F., de Oliveira Jr., S., 2007. Exergy analysis of sugarcane bagasse gasification. Energy 32, 314–327.

Peng, D., Robinson, D. B., 1976. A new two-constant equation of state. Industrial and Engineering Chemistry Fundamentals 15 (1), 59–64.

Perlmutter, M. J., Kimmel, H. E., Chiu, C., Paradowski, H., 2004. Economic and environmental benefits of two-phase LNG expanders. pp. 1121–1130.

Peterson, A. A., Vogel, F., Lachance, R. P., Fröling, M., Antal Jr., M. J., Tester, J. W., 2008a. Thermochemical biofuel production in hydrothermal media: A review of sub- and supercritical water technologies. Energy and Environmental Science 1 (1), 32–65.

Peterson, A. A., Vontobel, P., Vogel, F., Tester, J. W., 2008b. In situ visualization of the performance of a supercritical-water salt separator using neutron radiography. Journal of Supercritical Fluids 43 (3), 490–499.

Peterson, A. A., Vontobel, P., Vogel, F., Tester, J. W., 2009. Normal-phase dynamic imaging of supercritical-water salt precipitation using neutron radiography. Journal of Supercritical Fluids 49 (1), 71–78.

Pettersen, T., Lien, K., 1994. A new robust design model for gas separating membrane modules, based on analogy with counter-current heat exchangers. Computers and Chemical Engineering 18 (5), 427–439.

Pfeifer, C., Hofbauer, H., 2008. Development of catalytic tar decomposition downstream from a dual fluidized bed biomass steam gasifier. Powder Technology 180, 9–16.

Phair, J., Badwal, S., 2006. Materials for separation membranes in hydrogen and oxygen production and future power generation. Science and Technology of Advanced Materials 7, 792–805.

Pierucci, S., Ranzi, E., 2008. A general mathematical model for a moving bed gasifier. Computer Aided Chemical Engineering 25, 901–906.

Pilarczyk, E., Henning, K.-D., 1987. Natural gas from landfill gases. Resources and Conservation 14, 283–294.

Previdoli, P., Beck, M., 2001. Vergleich der Energiepreise in verschiedenen OECD-Ländern. Bundesamt für Energie, www.bfe.ch (last visited 11/2009).

Prins, M. J., Ptasinski, K. J., Janssen, F. J. J. G., 2006. More efficient biomass gasification via torrefaction. Energy 31, 3458–3470.

Prins, M. J., Ptasinski, K. J., Janssen, F. J. J. G., 2007. From coal to biomass gasification: Comparison of thermodynamic efficiency. Energy 32, 1248–1259.

Pröll, T., Hofbauer, H., 2008. H2 rich syngas by selective co2 removal from biomass gasification in a dual fluidized bed system – process modelling approach. Fuel Processing Technology 89, 1207–1217.

Ptasinski, K. J., 2008. Thermodynamic efficiency of biomass gasification and biofuels conversion. Biofuels, Bioproducts and Biorefining 2, 239–253.

Ptasinski, K. J., Prins, M. J., Pierik, A., 2007. Exergetic evaluation of biomass gasification. Energy 32, 568–574.

Qin, J., Rosenbauer, R. J., Duan, Z., 2008. Experimental measurements of vapor-liquid equilibria of the H2O+CO2+CH4 ternary system. Journal of Chemical and Engineering Data 53, 1246–1249.

References

Ragauskas, A. J., Williams, C. K., Davison, B. H., Britovsek, G., Cairney, J., Eckert, C. A., Frederick, William J., J., Hallett, J. P., Leak, D. J., Liotta, C. L., Mielenz, J. R., Murphy, R., Templer, R., Tschaplinski, T., 2006. The path forward for biofuels and biomaterials. Science 311 (5760), 484–489.

Rapagnà, S., Jand, N., Kiennemann, A., Foscolo, P., 2000. Steam-gasification of biomass in a fluidised-bed of olivine particles. Biomass and Bioenergy 19, 187–197.

Rauch, R., last visited 04/2009. www.ficfb.at.

Rauch, R., written around 2004. Stromerzeugung aus Biomasse durch Wasserdampfvergasung. Tech. rep., Institut für Verfahrens-, Brennstoff- und Umwelttechnik, TU Wien, www.ficfb.at, last visited 04/2009.

Rauch, R., Hofbauer, H., 2003. Wirbelschicht–Wasserdampf–Vergasung in der Anlage Güssing. Betriebserfahrungen aus zwei Jahren Demonstrationsbetrieb. In: 9. Internationale Fachtagung "Energetische Nutzung nachwachsender Rohstoffe". Freiberg, Deutschland.

Rauch, R., Hofbauer, H., Bosch, K., Siefert, I., Aichernig, C., Tremmel, H., Voigtlaender, K., Koch, R., Lehner, R., 2004. Steam gasification of biomass at CHP plant Guessing – status of the demonstration plant. In: 2nd World Conference and Technology Exhibition on Biomass for Energy, Idustry and Climate Protection. Rome.

Rautenbach, R., Dahm, W., 1985. The separation of multicomponent mixtures by gas permeation. Chemical Engineering and Processing 19 (4), 211–219.

Reimert, R., 1985. Methanol production based on synthesis gas from coal and biomass. In: Synthetic fuels. ECSC, Brussels.

Reimert, R., Schaub, G., 2009. Gas production, chap. 4: Gas production from coal, wood, and other solid feedstocks. In: Ullmann's encyclopedia of industrial chemistry, 7th Edition. Wiley-VCH.

Riquarts, H.-P., Leitgeb, P., 1985. Druckwechsel–Adsorptionsanlagen zur Methangewinnung aus Biogasen. GWF–Gas/Erdgas 126, 15–19.

Sander, R., 1999. Compilation of Henry's law constants for inorganic and organic species of potential importance in environmental chemistry (vers. 3). www.henrys-law.org, last visited 04/2009.

Sayyaadi, H., 2009. Multi-objective approach in thermoenvironomic optimization of a benchmark cogeneration system. Applied Energy 86 (6), 867–879.

Scharlemann, J. P. W., Laurance, W. F., 2008. How green are biofuels? Science 319 (5859), 43–44.

Schubert, M., Regler, J. W., Vogel, F., 2010a. Continuous salt precipitation and separation from supercritical water. Part 1: Type 1 salts. Journal of Supercritical Fluids 52, 99–112.

Schubert, M., Regler, J. W., Vogel, F., 2010b. Continuous salt precipitation and separation from supercritical water. Part 2: Type 2 salts and mixture of two salts. Journal of Supercritical Fluids 52, 113–124.

Schuster, G., Löffler, G., Weigl, K., Hofbauer, H., 2001. Biomass steam gasification – an extensive parametric modeling study. Bioresorce Technology 77, 71–79.

Spath, P., Dayton, D., 2003. Preliminary screening – technical and economic assessment of synthesis gas to fuels and chemicals with emphasis on the potential for biomass-derived syngas. Tech. rep., NREL, Colorado, USA.

Stahl, M., Granström, K., Berghel, J., Renström, R., 2004. Industrial processes for biomass drying and their effects on the quality properties of wood pellets. Biomass and Bioenergy 27, 621–628.

Stucki, S., 2005. Projet bois–methane. Rapport sur la clôture de la phase 1 du projet: Preuve de la faisabilité technique à l'échelle du laboratoire. Tech. rep., PSI, Villigen, Switzerland.

Stucki, S., Vogel, F., Ludwig, C., Haiduc, A. G., Brandenberger, M., 2009. Catalytic gasification of algae in supercritical water for biofuel production and carbon capture. Energy and Environmental Science 2 (5), 535–541.

SVGW, 2008. G13, Richtlinien für die Einspeisung von Biogas ins Erdgasnetz. Zürich.

Svoboda, K., Pohořelý, M., Hartman, M., Martinec, J., 2009. Pretreatment and feeding of biomass for pressurized entrained flow gasification. Fuel Processing Technology 90, 629–635.

Swanson, M. L., Musich, M. A., Schmidt, D. D., Schultz, J. K., 2002. Feed system innovation for gasification of locally economical alternative fuels (FIGLEAF). final report. Tech. Rep. DE-FC26-00NT40904, US Department of Energy.

Sweny, J. W., Valentine, J. P., 1970. Physical solvent stars in gas treatment / purification. Chemical Engineering 77, 54–56.

Szargut, J., Styrylska, T., 1964. Angenäherte Bestimmung der Exergie von Brennstoffen. Brennstoff-Wärme-Kraft 16, 589–636.

References

Tijmensen, J. A. M., Faaij, A. P. C., Hamelinck, C. N., van Hardeveld, M. R. M., 2002. Exploration of the possibilities for production of Fischer Tropsch liquids and power via biomass gasification. Biomass and Bioenergy 23, 129–152.

Tilman, D., Socolow, R., Foley, J. A., Hill, J., Larson, E., Lynd, L., Pacala, S., Reilly, J., Searchinger, T., Somerville, C., Williams, R., 2009. Beneficial biofuels – the food, energy, and environment trilemma. Science 325 (5938), 270–271.

Tock, L., Gassner, M., Maréchal, F., 2009. Thermo-economic process model for thermochemical production of liquid fuels from lignocellulosic biomass. Submitted to Biomass and Bionenergy.

Toffolo, A., Lazzaretto, A., 2002. Evolutionary algorithms for multi-objective energetic and economic optimization in thermal system design. Energy 27 (6), 549–567.

Torres, W., Pansare, S. S., Goodwin Jr., J. G., 2007. Hot gas removal of tars, ammonia, and hydrogen sulfide from biomass gasification gas. Catalysis Reviews - Science and Engineering 49, 407–456.

Türkay, M., Grossmann, I. E., 1996. Logic-based MINLP algorithms for the optimal synthesis of process networks. Computers and Chemical Engineering 20 (8), 959–978.

Turton, R., Bailie, R. C., Whiting, W. B., Shaeiwitz, J. A., 1998. Analysis, synthesis, and design of chemical processes. Prentice Hall, New York.

Ulrich, G.-D., 1984. A guide to chemical engineering process design and economics. Wiley, New York.

Ulrich, G. D., Vasudevan, P. T., 2004. Chemical engineering process design and economics. A practical guide, 2nd Edition. Process publishing, New Hampshire.

UOP LLC, last visited 04/2009. www.uop.com/gasprocessing/6010.html.

Urban, W., Girod, K., Lohmann, H., 2008. Technologien und Kosten der Biogasaufbereitung und Einspeisung in das Erdgasnetz. Ergebnisse der Markterhebung 2007-2008. Tech. rep., Fraunhofer-Institut für Umwelt-, Sicherheits- und Energietechnik.

Valin, S., Ravel, S., Guillaudeau, J., Thiery, S., 2010. Comprehensive study of the influence of total pressure on product yields in fluidized bed gasification of wood sawdust. Accepted for publication in Fuel Processing Technology.

van Stein, E. E., Juwono, E., Demetri, E. P., 2002. The impact of ITM oxygen on economics for coal-based IGCC. In: Proceedings of the 27th International Technical Conference on Coal Utilization & Fuel Systems. Clearwater, Florida.

References

Vogel, F., Waldner, M. H., Rouff, A. A., Rabe, S., 2007. Synthetic natural gas from biomass by catalytic conversion in supercritical water. Green Chemistry 9 (6), 616–619.

Vogel, F., Waldner, M. H., Truong, T.-B., De Boni, E., Stucki, S., 2005. Verfahren zur Erzeugung von Methan und Methanhydrat aus Biomasse (Process for the production of methane and methane hydrate from biomass). Paul Scherrer Institut, Patent application PCT 05021601.9/EP 05022101 (2005-10-04).

Waldner, M. H., 2007. Catalytic hydrothermal gasification of biomass for the production of synthetic natural gas. Ph.D. thesis, Eidgenössische Technische Hochschule Zürich.

Waldner, M. H., Vogel, F., 2005. Renewable production of methane from woody biomass by catalytic hydrothermal gasification. Industrial and Engineering Chemistry Research 44, 4543–4551.

Weller, S., Steiner, W. A., 1950. Separation of gases by fractional permeation through membranes. Journal of Applied Physics 21, 279–283.

Wilén, C., Rautalin, A., 1993. Handling and feeding of biomass to pressurized reactors: Safety engineering. Bioresource Technology 46, 77–85.

Wilson, G. M., 1964. Vapor-liquid equilibrium. XI. A new expression for the excess free energy of mixing. Journal of the American Chemical Society 86 (2), 127–130.

Wyssmont Inc., last visited 04/2009. www.techtp.com.

Yoshikawa, K., 2006. R&D (Research and Development) on distributed power generation from solid fuels. Energy 31, 1656–1665.

Zah, R., Böni, H., Gauch, M., Hischier, R., Lehmann, M., Wäger, P., 2007. Oekobilanz von Energieprodukten: Oekologische Bewertung von Biotreibstoffen. Tech. rep., Swiss Federal Laboratories for Materials Testing and Research (EMPA), Switzerland.

Zhang, S., Maréchal, F., Gassner, M., Périn-Levasseur, Z., Qi, W., Ren, Z., Yan, Y., Favrat, D., 2009. Process modeling and integration of fuel ethanol production from lignocellulosic biomass based on double acid hydrolysis. Energy and Fuels 23, 1759–1765.

Zhang, S., Yan, Y., Li, T., Ren, Z., 2005. Upgrading of liquid fuel from the pyrolysis of biomass. Bioresource Technology 96, 545–550.

Zwart, R. W. R., Boerrigter, H., 2005. High efficiency co-production of Synthetic Natural Gas (SNG) and Fischer-Tropsch (FT) transportation fuels from biomass. Energy and Fuels 19, 591–597.

Appendix A

Conceptual flowsheets of the process units

This appendix provides the conceptual flowsheets for the unit models of the process superstructure for SNG production discussed in Chapter 2. The schematics of Figures A.1 to A.5 are intended to illustrate the structure of the energy-flow models for the principal units and major heat exchanges. They do not include the details of a final design. As outlined in Chapter 1, the combustion reactor(s), heat exchanger network and steam cycle are modelled by MILP and thus not depicted here.

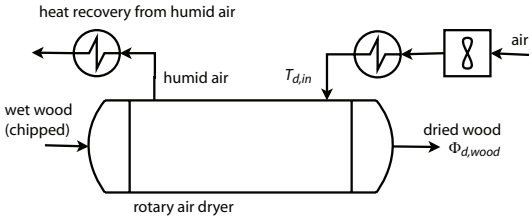

(a) Air drying.

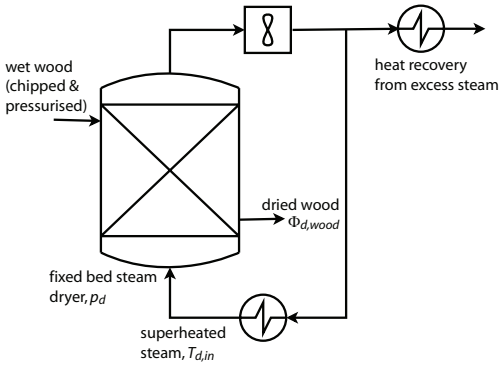

(b) Steam drying.

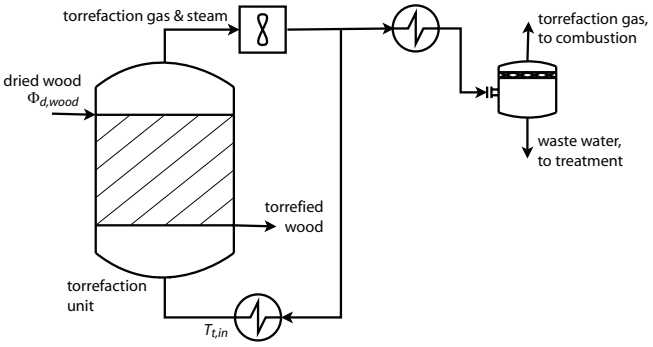

(c) Torrefaction.

Figure A.1—Thermal preatreatment units.

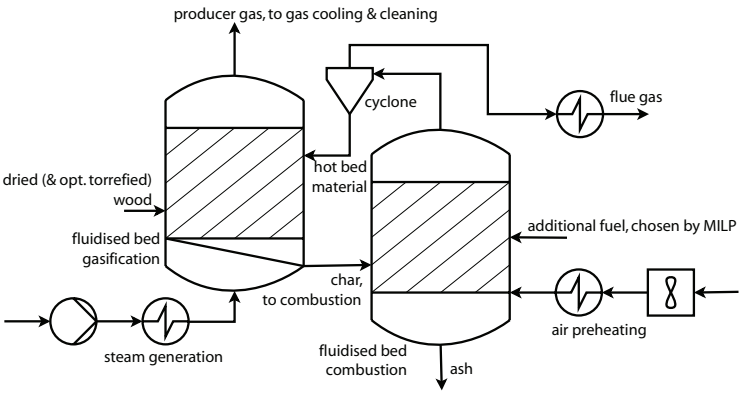

(a) Indirectly heated gasification. Note: As discussed in detail in Chapter 1, the combustion and gasification reactors are not coupled in the energy-flow model. Instead, the optimal fuels and air preheating to satisfy the gasifier's heat demand is determined in the energy-integration model by MILP.

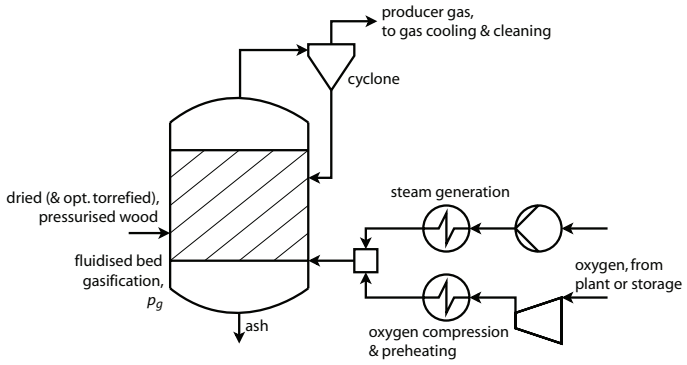

(b) Directly heated gasification.

FIGURE A.2—Gasification units.

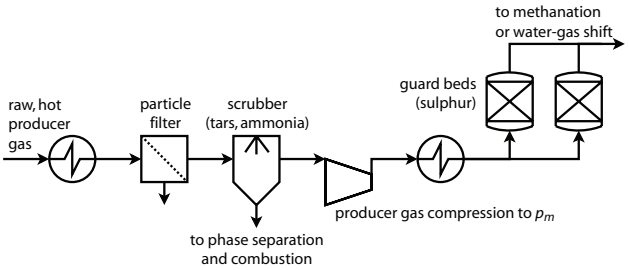

(a) Cold gas cleaning.

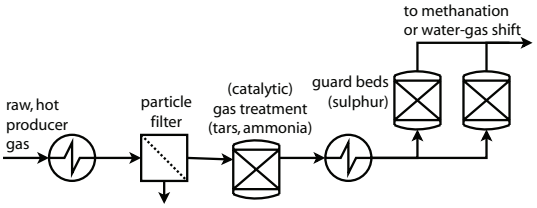

(b) Hot gas cleaning.

Figure A.3—Gas cleaning. Note: Gas cleaning is not modelling in detail and only the recovery of sensible heat of the producer gas is considered. The unit configuration may change.

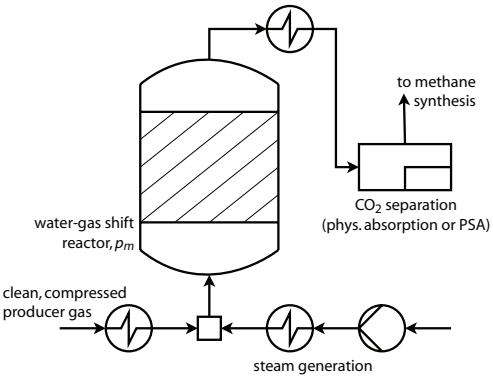

(a) Water-gas shift (optional).

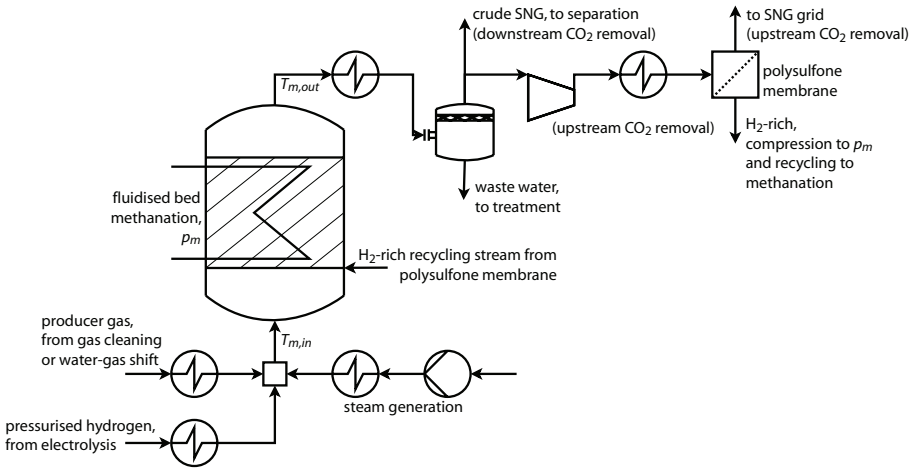

(b) Fluidised bed methanation.

FIGURE A.4—Methane synthesis and optional upstream stoichiometry adjustment by water-gas shift and CO_2 removal with one of the options depicted in Figure A.5(a) and (b).

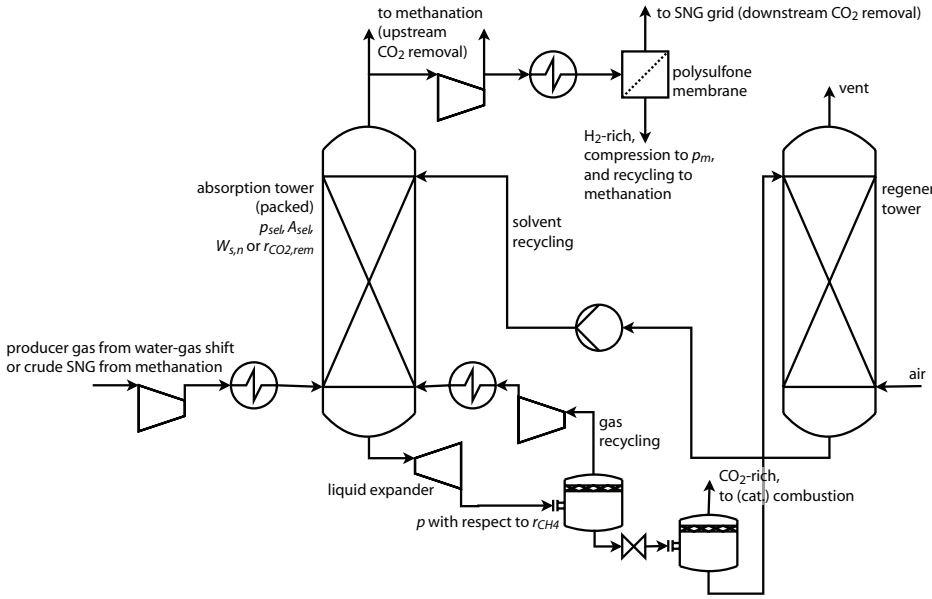

(a) Physical absorption (Selexol).

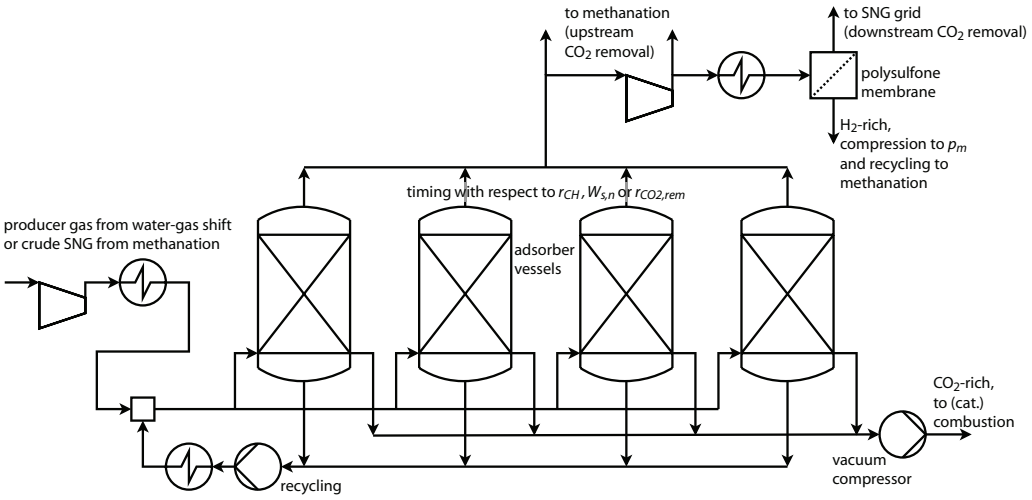

(b) Pressure swing adsorption.

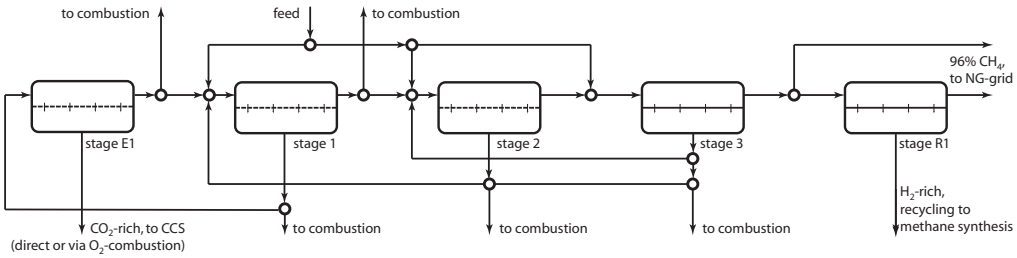

(c) Membrane cascade superstructure. Compressors and heat exchangers for conditioning of the feed streams are included in the model, but not shown here for the sake of clarity.

Figure A.5—SNG upgrading options.

Appendix B

Economic scaling of Pareto fronts

This appendix provides a comparison of the thermo-economic Pareto-fronts obtained at several reference scales for the optimisation formulation used in the typefaction (Chapter 6). At 24 test configurations, Figures B.1 to B.4 confirm the hypothesis that the operating conditions within a set of Pareto-optimal flowsheets do not substantially change with process scale, which makes it possible to select the optimal plants at different scales by extrapolating the optimised flowsheets from a reference scale. In more than half of the 24 test cases, the difference in investment cost is within 1-2%, in one third of the cases it is smaller than 5%, and in none of the cases bigger than 7%. For some configurations, the performance of the extrapolated flowsheets is even better than the one of the optimised configurations. This highlights that the error commited through the extrapolation is in the same order of magnitude than the incertainty of not finding the global optimum with an evolutionary algorithm that inherently lacks of a convergence criterion.

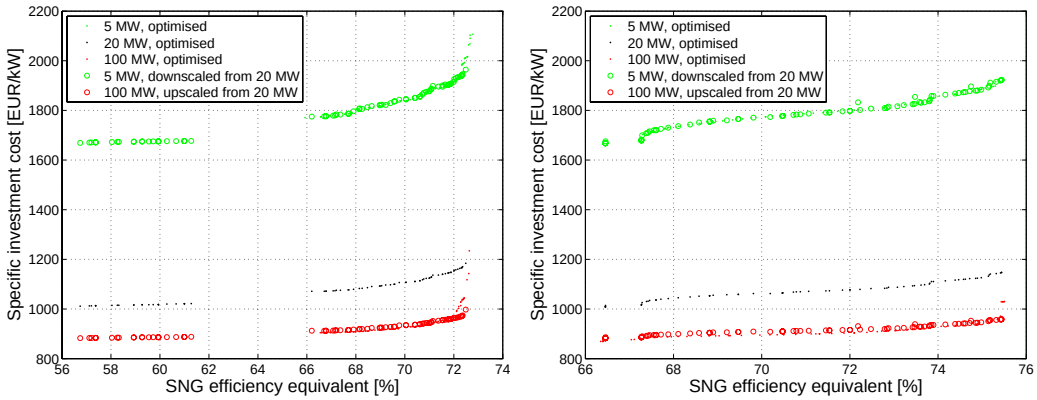

(a) PSA.

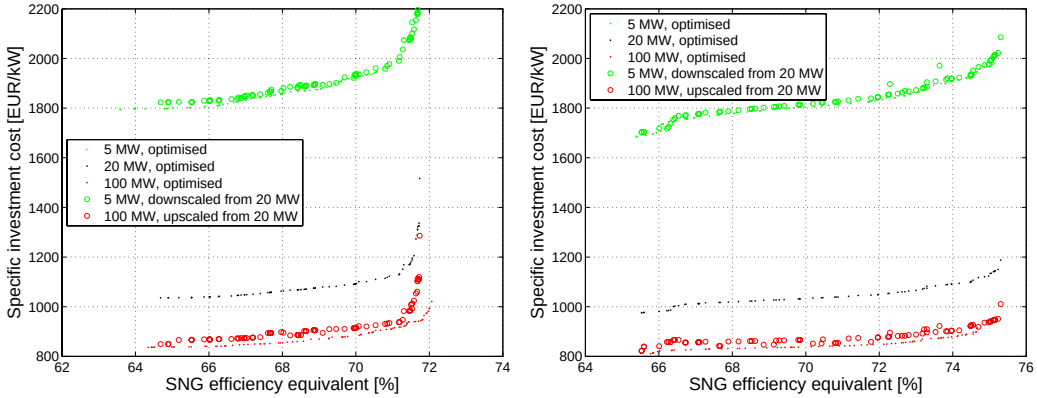

(b) Physical absorption.

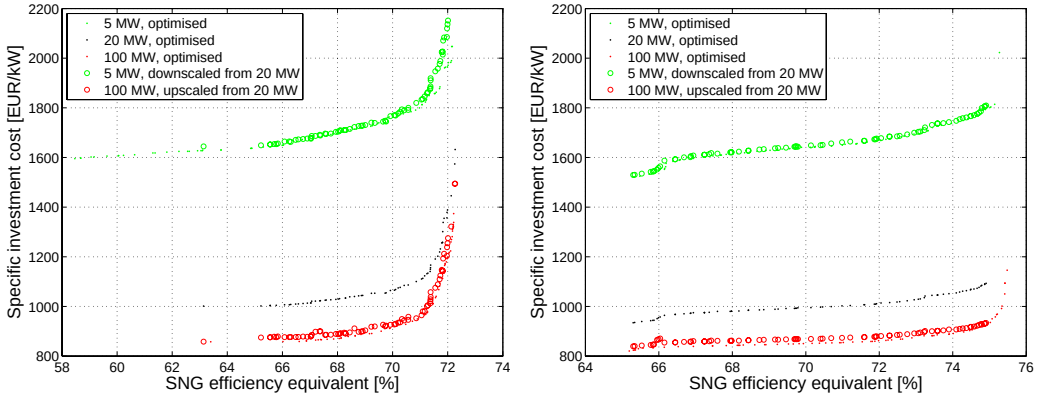

(c) Membranes.

Figure B.1—FICFB gasification with air drying. Without (left) and with heat cogeneration.

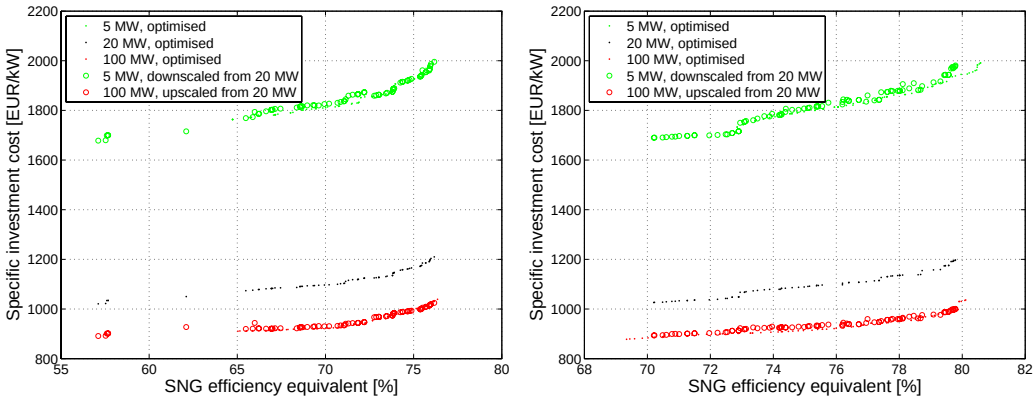

(a) PSA.

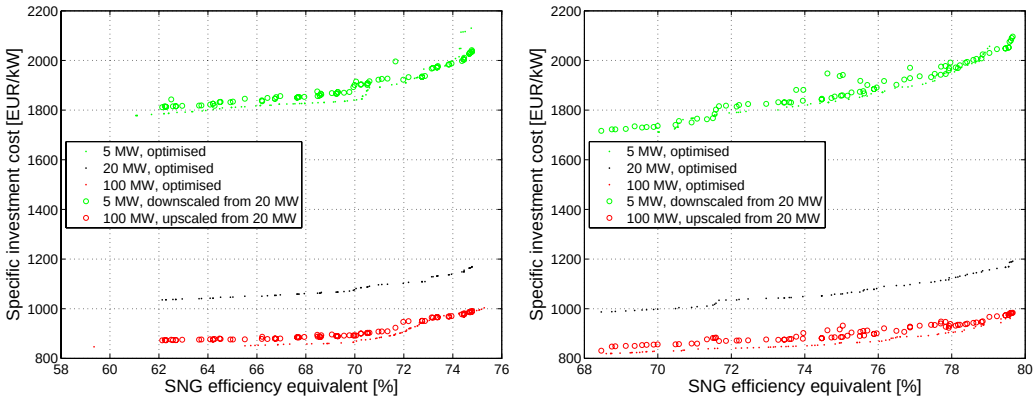

(b) Physical absorption.

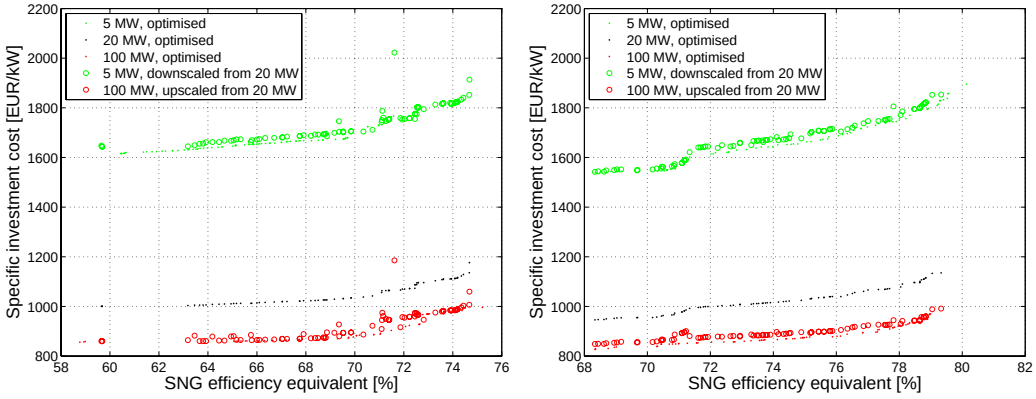

(c) Membranes.

FIGURE B.2—FICFB gasification with steam drying. Without (left) and with heat cogeneration.

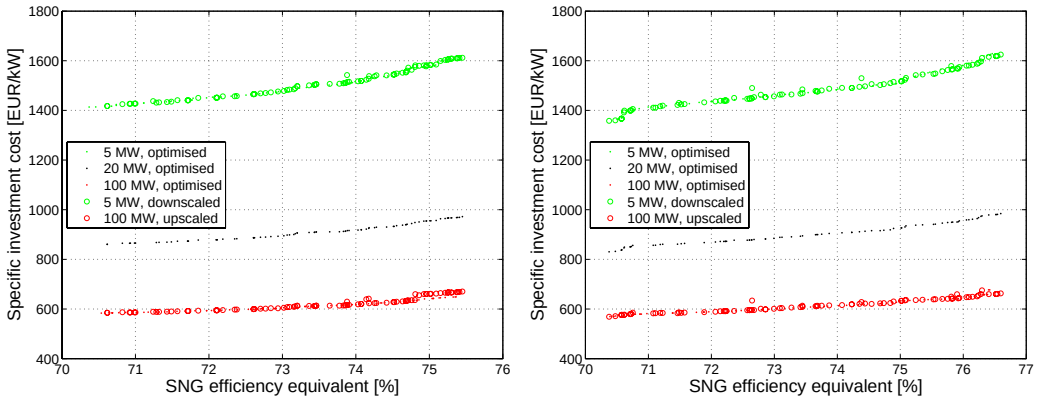

(a) PSA.

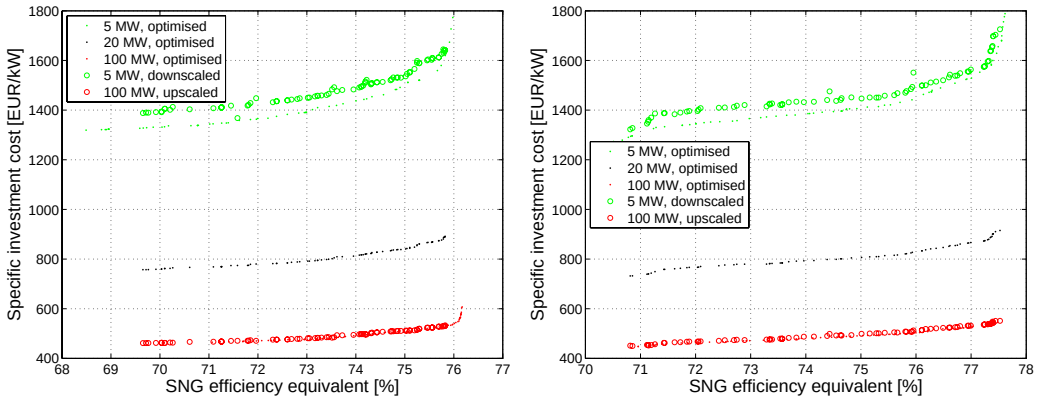

(b) Physical absorption.

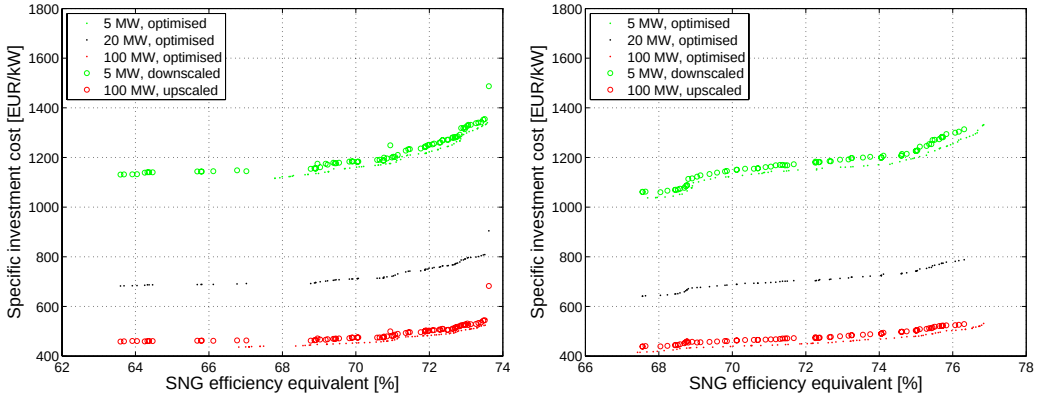

(c) Membranes.

Figure B.3—CFB-O2 gasification with air drying. Without (left) and with heat cogeneration.

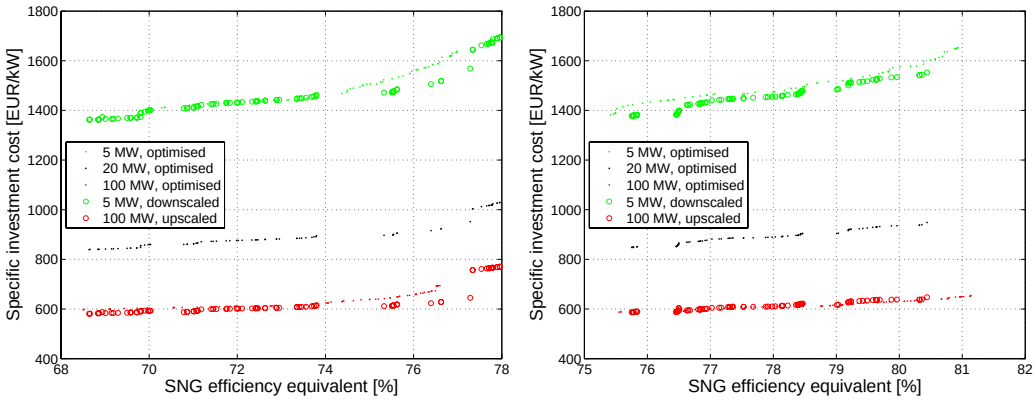

(a) PSA.

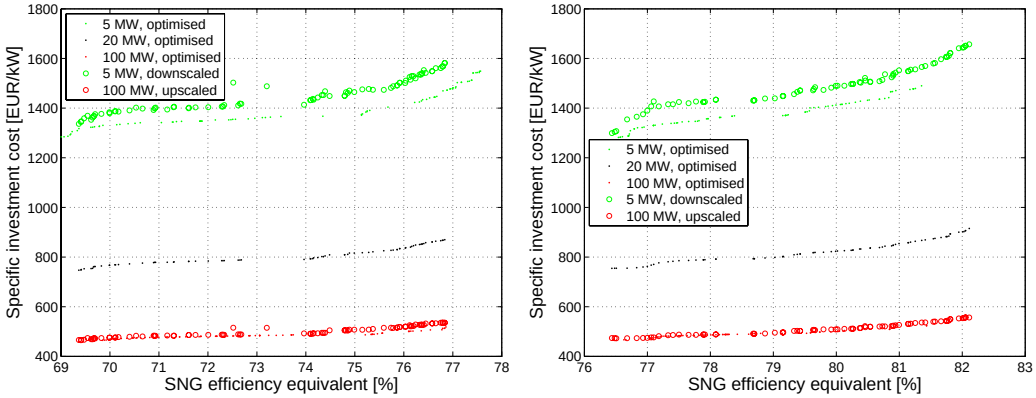

(b) Physical absorption.

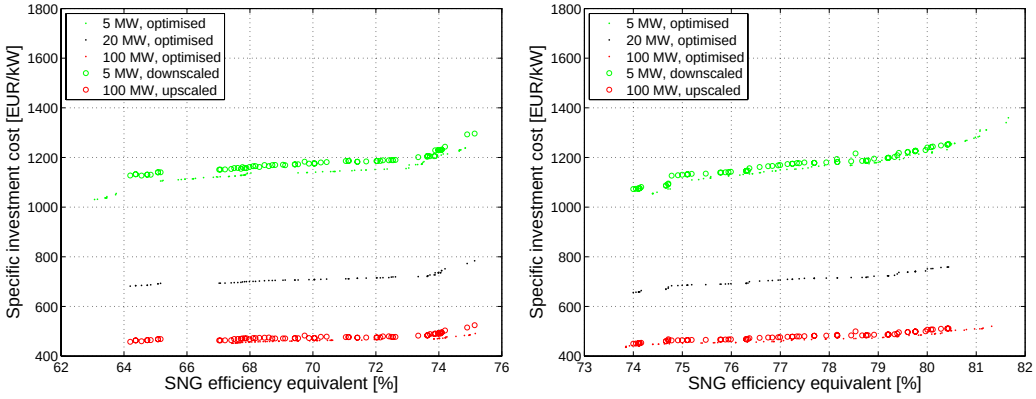

(c) Membranes.

FIGURE B.4—CFB-O2 gasification with steam drying. Without (left) and with heat cogeneration.

Appendix C

Thermodynamic model for hydrothermal gasification

This appendix details the thermodynamic property model adopted at the particular process conditions downstream to hydrothermal gasification discussed in Chapter 7, where reduced pressures $p_r = p/p_c$ up to 1.4 and temperatures $T_r = T/T_c$ in the range of 0.5 to 1.1 are encountered.

Equations of state

In an attempt to represent H_2O, CO_2 and CH_4 and its binary and ternary mixtures over a very large domain by one single thermodynamic model, Duan et al. (1992a,b) developed and parametrised a modified form of the Lee-Kesler equation of state (EOS). Mainly targeting the investigation of geological fluids and fluid inclusions, the purpose of their EOS is to predict both pTV and liquid-vapour equilibria in the range of 273(323)-1273 K and 0-8000(1000) bar. Since H_2O, CO_2 and CH_4 are the three bulk species in hydrothermal gasification and the encountered process conditions fall within this range, this EOS has been investigated and further developed in several studies. Luterbacher (2006) compared its prediction of molar volume and residual enthalpy with conventional equations of state for three different bulk compositions that are typically obtained from hydrothermal biomass gasification. In order to generalise the EOS to the minor species present in the crude product, Esser (2008) developed an approach that explores the similarity of Duan's equation with the Lee-Kesler EOS. In the latter, the compressibility factor Z is predicted by interpolating the compressibility factors of two reference fluids at their corresponding states (i.e. at the same T_r, p_r) by the acentric factor. The basic hypothesis in Esser's work is that interpolating

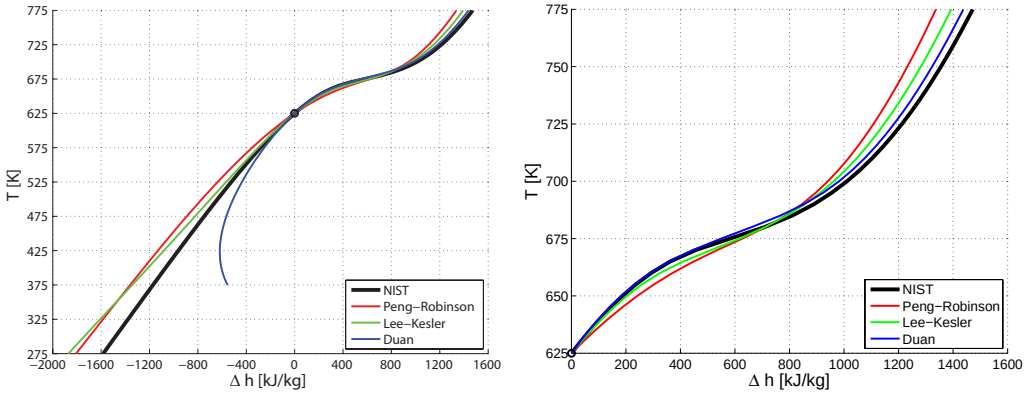

Figure C.1—Predicted hT-profiles for pure water at 300 bar over the entire domain (left) and detailed in the critical region (right). Values for different EOS are superposed at 625 K.

the parameters used for the evaluation of Z of the reference fluids instead of interpolating Z itself provides a similar estimation. He tested his approach on both the Lee-Kesler EOS and the Duan EOS and observed a good agreement with the results obtained from their original forms. By interpolating the unknown parameters in the Duan EOS from the similar parameters in the Lee-Kesler equation, it is thus possible to extend the specialised form to other species than H_2O, CO_2 and CH_4.

Although good agreement of Z and LVE with experimental data over a wide range of temperature and pressures is observed, the verifications of the Duan EOS revealed some major weaknesses which prevent its direct application in the process model. Figure C.1 shows the calculated enthalpy-temperature profile of pure water for the different candidate EOS in comparison with reliable data from NIST (Linstrom and Mallard, 2009). Although good agreement is observed in the critical region, Duan's model completely fails below 525 K. This may be partially due to the fact that the model has been developed for the prediction of pTV and liquid vapour equilibria, and no enthalpy data has been used in the calibration. Another reason is that the lower temperature limit for which the model is claimed valid is approached. In the domain below approximately 150°C, Heyen (2008a) doubts on the accuracy of the EOS also for LVE calculations, which is furthermore supported by the fact that its developer is continuing to publish dedicated solubility models and data in this range (e.g. Duan and Sun, 2003, Duan and Mao, 2006, Qin et al., 2008).

Hybrid approach

As none of the tested models allows for evaluating all relevant thermodynamic properties of the H_2O-CO_2-CH_4 system, a hybrid approach is adopted. Enthalpy is consistently evaluated with the standard Lee-Kesler equation, which provides a very good accuracy for the bulk water in the critical region. When used for all process streams throughout the plant, the divergence at moderate temperatures observed in Figure C.1 is thereby not a serious issue since the enthalpy requirements for heating and cooling the bulk before and after gasification is balanced. A combination of the pure substance's properties in an ideal model would better fit the moderate temperature region. However, the implementation of a consistent switch of the thermodynamic model between moderate and critical temperatures is problematic due to the complex structure of the product separation and expansion system.

The different developments of Duan et al. are used whenever it is necessary to calculate the liquid vapour equilibria with bulk water at high pressure. At temperatures above 523 K, evaluating the fugacities through the homogeneous EOS proves accurate and allows for coherency in the supercritical zone. Below 523 K, the calculation of the LVE is based on a heterogeneous solubility model (Duan and Sun, 2003, Duan and Mao, 2006). In their work, the chemical potential $\tilde{\mu}$ of the noncondensable species i in the gaseous and liquid phases of the binary H_2O-CO_2 and H_2O-CH_4 systems is developed as:

$$\begin{aligned}\tilde{\mu}_i^v &= \tilde{\mu}^{v0}_i + \tilde{R}T\ln(f_i^v) \\ &= \tilde{\mu}^{v0}_i + \tilde{R}T\ln(\varphi_i \tilde{c}_i^v p) \qquad \text{(C.1)} \\ \mu_i^l &= \tilde{\mu}^{l0}_i + \tilde{R}T\ln(a_i^l) \\ &= \tilde{\mu}^{l0}_i + \tilde{R}T\ln\left(\frac{\tilde{c}_i^l}{\tilde{c}^l_{H2O}\tilde{m}_{H2O}}\gamma_{i,H2O}\right) \qquad \text{(C.2)}\end{aligned}$$

where f^v and a^l term the fugacity and activity in the vapour and liquid phase, and φ and γ the coefficients thereof, respectively. Note that in this formulation, the activity coefficient of the noncondensables is dependent on the solvent and can be adjusted to the salt content in the aqueous phase. For convenience, the reference state of the binary mixtures is set to:

$$\tilde{\mu}^{v0}_i = 0 \qquad \text{(C.3)}$$

$$\gamma_{i,H2O} = 1 \qquad \text{(C.4)}$$

from which, at equilibrium ($\tilde{\mu}_i^v = \tilde{\mu}_i^l$):

$$\ln(f_i^v) = \frac{\tilde{\mu}^{l0}_i}{\tilde{R}T} + \ln\left(\frac{\tilde{c}_i^l}{\tilde{c}^l_{H2O}\tilde{m}_{H2O}}\right) \qquad \text{(C.5)}$$

Based on Equation (C.5), Duan and Sun (2003) and Duan and Mao (2006) propose to evaluate the fugacity from their EOS for pure CO_2 and CH_4 and adjust $\tilde{\mu}_i^{l0}/(\tilde{R}T)$ with a correlation in T and p of similar complexity than the other parameters in their EOS in order to represent the available data within the experimental error.

Although accurately predicting the binary systems, a recent experimental investigation of the same researchers shows that both CO_2 and CH_4 get up to 20% (CO_2) and 40% (CH_4) more soluble in the ternary system at 323 to 373 K and 100 to 500 bar (Qin et al., 2008). To account for this interaction, we suggest to complete Equation (C.5) with a supplementary interaction term in form of a fugacity coefficient $\ln(\varphi_i')$ for the gas phase composition[1]:

$$\ln(f_i^v) + \ln(\varphi_i') = \frac{\tilde{\mu}_i^{l0}}{\tilde{R}T} + \ln\left(\frac{\tilde{c}_i^l}{\tilde{c}_{H2O}^l \tilde{m}_{H2O}}\right) \tag{C.6}$$

Analoguous to the activity coefficient of Wilson (1964), it is convenient to write $\ln(\varphi_i')$ as:

$$\ln(\varphi_i') = 1 - \ln\left(\sum_j \Lambda_{i,j}\ \tilde{c}_j^{v\prime}\right) - \sum_k \frac{\tilde{c}_k^{v\prime}\ \Lambda_{k,i}}{\sum_j \Lambda_{k,j}\ \tilde{c}_j^{v\prime}} \tag{C.7}$$

$$\Lambda_{i,j} = \frac{Z_j}{Z_i} \exp\left(-\frac{\tilde{A}_{i,j}}{\tilde{R}T}\right) \tag{C.8}$$

where $\tilde{A}_{i,j}$ corresponds to an interaction energy between different molecules i and j. In our case, Equation (C.7) needs to be evaluated for indices i, j, k corresponding to CO_2 and CH_4, where the molar fractions $\tilde{c}_i^{v\prime}$ refer to the dry composition of the vapour phase.

The dataset of Qin et al. (2008) contains 14 binary and 21 ternary LVE measurements at 100-500 bar and approximately 323 K and 373 K. In the ternary data, the molar share of CO_2 in the noncondensable composition ($\tilde{c}_{CO2}{}'$) thereby varies between 46% and 83%. Neglecting the small variation of p, T in one dataset (max. $\pm$ 4 bar and $\pm$ 0.7 K), the interaction energies $\tilde{A}_{CO2,CH4}$ and $\tilde{A}_{CH4,CO2}$ of Equation (C.8) have been regressed by least squares fitting of the equilibrium ratios $\tilde{c}_{CO2}^v/\tilde{c}_{CO2}^l$ and $\tilde{c}_{CH4}^v/\tilde{c}_{CH4}^l$. The assessed constants and a comparison of the obtained errors in the binary and in the ternary systems with and without an interaction term are shown in Table C.1. For the binary measurements, the interaction term does obviously not

[1] In analogy to Wilson (1964), it would be more consistent to introduce the interaction as an activity in the liquid phase. However, this results in a poor fitting of the experimental data since the liquid composition does change only very little.

Error	Data	Model	$\tilde{c}^l_{CO2}$	$\tilde{c}^l_{CH4}$	$\tilde{c}^v_{CO2}$	$\tilde{c}^v_{CH4}$	$\frac{\tilde{c}^v_{CO2}}{\tilde{c}^l_{CO2}}$	$\frac{\tilde{c}^v_{CH4}}{\tilde{c}^l_{CH4}}$
mean	binary	(C.5), (C.6)	4.8	3.1	2.1	0.2	7.3	3.0
(of abs.	ternary	(C.5)	5.7	11.7	2.8	1.2	9.2	14.3
error)		(C.6)	3.1	3.9	1.6	1.2	4.4	3.2
max.	binary	(C.5), (C.6)	-7.0	-5.1	3.5	0.3	8.6	5.5
	ternary	(C.5)	-14.7	-28.0	8.5	4.5	27.2	44.4
		(C.6)	11.6	-7.9	3.5	4.0	-12.6	13.0

TABLE C.1—Mean and maximum relative errors (in %) of the solubility models with and without a CO_2-CH_4 interaction term. $\tilde{A}_{CO2,CH4}$ = 9.49 kJ/mol, $\tilde{A}_{CH4,CO2}$ = -20.8 kJ/mol.

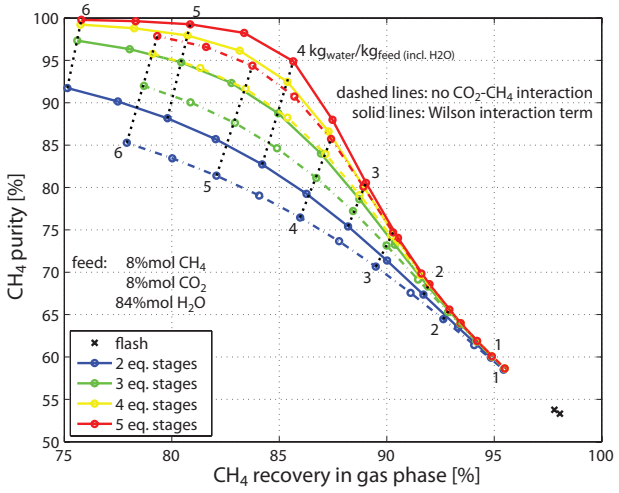

FIGURE C.2—Influence of the solubility model on the calculated performance for CO_2/CH_4-separation in an absorption column with water at 300 bar.

contribute and a mean error of 0 to 7% is observed[2], which falls in the accuracy range of the experimental system and the binary model. If the binary models are directly used to determine the LVE equilibrium of the ternary system, the assessed errors for the liquid composition and the equilibrium ratios increase considerably since the increase of CO_2- and CH_4-solubility

[2]Part of this error is thereby due to irreproducible values for the H_2O content in the vapour phase. Duan and Sun (2003) report to estimate $\tilde{c}^v_{H2O}$ by the steam saturation pressure. Qin et al. (2008) do not measure $\tilde{c}^v_{H2O}$, but compute it with their models. The reported values do however not correspond to this: at 375 K and 499 bar, their data suggests a vapour pressure of 18 bar in the H_2O-CO_2 system, although the steam saturation pressure is close to 1 bar. This contributes to an error of max. 3% in Table C.1.

cannot be represented. By introducing the interaction coefficients, the mean errors are reduced and the ternary model basically reaches the precision of the binary model, although the maximum errors are somewhat higher due to more scatter in the data.

In order to illustrate the influence of the solubility model, Figure C.2 shows the performance of the absorption column discussed in Section 7.3.2.4 as calculated with and without the correction for the CO_2-CH_4 interaction in the ternary. For elevated separation ratios approaching the required methane purity of 96%, the difference between the two models is appreciable and highlights the importance of a correct thermodynamic model for an accurate process design. Accounting for the interactions between CO_2 and CH_4, 96% purity is attained in 5 equilibrium stages with roughly 4 kg_{water}/kg_{feed} and recovering 85% of the methane feed. For the same purity and column size, almost 5.5 kg_{water}/kg_{feed} are required and only 82% of methane is recovered if the interactions are not considered.

Nomenclature

Abbreviations

CHP	Combined heat and power
EOS	Equation of state
(FIC)FB	(Fast internally circulating) Fluidised bed
HE(N)	Heat exchanger (network)
LV(E)	Liquid vapour (equilibrium)
MER	Minimum energy requirement
MI(N)LP	Mixed integer (non-)linear programming
POX	Partial oxidation
PSA	Pressure swing adsorption
(S)NG	(Synthetic) natural gas
TSA	Temperature swing adsorption
vol	Volume
WHSV	Weight hourly space velocity
wt	Weight

Greek letters

α	Convective heat transfer coefficient	$\mathrm{kW/(m^2K)}$
α	Selectivity	-
δ	Thickness of membrane layer	Å
Δh^0	Lower heating value	kJ/kg
$\Delta \tilde{h}_r^0$	Standard heat of reaction	kJ/mol
Δh_{vap}	Heat of vaporisation	kJ/kg
Δk^0	Exergy value	MJ/kg
Δp	Pressure drop	bar
ΔT_{eq}	Temperature difference to equilibrium	K
ΔT_{min}	Minimum approach temperature	K
ΔT_{ref}	Reference approach temperature	K
ϵ	Energy efficiency	%
ϵ_{cg}	Cold gas efficiency	%
ε	Mass efficiency	%
ε_{cc}	Carbon conversion efficiency	%
η	Exergy efficiency	%

$\gamma_{i,j}$	Activity coefficient of i in solution with j	bar $(\mathrm{mol/kg})_j$
Λ	Wilson interaction coefficient	-
μ	Mean value	
$\tilde{\mu}$	Chemical potential	kJ/mol
Π_r	Pressure ratio	-
φ	Fugacity coefficient	-
Φ	Humidity	$\mathrm{kg}_{H2O}/\mathrm{kg}_{tot}$
φ	Relative humidity	%
ρ	Correlation coefficient	-
ρ	Density	$\mathrm{kg/m^3}$
σ	Standard deviation	
θ	Molar stage cut	-
Roman letters		
A	Absorption factor	-
A	Area	$\mathrm{m^2}$
$\tilde{A}$	Wilson interaction energy	kJ/mol
a	Activity	bar
b	Cost exponent	-
C	Cost	€ or €/MWh
c	Specific cost	€/kW
c	Mass fraction	%
$\tilde{c}$	Molar fraction	%
c_1	Cost factor to account for contingencies and fees	-
c_2	Cost factor to account for site development and auxiliary facilities	-
c_p	Specific heat at constant pressure	kJ/(kg K)
d	Diameter	$\mathrm{m^2}$
$\dot{E}$	Mechanical or electrical power	kW
$\dot{E}$	Exergy	kW
e	Specific mechanical or electrical work	kJ/kg
e_{spec}	Specific power consumption	$\mathrm{kW}_{el}/\mathrm{MW}_{th}$
f	Fugacity	bar
f_s	Utilisation level of subsystem s	-
G	Gas mass flux	$\mathrm{kg/(s{\cdot}m^2)}$
$\tilde{g}$	Molar Gibbs free energy	kJ/mol
h	Mass enthalpy	kJ/kg
h	Height	m
i_r	Interest rate	%
K	Equilibrium constant	variable
$\hat{K}$	Apparent equilibrium constant	variable
$\hat{K}_{\tilde{c}}$	Apparent equilibrium constant with respect to molar fractions	variable
$\hat{K}_p$	Apparent equilibrium constant with respect to partial pressures	variable
$k_{C2/C1}$	Proportionality constant $\tilde{c}_{C2H4}/\tilde{c}_{CH4}$	-
$\dot{L}$	Exergy depletion	kW
l	Length	m
$\dot{m}$	Mass flow	kg/s

$\tilde{m}$	Molecular weight	kg/mol
n	Expected plant lifetime	years
n	Stoichiometric coefficient	mol
$\dot{n}$	Molar flow	kmol/s
P	Permeability	barrer
P_a	Yearly production	MWh_{SNG}/year
p	Pressure	bar
$\dot{Q}$	Heat	kW
R	Dimensionless permeation factor/area	-
$\dot{R}$	Cascaded energy	kW
$\tilde{R}$	Ideal gas constant	kJ/(K mol)
$r_{CO2,rem}$	Carbon dioxide removal in separation	%
r_{CH4}	Methane recovery	%
r_{SNG}	SNG recovery	%
$r_{S/B}$	Steam to dry biomass ratio	-
SN	Stoichiometric number	-
$s_{in,2}$	Fraction of membrane inlet to stage 2	-
$s_{p1,E1}$	Fraction of permeate 1 to stage E1	-
T	Temperature	K
t_{r1}	Relative duration of PSA adsorption	-
t_{r2}	Relative duration of PSA recycling	-
U	Overall transfer coefficient	variable
u	Velocity	m/s
V	Volume	m^3
$\dot{V}$	Volume flow	m^3/s
$W_{s,n}$	Wobbe Index	$\mathrm{kWh\ Nm}^{-3}$
y	Integer choices	-
Z	Compressibility factor	-

Subscripts

a	atmospheric
ad	adiabatic
BM	bare module
BP	by-products
be	break even
c	cold
c	combustion
c	critical
cat	catalyst
cc	carbon conversion
cg	cold gas
d	drying
daf	dry, ash-free
el	electric
eq	equilibrium
f	feed

GR	grass roots
GR,d	depreciated grass roots
g	gasification
h	hot
lm	log-mean
M	maintenance
m	methanation
max	maximum
$mean$	mean
min	minimum
OL	operating labour
OP	operation
P	production
p	permeate
q	heat
r	reduced
r	retentate
ref	reference
RM	raw materials
s	steam cycle
sat	saturation (or saturated)
ss	salt separation
t	torrefaction
th	thermal
tot	total
UT	utilities
vap	vaporisation (or vaporised)
y	material transformation

Superscripts

$*$	Corrected temperatures
$+$	Material or energy stream entering the system
$-$	Material or energy stream leaving the system
0	Standard conditions
l	Liquid phase
sep	Separation system
v	Vapour phase

List of Figures

List of Tables

List of Tables

Curriculum vitae

Personal details

Name	Martin GASSNER
Date of birth	12.05.1980
Citizenship	Liechtenstein
Contact	martin.gassner@epfl.ch

Scientific experience

2006 – 2010 PhD student, Laboratory for Industrial Energy Systems, Ecole Polytechnique Fédérale de Lausanne (EPFL), Switzerland.

2009 Research visit, Yoshikawa Laboratory, Tokyo Institute of Technology, Japan. Research interest: Processes for the conversion of waste to energy.

2005 – 2006 Research assistant, Laboratory for Industrial Energy Systems, EPFL. Experimental investigation and development of a system for direct ignition of a small-scale gas turbine with kerosene.

Education

2000 – 2005 MSc in mechanical engineering, EPFL, Switzerland.

2003 – 2004 Exchange student, Chalmers University of Technology, Sweden.

Awards

2006 Best paper of a young scientist at ECOS conference for "Thermo-economic optimisation of the integration of electrolysis in a wood to methane process."

2005 "Energy"-price of the canton of Vaud for MSc thesis at EPFL.